Genetic analysis of post-embryonic development in *Drosophila*

By

Sarah D. Neuman

A dissertation submitted in partial fulfillment of

the requirements for the degree of

Doctor of Philosophy

(Cellular and Molecular Biology)

at the

UNIVERSITY OF WISCONSIN-MADISON

2017

Date of final oral examination: 6/20/2017

The dissertation is approved by the following members of the Final Oral Committee:

Arash Bashirullah, Associate Professor, Pharmacy
Alan Attie, Professor, Biochemistry
Grace Boekhoff-Falk, Associate Professor, Cell & Regenerative Biology
Shigeki Miyamoto, Professor, Oncology
Bill Sugden, Professor, Oncology

TABLE OF CONTENTS

LIST OF FIGURES AND TABLES

CHAPTER 2: *Hobbit* couples retrograde trafficking and regulated exocytosis to drive insulin-dependent growth during *Drosophila* development

CHAPTER 3: Future Directions and Conclusions

CHAPTER 4: *Tango7* regulates cortical activity of caspases during *reaper*-triggered changes in tissue elasticity

CHAPTER 6: INO80-dependent regression of ecdysone-induced transcriptional responses regulates developmental timing in *Drosophila*

APPENDIX 1: Retinal expression of the *Drosophila eyes absent* gene is controlled by several cooperatively acting *cis*-regulatory elements

APPENDIX 2: Teashirt and Tiptop control growth and developmental plasticity within the *Drosophila* eye-antennal disc

ABSTRACT

Animal development is a complex and highly-coordinated process. Building an adult animal of the proper size and shape requires intricate regulation of every aspect of biology, from basic functions within single cells to systemic coordination between entire tissues and organs. The work presented in this dissertation explores the genetic mechanisms regulating post-embryonic development in *Drosophila*, with a specific focus on growth control, tissue morphogenesis, and developmental timing. I have identified *hobbit*, a novel and highly-conserved gene that reveals a new role for intracellular trafficking and regulated exocytosis in growth control. Additionally, I have explored the function of caspases as regulators of morphogenesis, providing new insights into how these enzymes remodel the salivary gland during development. I have also identified a new role for transcriptional repression mechanisms in the regulation of developmental timing. Finally, I present some collaborative studies examining the role of transcription in development of the *Drosophila* compound eye. Altogether, the work presented in this dissertation sheds new light on genetic mechanisms regulating post-embryonic development, a critical but poorly studied developmental stage.

ACKNOWLEDGEMENTS

There are many, many people to whom I owe great thanks in helping me reach my goal of completing a Ph.D. Reaching this milestone would not have been possible without the unfailing help and support from my family, friends, teachers, and mentors.

First and foremost, my advisor, Arash Bashirullah. Arash, I can't thank you enough for everything you've done for me during my time in graduate school. Thank you for allowing me to take the risk to work on *hobbit*, and encouraging me through every rough spot and setback that comes with trying to figure out something completely new. Thank you also for helping me to realize what I am capable of and pushing me to reach (and understand!) my full potential. Finally, thank you for the opportunities and freedom that you have given me to explore my interests, both at and beyond the bench.

To my committee members, Alan Attie, Grace Boekhoff-Falk, Shigeki Miyamoto, and Bill Sugden: Thank you for taking the time out of your busy schedules to come to my committee meetings each year. Your feedback and support played a critical role in my success as a graduate student. I truly looked forward to each of my committee meetings, knowing that I would get to have an engaging discussion about my science with you.

Yunsik Kang: You might be a cancerous, dominant negative, foreign bum with Asian genes, but you are also my best Korean friend. Thank you for all of the fun times in lab- all of the stupid conversations, GoT theories, and putting up with me being "nice" to you. Your ideas, input, and feedback played a huge role in helping my projects succeed. I miss you in lab, but I know that your raw passion for science will help you be wildly successful in your postdoc and beyond.

Robert Ihry: Thank you so much for everything you did for me during your time in the lab. I miss our late-night RNA-making and marathon white prepupa picking parties; every time I'm in lab late at night I remember those good (and tiring) times. Thank you also for your persistent harassment that eventually got me riding a bike, which has literally changed my life. I am so happy that you are doing well in your postdoc, and I know that you will change the world someday with your science.

Khailee Marischuk: I am so glad that we got to share our love of books, the Tenth Doctor, and cute animal videos. I hope you realize that every time I hear or see a really bad pun I will be sending it to you. I wish you all the best in your new lab, and I know that you will be amazing!

Doug Braun and Dena Johnson-Schlitz: Thank you to both of you for keeping the lab up and running, and for all of the help that you provided over the years.

To my amazing undergrads- Jessica Smoko, Lindsay Mosher, Kelci Marzahn, Bridget Stollfus, Erica Terry, and Cidnee Carrigan- watching each of you learn and grow as scientists during your time in lab was a tremendously rewarding experience. I hope you realize that I learned just as much from you as you (hopefully!) learned from me.

To my CMB friends and classmates: Thank you all for being all-around great people! It has been so much fun to get to know each of you, and I couldn't have asked for a more fantastic group of friends and colleagues to share the graduate school journey with. Best of luck to each of you as you move into the next phase of your careers!

Michelle Holland, Jessica Skarlupa, and Lauren Weitkamp- Thank you for all you did/do to keep the CMB program up and running.

David Wassarman: Thank you for your leadership of the CMB program over the last few years. Thank you also for giving me the opportunity to serve the program on the Coordinating Committee. I am glad to have been a part of efforts to make the program even better.

To Greg Smith, my undergraduate academic and research advisor: Greg, without you, I wouldn't have even known that a Ph.D. in the sciences was an option for me. Thank you for everything you did for me during my time at Lakeland, and for everything you continue to do as my mentor. I truly wouldn't be here without you.

To my 7th grade teacher, Mr. Jim Hardt: When I look back, your class stands out as one of the biggest things that ignited my passion and curiosity about the natural world. Thank you for opening my world to science.

And finally, to my parents, Dan and Carol Neuman: Mom and Dad, words cannot express how grateful I am for your love and support throughout graduate school, and indeed throughout every step of the way that led me to this point. You have always been my biggest fans and cheerleaders, and I know how proud you are of everything I've accomplished. Thank you for everything. I love you!

I'd also like to acknowledge my funding sources: National Science Foundation Graduate Research Fellowship Program (NSF GRFP DGE-1256259) and Straka Fellowship funding from the University of Wisconsin-Madison Graduate School.

PART ONE

Growth control: a new role for intracellular trafficking

CHAPTER 1

Introduction: Anterograde and Retrograde Trafficking in Secretory Cells

Secretory cells are a specialized cell type that produce and secrete large amounts of cargo proteins in response to specific stimuli. During the production and secretion of cargo-carrying secretory granules, secretory cells must ensure that the proper proteins are delivered to the correct subcellular compartments, a process called intracellular trafficking. These cells utilize two distinct intracellular trafficking pathways: the anterograde, or secretory, pathway, and the retrograde, or endocytic, pathway. This introduction will provide an overview of the molecular regulation of each step within these two trafficking pathways.

PART I: THE ANTEROGRADE TRAFFICKING PATHWAY

There are two types of anterograde trafficking, also referred to as secretion: the constitutive secretory pathway and the regulated secretory pathway. The constitutive secretory pathway is utilized by all cell types and is used to deliver proteins and phospholipids to the plasma membrane[1]. As the name implies, the constitutive pathway is always active in the cell, and constitutively-secreted vesicles fuse with the plasma membrane and release their contents in a stimulus-independent manner. In contrast, the regulated exocytosis pathway is only utilized in specialized secretory cells and is activated in a stimulus-dependent manner[1]. The regulated exocytosis pathway is critical for many basic biological functions in neuronal, endocrine, exocrine, and neuroendocrine tissues, including synaptic transmission and neuropeptide release in neurons, insulin release in pancreatic β-cells, and mucin secretion in airway epithelial cells[2]. This introduction will focus specifically on regulated exocytosis of secretory granules in professional secretory cells.

Secretory granule biogenesis

The first step of anterograde trafficking/regulated exocytosis is the production of secretory granules. These are specialized organelles that contain large amounts of specific secretory products. Some secretory granules, such as those containing neuropeptides or insulin, contain a crystallized, electron-dense core and are therefore called dense core vesicles[3,4]. Proteins destined for the regulated exocytosis pathway are targeted to the rough endoplasmic reticulum (ER) via signal peptides; these proteins are then translated on the rough ER[4]. Secretory proteins next traffic through the cisternae of the Golgi apparatus, where they are post-translationally modified, and ultimately reach the *trans*-Golgi Network (TGN)[4]. Upon reaching the TGN, regulated secretory proteins are sorted and packaged into immature secretory granules. There are different mechanisms used to target these proteins to granules. For insoluble cargoes, targeting appears to require a combination of calcium- and pH-dependent selective aggregation of secretory proteins and specific peptide motifs that act as sorting signals within the secretory proteins themselves[5]. For soluble cargoes, such as prohormones, targeting appears to require interaction with a sorting receptor and/or specific lipid domain located on the TGN membrane[5]. All of these mechanisms appear to be critical for properly sorting secretory proteins into immature secretory granules in different cell types; however, there is still much unknown about this critical step in regulated exocytosis. Once the cargo has been consolidated, secretory granules bud from the TGN membrane. This process requires members of the Arf and Rab families of small GTPases and cytoskeletal components, including F-actin and myosin II, to mediate membrane curvature and scission[5–7].

During the process of secretory granule biogenesis, a variety of transmembrane and membrane-associated proteins are loaded onto the surface of the granules. Studies in neuroendocrine cells have shown that immature granules are clathrin-coated[8,9]. Clathrin appears to be important for granule biogenesis, as loss of either clathrin or its adaptor *AP-1* in the acinar cells of the *Drosophila* larval salivary glands inhibits biogenesis of secretory granules containing mucin-like “glue” proteins[10]. Additionally, studies in neuroendocrine cell lines have found that Soluble NSF-Attachment Protein Receptor (SNARE) proteins, membrane-tethered proteins that are critical for membrane fusion events, are loaded onto immature secretory granules. In AtT-20 cells, VAMP2 and VAMP4 are both present on immature granule membranes[11], while syntaxin-6 is loaded onto immature granules in PC12 cells[12]. Similarly, in the *Drosophila* larval salivary gland, the SNARE SNAP-24 is loaded onto mucin-containing glue granules[13]. Synaptotagmins, specifically Synaptotagmin-I and Synaptotagmin-IV, which are calcium-sensitive mediators of membrane fusion, are also loaded onto immature secretory granules in AtT-20 neuroendocrine cells[11]. Although SNAREs and Synaptotagmins are present on immature secretory granules, it is not clear if they play a role during granule budding from the TGN membrane.

Secretory granule maturation

Upon exit from the TGN, immature secretory granules undergo a maturation process. Maturation occurs relatively rapidly, within a few hours of biogenesis in most cell types studied[5,14]. Secretory granule maturation is essential for exocytosis, as immature granules cannot be efficiently secreted[11]; furthermore, maturation is important for proper

processing and packaging of secretory cargo. The process of secretory granule maturation comprises three distinct, and largely sequential, steps.

The first step of secretory granule maturation involves homotypic fusion of nascent, small granules to generate larger granules[5]. This process was first observed in 1966 during morphological studies of mammotropic hormone-producing cells in the lactating rat[15], and has since been observed in many different cell types, including mammalian neuroendocrine (PC12) cells, mast cells, pancreatic acinar cells, and *Drosophila* larval salivary gland cells. In PC12 cells, homotypic fusion is mediated by the SNAREs syntaxin-6 and Synaptotagmin-IV[12,16], while the SNARE SNAP-24 mediates granule-granule fusion in the *Drosophila* larval salivary glands[13]. Loss of the Arf-family small GTPase *Arl1* in *Drosophila* salivary glands results in granules with dramatically reduced size[17], suggesting that this protein may regulate homotypic fusion through an unknown mechanism. Recent studies in a mouse model find that *HID-1*, a conserved membrane shuttling protein, is required for homotypic fusion of insulin secretory granules in pancreatic β-cells[18]. Studies in certain cell types, including mast cells and pancreatic acinar cells, suggest that homotypic fusion does not occur randomly to generate granules of varying size; instead, final granule size is determined by precise fusion of “unit granules” (reviewed in[19]). However, the biological significance of the unit granule fusion model is unclear.

The second step of secretory granule maturation involves budding of small vesicles, called immature secretory granule-derived vesicles (IDVs) or constitutive-like vesicles, off secretory granule membranes. This step serves as a sort of “quality control” by refining the content of the secretory granule and remodeling its membrane[5]. Many

different proteins have been observed to exit immature secretory granules in IDVs, including the homotypic fusion machinery proteins syntaxin-6, VAMP4, and Synaptotagmin-IV[11,12,20]. This step appears to be essential for efficient secretion, as retention of Synaptotagmin-IV on secretory granules in AtT-20 cells strongly inhibited exocytosis[11]. IDV budding also removes proteins that were aberrantly packaged into immature secretory granules. Studies in PC12 cells reveal that furin, a protease that is abundantly expressed in the TGN, is packaged into immature secretory granules but is absent from mature secretory granules[21]. The cytoplasmic domain of furin recruits the clathrin-adaptor AP-1, mediating removal of the protease from the immature secretory granule in small clathrin-coated vesicles. This data supports the idea that IDV budding acts as a quality control step to remove proteins that were aberrantly targeted to secretory granules. This step also presumably removes the immature secretory granule clathrin coat and excess membrane from homotypic fusion events[22,23]. Additionally, studies in mammalian pancreatic β-cells demonstrate that the mannose 6-phosphate receptor (M6PR), the sorting receptor for lysosomal proteins, is present on immature secretory granules but absent from mature granules[20]. Lysosomal enzymes have also been observed within secretory granules[24]. M6PR and its cognate lysosomal enzyme ligands are removed from immature granules through a mechanism similar to that described for furin above; however, after budding from the immature granule, M6PR-containing vesicles traffic to endosomes for eventual delivery of M6PR-ligand complexes to the lysosome[20,24]. Finally, poorly-aggregated cargo proteins are also removed during the process of IDV budding[3]. After budding from the immature secretory granule, IDVs traffic to endosomes, where they may be secreted via the constitutive pathway, targeted to the

lysosome, or recycled back to the TGN[5]. Two recent studies in *C. elegans* highlight the importance of proper regulation of IDV budding during maturation. These studies find that mutants of the small GTPase *Rab2* aberrantly lose dense-core vesicle neuropeptide cargo from immature secretory granules to endosomes during the process of maturation[25,26]. Two additional proteins that interact with *Rab2* (*rund-1* and *cccp-1*) also regulate the fidelity of dense core vesicle cargo trafficking during secretory granule biogenesis and maturation[27]. Taken together, the process of IDV budding plays a critical role in the refinement of cargo content within secretory granules, and proper regulation of this process is essential in order to prevent aberrant loss of cargo during the maturation process.

Studies of both biogenesis and maturation of secretory granules have led to two differing models for how cargo is sorted into granules (reviewed in[23]). The first, termed “sorting by entry,” posits that secretory cargoes are selectively packaged into granules at the TGN, and the TGN acts as the sole site of selectivity for granule content and determines the eventual delivery site of the secretory cargo. The second model, called “sorting by retention,” suggests that the TGN acts as initial sorting site for secretory cargo, but some non-specific proteins may be aberrantly packaged into secretory granules. These non-specific proteins are later removed by small vesicles that bud from the secretory granule. Experimental evidence supports both models, and different cell types may use both mechanisms to generate secretory granules that contain correct cargo and are targeted to the correct destination. However, a recent study suggests that a third mechanism may play a role in the packaging of secretory content. Analysis of *C. elegans* mutants of *Endosome-Associated Recycling Protein (EARP)-interacting protein 1* (*eipr-1*)

revealed that neuronal dense core vesicle cargoes traffic through endosomal compartments to reach secretory granules[28]. Taken together, experimental evidence indicates that multiple steps of sorting and packaging contribute to the production of secretory granules containing the correct amount and type of cargo.

The final step of secretory granule maturation involves acidification of the immature granule. This is accomplished by vacuolar ATPase (V-ATPase) proton pumps on granule membranes[29]. The pH of an immature secretory granule is ~6.3; once acidification is complete, mature granules have a pH of ~5-5.5[30]. This acidification step is critical for secretory granules containing prohormones and proneuropeptides, as the prohormone convertases (PCs) that process these biologically-inactive precursors into bioactive hormones are only active at an acidic pH[30,31]. Little is known about the regulation of secretory granule acidification, although a recent study in *C. elegans* revealed that *vps-50*, a conserved protein, plays a role in neuropeptide-containing granule acidification, likely by facilitating the recruitment or assembly of the V-ATPase complex[32]. Altogether, the process of secretory granule maturation ensures that granules contain only the correct, bioactive cargo and that they are competent to undergo efficient exocytosis.

Exocytosis of secretory granules

Once maturation is complete, secretory granules are competent to undergo exocytosis, releasing their cargo to the extracellular environment; however, there are several steps that precede cargo release. Secretory granules are transported from the TGN to the plasma membrane in a microtubule-dependent manner[4,33]. Upon reaching the plasma membrane, secretory granules are sorted into two pools: the “readily-releasable”

pool, which can immediately undergo exocytosis upon receipt of a stimulus, and the "reserve" pool, which can maintain exocytosis upon prolonged stimulation[5]. Only about 1 percent of the total secretory granule content in endocrine, neuroendocrine, and exocrine cells comprises the readily-releasable pool[2]. The granules that make up the readily-releasable pool undergo several tethering, docking and priming steps before they can undergo stimulus-dependent membrane fusion.

Granules destined for the readily-releasable pool first undergo tethering and docking to the plasma membrane. The initial tethering step represents a loose attachment of the secretory granule to the plasma membrane[2,34]. The exocyst complex, an 8-protein complex that is highly conserved throughout eukaryotes, plays a significant role in tethering during constitutive secretion, but also during certain regulated secretion events, including release of vesicles containing the glucose transporter GLUT4 in response to insulin[35]. Early work studying mutants of exocyst components in yeast showed that disruption of this protein complex resulted in an accumulation of secretory vesicles within the cell, suggesting that the complex plays a role prior to membrane fusion events[36,37]; however, the mechanism by which exocyst regulated tethering was unclear. A recent study used quantitative fluorescence microscopy to resolve the structure of the exocyst complex *in vivo*, and found that the proteins in the complex form intertwined rods that interact with both the plasma membrane and the vesicle membrane to bring them into close proximity[38]. Exocyst activity is Rab GTPase-dependent; in yeast, Sec4p (orthologous to mammalian *RAB8A*) is the primary regulator of exocyst function[37]. In pancreatic and salivary gland acinar cells, Rab3D, Rab27B, and synaptotagmin-like

proteins (Slps) are present on secretory granule membranes, and these proteins may play a role in tethering through unknown mechanisms[39].

Once tethered to the plasma membrane, secretory granules next undergo a docking step, which represents a more stable, tight interaction between the vesicle and target membrane. Docking is mediated by SNARE proteins, both vesicle SNAREs (v-SNAREs) on the secretory granule membrane, and target membrane SNAREs (t-SNAREs) on the plasma (or other target) membrane. SNARE proteins may also be classified as Q-SNAREs, which have a conserved glutamine in their SNARE motif, or R-SNAREs, which have a conserved arginine in their SNARE motif[2]. The human genome encodes at least 44 SNARE protein isoforms[40], most of which contain a C-terminal membrane anchor. SNAREs lacking a transmembrane domain are anchored to the appropriate membrane through posttranslational modifications or through interactions with other transmembrane SNAREs[41]. Different secretory cell types, and indeed, different types of secretory granules within the same cell, may use varying v- and t-SNAREs to regulate membrane fusion events; however, the basic mechanism of SNARE action remains the same across all cell types. Docking of secretory granules requires specific interactions between v-SNAREs and t-SNAREs, which bind to each other and form the "SNAREpin" complex, composed of four SNARE motifs assembled in a twisted, four-helical bundle[41]. The interaction of one v-SNARE and three t-SNAREs acts like a zipper to pull the secretory granule and target membrane into close proximity; this interaction is highly energetically-favorable and the resulting SNARE complex is very stable[42]. Certain proteins interact with SNAREs to facilitate SNAREpin formation; for example, Munc18-1,

a member of the conserved family of Sec1/Munc18 proteins, plays a critical role in dense core vesicle docking by facilitating SNAREpin formation[39,43].

Once docked, secretory granules undergo a priming step. Historically, docking was thought to precede priming; however, recent studies using high-pressure freezing electron microscopy suggest that docking and priming may occur nearly simultaneously[44]. Priming was originally defined as an ATP- and calcium-dependent step that occurs prior to granule release and is activated upon low-level calcium stimulation (0.1-2μM)[45]. This process was first described as the ATP-dependent disassembly of *cis*-SNARE complexes to enable *trans*-SNARE interactions, requiring the chaperones N-ethylmaleimide-Sensitive Factor protein (NSF) and Soluble NSF Attachment protein (α-SNAP)[46]. More recently, new proteins have been characterized that regulate vesicle priming. Calcium-dependent Activator Protein for Secretion (CAPS) and Mammalian Unc-13 (Munc13) are two proteins that play a critical role in dense core vesicle priming in many secretory cell types[47–50]. The 2 vertebrate CAPS proteins (CAPS1 and CAPS2) regulate priming by enhancing SNARE complex assembly; specifically, these proteins facilitate insertion of v-SNAREs into the overall SNARE complex[51]. Munc13 family proteins also appear to regulate SNARE complex assembly by facilitating the conversion of t-SNAREs from closed monomers to heterodimers, a critical step to enable interactions between v- and t-SNAREs[51]. SNAREpin formation alone is sufficient to drive membrane fusion if left unchecked; therefore, small inhibitory proteins called complexins interfere with the “zipper” action of v- and t-SNARES to hold granules in a docked state until receipt of a stimulus to trigger membrane fusion[39,52].

Once a secretory granule has been docked and primed, it is ready to undergo fusion with the plasma membrane in response to a stimulus. In most secretory cells, calcium is the major signal that drives granule release; calcium concentrations can reach several μM to drive membrane fusion[45]. Synaptotagmins are the major calcium-sensing proteins that promote membrane fusion. Mammals have 17 synaptotagmin isoforms that are differentially expressed and utilized in different secretory cell types; however, only 8 synaptotagmins can directly bind calcium[53]. These proteins contain two calcium-binding domains, called C2 domains, that mediate calcium-dependent interactions with phospholipids and with the SNARE complex[54,55]. The most well-characterized synaptotagmin is Synaptotagmin-1 (Syt-1), which plays a key role in both synaptic vesicle and dense core vesicle release in neurons, as well as secretory granule release in many other cell types[53]. Although the detailed molecular mechanism by which Syt-1 mediates membrane fusion is still unclear, it is thought that calcium stimulation alters interactions between Syt-1 and complexin, effectively releasing the SNARE complex to drive fusion of the granule membrane with the plasma membrane[52]. However, Syt-1 may also directly regulate membrane cross-linking and curvature to promote fusion[56,57]. SNARE complex “zippering” drives opening of the fusion pore, enabling release of secretory granule content to the extracellular environment. In the *Drosophila* larval salivary glands, the actin-myosin cytoskeleton plays a critical role in mucin-like glue protein secretion. Recent studies have found that the cortical filamentous actin (F-actin) cytoskeleton is transiently dismantled at exocytosis sites on the apical membrane; F-actin is then rapidly re-assembled around the secreting glue granule, and myosin-II generates a contractile force to expel granule contents into the lumen[58,59].

The anterograde trafficking pathway in secretory cells is a complex and tightly-regulated process that requires the biogenesis, maturation, and regulated release of cargo-containing secretory granules. Regulated secretion is critical for maintenance of physiological homeostasis in animals, and disruption of this process causes a myriad of human diseases, highlighting the importance of this trafficking pathway for human health and development.

PART II: THE RETROGRADE TRAFFICKING PATHWAY

A second critical trafficking pathway within eukaryotic cells is the retrograde, or endocytic, pathway. This trafficking pathway is used to bring molecules from the extracellular environment or the plasma membrane into the interior of the cell. Retrograde trafficking begins with classical endocytosis: the formation of plasma membrane invaginations that enclose specific cargo, forming a vesicle that is then brought inside the cell. Many different cargoes can be brought into the cell via endocytosis, and this process is highly regulated (reviewed in[60,61]). Once endocytic vesicles have entered the cell, they are trafficked to the endolysosomal system, composed of organelles that function as central hubs for cargo sorting, recycling, trafficking, and degradation. Endocytic cargoes first enter the early endosome, the central sorting hub for the endolysosomal system. Vesicular cargo may also enter the early endosome from other routes, including direct trafficking from the TGN or other organelles, including IDVs that bud from maturing secretory granules[23,62]. Early endosomes eventually mature into late endosomes, and late endosomes fuse with lysosomes to mediate cargo degradation. Cargo may also be redirected from the early endosome to the recycling endosome for trafficking back to the

plasma membrane. The endolysosomal system is highly dynamic, with constant maturation of endosomal compartments, making it very difficult to mark clear boundaries between early, late, and recycling endosomes[62]. Nonetheless, these compartments serve a critical function in the sorting and trafficking of vesicular cargo. This introduction will focus specifically on retrograde trafficking routes from endosomes to the TGN.

Early/late endosome to TGN trafficking: the retromer complex

The retromer complex plays a critical role in the recognition, sorting, and trafficking of cargo from early/late endosomes to the TGN. Initial studies of retromer function concluded that retromer regulated early endosome to TGN trafficking; however, more recent studies indicate that retromer regulates trafficking out of endosomes that have matured to a transitional state between an early and late endosome[63]. Recent work has found that retromer can also regulate direct recycling from endosomes to the plasma membrane and trafficking from mitochondria to peroxisomes (reviewed in[64]); however, this introduction will focus specifically on retromer function in endosome to TGN trafficking. Retromer was first discovered in yeast in a screen for regulators of endosome-to-TGN transport of Vps10p, a transmembrane sorting receptor[65]. Five proteins make up the retromer complex in yeast: a dimer of Vps5p and Vps17p and a trimer of Vps26p, Vps29p, and Vps35p[66]. The Vps26-Vps29-Vps35 trimer forms the “cargo-selective complex” (CSC), which, as the name implies, plays an important role in cargo identification and is highly conserved throughout eukaryotes[64,67]. Mammals have two Vps26 paralogs, Vps26A and Vps26B, that provide different specificities for cargo recognition[68]. Vps5p and Vps17p are homologus to the Sorting Nexin (SNX) protein family

in mammals, four of which function as core components in the retromer complex: SNX1, SNX2, SNX5, and SNX6[69]. The SNX proteins function as heterodimers (SNX1/5, SNX1/6, SNX2/5, or SNX2/6) and form the “tubulation complex,” which plays a critical role in bending membranes[70]. Other SNX proteins also play a role in the retromer complex, providing mechanisms for increased specificity and functional diversity for the complex[71,72].

In order to mediate retrograde trafficking, the retromer complex must first be recruited to the endosomal membrane. The molecular details of this process are still emerging, but two different models for retromer recruitment have been proposed. In one model, the CSC is the first complex to be recruited to the endosomal membrane[73]; conversely, in the second model, the tubulation complex is first to arrive[74]. There is evidence supporting both models, and further studies are needed to resolve this issue. Nonetheless, the four tubulation complex SNX proteins that function as core retromer components contain two critical protein domains: a phagocyte-oxidase (phox)-homology (PX) domain and a Bin/Amphiphysin/Rvs (BAR) domain[75]. The PX domain binds phophoinositides, a specific type of membrane phospholipid[76], while the BAR domain can “sense,” bind, and stabilize membrane curvature[69]. In this manner, the tubulation complex is recruited to the phosphatidylinositol-3-monophosphate (PI3P)-rich, highly-curved membrane of the maturing early endosome[64]. Lipid composition appears to be very important for retromer function, as a *Drosophila* mutant of type II PI4 kinase (PI4KII) exhibits aberrant retromer dynamics in the larval salivary glands during glue protein synthesis[77]. Additionally, the CSC component Vps35 can bind to the small GTPase Rab7, a protein on maturing early endosomes where retromer functions[78], and to the SNX

tubulation complex[64]. The combination of these protein and lipid interactions results in recruitment of the complete retromer complex to endosomal membranes.

After recruitment to the endosomal membrane, the retromer complex initiates cargo recognition, tubulation, and carrier biogenesis. Many different retromer cargoes have been identified (for details, see below); however, all interact with either the CSC and/or the SNX proteins, usually via specific peptide sequences that bind with one of the retromer components[64]. Once the appropriate cargoes are bound, the retromer complex begins the process of tubule formation. The BAR domain-containing SNX proteins (SNX1/2, SNX5/6) mediate membrane deformation through organization of heterodimeric BAR domains organized in helical arrays[74,79]. Expansion of these helical arrays results in formation of a narrow tubule that is coated with retromer complex components. Tubulation is assisted by cytoskeletal components, including the dynein/dynactin molecular motor[80,81] and the filamentous actin (F-actin)-binding Wiskott-Aldrich Syndrome Protein and SCAR Homolog (WASH) complex[82]. Following tubulation, a retromer-coated cargo carrier is excised from the end of the tubule. This process is poorly characterized, however, studies in both yeast and mammalian cells suggest that it requires the large GTPase dynamin[83,84]. Eps15 homology domain 1 (EHD1) is an ATPase that may also facilitate membrane scission during carrier biogenesis[85]. The cargo carrier is then transported to the TGN via microtubules and molecular motors; however, the specific mechanisms regulating this process have not yet been defined[64].

The retromer complex regulates retrograde trafficking of many different cargo proteins, some of which will be listed here. Recent reviews contain a more exhaustive list of retromer cargoes[64,70]. The first cargoes to be recognized were yeast Vps10p and its

mammalian orthologs, Sortilin and SorLA[65,86]. Subsequently, the list of retromer cargoes has exploded to include other transmembrane receptors, including the cation-independent mannose 6-phosphate receptor (CI-M6PR) in mammals[87], the bone morphogenetic protein (BMP) receptor SMA-6 in *C. elegans*[88], and various G-protein coupled receptors (GPCRs) in both *Drosophila* and mammals[89,90]. Retromer is also required for recycling of the morphogen carrier Wntless (Wls) in mammals, *Drosophila*, and *C. elegans*[91,92]. Wntless acts as a carrier for the morphogen Wnt from the TGN to the plasma membrane; once Wnt has been secreted, Wls traffics back to the TGN via retromer. Disruption retromer function traps Wls in endosomes and results in reduced Wnt secretion. Recent studies also find that retromer is required for recycling of the Notch receptor in *Drosophila*[93]. Finally, a number of SNARE proteins cycle between endosomes and the TGN[94], ensuring that SNAREs are located on the proper intracellular membrane to mediate fusion events during vesicular trafficking.

Retromer function also has important implications for human disease. Retromer dysfunction is associated with both Alzheimer's and Parkinson's Disease. In Alzheimer's, defects in retromer-mediated trafficking trap both amyloid precursor protein (APP) and β- and γ-secretase, the enzymes that process APP, in endosomes, resulting in higher levels of amyloid β (Aβ) production and facilitating amyloid plaque formation[95]. A mutation in Vps35 ($Vps35^{D620N}$) is associated with late-onset Parkinson's Disease, presumably by disrupting retromer interactions with the WASH complex, resulting in aberrant trafficking of proteins that regulate autophagy and promoting neuronal cell death[95]. Finally, a number of human pathogens co-opt the retromer machinery to mediate entry into cells. The bacterial Shiga toxin from *Shigella dysenteriae* and Cholera toxin from *Vibrio cholera* both

utilize retromer-mediated transport to enter human cells[96]. Viruses, including HPV-16, HVS, and HIV-1, also utilize the retromer complex to facilitate infectivity or viral capsid assembly[70].

Early/recycling endosome to TGN trafficking: clathrin and adaptors

The clathrin coat protein plays a critical role in mediating retrograde transport from early or recycling endosomes to the TGN. It is difficult to experimentally differentiate early endosomes from recycling endosomes, as there are no markers that are completely specific for the recycling endosome[97]. Nonetheless, clathrin is present on early endosomes, and mutation of clathrin traps cargo proteins in the early endosome[98,99]. Clathrin adaptor proteins are also critical for clathrin-mediated retrograde transport, including AP-1[100], EpsinR[99], and oculocerebrorenal syndrome of Lowe (OCRL)[101]. The use of different clathrin adaptors appears to mediate specificity in cargo selection. Disruption of clathrin function affects trafficking of many of the same proteins that undergo retromer-dependent retrograde transport, including the bacterial Shiga and Cholera toxins, Sortilin, and the lysosomal enzyme receptor M6PR[62]; however, it is unclear if retromer and clathrin play cooperative or sequential roles in trafficking of these cargo proteins. The most recent models suggest that clathrin first mediates cargo sorting and enrichment in early endosomes before retromer is recruited, then retromer binds near clathrin-coated regions and independently initiates tubulation[102]. However, further work is needed to verify this model.

A few studies have suggested that an independent recycling endosome to TGN trafficking pathway exists. One study using Shiga toxin as a marker found that expression

of a dominant-negative form of the small GTPase Rab11 inhibited retrograde transport of the toxin to the TGN, trapping it in a putative recycling endosomal compartment[103]. A second study of HIV-triggered endocytosis also suggested a role for Rab11 in recycling[104]. However, more work is needed to identify the mechanisms regulating Rab11-mediated retrograde trafficking from the recycling endosome.

Late endosome to TGN trafficking: Rab9/TIP47/p40

A third retrograde trafficking route moves cargoes specifically from late endosomes to the TGN. There are two primary cargo protein that are known to traffic via this route: M6PRs and the protease furin[62]. Although M6PRs are also trafficked by the retromer complex, it is likely that retromer “misses” some of these proteins, which are then identified in and recycled from the late endosome. Late endosome to TGN trafficking requires the late endosome-localized small GTPase Rab9[105]. During M6PR trafficking, Rab9 recruits an effector protein, M6PR tail-interacting protein of 47 kDa (TIP47), which binds to specific amino acid residues in the cytoplasmic domain of M6PR[106]. Disruption of TIP47 binding, either through RNAi knockdown of TIP47 or mutation of TIP47 binding sites in M6PR, inhibits retrograde trafficking of the protein. Rab9 also recruits a second effector protein, p40 (protein of 40 kDa), that promotes M6PR trafficking[107]. Together, Rab9, TIP47, and p40 recruit and package M6PR into transport vesicles that traffic back to the TGN through unknown mechanisms[62,108,109]. Furin also requires Rab9-mediated late endosome to TGN trafficking, although a role for TIP47 and p40 in this process is not clear[110]. Recent studies suggest that the Rho GTPase RhoBTB3 may also play a role in Rab9-mediated retrograde trafficking. RhoBTB3 was identified as a Rab9 interactor in a

yeast two-hybrid screen; additionally, RhoBTB3 binds with TIP47[111]. Studies of RhoBTB3 function in retrograde trafficking suggest that the protein may play a role in retrograde transport vesicle uncoating and/or fusion at the TGN.

Tethering and fusion at the TGN

Upon reaching the TGN, vesicles derived from the retrograde pathway must be tethered and fuse at the TGN membrane, similar to the steps that occur during secretory granule exocytosis. Two families of tethering factors are particularly important for retrograde transport: the Golgins and the Golgi-Associated Retrograde Proteins (GARP) complex[102]. Golgins form homodimers and are composed of long coiled-coil regions[112]. Recently, the importance of Golgins in tethering was tested using a "knock sideways" approach, where Golgins were engineered to be mis-targeted to mitochondria instead of the TGN, then checking to see if cargo was also misdirected to the mitochondria[113]. Using this approach, golgin-97, golgin-245, and GCC88 were identified as important tethers for endosome to TGN cargo, such as M6PR. Other studies have found that the Golgin GCC185 specifically plays a role in Rab9-dependent trafficking from the late endosome[114]. The Golgins interact directly with microtubules or microtubule-associated proteins to provide a direct track for retrograde trafficking vesicles to reach the TGN, and these proteins have a highly flexible structure that allows them to capture incoming vesicles and tether then to the TGN membrane[102]. The GARP complex is a second protein complex that plays a critical role in vesicle tethering at the TGN. This complex was first discovered in yeast and is composed of four proteins: Vps51 (Ang2 in mammals), Vps52, Vps53, and Vps54[115,116]. Vps52 binds proteins, such as Rabs, on the surface of

retrograde transport carriers, while Vps53 interacts with proteins on the TGN membrane, making the GARP complex an effective tether for incoming transport vesicles[102]. GARP appears to serve as a tether for retrograde cargoes derived from both the early and late endosome[117], and also facilitates SNARE complex formation during membrane fusion, which will be described below. Other membrane tethers, such as the Conserved Oligomeric Golgi (COG) complex and the Transport Protein Particle (TRAPPII) complex, also play a role in tethering during retrograde transport; however, these proteins appear to primarily regulate intra-Golgi trafficking and not direct tethering of transport vesicles to the TGN[102].

The final step of retrograde trafficking requires fusion of the transport carrier membrane with the TGN membrane. This process is very similar to membrane fusion during secretory granule exocytosis; specific SNARE proteins present on the TGN membrane and the transport carrier membrane drive fusion of the two membranes. There are about a dozen SNARES present within the Golgi complex; of these, the t-SNAREs syntaxin-5, syntaxin-6, syntaxin-10, syntaxin-16, Vti1a, GS28, and Ykt6 are known to play a role in retrograde trafficking[62]. These t-SNAREs can pair with v-SNAREs on transport carrier membranes, including VAMP3, VAMP4, and GS15[62]. Consequently, these SNAREs are themselves subject to anterograde and retrograde trafficking between endosomes and the TGN to ensure that a constant supply of these membrane fusion proteins is present in the appropriate subcellular compartment[94].

CONCLUSIONS

Anterograde and retrograde trafficking both play a critical role in ensuring that proteins reach the appropriate subcellular compartment. In secretory cells, episodes of regulated exocytosis result in a massive release of cargo proteins, which requires a correspondingly significant utilization of the secretory machinery, including synaptotagmins and SNAREs. It would be energetically unfavorable for the cell to synthesize this machinery *de novo* for each round of secretory granule biogenesis and secretion; therefore, it would make sense for secretory cells to utilize retrograde trafficking pathways to recycle these components for subsequent rounds of secretion. However, currently, there is no direct evidence linking retrograde trafficking of secretory proteins to defects in anterograde trafficking. This section describes the identification of an uncharacterized and highly conserved protein, named *hobbit*, that regulates retrograde trafficking of *Synaptotagmin-1* and the SNARE *SNAP-24* to feed-forward the maturation and secretion of cargo-containing secretory granules. This work provides new insights into the biological importance of retrograde trafficking during the process of regulated exocytosis.

REFERENCES

1. Burgess, T. L. & Kelly, R. B. Constitutive and Regulated Secretion of Proteins. *Annu. Rev. Cell Biol.* **3,** 243–293 (1987).

2. Burgoyne, R. D. & Morgan, A. Secretory Granule Exocytosis. *Physiol. Rev.* **83,** (2003).

3. Molinete, M., Irminger, J. C., Tooze, S. A. & Halban, P. A. Trafficking/sorting and granule biogenesis in the beta-cell. *Semin. Cell Dev. Biol.* **11,** 243–51 (2000).

4. Gondré-Lewis, M. C., Park, J. J. & Loh, Y. P. in *International Review of Cell and Molecular Biology* **299,** 27–115 (2012).

5. Kögel, T. & Gerdes, H.-H. Maturation of secretory granules. *Results Probl. Cell Differ.* **50,** 1–20 (2010).

6. Santiago-Tirado, F. H. & Bretscher, A. Membrane-trafficking sorting hubs: cooperation between PI4P and small GTPases at the trans-Golgi network. *Trends Cell Biol.* **21,** 515–25 (2011).

7. Lundmark, R., Doherty, G. J., Vallis, Y., Peter, B. J. & McMahon, H. T. Arf family GTP loading is activated by, and generates, positive membrane curvature. *Biochem. J.* **414,** 189–194 (2008).

8. Orci, L., Ravazzola, M., Amherdt, M., Louvard, D. & Perrelet, A. Clathrin-immunoreactive sites in the Golgi apparatus are concentrated at the trans pole in polypeptide hormone-secreting cells. *Proc. Natl. Acad. Sci.* **82,** 5385–5389 (1985).

9. Tooze, J. & Tooze, S. Clathrin-coated vesicular transport of secretory proteins during the formation of ACTH-containing secretory granules in AtT20 cells. *J. Cell Biol.* (1986).

10. Burgess, J. *et al.* AP-1 and clathrin are essential for secretory granule biogenesis in Drosophila. *Mol. Biol. Cell* **22,** 2094–2105 (2011).

11. Eaton, B. A., Haugwitz, M., Lau, D. & Moore, H. P. Biogenesis of regulated exocytotic carriers in neuroendocrine cells. *J. Neurosci.* **20,** 7334–44 (2000).

12. Wendler, F., Page, L., Urbé, S. & Tooze, S. A. Homotypic fusion of immature secretory granules during maturation requires syntaxin 6. *Mol. Biol. Cell* **12,** 1699–709 (2001).

13. Niemeyer, B.A. & Schwarz, T. L. SNAP-24, a Drosophila SNAP-25 homologue on granule membranes, is a putative mediator of secretion and granule-granule fusion in salivary glands. *J. Cell Sci.* **113 Pt 2,** 4055–4064 (2000).

14. Tooze, S. A., Flatmark, T., Tooze, J. & Huttner, W. B. Characterization of the immature secretory granule, an intermediate in granule biogenesis. *J. Cell Biol.* **115,** (1991).

15. Smith, R. E. & Farquhar, M. G. Lysosome function in the regulation of the secretory process in cells of the anterior pituitary gland. *J. Cell Biol.* **31,** 319–47 (1966).

16. Ahras, M., Otto, G. P. & Tooze, S. A. Synaptotagmin IV is necessary for the maturation of secretory granules in PC12 cells. *J. Cell Biol.* **173,** 241–51 (2006).

17. Torres, I. L., Rosa-Ferreira, C. & Munro, S. The Arf family G protein Arl1 is required for secretory granule biogenesis in Drosophila. *J. Cell Sci.* **127,** 2151–60 (2014).

18. Du, W. *et al.* HID-1 is required for homotypic fusion of immature secretory granules during maturation. *Elife* **5,** (2016).

19. Hammel, I., Lagunoff, D. & Galli, S. J. Regulation of secretory granule size by the precise generation and fusion of unit granules. *J. Cell. Mol. Med.* **14,** 1904–16 (2010).

20. Klumperman, J., Kuliawat, R., Griffith, J. M., Geuze, H. J. & Arvan, P. Mannose 6-phosphate receptors are sorted from immature secretory granules via adaptor protein AP-1, clathrin, and syntaxin 6-positive vesicles. *J. Cell Biol.* **141,** 359–71 (1998).

21. Dittie, A. S., Hajibagheri, N. & Tooze, S. A. The AP-1 adaptor complex binds to immature secretory granules from PC12 cells, and is regulated by ADP-ribosylation factor. *J. Cell Biol.* **132,** 523–36 (1996).

22. Tooze, S. A. Biogenesis of secretory granules in the trans-Golgi network of neuroendocrine and endocrine cells. *Biochim. Biophys. Acta* **1404,** 231–44 (1998).

23. Arvan, P. & Castle, D. Sorting and storage during secretory granule biogenesis: looking backward and looking forward. *Biochem. J.* **332 Pt 3,** 593–610 (1998).

24. Kuliawat, R., Klumperman, J., Ludwig, T. & Arvan, P. Differential Sorting of Lysosomal Enzymes Out of the Regulated Secretory Pathway in Pancreatic β-Cells. *J. Cell Biol.* **137,** (1997).

25. Edwards, S. L. *et al.* Impaired dense core vesicle maturation in Caenorhabditis elegans mutants lacking Rab2. *J. Cell Biol.* **186,** 881–895 (2009).

26. Sumakovic, M. *et al.* UNC-108/RAB-2 and its effector RIC-19 are involved in dense core vesicle maturation in Caenorhabditis elegans. *J. Cell Biol.* **186,** 897–914 (2009).

27. Ailion, M. *et al.* Two Rab2 Interactors Regulate Dense-Core Vesicle Maturation. *Neuron* **82,** 167–180 (2014).

28. Topalidou, I. *et al.* The EARP Complex and Its Interactor EIPR-1 Are Required for Cargo Sorting to Dense-Core Vesicles. *PLOS Genet.* **12,** e1006074 (2016).

29. Jefferies, K. C., Cipriano, D. J. & Forgac, M. Function, structure and regulation of the vacuolar (H+)-ATPases. *Arch. Biochem. Biophys.* **476,** 33–42 (2008).

30. Urbé, S., Dittié, A. S. & Tooze, S. A. pH-dependent processing of secretogranin II by the endopeptidase PC2 in isolated immature secretory granules. *Biochem. J.* **321 Pt 1,** 65–74 (1997).

31. Orci, L. *et al.* Conversion of proinsulin to insulin occurs coordinately with acidification of maturing secretory vesicles. *J. Cell Biol.* **103,** 2273–81 (1986).

32. Paquin, N. *et al.* The Conserved VPS-50 Protein Functions in Dense-Core Vesicle Maturation and Acidification and Controls Animal Behavior. *Curr. Biol.* **26,** 862–871 (2016).

33. van den Berg, R. & Hoogenraad, C. C. Molecular motors in cargo trafficking and synapse assembly. *Adv. Exp. Med. Biol.* **970,** 173–96 (2012).

34. Waters, M. G. & Hughson, F. M. Membrane Tethering and Fusion in the Secretory and Endocytic Pathways. *Traffic* **1,** 588–597 (2000).

35. Uhm, M. *et al.* Phosphorylation of the exocyst protein Exo84 by TBK1 promotes insulin-stimulated GLUT4 trafficking. *Sci. Signal.* **10,** eaah5085 (2017).

36. Novick, P., Field, C. & Schekman, R. Identification of 23 complementation groups required for post-translational events in the yeast secretory pathway. *Cell* **21,** 205–215 (1980).

37. TerBush, D. R., Maurice, T., Roth, D. & Novick, P. The Exocyst is a multiprotein complex required for exocytosis in Saccharomyces cerevisiae. *EMBO J.* **15,** 6483–94 (1996).

38. Picco, A. *et al.* The In Vivo Architecture of the Exocyst Provides Structural Basis for Exocytosis. *Cell* **168,** 400–412.e18 (2017).

39. Messenger, S. W., Falkowski, M. A. & Groblewski, G. E. Ca2+-regulated secretory granule exocytosis in pancreatic and parotid acinar cells. *Cell Calcium* **55,** 369–375 (2014).

40. Kienle, N., Kloepper, T. H. & Fasshauer, D. Differences in the SNARE evolution of fungi and metazoa. *Biochem. Soc. Trans.* **37,** 787–91 (2009).

41. Hong, W. SNAREs and traffic. *Biochim. Biophys. Acta - Mol. Cell Res.* **1744,** 120–144 (2005).

42. Fasshauer, D., Eliason, W. K., Brünger, A. T. & Jahn, R. Identification of a Minimal Core of the Synaptic SNARE Complex Sufficient for Reversible Assembly and Disassembly. *Biochemistry* **37,** 10354–10362 (1998).

43. Voets, T. *et al.* Munc18-1 promotes large dense-core vesicle docking. *Neuron* **31,** 581–91 (2001).

44. Siksou, L. *et al.* A common molecular basis for membrane docking and functional priming of synaptic vesicles. *Eur. J. Neurosci.* **30,** 49–56 (2009).

45. Sørensen, J. B. *et al.* The SNARE protein SNAP-25 is linked to fast calcium triggering of exocytosis. *Proc. Natl. Acad. Sci. U. S. A.* **99,** 1627–32 (2002).

46. Banerjee, A., Barry, V. A., DasGupta, B. R. & Martin, T. F. N-Ethylmaleimide-sensitive factor acts at a prefusion ATP-dependent step in Ca2+-activated exocytosis. *J. Biol. Chem.* **271,** 20223–6 (1996).

47. Walent, J. H., Porter, B. W. & Martin, T. F. A novel 145 kd brain cytosolic protein reconstitutes Ca(2+)-regulated secretion in permeable neuroendocrine cells. *Cell* **70,** 765–75 (1992).

48. Speidel, D. *et al.* CAPS1 and CAPS2 Regulate Stability and Recruitment of Insulin Granules in Mouse Pancreatic β Cells. *Cell Metab.* **7,** 57–67 (2008).

49. Sadakata, T. *et al.* The Secretory Granule-Associated Protein CAPS2 Regulates Neurotrophin Release and Cell Survival. *J. Neurosci.* **24,** 43–52 (2004).

50. Kang, L. *et al.* Munc13-1 is required for the sustained release of insulin from pancreatic β cells. *Cell Metab.* **3,** 463–468 (2006).

51. James, D. J. & Martin, T. F. J. CAPS and Munc13: CATCHRs that SNARE Vesicles. *Front. Endocrinol. (Lausanne).* **4,** 187 (2013).

52. Südhof, T. C. Neurotransmitter Release: The Last Millisecond in the Life of a Synaptic Vesicle. *Neuron* **80,** 675–690 (2013).

53. Pinheiro, P. S., Houy, S. & Sørensen, J. B. C2-domain containing calcium sensors in neuroendocrine secretion. *J. Neurochem.* **139,** 943–958 (2016).

54. Verdaguer, N., Corbalan-Garcia, S., Ochoa, W. F., Fita, I. & Gómez-Fernández, J. C. Ca2+ bridges the C2 membrane-binding domain of protein kinase Cα directly to phosphatidylserine. *EMBO J.* **18,** 6329–6338 (1999).

55. Li, C. *et al.* Ca(2+)-dependent and -independent activities of neural and non-neural synaptotagmins. *Nature* **375,** 594–9 (1995).

56. Seven, A. B., Brewer, K. D., Shi, L., Jiang, Q.-X. & Rizo, J. Prevalent mechanism of membrane bridging by synaptotagmin-1. *Proc. Natl. Acad. Sci. U. S. A.* **110,** E3243-52 (2013).

57. Hui, E., Johnson, C. P., Yao, J., Dunning, F. M. & Chapman, E. R. Synaptotagmin-mediated bending of the target membrane is a critical step in Ca(2+)-regulated fusion. *Cell* **138,** 709–21 (2009).

58. Rousso, T., Schejter, E. D. & Shilo, B.-Z. Orchestrated content release from Drosophila glue-protein vesicles by a contractile actomyosin network. *Nat. Cell Biol.* **18,** 181–90 (2015).

59. Tran, D. T., Masedunskas, A., Weigert, R. & Hagen, K. G. Ten. Arp2/3-mediated F-actin formation controls regulated exocytosis in vivo. *Nat. Commun.* **6,** 1–10 (2015).

60. Arlt, H. *et al.* Spatiotemporal dynamics of membrane remodeling and fusion proteins during endocytic transport. *Mol. Biol. Cell* **26,** 1357–70 (2015).

61. Shaw, J. D., Cummings, K. B., Huyer, G., Michaelis, S. & Wendland, B. Yeast as a Model System for Studying Endocytosis. *Exp. Cell Res.* **271,** 1–9 (2001).

62. Lu, L. & Hong, W. From endosomes to the trans-Golgi network. *Semin. Cell Dev. Biol.* **31,** 30–39 (2014).

63. Seaman, M. N. J. The retromer complex - endosomal protein recycling and beyond. *J. Cell Sci.* **125,** 4693–4702 (2012).

64. Liu, J.-J. Retromer-Mediated Protein Sorting and Vesicular Trafficking. *J. Genet. Genomics* **43,** 165–177 (2016).

65. Seaman, M. N., Marcusson, E. G., Cereghino, J. L. & Emr, S. D. Endosome to Golgi retrieval of the vacuolar protein sorting receptor, Vps10p, requires the function of the VPS29, VPS30, and VPS35 gene products. *J. Cell Biol.* **137,** 79–92 (1997).

66. Seaman, M. N., McCaffery, J. M. & Emr, S. D. A membrane coat complex essential for endosome-to-Golgi retrograde transport in yeast. *J. Cell Biol.* **142,** 665–81 (1998).

67. Haft, C. R. *et al.* Human orthologs of yeast vacuolar protein sorting proteins Vps26, 29, and 35: assembly into multimeric complexes. *Mol. Biol. Cell* **11,** 4105–16 (2000).

68. Bugarcic, A. *et al.* Vps26A and Vps26B Subunits Define Distinct Retromer

Complexes. *Traffic* **12,** 1759–1773 (2011).

69. Bonifacino, J. S. & Hurley, J. H. Retromer. *Curr. Opin. Cell Biol.* **20,** 427–436 (2008).

70. Trousdale, C. & Kim, K. Retromer: Structure, function, and roles in mammalian disease. *Eur. J. Cell Biol.* **94,** 513–521 (2015).

71. Xu, Y., Hortsman, H., Seet, L., Wong, S. H. & Hong, W. SNX3 regulates endosomal function through its PX-domain-mediated interaction with PtdIns(3)P. *Nat. Cell Biol.* **3,** 658–66 (2001).

72. Strochlic, T. I., Setty, T. G., Sitaram, A. & Burd, C. G. Grd19/Snx3p functions as a cargo-specific adapter for retromer-dependent endocytic recycling. *J. Cell Biol.* **177,** 115–25 (2007).

73. Harbour, M. E. *et al.* The cargo-selective retromer complex is a recruiting hub for protein complexes that regulate endosomal tubule dynamics. *J. Cell Sci.* **123,** 3703–17 (2010).

74. van Weering, J. R. T. *et al.* Molecular basis for SNX-BAR-mediated assembly of distinct endosomal sorting tubules. *EMBO J.* **31,** 4466–80 (2012).

75. Teasdale, R. D. & Collins, B. M. Insights into the PX (phox-homology) domain and SNX (sorting nexin) protein families: structures, functions and roles in disease. *Biochem. J.* **441,** 39–59 (2012).

76. Song, X. *et al.* Phox homology domains specifically bind phosphatidylinositol phosphates. *Biochemistry* **40,** 8940–4 (2001).

77. Burgess, J. *et al.* Type II phosphatidylinositol 4-kinase regulates trafficking of secretory granule proteins in Drosophila. *J. Cell Sci.* **125,** 3040–50 (2012).

78. Rojas, R. *et al.* Regulation of retromer recruitment to endosomes by sequential action of Rab5 and Rab7. *J. Cell Biol.* **183,** 513–26 (2008).

79. Carlton, J. *et al.* Sorting nexin-1 mediates tubular endosome-to-TGN transport through coincidence sensing of high- curvature membranes and 3-phosphoinositides. *Curr. Biol.* **14,** 1791–800 (2004).

80. Hong, Z. *et al.* The retromer component SNX6 interacts with dynactin p150(Glued) and mediates endosome-to-TGN transport. *Cell Res.* **19,** 1334–49 (2009).

81. Wassmer, T. *et al.* The retromer coat complex coordinates endosomal sorting and dynein-mediated transport, with carrier recognition by the trans-Golgi network. *Dev. Cell* **17,** 110–22 (2009).

82. Gomez, T. S. & Billadeau, D. D. A FAM21-Containing WASH Complex Regulates Retromer-Dependent Sorting. *Dev. Cell* **17,** 699–711 (2009).

83. Nicoziani, P. *et al.* Role for dynamin in late endosome dynamics and trafficking of the cation-independent mannose 6-phosphate receptor. *Mol. Biol. Cell* **11,** 481–95 (2000).

84. Chi, R. J. *et al.* Fission of SNX-BAR-coated endosomal retrograde transport carriers is promoted by the dynamin-related protein Vps1. *J. Cell Biol.* **204,** 793–806 (2014).

85. Gokool, S., Tattersall, D. & Seaman, M. N. J. EHD1 interacts with retromer to stabilize SNX1 tubules and facilitate endosome-to-Golgi retrieval. *Traffic* **8,** 1873–86 (2007).

86. Fjorback, A. W. *et al.* Retromer binds the FANSHY sorting motif in SorLA to regulate amyloid precursor protein sorting and processing. *J. Neurosci.* **32,** 1467–80 (2012).

87. Arighi, C. N., Hartnell, L. M., Aguilar, R. C., Haft, C. R. & Bonifacino, J. S. Role of the mammalian retromer in sorting of the cation-independent mannose 6-phosphate receptor. *J. Cell Biol.* **165,** 123–133 (2004).

88. Gleason, R. J., Akintobi, A. M., Grant, B. D. & Padgett, R. W. BMP signaling requires retromer-dependent recycling of the type I receptor. *Proc. Natl. Acad. Sci. U. S. A.* **111,** 2578–83 (2014).

89. Temkin, P. *et al.* SNX27 mediates retromer tubule entry and endosome-to-plasma membrane trafficking of signalling receptors. *Nat. Cell Biol.* **13,** 715–21 (2011).

90. Wang, S. *et al.* The Retromer Complex Is Required for Rhodopsin Recycling and Its Loss Leads to Photoreceptor Degeneration. *PLoS Biol.* **12,** e1001847 (2014).

91. Belenkaya, T. Y. *et al.* The retromer complex influences Wnt secretion by recycling wntless from endosomes to the trans-Golgi network. *Dev. Cell* **14,** 120–31 (2008).

92. Pan, C.-L. *et al.* C. elegans AP-2 and retromer control Wnt signaling by regulating mig-14/Wntless. *Dev. Cell* **14,** 132–9 (2008).

93. Gomez-Lamarca, M. J., Snowdon, L. A., Seib, E., Klein, T. & Bray, S. J. Rme-8 depletion perturbs Notch recycling and predisposes to pathogenic signaling. *J. Cell Biol.* **210,** 303–318 (2015).

94. Bonifacino, J. S. & Rojas, R. Retrograde transport from endosomes to the trans-Golgi network. *Nat. Rev. Mol. Cell Biol.* **7,** 568–579 (2006).

95. Wang, S. & Bellen, H. J. The retromer complex in development and disease. *Development* **142,** (2015).

96. Johannes, L. & Popoff, V. Tracing the Retrograde Route in Protein Trafficking. *Cell* **135,** 1175–1187 (2008).

97. Johannes, L. & Wunder, C. Retrograde Transport: Two (or More) Roads Diverged in an Endosomal Tree? *Traffic* **12,** 956–962 (2011).

98. Stoorvogel, W., Oorschot, V. & Geuze, H. J. A novel class of clathrin-coated vesicles budding from endosomes. *J. Cell Biol.* **132,** 21–33 (1996).

99. Saint-Pol, A. *et al.* Clathrin adaptor epsinR is required for retrograde sorting on early endosomal membranes. *Dev. Cell* **6,** 525–38 (2004).

100. Meyer, C. *et al.* μ1A-adaptin-deficient mice: lethality, loss of AP-1 binding and rerouting of mannose 6-phosphate receptors. *EMBO J.* **19,** 2193–2203 (2000).

101. Choudhury, R. *et al.* Lowe Syndrome Protein OCRL1 Interacts with Clathrin and Regulates Protein Trafficking between Endosomes and the Trans-Golgi Network. *Mol. Biol. Cell* **16,** 3467–3479 (2005).

102. Saimani, U. & Kim, K. Traffic from the endosome towards trans-Golgi network. *Eur. J. Cell Biol.* **96,** 198–205 (2017).

103. Wilcke, M. *et al.* Rab11 regulates the compartmentalization of early endosomes required for efficient transport from early endosomes to the trans-golgi network. *J. Cell Biol.* **151,** 1207–20 (2000).

104. Chaudhry, A. *et al.* HIV-1 Nef induces a Rab11-dependent routing of endocytosed immune costimulatory proteins CD80 and CD86 to the Golgi. *Traffic* **9,** 1925–35 (2008).

105. Lombardi, D. *et al.* Rab9 functions in transport between late endosomes and the trans Golgi network. *EMBO J.* **12,** 677–82 (1993).

106. Díaz, E. & Pfeffer, S. R. TIP47: a cargo selection device for mannose 6-phosphate receptor trafficking. *Cell* **93,** 433–43 (1998).

107. Díaz, E., Schimmöller, F. & Pfeffer, S. R. A Novel Rab9 Effector Required for Endosome-to-TGN Transport. *J. Cell Biol.* **138,** 283-90 (1997).

108. Carroll, K. S. *et al.* Role of Rab9 GTPase in facilitating receptor recruitment by TIP47. *Science* **292,** 1373–1376 (2001).

109. Barbero, P., Bittova, L. & Pfeffer, S. R. Visualization of Rab9-mediated vesicle transport from endosomes to the trans-Golgi in living cells. *J. Cell Biol.* **156,** 511–518 (2002).

110. Chia, P. Z. C., Gasnereau, I., Lieu, Z. Z. & Gleeson, P. A. Rab9-dependent retrograde transport and endosomal sorting of the endopeptidase furin. *J. Cell Sci.* **124,** 2401–2413 (2011).

111. Espinosa, E. J., Calero, M., Sridevi, K. & Pfeffer, S. R. RhoBTB3: A Rho GTPase-Family ATPase Required for Endosome to Golgi Transport. *Cell* **137,** 938–948 (2009).

112. Munro, S. The Golgin Coiled-Coil Proteins of the Golgi Apparatus. *Cold Spring Harb. Perspect. Biol.* **3,** a005256–a005256 (2011).

113. Wong, M. & Munro, S. The specificity of vesicle traffic to the Golgi is encoded in the golgin coiled-coil proteins. *Science* **346,** 1256898 (2014).

114. Reddy, J. V *et al.* A functional role for the GCC185 golgin in mannose 6-phosphate receptor recycling. *Mol. Biol. Cell* **17,** 4353–63 (2006).

115. Siniossoglou, S. & Pelham, H. R. B. Vps51p links the VFT complex to the SNARE Tlg1p. *J. Biol. Chem.* **277,** 48318–24 (2002).

116. Pérez-Victoria, F. J. *et al.* Ang2/fat-free is a conserved subunit of the Golgi-associated retrograde protein complex. *Mol. Biol. Cell* **21,** 3386–95 (2010).

117. Pérez-Victoria, F. J., Mardones, G. A. & Bonifacino, J. S. Requirement of the human GARP complex for mannose 6-phosphate-receptor-dependent sorting of cathepsin D to lysosomes. *Mol. Biol. Cell* **19,** 2350–62 (2008).

CHAPTER 2

Hobbit couples retrograde trafficking and regulated exocytosis to drive insulin-dependent growth during *Drosophila* development

This chapter has been submitted for publication.

Neuman SD, Bashirullah A. *Hobbit* couples retrograde trafficking and regulated exocytosis to drive insulin-dependent growth during *Drosophila* development. Submitted to *Cell Reports*.

SUMMARY

All animals must coordinate growth rate and the timing of maturation to reach the appropriate final body size. Here we describe *hobbit*, a novel and conserved gene identified in a forward genetic screen for *Drosophila* animals with a small body size. We demonstrate that *hobbit* mutant animals have systemic growth defects because they fail to secrete insulin. Without *hobbit*, regulated secretion fails during post-embryonic development because of defects in retrograde intracellular trafficking. Our data indicates that *hobbit* regulates a recycling shunt that promotes the trafficking of endocytosed secretory granule membrane proteins from endosomes back to the *trans*-Golgi network, where they can be re-used to drive future rounds of regulated secretion. In this manner, *hobbit* couples the retrograde and anterograde trafficking pathways, revealing a mechanistic role for this coupling to sustain prolonged secretory events during development.

INTRODUCTION

Body size is exquisitely regulated during metazoan development. In *Drosophila*, an explosive period of growth occurs during larval development; however, this systemic growth ceases and final body size is specified at the onset of metamorphosis (Nijhout et al., 2014). One of the most critical regulators of body size in *Drosophila* is the insulin signaling pathway. In this pathway, *Drosophila* insulin-like peptides (Dilps) are secreted from the insulin producing cells (IPCs), which are neuroendocrine cells located in the larval central nervous system. The IPCs function in a manner that is analogous to mammalian pancreatic β-cells (Geminard et al., 2006). Dilps then circulate systemically and bind to the insulin receptor (*InR*) on the membrane of target cells, triggering a downstream signaling cascade that regulates both metabolism and cellular growth (Brogiolo et al., 2001; Rulifson et al., 2002). Disruption of the insulin signaling pathway has a profound effect on *Drosophila* body size. Ablation of the IPCs (Rulifson et al., 2002), genetic deletion of Dilps (Grönke et al., 2010), or mutation of targets downstream of *InR* (Böhni et al., 1999; Brogiolo et al., 2001; Murillo-Maldonado et al., 2011) all result in dramatic reduction in body size. However, despite the importance of the insulin signaling pathway for systemic growth in flies and for disease in humans, the factors regulating insulin secretion remain largely unknown.

Insulin secretion in both flies and mammals occurs via regulated exocytosis. This intracellular trafficking pathway, also known as the anterograde trafficking pathway, begins with the biogenesis of secretory granules at the *trans*-Golgi Network (TGN). Specific cargo proteins are selectively packaged into these specialized organelles, which bud from the TGN as immature secretory granules (Kögel and Gerdes, 2010). The

immature granules then undergo a maturation process to refine their content and membrane composition, rendering them competent for exocytosis (Kögel and Gerdes, 2010). Mature secretory granules traffic to the plasma membrane, where they undergo tethering, docking, and priming steps, attaching them to the membrane so they can be quickly released to the extracellular environment in a stimulus-dependent manner (Burgoyne and Morgan, 2003). Membrane fusion events are mediated by Synaptotagmins and Soluble NSF Attachment Protein Receptors (SNAREs) that are present on both secretory granule membranes and the plasma membrane; these proteins bind with each other to form a stable complex that facilitates the opening of a fusion pore and the release of secretory granule content (Burgoyne and Morgan, 2003; Hong, 2005). However, there is a second intracellular trafficking pathway, called the retrograde trafficking pathway, that regulates cargo trafficking in the reverse direction. In this pathway, proteins are removed from the plasma membrane via endocytosis and trafficked to the endosomal system, a central sorting hub for endocytosed material. From endosomes, cargoes can be sorted for immediate recycling back to the plasma membrane, degradation via lysosomes, or retrograde trafficking to the TGN (Scott et al., 2014). Despite the many trafficking pathways between endosomes and other organelles, regulated exocytosis and retrograde trafficking are thought to be independent processes; there is no direct evidence linking these two intracellular trafficking pathways.

Here, we report the identification and characterization of *hobbit*, a novel and conserved protein that couples retrograde trafficking and regulated exocytosis. We identified *hobbit* in a chemical mutagenesis screen for *Drosophila* mutant animals with a small body size. *Hobbit* is highly conserved throughout eukaryotes, but the protein has

not been functionally characterized. We find that *hobbit* mutant animals have a small body size because they fail to secrete insulin, and demonstrate that *hobbit* is required for maintenance of the major endocrine signaling axis that regulates insulin release. Furthermore, other regulated exocytosis events are also disrupted in *hobbit* mutant animals, including the secretion of mucin-like “glue” proteins from the larval salivary glands at the onset of metamorphosis. Regulated exocytosis fails in *hobbit* mutant tissues because secretory granules lack SNAREs and Synaptotagmins and therefore are not competent for release. These membrane fusion proteins instead accumulate inside dramatically enlarged *Rab7*-positive endosomes in *hobbit* mutant cells. Moreover, the Hobbit protein itself localizes to *Rab7*-associated tubular structures and the Golgi. These results suggest that *hobbit* is required for retrograde transport of internalized secretory granule membrane proteins from endosomes back to the TGN, where they can be reused for future regulated exocytosis events.

EXPERIMENTAL PROCEDURES

Fly stocks, food, and developmental staging

The following stocks were obtained from the Bloomington *Drosophila* Stock Center: w^{1118}, *Df(3R)BSC677, Df(3R)ED6058*, *Df(3R)BSC678*, *Df(3R)Exel6186*, InR^{E19}, InR^{93Dj-4}, InR^{05545}, *UAS-Dcr-2*, *tub-GAL4*, *act-GAL4*, *hs-flp*, *neoFRT80B*, *Ubi-GFP 61EF*, *Sgs3-GFP*, *Dilp2-GAL4*, *UAS-GFP*, *ppl-GAL4*, *Cg-GAL4*, *Ubi-mRFP-nls* 3L, *UAS-Syt1-GFP*, *hs-GAL4*, *Rab7-EYFP*, *UAS-Golgi-RFP*, *Sgs3-GAL4*. *Sgs3-DsRED* was kindly provided by A. Andres (University of Nevada Las Vegas). The five *hobbit* mutations and InR^{sP1} were generated in an EMS-mutagenesis screen (Wang et al., 2008); the methods used to map these mutations are described elsewhere (Sapiro et al., 2013). All experiments were performed in temperature-controlled incubators at 25°C in uncrowded bottles or vials. For insulin secretion assays, larvae were picked at 0-4 h after hatching from the embryo and grown on food containing 34 g inactivated yeast, 83 g corn flour, 60 g sucrose, and 10 g agar per liter. 48 h later, at the start of the third larval instar, these larvae were starved on agar plates containing PBS/1% sucrose for 24 h. Larvae were then re-fed for the appropriate time on the food described above. To generate somatic clones in the salivary glands, embryos were heat-shocked at 37°C for 30 min at 0-4 h after egg lay (AEL); for wing discs, the same heat-shock treatment was given to larvae at 72-76 h AEL. For developmental timing experiments, larvae containing the *Sgs3-GFP* transgene were collected at 88 h AEL and scored for the absence of Sgs3-GFP expression. These larvae were then checked every 4 h for induction of Sgs3-GFP; once expressed, larvae were allowed to age at 25°C on grape agar plates with yeast paste until puparium formation.

Phylogenetic tree and identity plot analysis

Hobbit orthologs were identified using the HMMER web server (Finn et al., 2015) with the CG14967 protein sequence as the query sequence. Significant hits ($p \leq 0.0001$) were submitted to phyloT (http://phylot.biobyte.de/) to generate a phylogenetic tree based on NCBI taxonomy information. We used Interactive Tree of Life (Letunic and Bork, 2016) to visualize, edit, and annotate the final tree. To assay amino acid conservation, we used ClustalOmega (Sievers et al., 2011) to generate a protein alignment between fly *hobbit* and its orthologs in *C. elegans*, *B. mori*, *A. gambiae*, *D. rerio*, *X. tropicalis*, *G. gallus*, *O. cuniculus*, *R. norvegicus*, *M. musculus, M. mulatta*, *P. troglodytes*, and *H. sapiens*. The resulting alignment was visualized in JalView (Waterhouse et al., 2009), and similarity scores at each amino acid position were extracted to generate the final identity plot.

Molecular cloning and transgenic animal generation

To generate the *UAS-hobbit* transgene, the full-length *hobbit* coding sequence was amplified from w^{1118} cDNA using the following primers: 5' AAA AGG TAC CAT GAT GCT ACA GCT ACT TCT ATT CTG CCT GG 3' and 5' AAA AAA GCG GCC GCT CAA TCA TTT CCC GAT CTC TTT CCG 3'. The resulting ~6.9 kb product was digested with *KpnI* and *NotI*, ligated into the Gateway entry vector pENTR 1A (Invitrogen), and sequence-verified. LR Clonase (Invitrogen) was used to recombine the entry clone into the pTW (DGRC) destination vector. Successful recombination was confirmed by sequencing. The resulting *UAS-hobbit* plasmid was then injected into w^{1118} flies using standard methods (Genetic Services, Inc.). A similar strategy was used to generate the *UAS-KIAA0100* transgene. The *KIAA0100* coding sequence was amplified from oligo(dT)-primed qPCR

human reference cDNA (Clontech) using the following primers: 5’ CCC CCC TTT AAA ACC ATG CCT CTG TTC TTC TCC GC 3’ and 5’ AAA AAA GCG GCC GCT TTC ATT TGC GCC TGC CAA A 3’. The resulting ~6.2 kb product was digested with *DraI* and *NotI*, and entry and destination clones were generated as described above. *KIAA0100* has many predicted isoforms; therefore, only the full-length product matching the NCBI consensus coding sequence (CCDS) was used. Sequence-verified plasmids were injected into w^{1118} flies using standard protocols (Genetic Services, Inc.). To generate *UAS-hobbit-GFP*, we first amplified the GFP coding sequence from pTGW (DGRC) using the following primers: 5’ AAA AAA GGT ACC AGT GAG CAA GGG CGA GGA GCT 3’ and 5’ AAA AAA TCT AGA CTT GTA CAG CTC GTC CAT GC 3’. The resulting PCR product was digested with *KpnI* and *XbaI* and ligated into pBID-UASC-G (Wang et al., 2012). The plasmid was sequence-verified, and the *hobbit* entry clone was recombined into this destination vector as described above. Sequence-verified plasmids were injected into *VK00027* flies for phiC31-mediated site-directed integration (Rainbow Transgenic Flies, Inc.). To generate the *UAS-hobbit-RNAi* lines, we followed the strategy outlined by the Transgenic RNAi Project (TRiP) (Ni et al., 2011). The primers for *hobbit-RNAi 1* were: 5’ CTA GCA GTA TGA TGC TAC AGC TAC TTC TAT AGT TAT ATT CAA GCA TAT AGA AGT AGC TGT AGC ATC ATG CG 3’ and 5’ AAT TCG CAT GAT GCT ACA GCT ACT TCT ATA TGC TTG AAT ATA ACT ATA GAA GTA GCT GTA GCA TCA TA C 3’. The primers for *hobbit-RNAi 2* were: 5’ CTA GCA GTA TGC AGC GAA TTG TTG TTA AAT AGT TAT ATT CAA GCA TAT TTA ACA ACA ATT CGC TGC ATG CG 3’ and 5’ AAT TCG CAT GCA GCG AAT TGT TGT TAA ATA TGC TTG AAT ATA ACT ATT TAA CAA CAA TTC GCT GCA TAC TG 3’. The primers were annealed, phosphorylated, and

ligated into pVALIUM20 (TRiP) that had been linearized by digestion with *NheI* and *EcoRI*. The resulting plasmids were sequence verified and injected for phiC31-mediated site-directed integration into *attP2*-containing flies (Rainbow Transgenic Flies, Inc.). To generate the endogenous *hobbit-GFP*, we obtained a fosmid containing C-terminal superfolder GFP (sGFP)-tagged *hobbit* and the surrounding genomic sequences (~15 kb upstream and ~9 kb downstream) (*Drosophila* TransgeneOme; Sarov et al. 2016). We sequence-verified the presence, orientation, and reading frame of the sGFP tag, and injected the fosmid into *VK00027* flies for phiC31-mediated site-directed integration (Rainbow Transgenic Flies, Inc.).

Pupa volume quantification and lethal phase analysis

All light microscope images of pupae were captured on an Olympus SXZ16 stereomicroscope coupled to an Olympus DP72 digital camera with DP2-BSW software. To quantify body size, we used Photoshop CS6 to measure the length and width of each pupa, and calculated pupa volume using a published formula (Delanoue et al., 2016). Animals were grown at controlled density to avoid any nutritional effects on body size. After image capture, the pupae were transferred to a grape agar plate and aged at 25^{o}C for one week for lethal phase analysis. Lethal phases were determined using Bainbridge and Bownes staging criteria (Bainbridge and Bownes, 1981).

Quantitative real-time PCR (qPCR)

qPCR was performed as previously described (Ihry et al., 2012). Total RNA was extracted from whole animals of the appropriate developmental stage and genotype using the

RNeasy Plus Mini Kit (Qiagen), and cDNA was synthesized from 100 ng of total RNA using SuperScript III First-Strand Synthesis System (Invitrogen). qPCR was performed on a Roche LightCycler 480 using LightCycler 480 SYBR Green I Master Mix (Roche). In all experiments, samples were run simultaneously in biological triplicate, and amplification efficiencies were calculated for each primer pair. The Relative Expression Software Tool (REST) (Pfaffl et al., 2002) was used to calculate relative expression. Primer sequences for *rp49* were published previously (Ihry et al., 2012). New primers were designed using ApE (for *hobbit*) or FlyPrimerBank (Hu et al., 2013) for *InR*. *hob* F: 5' TTT GGT GAA GAG GTT TCG GGT C 3'; *hob* R: 5' TCT TTG TTG ATG CGA ATG TCA CG 3'. *InR* F: 5' GAA GTG GAG ACG ACG GGT AAA 3'; *InR* R: 5' TCG CGC TGT TGT CGA TTG TT 3'.

Immunofluorescent staining and confocal microscopy

Tissues were dissected from the appropriate animals, fixed for 30 min in PBS with 0.1% Triton-X 100 (PBST) and 4% formaldehyde, blocked overnight in PBST/4% BSA at 4^{o}C, and stained using the appropriate primary and secondary antibodies diluted in PBST/4% BSA. Primary antibodies used were 1:200 rat α-Dilp2 (Géminard et al., 2009), 1:800 rabbit α-Dilp5 (Géminard et al., 2009) (both a gift from P. Leopold, University Nice Sophia Antipolis), 1:200 rabbit α-SNAP-24 (Niemeyer and Schwarz, 2000) (gift from T. Schwarz, Harvard Medical School), 1:50 mouse α-Syt1 (Developmental Studies Hybridoma Bank 3H2 2D7), 1:50 mouse α-Rab7 (Riedel et al., 2016) (Developmental Studies Hybridoma Bank Rab7). Secondary antibodies were diluted at 1:200 and included α-rat AlexaFluor 568 (Invitrogen A11077), α-rabbit AlexaFluor 633 (Invitrogen A21071), α-rabbit Cy3 (Jackson Immuno-Research Labs 711-165-152), α-mouse Cy3 (Jackson Immuno-

Research Labs 715-165-150). DAPI was used to label nuclei (1:1000, Invitrogen). Stained tissues were mounted in Vectashield (Vector Laboratories). Images were captured on an Olympus FluoView FV1000 confocal microscope and optimized with FV10-ASW software. For live tissue imaging, tissues were dissected and mounted in PBS and imaged for no longer than 5 min after dissection. Insulin producing cell (IPC) images were acquired from a z-series comprising 40 slices at a 0.59 µm step size. Identical laser settings and optimization parameters were used for all samples; images shown as sum-intensity projections generated by FV10-ASW software. Quantification of clone:twin spot area ratios and glue granule areas was done using ImageJ.

RESULTS

A chemical mutagenesis screen for new regulators of body size

To find new regulators of body size in *Drosophila*, we conducted a large-scale EMS mutagenesis screen on the third chromosome to identify metamorphosis-specific lethal mutations. We screened over 26,000 mutagenized chromosomes and identified 8,636 lethal mutations; of these, 566 were pupal lethal mutations (Wang et al., 2008). Among the 566, we identified 26 mutant strains in 19 complementation groups that displayed a dramatic small pupa (sP) phenotype. We first focused on mapping the mutant with the smallest body size: *sP1*. Recombination mapping with pairs of dominant markers (Sapiro et al., 2013) followed by complementation tests with chromosomal deficiencies and known lethal mutations identified *sP1* as an allele of the insulin receptor (*InR*) (Fig. S1A-C), a protein that has previously been shown to play a critical role in body size determination (Chen et al., 1996; Fernandez et al., 1995). InR^{sP1} does not contain any sequence changes within the *InR* coding sequence; however, *InR* mRNA transcript levels are significantly reduced in the mutant animals (Fig. S1D), suggesting that this allele contains a lesion disrupting critical regulatory sequences. The identification of a novel allele of *InR* confirms that our screening approach has uncovered *bona fide* regulators of systemic growth.

Identification of *hobbit*, a novel and conserved regulator of body size

We next mapped the most frequently mutated locus (*sP2*), which contained five alleles. Recombination mapping with dominant markers placed this mutation between *Roughened (R*) and *Dichaete* (*D*); however, the mutant animals complemented all

chromosomal deficiencies in this region, indicating that the disrupted gene was located in a gap between chromosomal deletions (Fig. S2A). Subsequent Sanger sequencing of candidate genes revealed lesions in a previously uncharacterized gene, *CG14967* (Fig. S2A). We named this gene *hobbit* because of the dramatic small pupa phenotype displayed by the mutant animals (Fig. 1A, Fig. 2). All five *hobbit* alleles contained nonsense mutations (Fig. 1C, Fig. S2A), and all exhibited the same small body size and lethal phase (Fig. S2B), indicating that these are likely loss-of-function alleles. Importantly, *hobbit* is conserved across eukaryotes, with orthologs in fungi, green plants, protists, and animals (Fig. 1B). Additionally, a protein sequence identity plot among 13 animal model organisms (from worms to humans) reveals a high degree of primary sequence conservation across the length of the protein (Fig. 1C). However, no functionally-characterized domains are predicted beyond a possible transmembrane domain at the N-terminus. Additionally, sequence homology searches do not reveal any hits outside of *hobbit* and its orthologs. These results indicate that *hobbit* encodes a truly novel protein.

Without any obvious molecular signatures or protein domains to guide our studies, we relied on phenotypic clues to characterize the function of *hobbit*. We began these phenotypic studies by validating our *hobbit* mutations using RNAi knockdown and rescue experiments. Publicly available RNAi lines did not affect *hobbit* expression levels; therefore, we generated two new RNAi constructs that did significantly reduce *hobbit* levels (Fig. S3). Importantly, ubiquitous *hobbit* RNAi knockdown phenocopied both the small body size and lethality of our mutant animals (Fig. 2). To conduct a rescue experiment, we cloned the wild-type fly Hobbit protein and ubiquitously overexpressed it

in the *hobbit* mutant background. This treatment rescued both the small body size and metamorphosis lethality of *hobbit* mutant animals (Fig. 1A, Fig. 2). Additionally, we cloned the human *hobbit* ortholog, *KIAA0100*, and ubiquitously overexpressed it in the *hobbit* mutant background; this treatment also rescued both body size and lethality (Fig. 1A, Fig. 2), suggesting that the function of *hobbit* is evolutionarily conserved.

Hobbit **regulates body size in a non-cell autonomous manner**

As a first step toward understanding the function of *hobbit*, we sought to determine why the mutant animals are small. First, to determine if *hobbit* had a cell-autonomous effect on growth, we generated somatic clones in both mitotic (wing disc) and endocycling (salivary gland) cells and measured the area of the mutant clones and twin spots. Although *hobbit* mutant tissues are small (Fig. 3A), the ratio of clone:twin spot area in both wing disc and salivary gland cells is 1:1 (Fig. 3B,C). Because the mutant clones are the same size as the paired twin spots, these results indicate that *hobbit* does not have a cell-autonomous effect on growth and therefore must regulate body size in a non-cell autonomous manner.

We next began to investigate known causes of non-cell autonomous growth defects in *Drosophila*. Developmental timing abnormalities leading to a shortened larval growth phase and precocious entry into metamorphosis can cause reduced body size through non-cell autonomous mechanisms (King-Jones et al., 2005). Larvae with this defect develop normally until the third larval instar, but then prematurely enter metamorphosis. We used a marker, called *Sgs3-GFP*, which is induced in the larval salivary glands at the mid-third larval instar transition, to synchronize animals at this

developmental timepoint and then measure the duration of the third larval instar. All control animals entered metamorphosis within 24 h after *Sgs3-GFP* expression (Fig. 3D, solid line). However, *hobbit* mutant animals were developmentally delayed, with some animals taking >40 h to pupariate after induction of *Sgs3-GFP* (Fig. 3D, dotted line). These results indicate that developmental timing defects are not responsible for the small body size of *hobbit* mutant animals.

Insulin secretion fails in *hobbit* mutant animals

The insulin signaling pathway plays a central role in the regulation of *Drosophila* body size. Interestingly, *hobbit* mutant animals exhibit a dominant genetic interaction with our mutant allele of *InR*; double heterozygous animals are smaller than either single heterozygote (Fig. S2C), suggesting that *hobbit* may play a role in the insulin pathway. Like loss of insulin itself, *hobbit* has a non-cell autonomous effect on growth, leading us to test if *hobbit* mutant animals had defects in insulin secretion. Consistent with previous reports (Géminard et al., 2009), control animals that are feeding secrete insulin and therefore exhibit little staining for Dilp2 or Dilp5 in the IPCs; however, starved animals retain insulin, resulting in bright Dilp2/5 signal which returns to steady-state levels within 2 h after re-feeding (Fig. 4A, Fig. S4A). In contrast, *hobbit* mutant animals exhibited bright Dilp2 and Dilp5 signal under fed, starved, and re-fed states (Fig. 4B, Fig. S4B), indicating that these animals do not properly secrete insulin and suggesting that this defect may underlie the small body size of *hobbit* mutant animals.

We next wanted to determine which tissues required *hobbit* function for insulin secretion. IPC-specific *hobbit* RNAi knockdown significantly reduced body size (Fig. 4C),

suggesting that *hobbit* is required in the IPCs for insulin secretion. However, IPC-specific expression of *hobbit* in the mutant background did not rescue body size (Fig. 4C) or insulin secretion, suggesting that additional tissues may require *hobbit* function for insulin release. Previous studies have shown that the *Drosophila* fat body functions as a nutrient sensor, releasing secreted signals that circulate systemically and promote insulin release in response to dietary inputs (Delanoue et al., 2016; Géminard et al., 2009; Rajan and Perrimon, 2012), prompting us to test if *hobbit* was also required in the fat body. Fat body-specific expression of *hobbit* in mutant animals did not rescue body size (Fig. 4C, Fig. S4C) or insulin secretion; however, expression of *hobbit* in both the IPCs and fat body significantly rescued the small body size of *hobbit* mutant animals and restored the ability to secrete insulin (Fig. 4C-D, Fig. S4C-D). Taken together, these results indicate that *hobbit* regulates body size by maintaining the major endocrine axis required for insulin secretion.

Secretion of mucin-like glue proteins is disrupted in *hobbit* mutant salivary glands

Although *hobbit* expression in both the IPCs and fat body rescued body size, it did not rescue lethality (Fig. 4C, Fig. S4C), suggesting that *hobbit* has essential functions in other tissues. Because the fat body and IPCs both utilize regulated exocytosis, we tested if other regulated secretion events were disrupted in *hobbit* mutant animals. First, *hobbit* mutant pupae have a soft cuticle, suggesting that *hobbit* function may be required for deposition of chitin. Another conspicuous regulated exocytosis event during *Drosophila* development is the secretion of mucin-like “glue” proteins from the larval salivary glands at the onset of metamorphosis (Biyasheva et al., 2001). Glue proteins are synthesized in

the acinar cells of the salivary glands during the final day of larval development, secreted into the lumen via regulated exocytosis just prior to puparium formation, and expelled onto the surface of the animal at puparium formation, allowing it to adhere to a solid surface during metamorphosis (Biyasheva et al., 2001; Rousso et al., 2015; Tran et al., 2015). Interestingly, glue secretion, assayed by imaging GFP-tagged glue protein (*Sgs3-GFP*), fails in *hobbit* mutant animals (Fig. S5A), and this effect is cell-autonomous, as *hobbit* mutant flp/FRT clones also fail to secrete glue (Fig. 5A). Taken together, these results demonstrate that *hobbit* plays a critical, cell-autonomous role in regulated exocytosis.

Secretory granules in *hobbit* mutant tissues lack membrane proteins required for maturation and exocytosis

Our next goal was to identify the mechanism by which *hobbit* regulates secretion. We first analyzed the morphology of the glue-containing secretory granules in *hobbit* mutant salivary glands to determine if there were any defects. We found that these granules are significantly smaller compared to controls (Fig. 5B), suggesting that the granules do not mature properly, since glue granules are known in increase in size prior to release (Niemeyer and Schwarz, 2000). Exocytosis is mediated by the presence and activity of membrane fusion proteins, such as SNAREs and Synaptotagmins, that are present on both secretory granules and target membranes. Strikingly, secretory granules in *hobbit* mutant salivary glands do not contain these membrane fusion proteins. Salivary gland-specific expression of GFP-tagged *Synaptotagmin-1 (Syt1*-GFP) shows that this protein is present around secretory granules in control glands but absent from granule

membranes in *hobbit* mutant glands (Fig. 5C, Fig. S5B). Immunofluorescent staining with an α-Syt1 antibody confirms these results (Fig. S5C). Furthermore, immunofluorescent staining for the SNARE protein *SNAP-24* also shows that this protein is present around secretory granules in controls but absent from granules in *hobbit* mutant glands (Fig. S5D). Because secretory granules in *hobbit* mutant cells do not contain membrane fusion proteins, these granules are not competent to undergo maturation or exocytosis, explaining why regulated exocytosis fails in *hobbit* mutant cells.

Hobbit **regulates a recycling shunt for replenishing secretory granule membrane proteins**

To gain further insights into how *hobbit* regulates exocytosis, we analyzed where Hobbit protein localizes within the cell. We first generated a GFP-tagged *hobbit* overexpression construct, which localized in small punctate structures that were distinct from glue granules (Fig. 6A). Although this construct rescued *hobbit* mutant animals and therefore generates functional protein, overexpression of proteins can sometimes alter trafficking dynamics. Therefore, we further analyzed Hobbit localization using an endogenous tagged protein. We obtained and validated a DNA construct containing *hobbit* with a C-terminal superfolder-GFP (sGFP) tag and the surrounding ~20kb of DNA sequence (Sarov et al., 2016) (Fig. S6A), which likely recapitulates endogenous expression levels and patterns. This construct generates functional Hobbit protein, as one copy is sufficient to rescue both *hobbit* mutant body size and lethality (Fig. S6B). Endogenous Hobbit-sGFP again exhibits punctate localization patterns and partially co-localizes with both a Golgi body marker and with *Rab7*, a marker for maturing endosomes

(Fig. 6B). However, endogenous Hobbit can also be observed in thin filamentous structures extending from *Rab7*-positive endosomes (Fig. 6B), suggesting that the protein may localize to endosomal tubules, structures that play a critical role in retrograde trafficking from *Rab7*-positive endosomes to the TGN (Bonifacino and Hurley, 2008). This localization pattern suggests that *hobbit* may play a role in retrograde trafficking via endosomal tubules.

Given that the Hobbit protein appears to localize to endosomal tubules, we next tested for defects in endocytic trafficking or endosomal morphology in *hobbit* mutant salivary glands. To do this, we used a collection of endogenously-regulated, EYFP-tagged Rab proteins (Dunst et al., 2015) to compare Rab protein localization in control and *hobbit* mutant salivary glands. We focused specifically on Rab proteins that are known to localize to endosomal compartments. The most striking defects were observed with *Rab7*; we found that *hobbit* mutant salivary glands contained numerous enlarged *Rab7*-positive endosomes (Fig. 6C). These results indicate a specific defect in the same endosomal compartment where Hobbit protein localizes. Furthermore, as mentioned earlier, in *hobbit* mutant glands, *Syt1* and *SNAP-24* are absent from secretory granule membranes. Instead, these proteins aberrantly accumulate inside the enlarged *Rab7*-positive endosomes (Fig. 6D, Fig. S5B-D). This accumulation of secretory granule membrane proteins within endosomes suggests that these proteins are trapped in endosomal compartments and cannot be trafficked to the TGN to replenish the available pool to coat nascent secretory granules. Taken together, our Hobbit localization studies and mutant phenotypic analyses suggest that *hobbit* regulates a recycling shunt to shuttle

secretory granule membrane proteins from the endocytic pathway to the secretory pathway.

DISCUSSION

Regulated exocytosis is a critical process for both systemic signaling and homeostatic mechanisms in multicellular organisms. SNAREs and Synaptotagmins are indispensable for regulated exocytosis; without these proteins, secretory granules cannot fuse with the plasma membrane. Therefore, the availability of these proteins becomes a rate-limiting factor during prolonged secretory functions. In turn, the endocytic/retrograde pathway plays a critical role in cellular homeostasis by removing proteins from the plasma membrane and recycling them; however, there is no established connection between retrograde trafficking and regulated exocytosis. *Hobbit* provides such a link, acting as a "recycling shunt" to direct secretory granule membrane proteins from the endocytic system back to the TGN, where they are loaded onto nascent secretory granules.

The biosynthesis of secretory granule membrane proteins is a complex process. SNAREs contain C-terminal transmembrane domains; therefore, these proteins are synthesized by ribosomes in the cytoplasm and translocated into the endoplasmic reticulum (ER) lumen post-translationally (Kutay et al., 1995). This process requires the use of chaperone proteins to prevent the nascent SNARE protein from forming a complex with other SNAREs on organelle membranes; additionally, the hydrophobic membrane anchor must be sheltered to prevent aggregation (Gristick et al., 2015). From the ER, SNAREs then traffic through the Golgi cisternae, until they are loaded onto secretory granules budding from the TGN (Kutay et al., 1995). However, little is known about the fate of these proteins after fusion of secretory granules with the plasma membrane. Our results suggest that *hobbit* defines a new pathway that recycles these proteins via retrograde trafficking, allowing them to be retrieved from the plasma membrane, traffic

through the endosomal system, and ultimately reach the TGN, where they can be re-used as new secretory granules are produced. Given the considerable energy investment that *de novo* protein synthesis and processing requires, it is likely that this new *hobbit*-dependent pathway plays a particularly important role in secretory cells that must sustain regulated exocytosis for prolonged periods of time, such as the *Drosophila* IPCs. However, the prevalence of *hobbit*-dependent recycling among other types of secretory cells poses an interesting question for future studies.

The precise molecular function of *hobbit* during secretion events remains unclear. The Hobbit protein appears to localize to endosomal tubules, structures that are known to play a functional role in retrograde trafficking. Endosomal tubule formation and function requires the retromer complex, a protein coat complex that is conserved from yeast to humans (Bonifacino and Hurley, 2008), raising the possibility that *hobbit* may regulate retromer complex assembly or function. However, unlike *hobbit* mutants, *Drosophila* retromer mutants exhibit lethality early in development, prior to metamorphosis (Franch-Marro et al., 2008; Wang et al., 2014), suggesting that *hobbit* may play a role in retrograde trafficking through an independent mechanism or may regulate a specific subset of retromer-dependent processes. For example, *hobbit* could serve as a cargo-specific adaptor for the retromer complex, allowing retromer to bind and traffic secretory granule membrane proteins. Further studies, such as the identification of proteins that physically interact with *hobbit*, will be needed to resolve these potential models.

Despite the evolutionary conservation of *hobbit*, the protein does not contain any functionally-characterized domains or obvious signatures that provide clues to its molecular function. Therefore, detailed structure-function studies will be necessary in

order to identify the critical sequences and protein domains that regulate *hobbit* localization and function. Some bioinformatic prediction programs detect a possible transmembrane domain at the N-terminus of the protein, suggesting that *hobbit* itself may be targeted to the constitutive secretory pathway, which is used to deliver membrane proteins to the plasma membrane or specific organelles, including endosomes. Our results are consistent with this finding; Hobbit protein localizes to both the Golgi body and endosomal tubules, indicating that Hobbit itself may be a protein that shuttles between the TGN and endosomes. Additional protein modeling and structure-function studies will reveal new insights into the molecular function of *hobbit*, and may also identify new protein domains and sequences that are critical for intracellular trafficking.

In conclusion, our studies reveal a new process that allows for the maintenance of sustained secretion events during development by promoting the retrograde transport and subsequent recycling of critical secretory granule membrane proteins. We provide a functional link between the retrograde and anterograde trafficking pathways, revealing a previously unknown coupling between these two intracellular trafficking routes. Our results also provide a new link between the regulation of intracellular trafficking and the systemic control of development, highlighting a novel role for trafficking in the control of animal physiology. This work also demonstrates the continued importance of chemical mutagenesis approaches to identify new and unexpected regulators of biology.

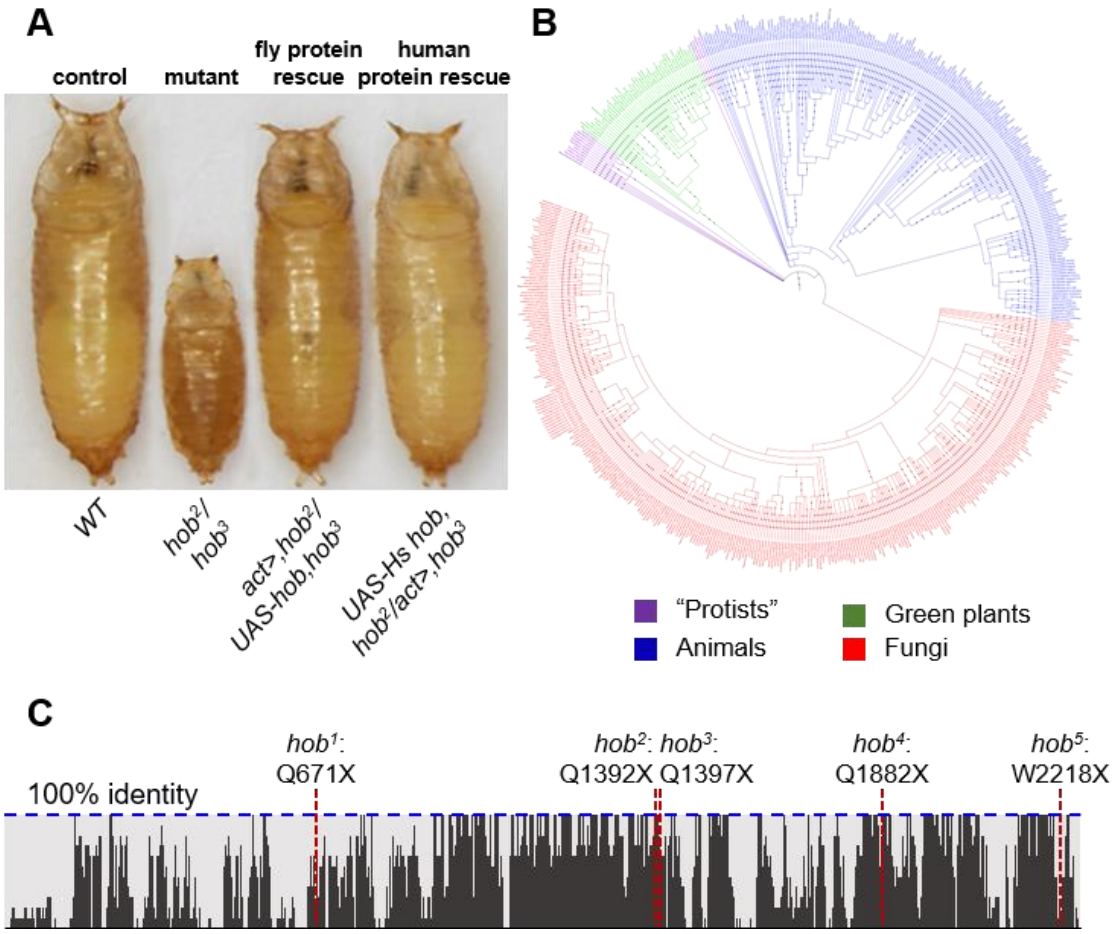

Fig. 1. Identification of *hobbit*, a novel and conserved regulator of systemic growth. **(A)** *hobbit* mutant animals have a dramatic small pupa phenotype that can be rescued by ubiquitous overexpression of the wild-type *Drosophila* protein (CG14967) or the human ortholog (KIAA0100). **(B)** "Tree of life" phylogeny showing *hobbit* orthologs throughout Eukaryota, in green plants (green), animals (blue), fungi (red), and some protists (purple). **(C)** Protein identity plot showing primary sequence conservation between *D. melanogaster hobbit* and 12 metazoan orthologs (*C. elegans*, *B. mori*, *A. gambiae*, *D. rerio*, *X. tropicalis*, *G. gallus*, *O. cuniculus*, *R. norvegicus*, *M. musculus, M. mulatta*, *P. troglodytes*, and *H. sapiens*); horizontal blue dotted line shows 100% identity. Vertical red

dotted lines indicate the position of *Drosophila hobbit* mutant nonsense mutations. See also Fig. S1, S2. *hob*: *hobbit*.

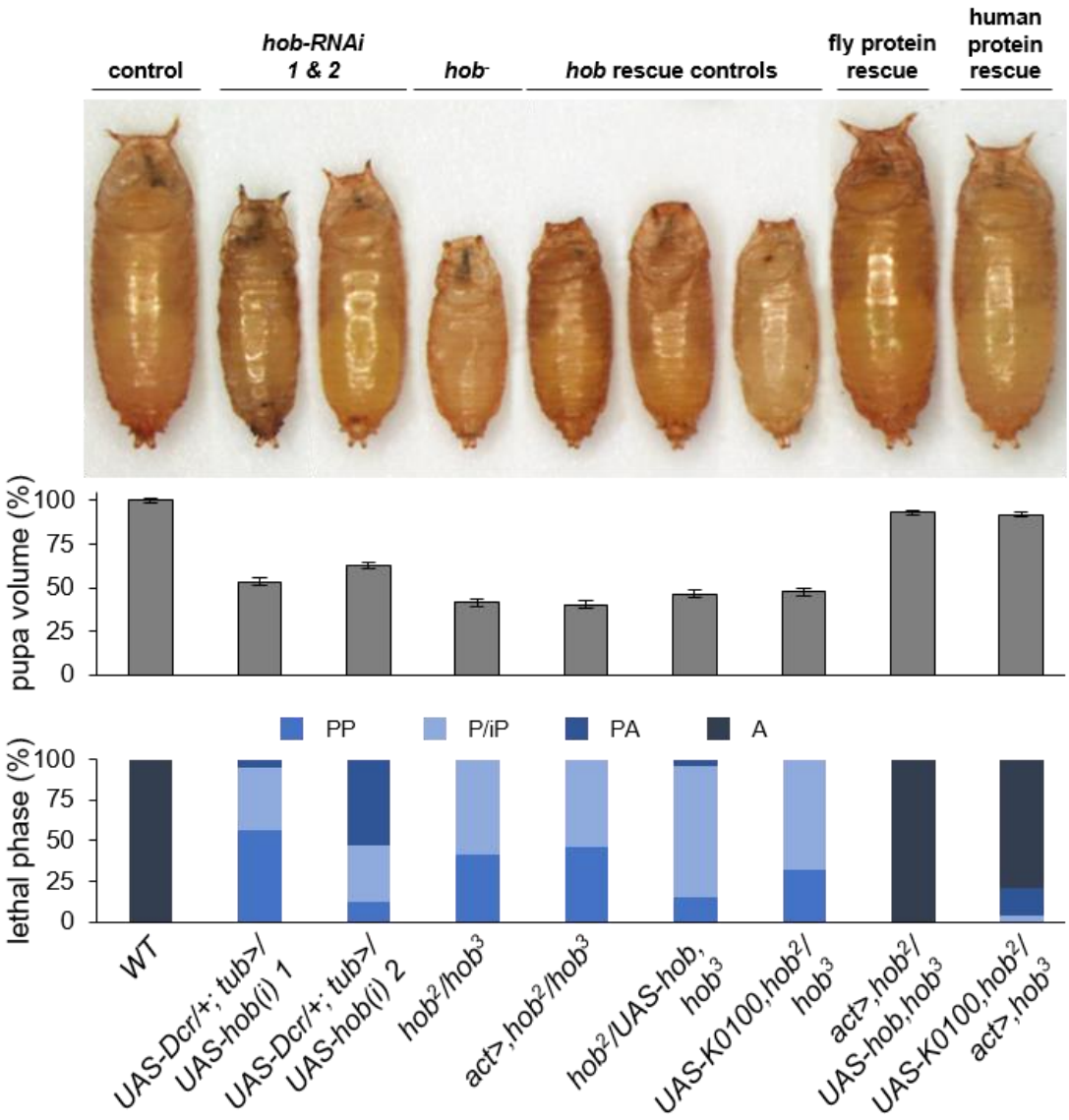

Fig. 2. *Hobbit* mutant animals can be rescued by fly and human proteins. Size quantification and lethal phase analysis for control, ubiquitous *hobbit-RNAi* (*UAS-Dcr/+; tub>/UAS-hob(i) 1* and *2*), *hobbit* mutants (hob^2/hob^3), *hobbit* mutant controls for rescue experiments (*act>,*hob^2/hob^3, hob^2*/UAS-hob,*hob^3, and *UAS-K0100,* hob^2/hob^3), fly *hobbit* mutant rescue (*act>,*hob^2*/UAS-hob,*hob^3), and human ortholog rescue (*UAS-K0100,*hob^2*/act>,*hob^3). Ubiquitous expression of *hobbit-RNAi* reduces body size and results in lethality during metamorphosis. Controls for rescue experiments don't

significantly alter body size or lethality compared to *hob*^{2}/*hob*^{3} mutant animals. Expression of fly *hobbit* or the human ortholog (*K0100*) both rescue body size and lethality. Body size quantified by pupa volume expressed as a percentage relative to wild-type (100%). Data shown as mean +/- SEM. Volume quantification and lethal phase analysis were done on the same animals; *n*=100 animals per genotype. See also Fig. S3. PP: Prepupa; P/iP: Pupa/incomplete Pupa; PA: Pharate Adult; A: Adult.

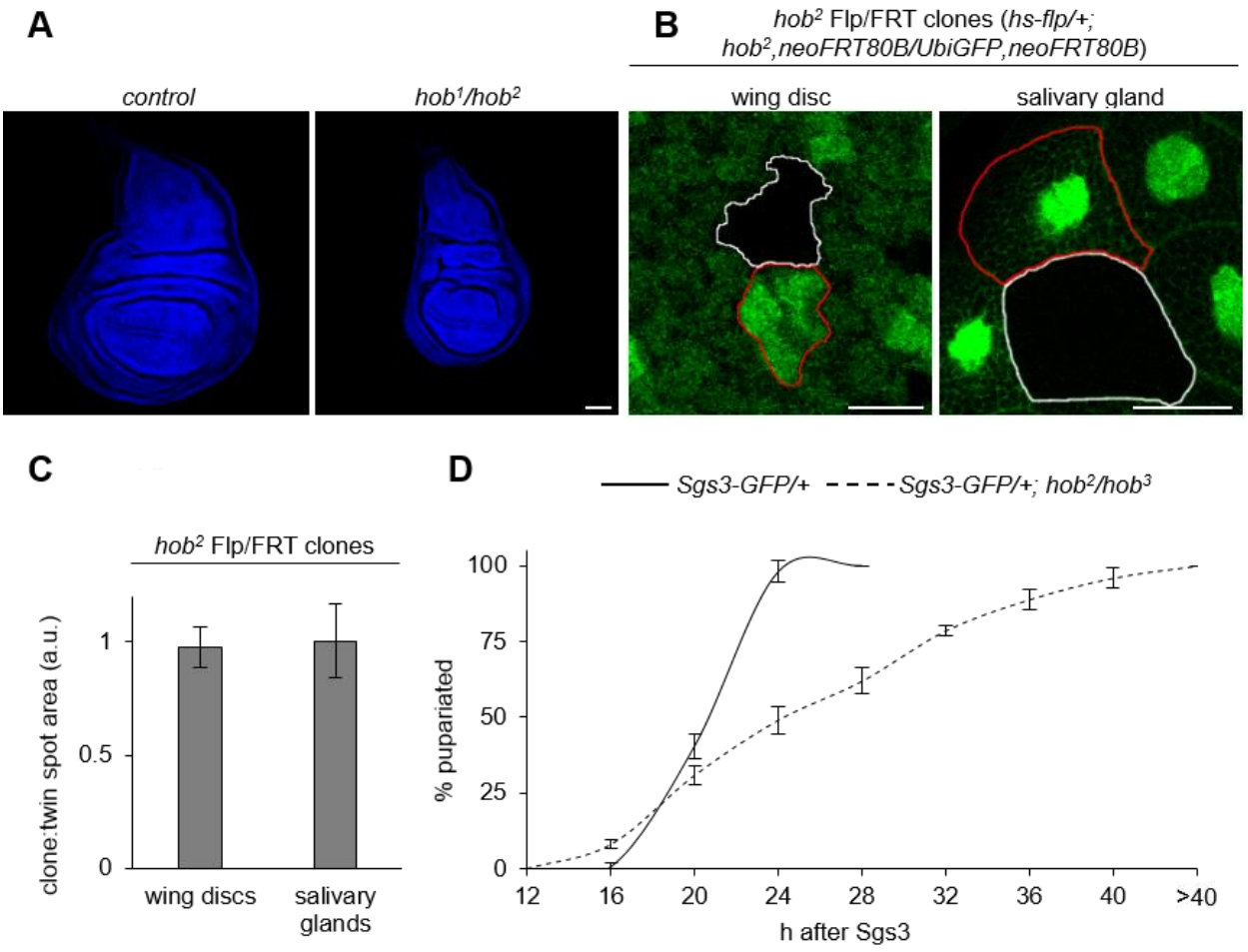

Fig. 3. *Hobbit* has a non-cell autonomous effect on growth. (A) Wing imaginal discs dissected from wandering L3 (wL3) larvae of control and *hobbit* mutant (*hob*^{1}/*hob*^{2}) animals show that tissues are small in *hobbit* mutant animals. Nuclei stained with DAPI (blue); scale bar 50µm. **(B)** *hob*^{2} mutant Flp/FRT clones (marked by loss of GFP and outlined in white) are the same size as paired twin spots (marked by 2x GFP and outlined in red) in both salivary glands and wing discs. Salivary gland scale bar 50µm, wing disc 5µm. **(C)** Quantification of the ratio of clone:twin spot area (in arbitrary units, a.u.) confirms a 1:1 ratio between clone area:twin spot area. Data shown as mean +/- SD; *n*=10 clones/twin spots per tissue. **(D)** Analysis of developmental timing in control and *hobbit*

mutant animals. Animals were synchronized at 0-4 h after the start of the mid-third larval instar transition (0-4 h after *Sgs3-GFP* expression), then allowed to age until the onset of metamorphosis (puparium formation). All control animals pupariate within 24 h of Sgs3-GFP expression; in contrast, *hobbit* mutants take longer than 40 h to pupariate. *y*-axis shows percentage of animals pupariated, *x*-axis shows developmental timepoint in h after Sgs3 expression. Triplicate $n>40$ animals (control total $n=146$, hob^{2}/hob^{3} total $n=137$) analyzed; data shown as mean +/- SD.

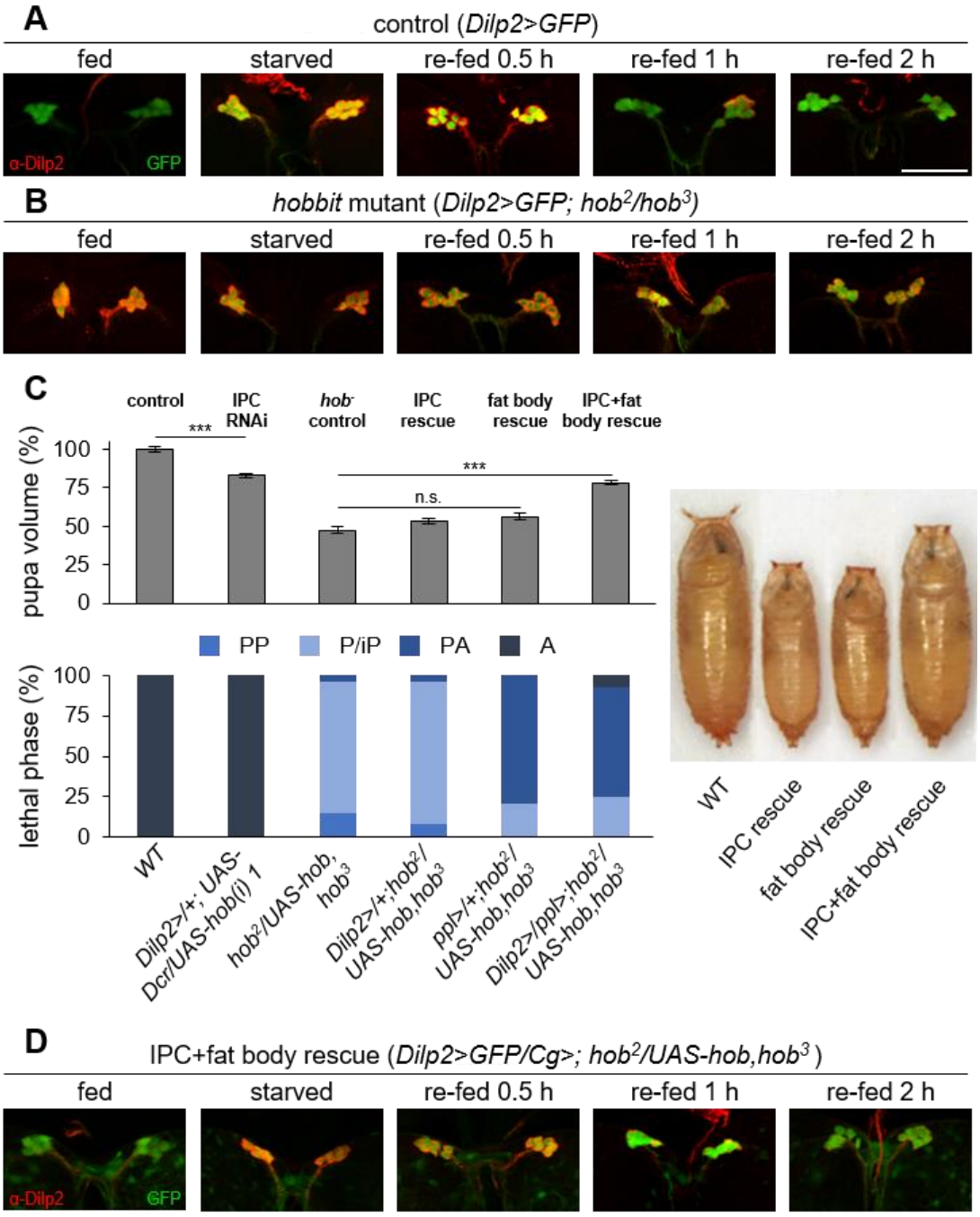

Fig. 4. *Hobbit* is required for insulin secretion. (A) Immunofluorescent staining for *Drosophila* insulin-like peptide Dilp2 (in red) in insulin producing cells (IPCs, marked with GFP in green) of control animals shows that Dilp2 is secreted under fed conditions, retained under starved conditions, and secreted within 2 h of re-feeding. **(B)** Dilp2 staining in *hobbit* mutant IPCs under fed, starved, and re-fed states shows that Dilp2 is not

secreted under any condition. **(C)** IPC-specific *hobbit* RNAi knockdown (with *Dilp2-GAL4*) reduces body size. However, IPC- or fat body-specific (with *ppl-GAL4*) *hobbit* expression does not rescue *hobbit* mutant small pupae, while expression in both IPCs and fat body does rescue size. None of these treatments rescue *hobbit* mutant lethality. Size quantified by pupa volume and expressed relative to wild-type (100%); data shown as mean +/- SEM. Volume and lethal phase data shown for $hob^{2}/UAS\text{-}hob,hob^{3}$ is the same as that shown in Fig. 2 but is included here for comparison. Volume measurements and lethal phase analysis were done on the same animals; n=100 per genotype. Asterisks indicate $p<0.0001$ calculated by two-tailed T-test. **(D)** Expression of *hobbit* in IPCs (marked with GFP in green) and fat body (with *Cg-GAL4*) rescues Dilp2 (in red) secretion in *hobbit* mutant animals. IPC images in all panels representative of $n\geq20$ analyzed per condition/genotype. Scale bar 50µm. See also Fig. S2C, Fig. S3, and Fig. S4. *hob*: *hobbit*; IPC: insulin producing cells; n.s.: not significant; PP: Prepupa; P/iP: Pupa/incomplete Pupa; PA: Pharate Adult; A: Adult.

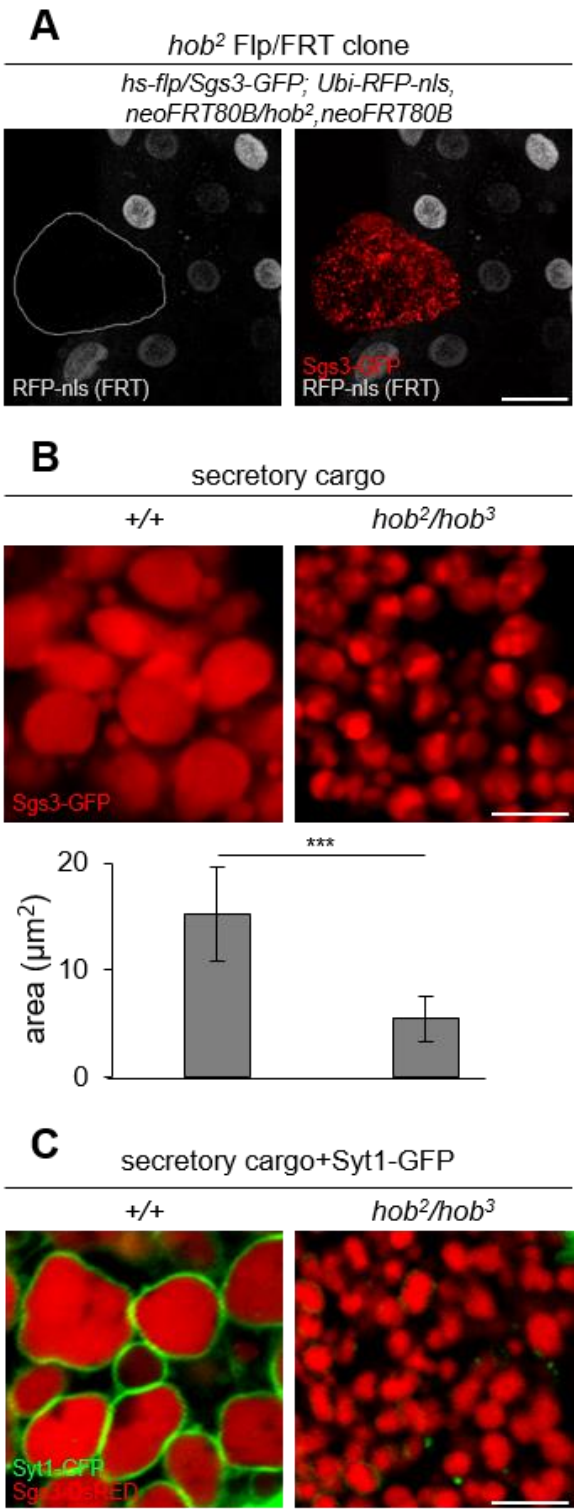

Fig. 5. Secretory granules in *hobbit* mutant cells are not competent for exocytosis.

(A) Flp/FRT *hob²* clone, marked by loss of RFP-nls (in gray) and outlined in white, shows

that Sgs3-GFP glue proteins (in red) are not secreted in *hobbit* mutant salivary gland cells dissected from prepupal animals. Scale bar 50µm. **(B)** Sgs3-GFP glue granules in *hobbit* mutant salivary glands are significantly smaller than controls. Graph shows quantification by granule area; data shown as mean +/- SD; $n \geq 60$ granules per genotype. Asterisks indicate $p < 0.001$, calculated by two-tailed T-test. Scale bar 5µm. **(C)** *Synaptotagmin-1-GFP* (Syt1-GFP, in green), is loaded onto glue granule membranes in control glands but not in *hobbit* mutant glands. Glue protein shown in red. Scale bar 5µm. All images acquired from live, unfixed tissue. See also Fig. S5. *hob*: *hobbit*.

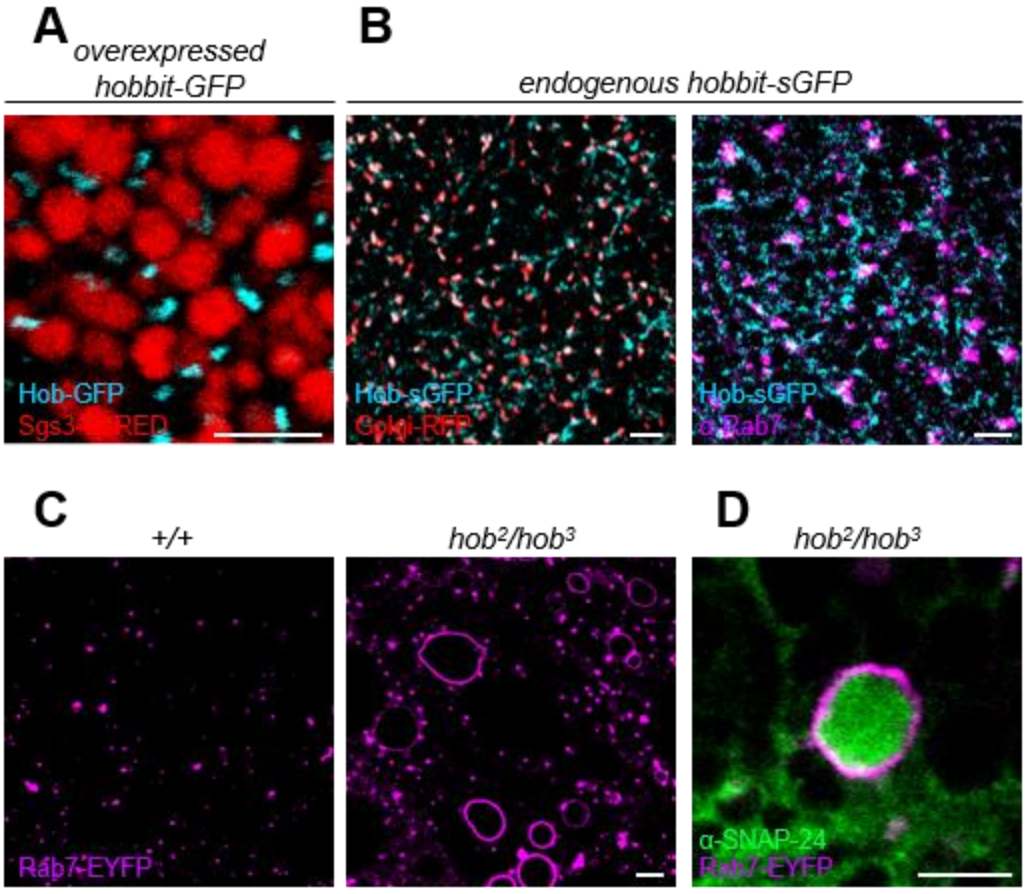

Fig. 6. *Hobbit* is required for retrograde trafficking of secretory granule membrane proteins. (A) Overexpression of Hobbit-GFP (with *Sgs3-GAL4*), in cyan, localizes in punctae that are distinct from glue granules, in red. **(B)** Endogenously-regulated superfolder GFP (sGFP)-tagged Hobbit (in cyan) shows partial co-localization with *Golgi-RFP* (in red, expression driven by *Sgs3-GAL4*) and the endosomal marker *Rab7* (in magenta); however, Hobbit is also observed in filamentous structures adjacent to *Rab7*-positive endosomes. **(C)** *Rab7*-positive endosomes (magenta) are dramatically enlarged in *hobbit* mutant salivary glands. Images acquired from live, unfixed tissue. *Rab7-EYFP* is an endogenously-regulated fluorescent fusion protein (Dunst et al., 2015). **(D)** *Rab7*-positive endosomes (magenta) contain accumulations of the SNARE protein *SNAP-24*

(in green) in *hobbit* mutant glands. Scale bars 5µm. See also Fig. S5 and Fig. S6. *hob*: *hobbit*.

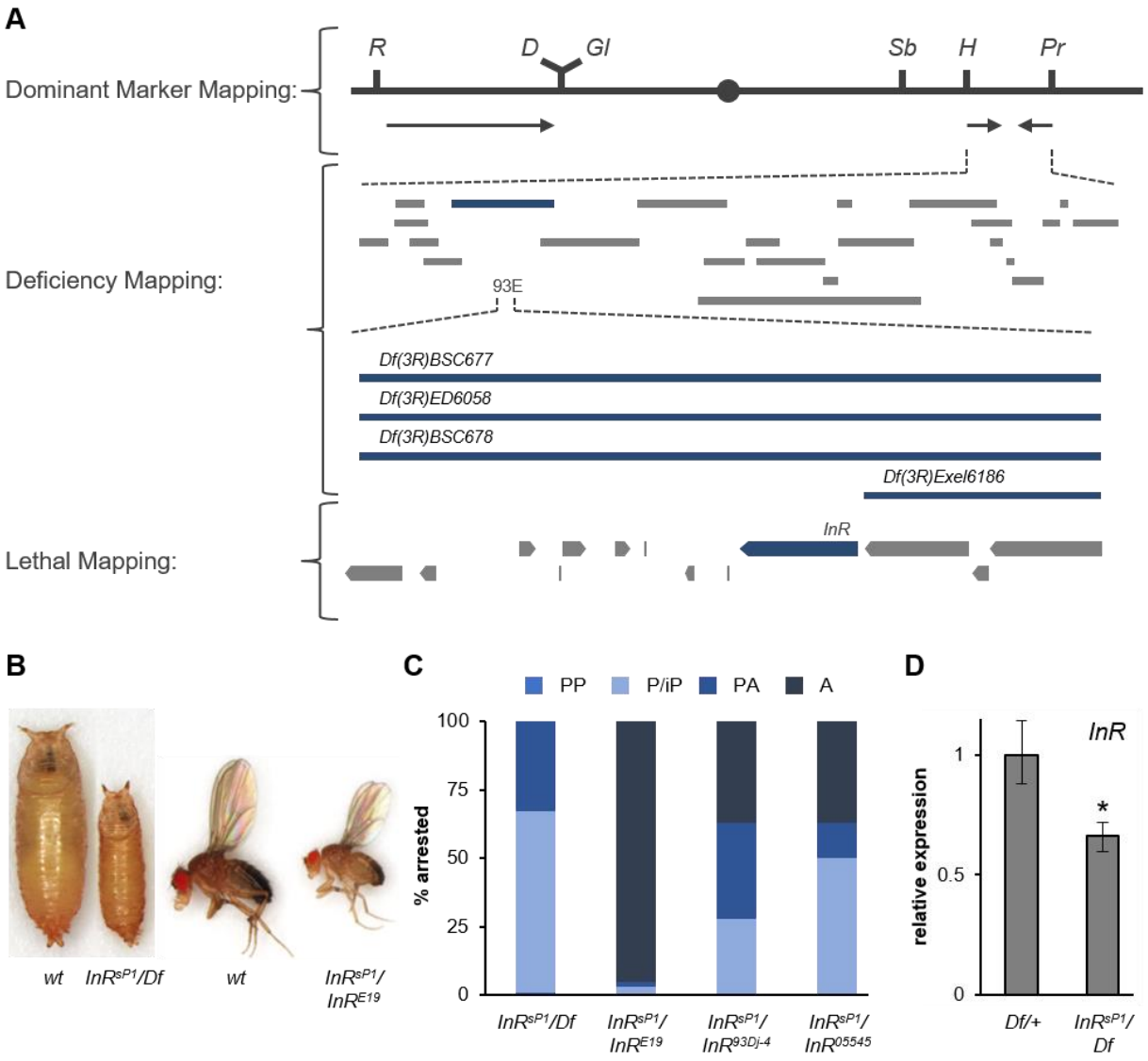

Fig. S1. Related to Fig. 1. Identification of a novel allele of the insulin receptor (*InR*). **(A)** Summary of mapping results to identify the gene disrupted in mutant *sP1*. Dominant marker mapping (Sapiro et al., 2013) placed the mutation between *Hairless* (*H*) and *Prickly* (*Pr*). *sP1* then failed to complement four overlapping chromosomal deficiencies/deletions (colored blue). *sP1/Df(3R)Exel6186* resulted in animals that were reduced in size but viable; the other three deficiencies produced animals that were small and metamorphosis-lethal. *sP1* then failed to complement three alleles of *InR*. Sanger

sequencing did not identify any mutations within the coding sequence of *InR* in *sP1*. **(B)** Hemizygous (*InR^{sP1}/Df(3R)ED6058*) *InR^{sP1}* animals are metamorphosis-lethal and small; *trans*-heterozygous (*InR^{sP1}/InR^{E19}*) *InR^{sP1}* animals are small and viable. **(C)** Lethal phase analysis for *InR^{sP1}* with *Df(3R)ED6058* and three known *InR* mutant alleles (*InR^{E19}* (Chen et al., 1996), *InR^{93Dj-4}* (Chen et al., 1996), *InR^{05545}* (Fernandez et al., 1995). *n*=100 animals per genotype. **(D)** qPCR analysis of *InR* expression levels in control (*Df(3R)ED6058/*+) and *sP1* mutant (*InR^{sP1}/Df(3R)ED6058*) whole animals collected at puparium formation (0 h PF) confirms that *InR* expression is significantly reduced in the mutant. This suggests that *InR^{sP1}* contains a lesion disrupting *InR* regulatory regions. *y*-axis shows relative expression, *x*-axis shows genotypes analyzed. Samples run in biological triplicate and expression normalized to the reference gene *rp49*. Error bars and statistics calculated by REST analysis, asterisks indicate $p<0.05$. PP: Prepupa; P/iP: Pupa/incomplete Pupa; PA: Pharate Adult; A: Adult.

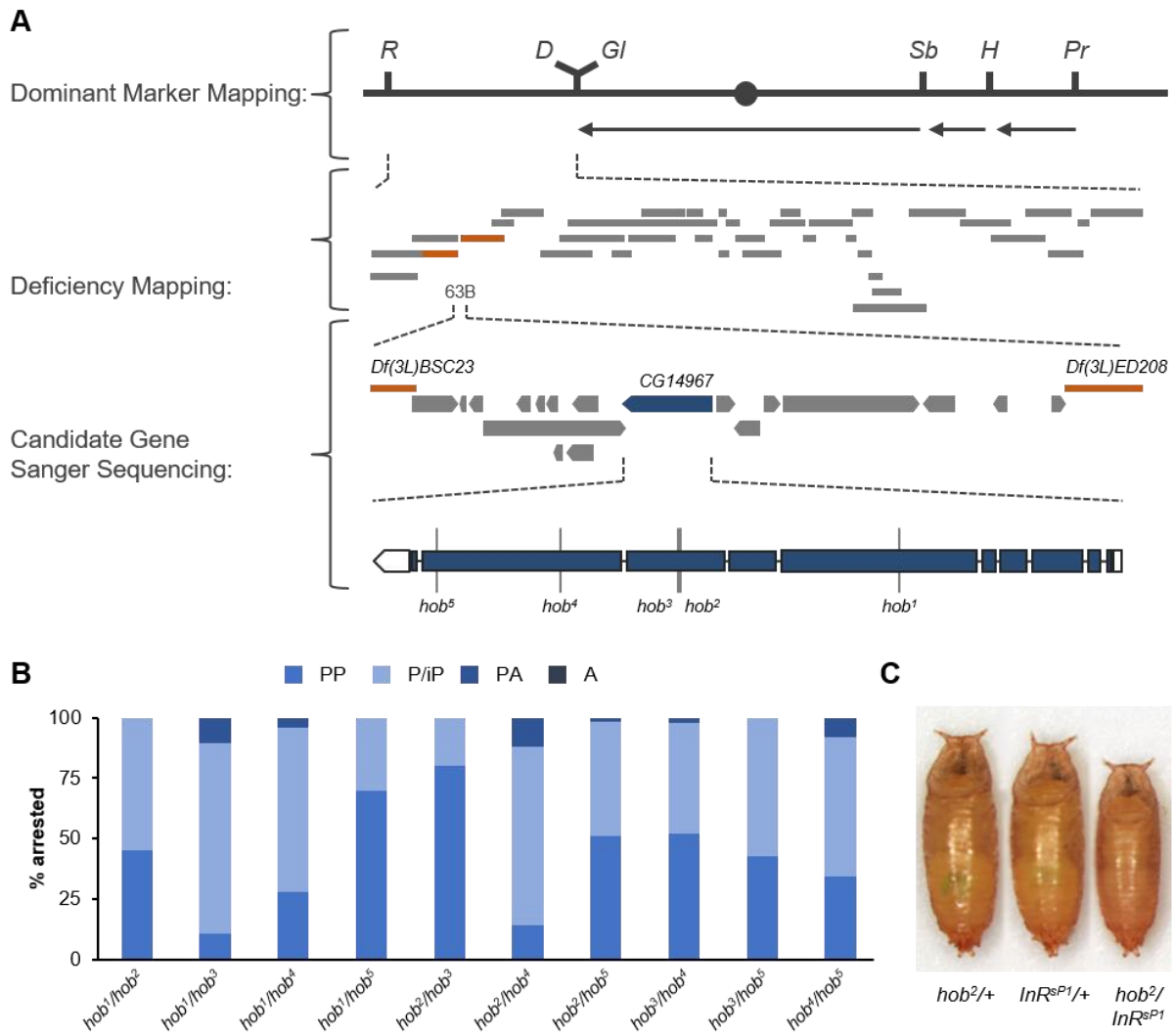

Fig. S2. Related to Fig. 1 and Fig. 4. Mapping of *hobbit* mutants. (A) Dominant marker mapping placed all five alleles of the largest small pupa complementation group (*sP2*) between *Roughened* (*R*) and *Dichaete* (*D*); however, the mutants did not fail to complement any deficiencies within this region, indicating that the causative gene was located in a gap between chromosomal deletions. Sanger sequencing of candidate genes revealed nonsense mutations in *CG14967* (subsequently named *hobbit*) in all five alleles. Deficiencies colored orange are located to the left and right of the *hobbit* gene. **(B)** Lethal phase analysis for all *trans*-heterozygous *hobbit* allelic combinations. All exhibit

metamorphosis lethality and a small body size. *n*≥10 animals per genotype. **(C)** *hobbit* mutants exhibit a dominant genetic interaction with InR^{sP1}; double heterozygous animals (hob^{2}/InR^{sP1}) are smaller than either single heterozygote. *hob*: *hobbit*; PP: Prepupa; P/iP: Pupa/incomplete Pupa; PA: Pharate Adult; A: Adult.

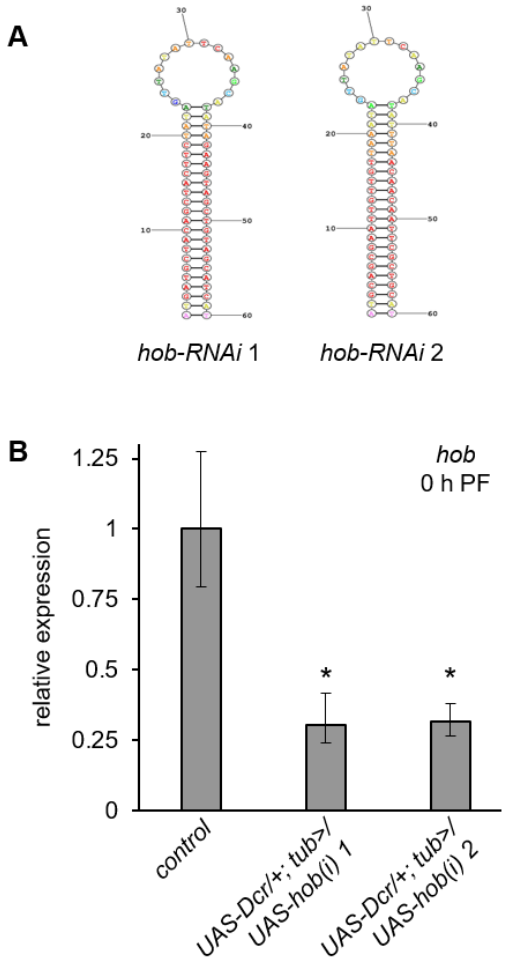

Fig. S3. Related to Fig. 2 and Fig. 4. Generation and validation of *hobbit-RNAi* constructs. (A) Structure and sequence of shRNA hairpins in transgenic RNAi constructs (see Methods for details of hairpin design and cloning). Images generated using RNAStructure (http://rna.urmc.rochester.edu/RNAstructureWeb/index.html). A newly-generated RNAi construct from the Transgenic RNAi Project (TRiP) contains the same shRNA hairpin as *hobbit-RNAi 2* inserted on chromosome 2; *hobbit-RNAi 2* is inserted on chromosome 3. **(B)** qPCR analysis verifies that *hobbit-RNAi* lines significantly reduce *hobbit* expression levels in whole animals collected at puparium formation (0 h PF). *y*-axis shows relative expression, *x*-axis shows genotypes analyzed. Samples run in

biological triplicate and expression normalized relative to the reference gene *rp49*. Error bars and statistics calculated by REST analysis, asterisks indicate $p<0.001$. *hob*: *hobbit*; PF: puparium formation.

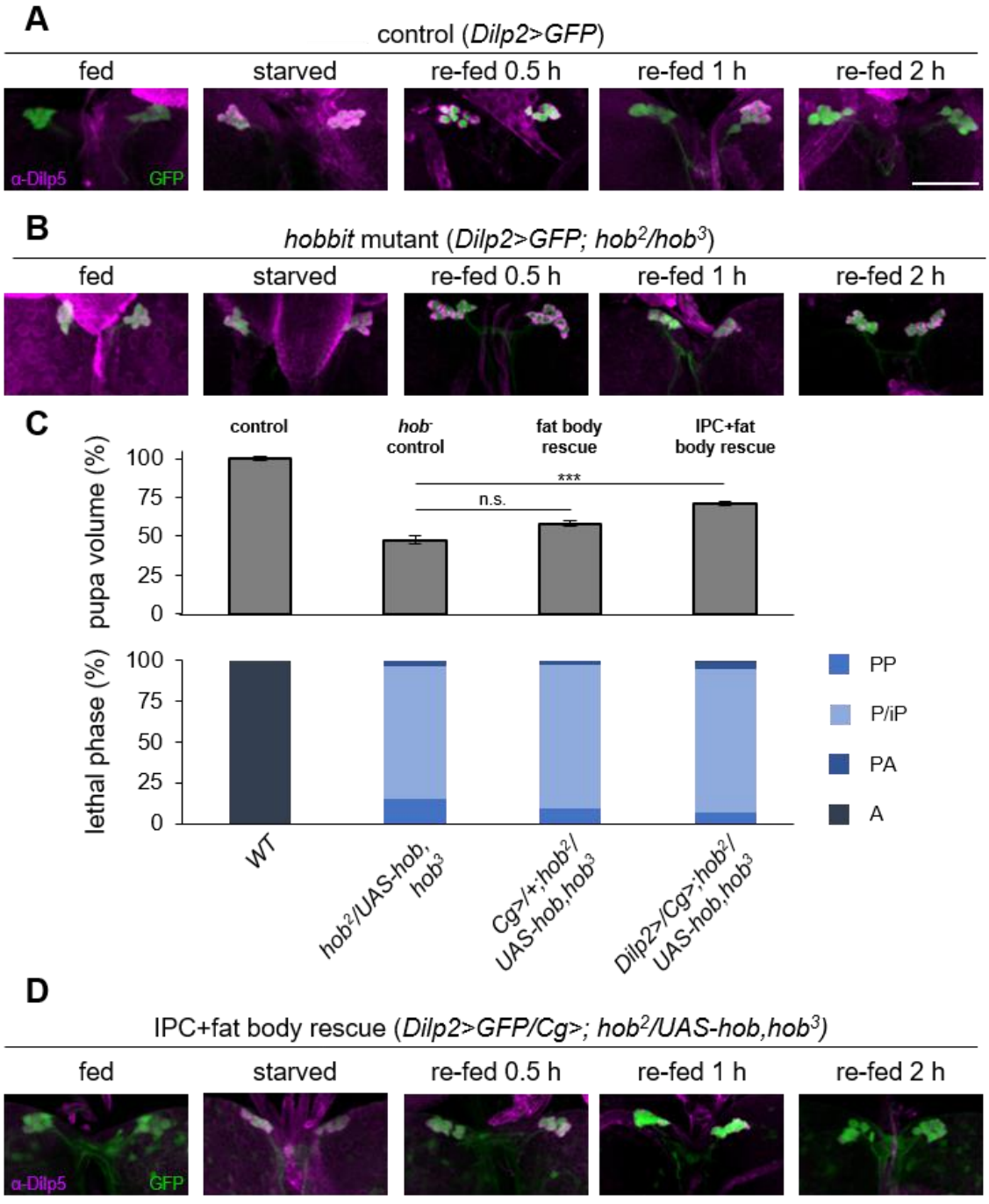

Fig. S4. Related to Fig. 4. *Hobbit* is required for Dilp5 secretion from IPCs. (A) Immunofluorescent staining for *Drosophila* insulin-like peptide Dilp5 (in magenta) in insulin producing cells (IPCs, marked with GFP in green) of control animals shows that Dilp5 is secreted under fed conditions, retained under starved conditions, and secreted

within 2 h of re-feeding. **(B)** Dilp5 staining in *hobbit* mutant IPCs under fed, starved, and re-fed states shows that Dilp5 is not secreted under any condition. **(C)** Fat body-specific (with *Cg-GAL4*) expression of *hobbit* does not rescue *hobbit* mutant small body size, while expression in both IPCs (with *Dilp2-GAL4*) and fat body (with *Cg-GAL4*) does rescue size. However, none of these treatments rescue *hobbit* mutant lethality. Size quantified by pupa volume and expressed relative to wild-type (100%); data represented as mean +/- SEM. Volume measurements and lethal phase analysis were done on the same animals; n=100 per genotype. Asterisks indicate p<0.0001 calculated by two-tailed T-test. *WT* and hob^{2}/*UAS-hob,*hob^{3} pupa volume and lethal phase data is the same as that shown in Fig. 4 and Fig. 2, respectively, but included here for comparison. **(D)** Expression of *hobbit* in the IPCs (marked with GFP in green) and fat body (with *Cg-GAL4*) rescues the ability to secrete Dilp5 (in magenta) in *hobbit* mutant animals. Scale bar 50µm. IPC images shown in all panels are representative of n≥20 analyzed per condition/genotype. *hob*: *hobbit*; IPC: insulin producing cells; PP: Prepupa; P/iP: Pupa/incomplete Pupa; PA: Pharate Adult; A: Adult.

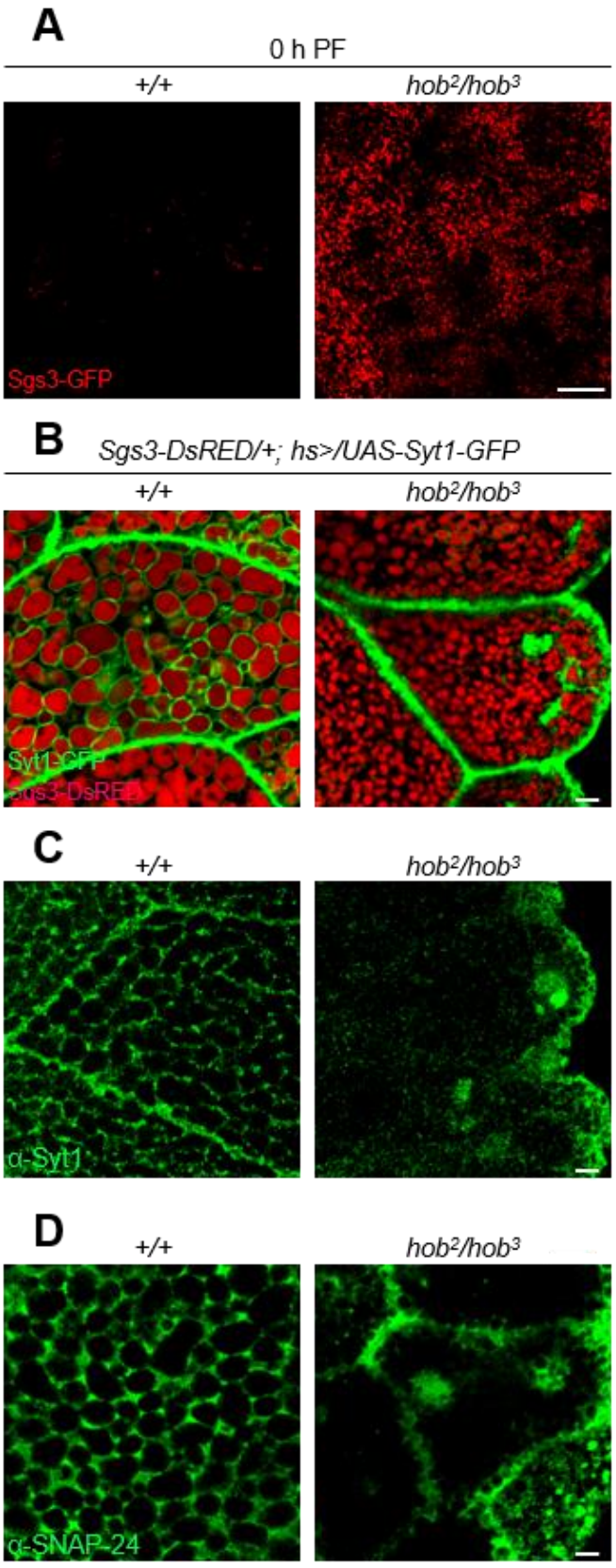

Fig. S5. Related to Fig. 5 and Fig. 6. Analysis of secretion and trafficking phenotypes in control and *hobbit* mutant salivary glands. (A) *Sgs3-GFP* glue proteins, shown in red, are not secreted in *hobbit* mutant salivary glands at the onset of metamorphosis (puparium formation). Control glands contain minimal glue content at puparium formation; in contrast, *hobbit* mutant glands are filled with glue at puparium formation. Images acquired from live, unfixed tissue. **(B)** *Synaptotagmin1-GFP* (*Syt1-GFP*) is not loaded onto glue granules in *hobbit* mutant salivary glands. In control glands, glue granules (in red) are surrounded by *Syt1-GFP* (in green); in contrast, *Syt1-GFP* is not present around glue granules in hob^2/hob^3 mutant salivary glands. Note the large accumulations of *Syt1-GFP* that are distinct from glue granules in *hobbit*

mutant glands. Images were taken in live, unfixed tissues. **(C)** Immunofluorescent staining using an α-Syt1 antibody confirms that Syt1 (green) is expressed and present around glue granules in control but not *hobbit* mutant salivary glands. Syt1 again accumulates in large structures in *hobbit* mutant glands. **(D)** Immunofluorescent staining to detect the SNARE protein SNAP-24 (in green) shows that this protein is present around glue granules in controls but not *hobbit* mutants; SNAP-24 also accumulates in large structures in *hobbit* mutant glands. These large structures in B-D represent accumulations of granule membrane proteins in enlarged *Rab7*-positive endosomes (see Fig. 6). Scale bar in (A) is 50µm; scale bar in (B-D) is 5µm.

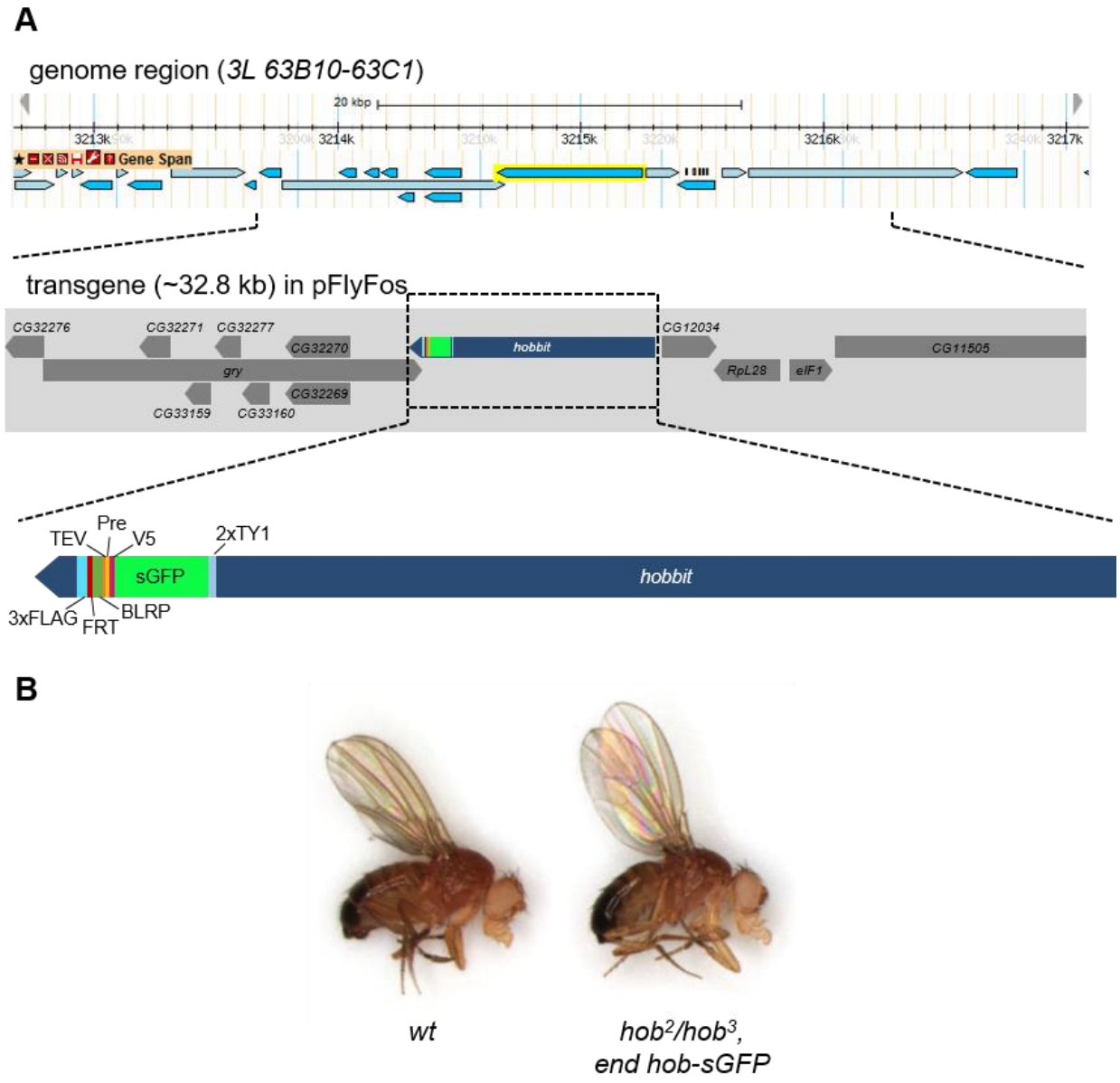

Fig. S6. Related to Fig. 6. Generation and validation of *endogenous hobbit-sGFP*. **(A)** Schematic of the transgene containing *hobbit-sGFP*. We obtained a fosmid containing ~32.8kb of chromosome *3L*, including *hobbit* tagged at the C-terminus with superfolder GFP (sGFP) and other epitope tags (Sarov et al., 2016). Sanger sequencing was used to confirm that the endogenous *hobbit* stop codon was deleted, and that the sGFP and other tags were present and in the correct reading frame. We then generated transgenic flies

containing this construct inserted on chromosome *3R* at *89E11*. **(B)** Rescue of *hobbit* mutant animals with *endogenous hobbit-sGFP*. The *endogenous hobbit-sGFP* construct generates a functional protein that recapitulates endogenous expression patterns, as one copy is sufficient to fully rescue the size and lethality of hob^{2}/hob^{3} mutant animals. Recombination of hob^{3} with *endogenous hobbit-sGFP* was confirmed using Sanger sequencing, looking for a double peak in the sequencing read at the position of the hob^{3} nonsense mutation, corresponding to one mutant copy (from hob^{3}) and one wild-type copy (from *endogenous hobbit-sGFP*).

REFERENCES

Bainbridge, B.S.P., and Bownes, M. (1981). Staging the metamorphosis of Drosophila melanogaster. *66*, 57–80.

Biyasheva, A., Do, T. V, Lu, Y., Vaskova, M., and Andres, A.J. (2001). Glue secretion in the Drosophila salivary gland: a model for steroid-regulated exocytosis. Dev. Biol. *231*, 234–251.

Böhni, R., Riesgo-Escovar, J., Oldham, S., Brogiolo, W., Stocker, H., Andruss, B.F., Beckingham, K., and Hafen, E. (1999). Autonomous control of cell and organ size by CHICO, a Drosophila homolog of vertebrate IRS1-4. Cell *97*, 865–875.

Bonifacino, J.S., and Hurley, J.H. (2008). Retromer. Curr. Opin. Cell Biol. *20*, 427–436.
Brogiolo, W., Stocker, H., Ikeya, T., Rintelen, F., Fernandez, R., and Hafen, E. (2001). An evolutionarily conserved function of the Drosophila insulin receptor and insulin-like peptides in growth control. Curr. Biol. *11*, 213–221.

Burgoyne, R.D., and Morgan, A. (2003). Secretory granule exocytosis. Physiol. Rev. *83*, 581–632.

Chen, C., Jack, J., and Garofalo, R. (1996). The Drosophila insulin receptor is required for normal growth. Endocrinology *137*, 846–856.

Delanoue, R., Meschi, E., Agrawal, N., Mauri, A., Tsatskis, Y., McNeill, H., and Leopold, P. (2016). Drosophila insulin release is triggered by adipose Stunted ligand to brain Methuselah receptor. Science *353*, 1553–1556.

Dunst, S., Kazimiers, T., von?Zadow, F., Jambor, H., Sagner, A., Brankatschk, B., Mahmoud, A., Spannl, S., Tomancak, P., Eaton, S., et al. (2015). Endogenously tagged rab proteins: a resource to study membrane trafficking in Drosophila. Dev. Cell *33*, 351–365.

Fernandez, R., Tabarini, D., Azpiazu, N., Frasch, M., and Schlessinger, J. (1995). The Drosophila insulin receptor homolog: a gene essential for embryonic development encodes two receptor isoforms with different signaling potential. EMBO J. *14*, 3373–3384.

Finn, R.D., Clements, J., Arndt, W., Miller, B.L., Wheeler, T.J., Schreiber, F., Bateman, A., and Eddy, S.R. (2015). HMMER web server: 2015 Update. Nucleic Acids Res. *43*, W30–W38.

Franch-Marro, X., Wendler, F., Guidato, S., Griffith, J., Baena-Lopez, A., Itasaki, N., Maurice, M.M., and Vincent, J.-P. (2008). Wingless secretion requires endosome-to-Golgi retrieval of Wntless/Evi/Sprinter by the retromer complex. Nat. Cell Biol. *10*, 170–177.

Geminard, C., Arquier, N., Layalle, S., Bourouis, M., Slaidina, M., Delanoue, R., Bjordal, M., Ohanna, M., Ma, M., Colombani, J., et al. (2006). Control of Metabolism and Growth Through Insulin-Like Peptides in Drosophila. Diabetes *55*, S5–S8.

Géminard, C., Rulifson, E.J., and Léopold, P. (2009). Remote Control of Insulin Secretion by Fat Cells in Drosophila. Cell Metab. *10*, 199–207.

Gristick, H.B., Rome, M.E., Chartron, J.W., Rao, M., Hess, S., Shan, S.O., and Clemons, W.M. (2015). Mechanism of assembly of a substrate transfer complex during tail-anchored protein targeting. J. Biol. Chem. *290*, 30006–30017.

Grönke, S., Clarke, D.-F., Broughton, S., Andrews, T.D., and Partridge, L. (2010). Molecular evolution and functional characterization of Drosophila insulin-like peptides. PLoS Genet. *6*, e1000857.

Hong, W. (2005). SNAREs and traffic. Biochim. Biophys. Acta - Mol. Cell Res. *1744*, 120–144.

Hu, Y., Sopko, R., Foos, M., Kelley, C., Flockhart, I., Ammeux, N., Wang, X., Perkins, L., Perrimon, N., and Mohr, S.E. (2013). FlyPrimerBank: An Online Database for Drosophila melanogaster Gene Expression Analysis and Knockdown Evaluation of RNAi Reagents. G3 *3*, 1607–1616.

Ihry, R.J., Sapiro, A.L., and Bashirullah, A. (2012). Translational Control by the DEAD Box RNA Helicase belle Regulates Ecdysone-Triggered Transcriptional Cascades. PLoS Genet. *8*, e1003085.

King-Jones, K., Charles, J.P., Lam, G., and Thummel, C.S. (2005). The ecdysone-induced DHR4 orphan nuclear receptor coordinates growth and maturation in Drosophila. Cell *121*, 773–784.

Kögel, T., and Gerdes, H.-H. (2010). Maturation of secretory granules. Results Probl. Cell Differ. *50*, 1–20.

Kutay, U., Ahnert-Hilger, G., Hartmann, E., Wiedenmann, B., and Rapoport, T.A. (1995). Transport route for synaptobrevin via a novel pathway of insertion into the endoplasmic reticulum membrane. EMBO J. *14*, 217–223.

Letunic, I., and Bork, P. (2016). Interactive tree of life (iTOL) v3: an online tool for the display and annotation of phylogenetic and other trees. Nucleic Acids Res. *44*, W242-W245.

Murillo-Maldonado, J.M., Sánchez-Chávez, G., Salgado, L.M., Salceda, R., and Riesgo-Escovar, J.R. (2011). Drosophila insulin pathway mutants affect visual physiology and brain function besides growth, lipid, and carbohydrate metabolism. Diabetes *60*, 1632–1636.

Ni, J.-Q., Zhou, R., Czech, B., Liu, L.-P., Holderbaum, L., Yang-Zhou, D., Shim, S., Handler, D., Karpowicz, P., Binari, R., et al. (2011). A genome-scale shRNA resource for transgenic RNAi in Drosophila. Nat. Methods *8*, 405–407.

Niemeyer, B. a, and Schwarz, T.L. (2000). SNAP-24, a Drosophila SNAP-25 homologue on granule membranes, is a putative mediator of secretion and granule-granule fusion in salivary glands. J. Cell Sci. *113 (Pt 2*, 4055–4064.

Nijhout, H.F., Riddiford, L.M., Mirth, C., Shingleton, A.W., Suzuki, Y., and Callier, V. (2014). The developmental control of size in insects. Wiley Interdiscip. Rev. Dev. Biol. *3*, 113–134.

Pfaffl, M.W., Horgan, G.W., and Dempfle, L. (2002). Relative expression software tool (REST) for group-wise comparison and statistical analysis of relative expression results in real-time PCR. Nucleic Acids Res. *30*, e36.

Rajan, A., and Perrimon, N. (2012). Drosophila Cytokine Unpaired 2 Regulates Physiological Homeostasis by Remotely Controlling Insulin Secretion. Cell *151*, 123–137.

Riedel, F., Gillingham, A.K., Rosa-Ferreira, C., Galindo, A., and Munro, S. (2016). An antibody toolkit for the study of membrane traffic in Drosophila melanogaster. Biol. Open *84*, bio.018937.

Rousso, T., Schejter, E.D., and Shilo, B.-Z. (2015). Orchestrated content release from Drosophila glue-protein vesicles by a contractile actomyosin network. Nat. Cell Biol. *18*, 181–190.

Rulifson, E.J., Kim, S.K., and Nusse, R. (2002). Ablation of insulin-producing neurons in flies: growth and diabetic phenotypes. Science *296*, 1118–1120.

Sapiro, A.L., Ihry, R.J., Buhr, D.L., Konieczko, K.M., Ives, S.M., Engstrom, A.K., Wleklinski, N.P., Kopish, K.J., and Bashirullah, A. (2013). Rapid recombination mapping for high-throughput genetic screens in Drosophila. G3 (Bethesda). *3*, 2313–2319.

Sarov, M., Barz, C., Jambor, H., Hein, M.Y., Schmied, C., Suchold, D., Stender, B., Janosch, S., Vinay Vikas, K.J., Krishnan, R.T., et al. (2016). A genome-wide resource for the analysis of protein localisation in Drosophila. Elife *5*, e12068.

Scott, C.C., Vacca, F., and Gruenberg, J. (2014). Endosome maturation, transport and functions. Semin. Cell Dev. Biol. *31*, 2–10.

Sievers, F., Wilm, A., Dineen, D., Gibson, T.J., Karplus, K., Li, W., Lopez, R., McWilliam, H., Remmert, M., Söding, J., et al. (2011). Fast, scalable generation of high-quality protein multiple sequence alignments using Clustal Omega. Mol. Syst. Biol. *7*, 539.

Tran, D.T., Masedunskas, A., Weigert, R., and Hagen, K.G. Ten (2015). Arp2/3-mediated F-actin formation controls regulated exocytosis in vivo. Nat. Commun. *6*, 1–10.

Wang, J.-W., Beck, E.S., and McCabe, B.D. (2012). A Modular Toolset for Recombination Transgenesis and Neurogenetic Analysis of Drosophila. PLoS One *7*, e42102.

Wang, L., Evans, J., Andrews, H.K., Beckstead, R.B., Thummel, C.S., and Bashirullah, A. (2008). A genetic screen identifies new regulators of steroid-triggered programmed cell death in Drosophila. Genetics *180*, 269–281.

Wang, S., Tan, K.L., Agosto, M.A., Xiong, B., Yamamoto, S., Sandoval, H., Jaiswal, M., Bayat, V., Zhang, K., Charng, W.-L.L., et al. (2014). The Retromer Complex Is Required for Rhodopsin Recycling and Its Loss Leads to Photoreceptor Degeneration. PLoS Biol. *12*, e1001847.

Waterhouse, A.M., Procter, J.B., Martin, D.M.A., Clamp, M., and Barton, G.J. (2009). Jalview Version 2-A multiple sequence alignment editor and analysis workbench. Bioinformatics *25*, 1189–1191.

CHAPTER 3

Future Directions and Conclusions

FUTURE DIRECTIONS

Detailed characterization of the molecular function of *hobbit*

The Hobbit protein does not contain any functionally characterized domains, making it difficult to predict the molecular function of the protein from sequence analysis alone. My characterization of *hobbit* function indicates that the protein localizes to endosomal tubules and plays a role in retrograde trafficking, however, further work will be needed to determine the precise molecular mechanisms by which *hobbit* acts. As a first step, it will be necessary to identify the specific Hobbit protein sequences that are critical for localization and function. We can begin to address these questions by generating GFP-tagged Hobbit protein fragments, and looking to see if any of these fragments recapitulate the normal Hobbit localization pattern or rescue *hobbit* mutant phenotypes. We will likely need to start with large fragments of the protein, then make progressively smaller fragments until we identify the specific sequences that regulate localization and/or function. The hob^{5} nonsense mutation provides an interesting starting point; this lesion is located only 60 amino acids from the end of the 2300 amino acid protein, yet hob^{5} mutants exhibit the same phenotypes as the other alleles, suggesting that critical information for localization and/or function may be encoded at the C-terminus. I have already generated an overexpression construct containing the hob^{5} truncated protein, and it does not rescue *hobbit* mutant phenotypes, confirming that critical information is encoded at the C-terminus. This Hobbit protein fragment is therefore a conspicuous candidate for GFP-tagging and functional analysis. We can then extend these analyses to other Hobbit protein fragments, using the regions of high primary sequence conservation as a guide. Additionally, these constructs can be used for biochemical analyses to identify the

proteins that physically interact with Hobbit. These experiments will provide new molecular insights into how *hobbit* regulates retrograde trafficking.

To begin to identify proteins that functionally interact with *hobbit*, I have taken a candidate approach with known regulators of retrograde trafficking. The retromer complex is a protein coat complex that regulates retrograde transport from *Rab7*-positive endosomes to the TGN[1], raising the possibility that *hobbit* and retromer may work together. I found that salivary gland-specific RNAi-knockdown of all the retromer complex components resulted in enlarged *Rab7*-positive endosomes and glue secretion defects (Fig. 1A). Additionally, the SNARE protein *SNAP-24* accumulated inside the enlarged *Rab7*-positive endosomes upon retromer knockdown (Fig. 1C). Therefore, disruption of retromer complex function effectively phenocopied the trafficking and secretion defects observed in *hobbit* mutant cells. I then tested if retromer exhibited any localization defects in *hobbit* mutant cells. Normally, the retromer complex component *Vps35* exhibits a punctate pattern that partially co-localizes with *Rab7*; however, in *hobbit* mutant cells, *Vps35* completely co-localizes with *Rab7* and becomes uniformly distributed around the endosomal membrane (Fig. 1B), suggesting that *hobbit* may be required for normal assembly and/or function of the retromer complex. I also tested the role of the retromer complex in the regulation of body size. Ubiquitous RNAi-knockdown of retromer complex components reduced body size (Fig. 1A,D), suggesting that retromer also plays a critical role in insulin release. Interestingly, a recent Genome Wide Association Study (GWAS) identified human Vps26B as a type 2 diabetes susceptibility locus[2], suggesting that a new pathway requiring *hobbit* and the retromer complex may be critical for insulin secretion in both flies and humans. Future studies, including the structure-function analyses described

above, will provide additional insights into how *hobbit* and the retromer complex cooperate during retrograde trafficking.

A third, independent approach to gain new insights into *hobbit* function would require the use of advanced imaging techniques. Super resolution microscopy, such as stimulated emission depletion (STED) microscopy, would provide clearer images of Hobbit localization in endosomes, tubules, and the Golgi body. STED microscopy could also be used to analyze Hobbit localization relative to other cellular factors known to regulate retrograde trafficking, including the retromer complex itself, microtubules, and the WASH complex (see Chapter 1 for details). These studies can be complemented with electron microscopy (EM). Is Hobbit visible on endosomal tubules using EM? If so, where on the tubule does Hobbit localize? New high-pressure freezing sample preparation techniques would aid in preservation of these fragile structures. Expanding Hobbit subcellular localization and co-localization studies will provide additional information about the molecular mechanism by which *hobbit* regulates retrograde trafficking. Finally, it is likely that Hobbit exhibits dynamic localization patterns and trafficks between multiple organelles. Therefore, the use of spinning disk confocal microscopy would allow analysis of Hobbit dynamics in living cells. Overall, the use of advanced imaging techniques will provide important new insights into *hobbit* localization and function in retrograde trafficking.

Analysis of *hobbit* function in tissue homeostasis

My results suggest that *hobbit* may play a role in regulated exocytosis in many different tissue types and developmental contexts. For example, I have found that *hobbit*

may play a role in tissue homeostasis by regulating secretion of critical morphogens. The external tissues of the adult fly, such as the wings, legs, and antennae, develop from partially-differentiated tissues in the larva called imaginal discs. These imaginal discs have an incredible capacity to regenerate after tissue damage; in fact, experiments in the 1960s demonstrated that fragments of wing imaginal discs that were surgically implanted into adult female abdomens could fully regenerate to produce a complete disc[3]. Tissue damage can also be induced by ectopically expressing pro-apoptotic genes, such as the inhibitor of apoptosis protein (IAP) antagonist *reaper*. Induction of *reaper* expression releases a caspase cascade, resulting in apoptosis (for details of *reaper*-induced caspase cascades, see Part 2). In control animals, transient ectopic expression of *reaper* triggers apoptosis in wing imaginal discs; however, given time, these discs will recover and regenerate. However, *hobbit* mutant discs given the same *reaper* treatment activate apoptosis but fail to regenerate properly. Conversely, *hobbit* overexpression strongly inhibits caspase activation in response to *reaper* expression, as seen when *hobbit* is overexpressed in the posterior region of the wing disc (Fig. 2). However, interestingly, *hobbit* overexpression also inhibits caspase activation in portions of the anterior half of the wing disc (Fig. 2D, see arrowheads), suggesting that *hobbit* has both a cell-autonomous and non-cell autonomous effect on sensitivity to apoptosis. Given that *hobbit* regulates exocytosis in many other tissue types, it is possible that the non-cell autonomous suppression of caspase activation is mediated by increased secretion of morphogens from the posterior region of the wing disc upon *hobbit* overexpression. Morphogens are known to be anti-apoptotic and also play critical roles in tissue regeneration after damage[4,5]. Currently, it is unclear which morphogen(s) are secreted

via *hobbit*-dependent mechanisms. However, a conspicuous candidate is *wingless*, the *Drosophila* ortholog of *Wnt*. Given the known role of the retromer complex in recycling the *wingless/Wnt* carrier *wntless*[6,7], it is possible that *hobbit* overexpression facilitates faster trafficking and recycling of this protein, resulting in increased *wingless* secretion. Excellent antibodies to detect *wingless* are commercially available, making it straightforward to test if *hobbit* overexpression does promote increased secretion of this protein. Many other morphogens, including the BMP protein *decapentaplegic* (*dpp*) and *hedgehog*, also have reagents available, making it possible to also test secretion of these proteins upon *hobbit* overexpression. These experiments will further characterize the role of *hobbit* in regulated exocytosis, but will also highlight another novel function of this highly conserved but poorly characterized protein.

Mapping and analysis of other small pupa mutants

In addition to *hobbit*, our screen identified 18 other complementation groups of mutants with a small pupa phenotype. These mutants provide exciting opportunities for future studies of systemic growth during *Drosophila* development. As a first step to identifying other mutants that may have a small pupa phenotype because of exocytosis defects, I conducted a secondary screen to identify additional mutants with glue secretion defects. This screen revealed six new complementation groups with defects in this process (Fig. 3). Using standard methods developed in our lab[8], I began mapping these mutations, and so far, I have mapped three of them to genes: *sulfateless*, *Vps15*, and *atlastin*. *sulfateless* is conserved throughout animals and is homologous to mammalian *N-deacetylase and N-sulfotransferase 2* (*NDST2*). This protein is part of the heparan-

sulfate proteoglycan (HSPG) biosynthesis pathway[9]. HSPGs play many roles during animal development; however, the most interesting for my studies is the characterized function of these proteins in secretory granule biogenesis and maturation in mammalian mast cells[10]. *sulfateless* has also been shown to regulate *wingless* secretion in *Drosophila* cells[11]. *Vps15* is a class III phosphatidylinositol-3 kinase (PI3K) that is conserved from yeast to humans; it is homologous to mammalian *PIK3R4*. This protein is required for production of PI3P, a lipid moiety that is abundant in endosomal membranes (see Chapter 1). *Vps15* primarily functions in autophagy; however, this protein was also recently reported to inhibit glue secretion in the *Drosophila* larval salivary glands through an unknown mechanism[12]. Finally, *atlastin* is conserved throughout animals and is homologous to mammalian *atlastin GTPase 2* (*ATL2*). *atlastin* plays critical roles in ER and Golgi morphogenesis and organization by acting as a membrane tether[13,14]. Loss of *atlastin* function also results in impaired synaptic transmission[14]. The final three glue secretion mutants have been mapped to small chromosomal regions, but I have not yet identified the specific gene that is disrupted.

Each of these small pupa mutants with glue secretion phenotypes represent interesting candidates for future study. First, do any of these proteins play a role in *hobbit*-dependent trafficking? We can first test if the salivary glands exhibit phenotypes similar to *hobbit* mutants, such as small glue granules and enlarged *Rab7*-positive endosomes. We can also test if Hobbit protein localization is altered in any of these mutant backgrounds. It will also be interesting to test if insulin secretion is disrupted in these mutant animals. Finally, even if these proteins don't function in the same molecular pathway as *hobbit*, analysis of their function will provide new mechanistic insights into

regulated exocytosis. We also intend to continue to map the other small pupa mutants, one of which has already been identified as a novel allele of the insulin receptor (*InR*), suggesting that some of these mutants may play a role in insulin action and/or signaling in peripheral tissues.

A

retromer complex component	enlarged Rab7 endosomes?	glue secretion defects?	small pupae?
Snx1-RNAi	yes	yes	yes
Snx3-RNAi	yes	yes	yes
Snx6-RNAi	yes	yes	n/a
Vps26-RNAi	yes	yes	yes
Vps29-RNAi	yes	yes	yes
Vps35-RNAi	yes	yes	yes

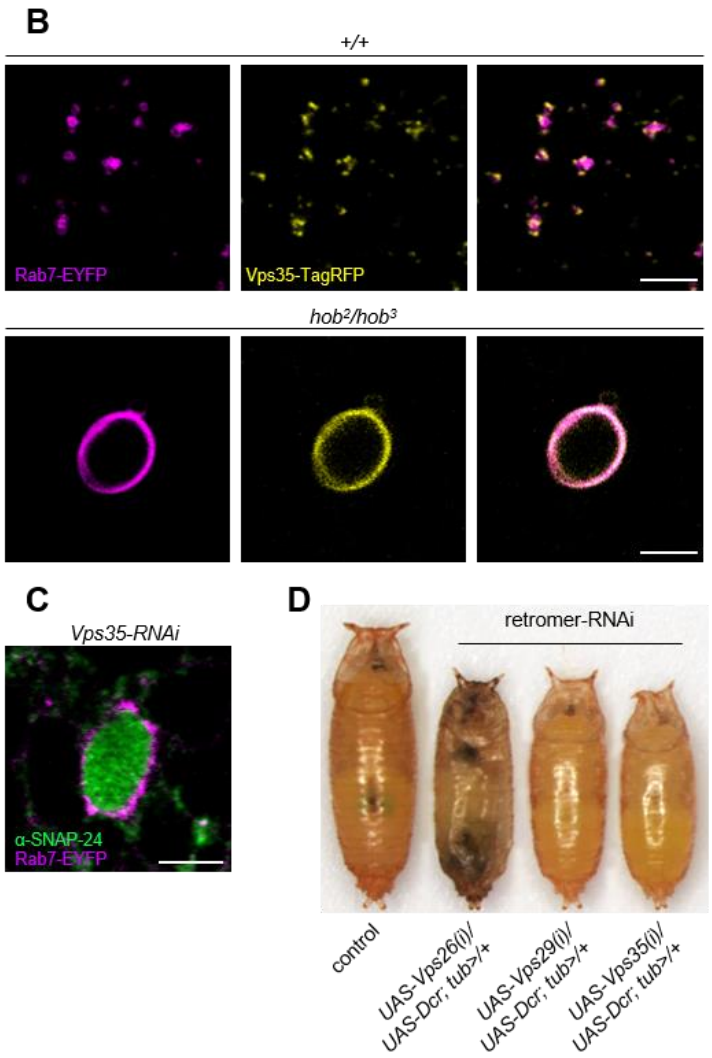

Figure 1. *Hobbit* is required for retromer complex function during regulated exocytosis. (A) Salivary gland-specific (with *Sgs3-GAL4*) RNAi knockdown of retromer

complex components results in enlarged *Rab7*-positive endosomes and impaired glue secretion. Ubiquitous RNAi knockdown (*UAS-Dcr; tub-GAL4*) of retromer components results in reduced body size; *Snx6* knockdown causes lethality during early larval development. **(B)** Retromer localization is altered in *hobbit* mutant salivary glands. *Vps35-TagRFP* (in yellow) partially co-localizes with *Rab7* (in magenta) in control glands; in *hobbit* mutant glands, *Vps35-TagRFP* is uniformly distributed around the endosomal membrane. All images acquired from live, unfixed tissue. *Vps35-TagRFP* is an endogenously-regulated fluorescent fusion protein[15]. **(C)** Enlarged *Rab7*-positive endosomes (magenta) contain *SNAP-24* (green) upon salivary gland-specific *Vps35* RNAi knockdown (with *Sgs3-GAL4*). **(D)** Ubiquitous RNAi knockdown of retromer cargo selective complex (CSC) components reduces animal body size. Scale bars 5µm.

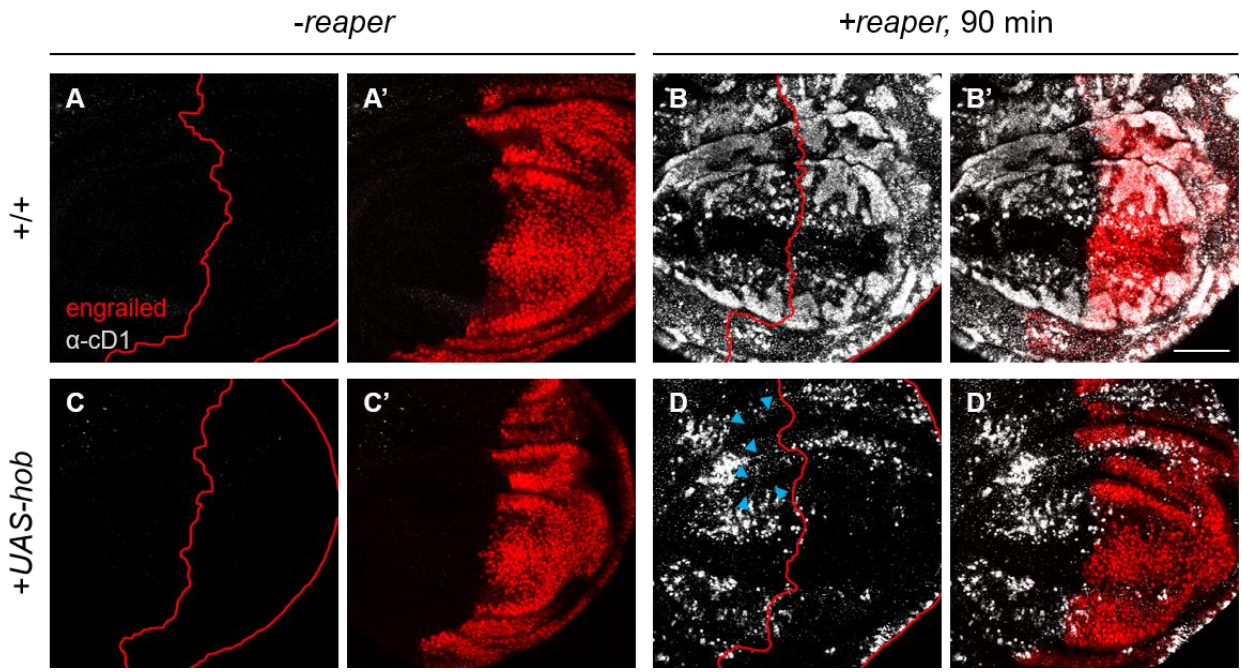

Figure 2. *hobbit* overexpression blocks caspase activation in response to an apoptotic stimulus. (A-A') Control wing imaginal discs do not exhibit caspase activation, assayed by staining for cleaved-Dcp-1 (α-cD1, in gray), without *reaper* expression. **(A)** Anti-cD1 staining in control discs (*en>RFP, hs-reaper/+*) without heat-induced expression of *reaper*. Posterior region of the wing disc outlined in red. **(A')** Merged image showing anti-cD1 staining and RFP expression in the poster region of the wing disc. **(B-B')** Control wing discs exhibit widespread anti-cD1 staining 90 min after heat-induced expression of *reaper*. **(B)** Anti-cD1 staining; posterior compartment of wing disc outlined in red. **(B')** Merged image of anti-cD1 staining and RFP expression in the posterior compartment. **(C-C')** No anti-cD1 staining is observed in wing imaginal discs overexpressing *hobbit* in the posterior compartment of the wing disc (*en>RFP, hs-reaper/UAS-hob*) without heat-induced expression of *reaper*. **(C)** Anti-cD1 staining in gray, posterior compartment outlined in red. **(C')** Merged image showing anti-cD1 staining and RFP expression in the

posterior compartment of the wing disc. **(D-D')** *hobbit* overexpression inhibits caspase activation 90 min after heat-induced expression of *reaper*. **(D)** *hobbit* overexpression in the posterior compartment of the wing disc (outlined in red) results in reduced anti-cD1 staining in both the posterior and anterior compartments. Blue arrowheads mark areas of strong suppression of caspase activation in the anterior compartment. **(D')** Merged image showing anti-cD1 staining and RFP expression in the posterior compartment of the wing disc. Scale bar is 50 µm.

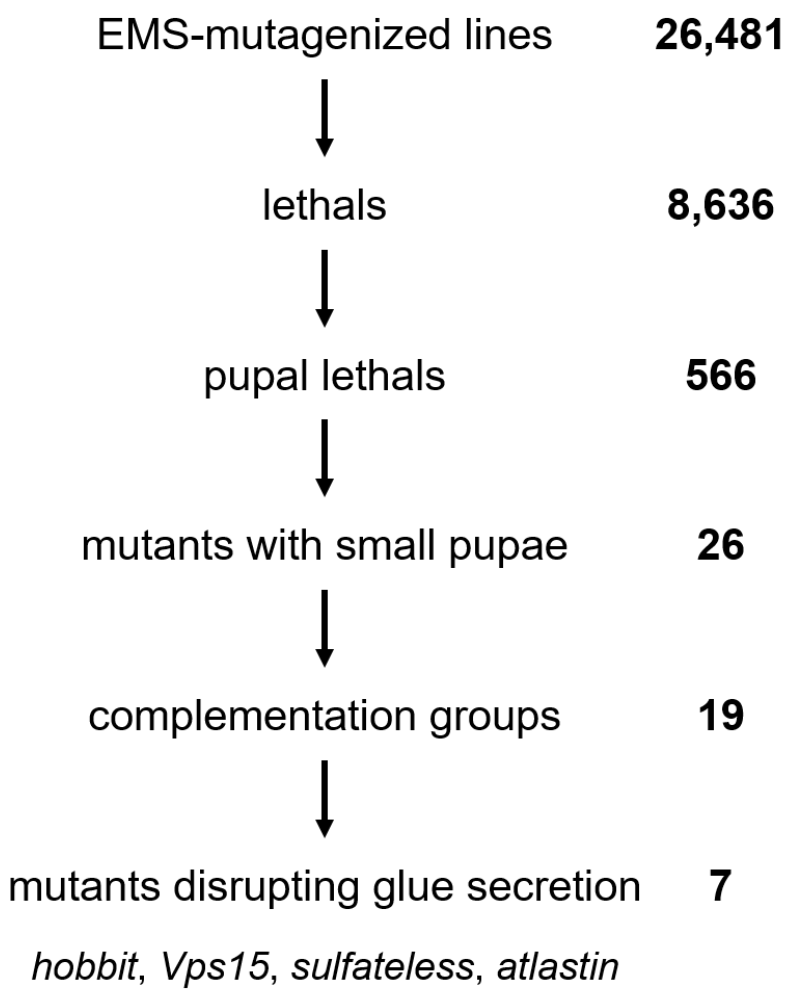

Figure 3. Screening and mapping summary of small pupa mutants with glue secretion defects. From our large-scale EMS mutagenesis on the third chromosome, we identified 566 pupal lethal mutations; of these, 26 exhibited a small pupa phenotype. These 26 mutants fit into 19 complementation groups. Subsequent screening for defects in glue secretion from the larval salivary glands uncovered seven complementation groups disrupting this process; of the seven, four have been mapped to the causative gene.

REFERENCES

1. Bonifacino, J. S. & Hurley, J. H. Retromer. *Current Opinion in Cell Biology* **20,** 427–436 (2008).

2. Kooner, J. S. *et al.* Genome-wide association study in individuals of South Asian ancestry identifies six new type 2 diabetes susceptibility loci. *Nat. Genet.* **43,** 984–989 (2011).

3. Hadorn, E. & Buck, D. On the differentiation of transplanted wing imaginal disc fragments of Drosophila melanogaster. *Rev. Suisse Zool.* **69,** 302–10 (1962).

4. Smith-Bolton, R. K., Worley, M. I., Kanda, H. & Hariharan, I. K. Regenerative Growth in Drosophila Imaginal Discs Is Regulated by Wingless and Myc. *Dev. Cell* **16,** 797–809 (2009).

5. Ryoo, H. D., Bergmann, A., Gonen, H., Ciechanover, A. & Steller, H. Regulation of Drosophila IAP1 degradation and apoptosis by reaper and ubcD1. *Nat. Cell Biol.* **4,** 432–438 (2002).

6. Port, F. *et al.* Wingless secretion promotes and requires retromer-dependent cycling of Wntless. *Nat. Cell Biol.* **10,** 178–185 (2008).

7. Franch-Marro, X. *et al.* Wingless secretion requires endosome-to-Golgi retrieval of Wntless/Evi/Sprinter by the retromer complex. *Nat. Cell Biol.* **10,** 170–177 (2008).

8. Sapiro, A. L. *et al.* Rapid Recombination Mapping for High-Throughput Genetic Screens in Drosophila. *G3 Genes|Genomes|Genetics* **3,** 2313–2319 (2013).

9. Toyoda, H., Kinoshita-Toyoda, A., Fox, B. & Selleck, S. B. Structural analysis of glycosaminoglycans in animals bearing mutations in sugarless, sulfateless, and tout-velu:Drosophila homologues of vertebrate genes encoding glycosaminoglycan biosynthetic enzymes. *J. Biol. Chem.* **275,** 21856–21861 (2000).

10. Sarrazin, S., Lamanna, W. C. & Esko, J. D. Heparan sulfate proteoglycans. *Cold Spring Harb. Perspect. Biol.* **3,** 1–33 (2011).

11. Lin, X. & Perrimon, N. Dally cooperates with Drosophila Frizzled 2 to transduce Wingless signalling. *Nature* **400,** 281–4 (1999).

12. Anding, A. L. & Baehrecke, E. H. Vps15 is required for stress induced and developmentally triggered autophagy and salivary gland protein secretion in Drosophila. *Cell Death Differ.* **22,** 457–64 (2015).

13. Orso, G. *et al.* Homotypic fusion of ER membranes requires the dynamin-like GTPase Atlastin. *Nature* **460,** 978–983 (2009).

14. Lee, M. *et al.* Drosophila Atlastin regulates the stability of muscle microtubules and is required for synapse development. *Dev. Biol.* **330,** 250–262 (2009).

15. Koles, K., Yeh, A. R. & Rodal, A. A. Tissue-specific tagging of endogenous loci in Drosophila melanogaster. *Biol. Open* **5,** 83–89 (2016).

CONCLUSIONS

The work described here highlights the continued importance of chemical mutagenesis screens to enable the discovery of new genes and new biological processes. These screens harness the power of random, unbiased mutagenesis to allow the animal to reveal what is biologically important. Indeed, *hobbit* could not have been identified by any other means. The identification of a novel, highly-conserved gene that regulates exocytosis could have far-reaching impacts for both our understanding of this fundamental cell-biological process and for human health. Analysis of *hobbit* function also revealed a previously uncharacterized role for retrograde trafficking in the control of exocytosis. Disruption of retromer function is known to play a role in neurodegenerative diseases, including Alzheimer's and Parkinson's; additionally, my work suggests that retromer dysfunction appears to affect insulin secretion in *Drosophila*, raising the tantalizing possibility of a genetic link between neurodegenerative diseases and type 2 diabetes. Continued analysis of *hobbit*-dependent intracellular trafficking will likely reveal other new insights into both basic cell biology and human disease.

PART TWO

Tissue morphogenesis: new functions for caspases

CHAPTER 4

Tango7 regulates cortical activity of caspases during *reaper*-triggered changes in tissue elasticity

This chapter is in press for publication in *Nature Communications*

Kang Y, Neuman SD, Bashirullah A. *Tango7* regulates cortical activity of caspases during *reaper*-triggered changes in tissue elasticity. *Nat Commun.* In press.

ABSTRACT

Caspases perform critical functions in both living and dying cells; however, how caspases perform physiological functions without killing the cell remains unclear. Here we identify a novel physiological function of caspases at the cortex of *Drosophila* salivary glands. In living glands, activation of the initiator caspase *dronc* triggers cortical F-actin dismantling, enabling the glands to stretch as they accumulate secreted products in the lumen. We demonstrate that *tango7*, not the canonical Apaf-1-adaptor *dark*, regulates *dronc* activity at the cortex; in contrast, *dark* is required for cytoplasmic activity of *dronc* during salivary gland death. Therefore, *tango7* and *dark* define distinct subcellular domains of caspase activity. Furthermore, *tango7*-dependent cortical *dronc* activity is initiated by a sublethal pulse of the IAP-antagonist *reaper*. Our results support a model in which biological outcomes of caspase activation are regulated by differential amplification of IAP-antagonists, unique caspase adaptor proteins, and mutually-exclusive subcellular domains of caspase activity.

INTRODUCTION

Caspases are cysteine-aspartic proteases best known for their roles in initiating cellular demolition during apoptosis[1,2]. These proteins are maintained within the cell as inactive zymogens. However, once activated, a caspase cascade is released, resulting in critical consequences for the cell. Initiator caspases sit at the top of this cascade. These proteins exist in the cell as inactive monomers, but upon receipt of an activating stimulus, they form active dimers, mediated by adaptor proteins[3]. The best characterized activation platform, which is required during apoptosis, is the apoptosome[4,5]. The apoptosome consists of the initiator caspase, caspase-9 (*dronc* in *Drosophila*), and the adaptor protein Apaf-1 (*dark* in *Drosophila*). In mammals, release of cytochrome c activates the apoptosome, allowing caspase-9 to cleave a second class of caspases, the effector caspases. The effector caspases exist in the cell as inactive dimers, and require cleavage by initiator caspases for activation[6,7]. The major effector caspases in *Drosophila* are *drice* and *dcp-1*. Activated effector caspases then cleave critical cellular targets as well as other effector caspases, generating a cascade of caspase activity that eventually results in cellular demolition. This self-perpetuating cascade of caspase activation led to the widespread notion that caspase activation represents a “point of no return” in the life of a cell. However, over the last decade, there have been many examples of caspases playing non-lethal, or “non-apoptotic,” roles in cells that do not die.

The list of non-lethal, non-apoptotic roles of caspases has been steadily growing[8-13]. For example, the initiator caspase, caspase-9, and the effector caspase, caspase-3, have been shown to mediate axon pruning during local deprivation of NGF[14]. Additionally, mouse hair follicles and the surrounding cells require non-apoptotic functions of the

effector caspase, caspase-7, for proper development[15]. In *Drosophila*, the initiator caspase *dronc* (homolog of mammalian caspase-9) plays a critical role in dendrite pruning of the sensory neurons of the peripheral nervous system[16,17], and also plays an important role in sperm individualization[18-20]. Although many non-apoptotic functions of caspases have been identified, how caspases function without executing the cell has remained a mystery. Unfortunately, these lethal and non-lethal outcomes of caspase activation have been studied in different cell types, making mechanistic comparisons very difficult.

We have found that the *Drosophila* larval salivary glands provide an ideal model to study developmentally-regulated non-lethal and lethal functions of caspases in a single cell type. Here we examine two distinct caspase activation events during salivary gland development: one resulting in a non-apoptotic, non-lethal outcome and the second resulting in a lethal outcome. We find that these two events are both regulated by the steroid hormone ecdysone; however, differential signaling mechanisms selectively amplify the activating signal, IAP-antagonist expression, to generate a lethal outcome instead of a non-lethal response. Moreover, we also demonstrate that caspases can be activated in mutually-exclusive subcellular domains to accomplish different biological functions, and the use of different adaptor proteins mediates this mutually-exclusive activation. Finally, our results highlight a novel, non-lethal function for caspases in the control tissue elasticity during exocrine secretion events. Altogether, we provide a new model for how caspases can be activated and perform cellular functions without triggering cell death during development.

RESULTS

A regulated sublethal pulse of *rpr* in salivary glands

In *Drosophila*, caspase activation hinges on transcriptional induction of IAP-antagonists[21], proteins that remove Inhibitor of Apoptosis proteins (IAPs) and initiate a caspase cascade. The primary IAP-antagonists in *Drosophila* are *reaper* (*rpr*) and *head involution defective* (*hid*), and these proteins play a critical role in the programmed cell death of the larval salivary glands during metamorphosis[22,23]. Our gene expression studies in the larval salivary glands at the onset of metamorphosis revealed a 1000-fold induction of *hid* at the start of pupal development (Fig. 1a). In contrast, we observed two distinct pulses of *rpr* expression: a 30-fold induction at the end of larval development, and a 1000-fold induction at the start of pupal development (Fig. 1a). The late, large pulse of *rpr* and *hid* has previously been characterized as part of the larval salivary gland cell death response[22,23]; however, the early, small pulse of *rpr* has not been described before. We wanted to confirm that this small *rpr* pulse was biologically relevant, so we first tested if the pulse was developmentally-regulated. The large, lethal pulse of IAP-antagonists is induced by the prepupal pulse of the steroid hormone 20-hydroxyecdysone (henceforth called ecdysone)[23]. Another ecdysone pulse occurs at the end of larval development[24], and peak steroid hormone levels coincide with the timing of the small pulse of *rpr* expression. We therefore tested if this small *rpr* pulse was regulated by ecdysone signaling. We found that tissue-specific expression of a dominant negative form of the ecdysone receptor (*EcR*^{F645A}) abolished *rpr* expression at the end of larval development (Supplementary Fig. 1a), indicating that this small *rpr* pulse is developmentally-regulated by the late larval pulse of ecdysone.

Although ecdysone signaling initiates induction of both the small and large *rpr* pulses, the mechanisms mediating the difference in magnitude between these pulses were unclear. We tested if this expression difference was regulated by different downstream targets of ecdysone. Several transcription factors, including *BR-C*, *E74A*, and *Med24*, are required for salivary gland cell death, and these transcription factors are themselves induced by ecdysone[23,25,26]. We found that *BR-C*, *E74A*, and *Med24* mutant salivary glands had reduced expression of *rpr* at the late, lethal pulse (Supplementary Fig. 1b). In *BR-C* mutant salivary glands (rbp^5), this resulted in *rpr* expression levels that resembled the magnitude of the early, small larval pulse. Interestingly, these same three mutants did not affect *rpr* expression at the small, early pulse (Supplementary Fig. 1a). Taken together, these results indicate that downstream targets of ecdysone, like *BR-C*, *E74A*, and *Med24*, differentially amplify *rpr* expression during the death response, making it possible to generate both sublethal and lethal pulses of the IAP-antagonist. Furthermore, the early, sublethal pulse of *rpr* was induced in a tissue-specific manner. Although all tissues tested responded to ecdysone by inducing expression of the primary target gene *E74A*, only the salivary glands and midgut induced *rpr* expression, while the wing discs and central nervous system did not (Supplementary Fig. 2). These results suggest that lethal vs. sublethal pulses of *rpr* are developmentally-controlled, raising the intriguing possibility that differential amplification and tissue-specific expression of IAP-antagonists may play a role in determining apoptotic versus non-apoptotic outcomes of caspase activation.

Sublethal *rpr* pulse initiates cortical caspase activation

To determine if the sublethal pulse of *rpr* in salivary glands had a function, we first examined if caspases were activated at this stage. We have previously shown that staining glands at this stage with antibodies directed to cleaved-caspase-3 (anti-cC3) does not show any signs of caspase activation[27]. Staining with antibodies directed to cleaved-Dcp-1 (anti-cD1), however, showed staining primarily at the cell cortex, with the intensity of staining peaking at -4 h PF (4 hours before puparium formation) (Fig. 1b). This Dcp-1 activation profile coincides with the peak of *rpr* expression, suggesting that the two events may be related. Indeed, in *rpr* mutant glands, anti-cD1 staining was disrupted (Fig. 1c). Furthermore, anti-cD1 staining required the initiator caspase *dronc* and the effector caspase *dcp-1*, but not the effector caspase *drice* (Fig. 1c). Importantly, these results indicate that the small, sublethal pulse of *rpr* initiates activation of specific caspases at the cortex of developing larval salivary glands.

Caspases dismantle cortical F-actin in living glands

To identify the consequence of caspase activation at the cortex of the larval salivary glands, we tested several vital dyes and antibodies known to stain the cell cortex. Only phalloidin, a vital dye that binds to filamentous actin (F-actin), showed a dramatic difference in staining between -8 h PF and 0 h PF glands. The cortex of most living cells features a meshwork of F-actin bundles that confers shape and structural stability to the cell. Accordingly, we observed a meshwork of cortical F-actin framing every cell in the larval salivary glands (Fig. 2a). The acinar cells of the salivary gland form a radially-symmetric polarized epithelium; the apical membrane, visualized by expression of a membrane-targeted GFP (CD8-GFP) (Fig. 2a-b), outlines the lumen of the glands, while

the basal membrane faces the exterior of the gland. A coronal view of the salivary glands revealed a clear F-actin cytoskeleton outlining each cell (Fig. 2c). However, we found that this cortical F-actin cytoskeleton was dismantled at the end of larval development. At -8 h PF, phalloidin staining showed tight bundles of cortical F-actin (Fig. 2d). Lifeact-Ruby, a fluorescently-tagged peptide that binds actin[28,29], also showed that most of the actin within the cell at -8 h PF is present at the cortex (Fig. 2e). These phalloidin-stained F-actin bundles became less distinct at -4 and -1 h PF, and disappeared by PF (Fig. 2d). Consistently, Lifeact-Ruby imaging showed that this loss of cortical F-actin was associated with a gradual redistribution of actin from the cortex to the cytoplasm (Fig. 2e). This dissolution of F-actin appeared to start at -4 h PF, when the decrease in phalloidin staining was accompanied by increased Lifeact-Ruby signal at the cortex, as well as an increase in Lifeact-Ruby signal in the cytoplasm (*cf.* Lifeact-Ruby versus phalloidin staining; Fig. 2d-e). These results reflect a rapid disassembly of cortical actin filaments into cytoplasmic monomers beginning at -4 h PF, at the peak of cortical caspase activation.

We next tested if cortical F-actin breakdown depended on the sublethal pulse of *rpr* and subsequent caspase activation at this stage. Indeed, loss of *rpr* function blocked dismantling of the F-actin cytoskeleton (Fig. 2f). Moreover, F-actin disassembly required *dronc* and *dcp-1* but not *drice* (Fig. 2f), mirroring the caspase cascade required for cortical staining of anti-cD1 during this stage (Fig. 1c). To further validate the role of caspases in F-actin disassembly, we tested the effect of inhibitors of caspase activation. Salivary gland-specific expression of *diap1*, the primary *Drosophila* IAP, disrupted F-actin breakdown, while expression of *p35*, the Baculovirus-derived effector caspase inhibitor,

slightly inhibited this process (Fig. 2g). Importantly, salivary gland-specific RNAi knockdown of *rpr* or *dronc* strongly inhibited F-actin disassembly (Fig. 2g). These results indicate a cell-autonomous requirement for *rpr*-dependent antagonism of *diap1* and activation of *dronc* during F-actin breakdown in the larval salivary glands.

Given that the small pulse of *rpr* is dependent on ecdysone signaling, we also tested if ecdysone directly triggered the loss of cortical F-actin in salivary glands. We found that cell-autonomous disruption of ecdysone signaling through expression of the dominant negative EcR^{F645A} in salivary glands blocked the loss of F-actin (Supplementary Fig. 3a). Conversely, addition of ecdysone to *ex vivo* cultures of salivary glands dissected at -8 h PF was sufficient to trigger F-actin breakdown, while addition of the translational inhibitor cycloheximide prevented ecdysone-triggered F-actin breakdown (Supplementary Fig. 3b), suggesting that translation of ecdysone-induced transcripts is critical for dismantling of cortical F-actin. Taken together, these results indicate that an ecdysone-induced sublethal pulse of *rpr* triggers caspase activation at the cortex, which, in turn, initiates dismantling of the cortical F-actin cytoskeleton.

F-actin breakdown requires *dronc* localization and activity

Our data thus far suggests that *rpr* activates caspases at the cortex, and it is this cortically- restricted activity that breaks down the F-actin cytoskeleton. To understand the mechanisms that restrict caspase activity to the salivary gland cell cortex, we first examined the subcellular localization of Dronc protein. Staining with an anti-Dronc antibody showed that Dronc protein is enriched at the cortex at -8 and -4 h PF (Supplementary Fig. 4a). Accordingly, overexpression of full-length Dronc showed

preferential targeting to the cortex at -8 and -4 h PF, but this cortical localization disappeared at PF (Fig. 3a; Supplementary Fig. 4b). Salivary gland-specific expression of *dronc-RNAi* abolished all Dronc staining at -8 h PF (Fig. 3a), confirming both the specificity of the antibody and efficiency of RNAi-knockdown. Dronc protein localized to the cortex before induction of the *rpr* pulse that triggers cortical cleaved-Dcp-1 activation, suggesting that subcellular targeting of the initiator caspase may be responsible for restricting the *rpr*-initiated caspase cascade to the cell cortex. We next wanted to test the role of Dronc activity in F-actin remodeling, as caspases have previously been shown to regulate other non-apoptotic functions independently of their catalytic activity[30,31]. Overexpression of Dronc accelerated the kinetics of F-actin breakdown in response to the small *rpr* pulse; in contrast, overexpression of a catalytically-inactive *dronc* (*dronc*$^{C\text{-}A}$) prevented the breakdown of cortical F-actin (Fig. 3b). *dronc*$^{C\text{-}A}$ still localized appropriately (Fig. 3b), suggesting that it may inhibit F-actin breakdown by displacing endogenous Dronc from the cortex. Taken together, these results demonstrate that both cortical localization and activity of Dronc are essential for F-actin dismantling during salivary gland development.

tango7 not *dark* regulates *dronc* localization and activity

We next wanted to determine how Dronc is localized to the cell cortex. Given that initiator caspases require adaptor proteins for activation and function[3,5,32], we tested if the Apaf-1 adaptor protein *dark*, which is the canonical regulator of *dronc* activity in *Drosophila*[33,34], was required for localization and/or function of *dronc* at the cortex. To our surprise, knockdown of *dark* had no effect on the cortical localization of Dronc protein

(Fig. 3c). Moreover, *dark* null mutant glands still showed cortical anti-cD1 staining, and dismantling of cortical F-actin occurred normally (Fig. 3e). These results demonstrate that *dark* is not required for the localization or function of *dronc* at the salivary gland cell cortex. To identify other potential adaptor proteins for *dronc* in salivary glands, we conducted an RNAi-based screen among candidate proteins known to physically interact with *dronc*[35-38]. The strongest suppressor of F-actin breakdown in our screen was *tango7* (Supplementary Fig. 5a). Salivary gland-specific knockdown of t*ango7* also disrupted cortical Dcp-1 activation (Supplementary Fig. 5b,c), indicating that *tango7* plays a cell-autonomous role in caspase-dependent F-actin dismantling. *tango7* mutant glands also disrupted both the cortical activation of Dcp-1 and the dismantling of cortical F-actin (Fig. 3f). Consistent with a function in F-actin breakdown, we found that Tango7 protein localized to the salivary gland cell cortex. Analysis of Tango7 localization using recently-generated endogenous superfolder GFP (sGFP)-tagged *tango7*[39] showed that Tango7 protein displayed subcellular dynamics similar to Dronc, with robust cortical localization at -8 h PF that was lost at 0 h PF (Supplementary Fig. 5d,e). This places Tango7 protein at the right time and place to function with Dronc in F-actin dismantling. We also investigated the effect of *tango7* knockdown on Dronc protein stability, as previous studies have shown that loss of *tango7* reduces Dronc protein levels[37]. However, western blot analysis of Dronc protein levels showed that knockdown of *tango7* did not reduce Dronc expression in salivary glands (Fig. 3d). Importantly, *tango7* appeared to be critical for proper cortical localization of Dronc. In *tango7* knockdown glands, Dronc protein no longer displayed tight cortical localization and appeared instead to diffuse towards the cytoplasm, with conspicuous gaps lacking Dronc protein at the cortex (Fig. 3c). Taken

together, these results demonstrate that *tango7* is required for localization, activation, and function of *dronc* in F-actin dismantling at the salivary gland cell cortex.

Caspase activation in mutually-exclusive subcellular domains

Both *dronc* and *dark* play a critical role in caspase activation during the death response in salivary glands[40-42], about half a day after the events discussed so far. To further examine the roles of *tango7* and *dark* in the activation of *dronc*, we tested the role of these adaptors during the death response in salivary glands. At this later stage, anti-cD1 staining still showed robust signal at the cortex, but now also showed significant signal in the cytoplasm (Fig. 4a). Analysis of a timecourse of anti-cD1 staining showed that cortical activation is short-lived at this stage, while the cytoplasmic activation persisted longer (Supplementary Fig. 6), suggesting that cortical activation may be a transient event in response to the high-magnitude induction of *rpr*. Loss of *dronc* disrupted all anti-cD1 staining (Fig. 4a), indicating that Dcp-1 activation in both the cortical and cytoplasmic subcellular domains requires *dronc* activity. Strikingly, salivary gland-specific knockdown of *tango7* disrupted anti-cD1 staining at the cortex without affecting anti-cD1 staining in the cytoplasm (Fig. 4a). Conversely, RNAi knockdown of *dark* disrupted anti-cD1 staining in the cytoplasm but not at the cortex (Fig. 4a). Consistent with previously published results, *dark* was required for anti-cC3 staining at this stage, which appeared to be only cytoplasmic (Fig. 4b). In contrast, knockdown of *tango7* did not appear to affect cytoplasmic anti-cC3 staining (Fig. 4b), although *tango7* knockdown appeared to disturb normal morphological breakdown during the death response. Anti-cC3 staining has previously been reported to detect *dronc* activity[43], but our results suggest that this

antibody specifically detects *dark*-dependent *dronc* activity in *Drosophila* tissues. Taken together, these results demonstrate that *tango7* is only required for caspase activation at the cortex, while *dark* is required for caspase activation in the cytoplasm. Importantly, activation of caspases in one subcellular domain does not appear to affect activation of caspases in the other domain, suggesting that caspase activation within these subcellular domains is restricted and compartmentalized.

We next tested if subcellular domain-specific activation of caspases resulted in compartment-specific functions. Cortical F-actin, which is transiently dismantled after the small pulse of *rpr* at PF, was dismantled once again during the death response (Fig. 4c). Similar to F-actin dismantling at PF, this second dismantling of cortical F-actin in dying glands also required *dronc* and *dcp-1*, but not *drice* (Fig. 4d), demonstrating that a similar caspase cascade is responsible for the cortical function of caspases in both living and dying cells. Importantly, knockdown of *tango7* blocked breakdown of cortical F-actin in dying glands, despite the robust activation of caspases in the cytoplasm (Fig. 4a,b,d). Conversely, although loss of *dark* blocked activation of caspases in the cytoplasm (Fig. 4b), absence of *dark* did not disrupt *dronc*-dependent dismantling of cortical F-actin (Fig. 4d). Thus, contrary to commonly-held assumptions, cytoplasmic activation of caspases does not result in widespread cellular caspase activity; instead, *tango7* and *dark* appear to define mutually-exclusive subcellular domains of *dronc* activation and function in dying salivary glands.

tango7 is required for _dronc_-dependent dendrite pruning

To determine the extent to which *tango7*-dependent control of *dronc* activity is used in other physiological contexts, we examined the role of *tango7* in *dronc*-dependent pruning of dendritic arborizations during metamorphosis. Dendrites of the class IV ddaC sensory neurons are pruned in an ecdysone-dependent manner, and this pruning involves remodeling of the cortical F-actin cytoskeleton[16,44-46]. We found, consistent with earlier reports[16,17,44,45], that blocking ecdysone signaling or loss of *dronc* disrupted dendritic pruning (Fig. 5a-d); however, in contrast to a previous report[16], we found that pruning occurred normally in *dark* mutant animals (Fig. 5g). Our result is consistent with axonal pruning in mammals, which requires caspase-9 activity, but not Apaf-1[14]. We also found that loss of *drice* did not block dendrite pruning (Fig. 5h), while knockdown of *tango7* did (Fig. 5e,f). Although ddaC sensory neurons formed fewer dendritic branches upon knockdown of *tango7*, these branches were not properly pruned. These results demonstrate that the caspase cascade and regulatory mechanisms we defined in larval salivary glands also function during dendrite pruning, suggesting that the *tango7*-dependent pathway outlined here may represent a conserved and widely-utilized mechanism for regulating cortical functions of caspases.

Caspase-dependent control of elasticity and timely secretion

In dying salivary glands, cortical F-actin is likely dismantled as a step toward cellular demolition; however, the function of F-actin breakdown in glands at the end of larval development was unclear. To understand why the cortical F-actin cytoskeleton is dismantled at the end of larval development, we first examined the most conspicuous function of glands at this stage: the secretion of mucin-like “glue” proteins. Glue secretion

occurs in two discrete steps: first, exocytosis of glue-containing vesicles from acinar cells to the lumen (Fig. 6a); and second, expulsion of glue proteins from the lumen to the exterior, allowing the soon-to-be stationary pupa to adhere to a solid surface (Fig. 6b). Exocytosis of glue-containing vesicles has recently been shown to require the actin cytoskeleton[47,48]. However, imaging and western blot analysis showed that glue exocytosis occurred normally in *dronc* mutant glands (Supplementary Fig. 7), indicating that *dronc*-dependent breakdown of cortical F-actin is not required for this step of glue secretion.

Exocytosis of glue proteins results in a dramatic morphological change in the salivary glands. By -1 h PF, glue exocytosis is nearly complete, but expulsion from the lumen onto the animal surface has not yet occurred. As a result, all of the secretory content is held within the lumen of the glands (Fig. 6a). Glue proteins are hygroscopic mucins which increase considerably in volume upon contact with water; therefore, the exocytosis and accumulation of secretory content resulted in a dramatic expansion of the lumen of the salivary glands (Fig. 6c,d). Luminal expansion began at -4 h PF: the same time as F-actin breakdown, raising the question of whether there is a functional relationship between these two processes. We found that mutants of the ecdysone primary response gene *BR-C* (*rbp*^{5}) produce very few glue-containing vesicles; however, the vesicles that are produced are secreted normally. A reduced load of secretory content results in only slight luminal expansion in these glands, enabling a more detailed analysis of F-actin breakdown. Importantly, we found that F-actin is still dismantled in *rbp*^{5} mutant salivary glands (Supplementary Fig. 8a), indicating that F-actin does not passively break as a result of luminal expansion. Additionally, high magnification analysis reveals clear

“fraying” of the F-actin structure at -1 h PF, causing F-actin to drop away from the cortex; this fraying is accompanied by complete dissolution of the F-actin meshwork (Supplementary Fig. 8b). Importantly, the fraying of F-actin is blocked in *rbp*^{5} mutant salivary glands upon overexpression of *diap1* or RNAi knockdown of *rpr* or *tango7*, further confirming that this process is caspase-dependent (Supplementary Fig. 8c), and suggesting that caspases may sever F-actin branchpoints during the breakdown process. Taken together, these results demonstrate that F-actin dismantling is an independently-regulated process during salivary gland development.

We next tested if F-actin played a role in the second step of glue secretion: expulsion from the lumen onto the surface of the animal. Interestingly, the lumen of *dcp-1* mutant or *tango7* knockdown glands, which both failed to dismantle cortical F-actin, did not expand upon glue exocytosis (Fig. 5c,d; Supplementary Fig. 9), raising the possibility that F-actin dismantling facilitates “stretching” of the glands to accommodate increasing amounts of secretory content in the lumen. Consistently, at PF, when all cortical F-actin is gone, wild type salivary glands were extremely “elastic” and could easily be stretched well beyond their normal length (Fig. 5e). In contrast, glands at -8 h PF, with an intact cortical F-actin cytoskeleton, tore when pulled (Fig. 5e). Finally, *dcp-1* mutant salivary glands precociously expelled their secretory content prior to the onset of metamorphosis (Fig. 5f), indicating that the retained rigidity of the F-actin cytoskeleton in these animals did not permit luminal expansion to accommodate the large volume of secreted glue proteins. These results highlight a novel aspect of exocrine biology, in which caspase-dependent remodeling of cortical F-actin in acinar cells regulates tissue elasticity and facilitates storage of luminal content prior to its timely expulsion.

DISCUSSION

Principles that govern the activation and function of caspases have fallen short in providing an understanding for how these enzymes can be activated to perform both delicate intracellular remodeling in living cells and total destruction in dying cells. In this paper, we provide new insights into the mechanisms that regulate caspase activation by comparing two completely different biological outcomes in the same tissue that both require caspase function. We show that the *Drosophila* homolog of caspase-9, *dronc*, is required for dismantling of the cortical F-actin cytoskeleton during salivary gland development—a role that is distinct from its known function in the salivary gland death response during metamorphosis. By systematically dissecting the regulation of *dronc* function at the cortex, we show that cortical functions of *dronc* are regulated independently from its cytoplasmic functions. The cytoplasmic functions of activated *dronc* require the canonical adaptor protein *dark*, while the cortical roles of *dronc* require *tango7*. In this manner, *tango7* and *dark* restrict the function of *dronc* to distinct subcellular domains. Moreover, we also show that these two functions can be initiated independently through differential amplification of IAP-antagonist expression, providing a model for how lethal and vital roles of caspases can be differentially activated in the same cell. Finally, we identify a new non-apoptotic function for caspases in the control of tissue elasticity to accommodate buildup of secreted products in the lumen of secretory tissues, facilitating their timely release.

Our results demonstrate that caspases can be activated in distinct, mutually-exclusive subcellular domains within a single cell, and that these subcellular domains are generated by use of unique caspase adaptor proteins. Local activation of caspases, as

detected by staining with antibodies to activated caspases, has been reported before[16-18,20,49]; however, here we demonstrate that local activation is achieved by targeting caspases to subcellular domains, and this targeting is necessary for subcellular functions of these caspases. Importantly, we show that caspases can be activated specifically in one domain without being activated in another, providing a mechanism that allows control of caspase activity with a previously unknown level of subcellular precision. However, the mechanisms that restrict caspase cascades to distinct subcellular compartments remain unclear. It is possible that caspase expression levels are intentionally kept low during non-lethal responses, and localized enrichment mediates subcellular-domain specific activation. For example, if most of the Dronc protein present in the cell localizes to the cortex, then this specific localization may restrict caspase functions to the cortical compartment. This model fits with our results at the end of larval development; however, in dying glands, caspases are independently activated in cortical and cytoplasmic compartments, suggesting that additional mechanisms are in play to restrict caspase activity to the appropriate subcellular compartment. For example, it is possible that caspase cascades occur within a physical complex consisting of initiator caspases, their adaptor proteins, effector caspases, and their substrates. In this model, only one of these proteins, likely the initiator caspase, would need to be subcellularly localized in order to generate a compartment-specific caspase cascade. However, resolution of this possible mechanism will require further studies. This subcellular domain-specific model for caspase activation contrasts with the commonly-held belief that activated caspase cascades passively perpetuate themselves and spread throughout the cell, and also

opens the possibility that caspases, through specific subcellular localization mediated by adaptor proteins, may play a role in many yet-to-be-identified biological processes.

We demonstrate that differential amplification of IAP-antagonists at specific developmental stages determines lethal vs. non-lethal outcomes of caspase activation. In our system, differential amplification is accomplished through the use of transcription factors that function downstream of a steroid hormone signal. However, caspases must have an ability to “sense” the magnitude of the IAP-antagonist pulse, ensuring that they initiate the appropriate lethal or non-lethal responses. One possible “sensing” mechanism may involve the aforementioned selectivity of initiator caspase adaptor proteins, like we observed with *tango7* and *dark*. In this model, some adaptor protein complexes would require a lower IAP-antagonist threshold for initiator caspase activation than others. However, elucidation of the detailed molecular mechanisms mediating “sensing” of IAP-antagonist expression levels will require further study. Finally, our results indicate that small pulses of IAP-antagonist expression are tissue-specific, raising the possibility that many more of these pulses are generated in other tissues and developmental stages that have not yet been detected or characterized. Our data suggests that non-lethal, physiological functions of caspases may be more widespread than previously thought.

Our results show that caspases play a novel role during the secretion of glue proteins. Glue proteins are essential to allow a newly-formed prepupa to adhere to a solid surface; however, when cortical F-actin dismantling fails, glue precociously “leaks” onto the surface of the animal. Although precocious expulsion of glue does not appear to have a deleterious effect in the lab, in the wild, it may adversely affect fitness by inhibiting larval movement or reducing the ability of the animal to stick securely to a surface during

metamorphosis. Additionally, our results raise the question of whether other exocrine tissues in different species, such as the mammary gland, may utilize caspases in a similar manner to accommodate large amounts of secreted luminal products prior to their release.

In conclusion, systematic analysis of vital and lethal responses to caspase activation in the same cells has revealed mechanisms that allow caspases to be activated without killing the cell. Our results demonstrate that caspases can be activated in mutually-exclusive subcellular domains, where activation of caspases in one domain does not trigger activation of caspases in another domain. We show that these subcellular domains are generated by different caspase adaptor proteins. It is likely that yet-to-be-identified adaptor proteins define other subcellular domains and, in so doing, help regulate the many physiological functions of caspases. Moreover, our results demonstrate that some of these subcellular domains have lower thresholds for activation of caspases, thereby allowing sublethal pulses of IAP-antagonists to selectively initiate physiological functions of caspases. Together, these results outline a simple conceptual framework for controlling caspase activation during normal development and physiology.

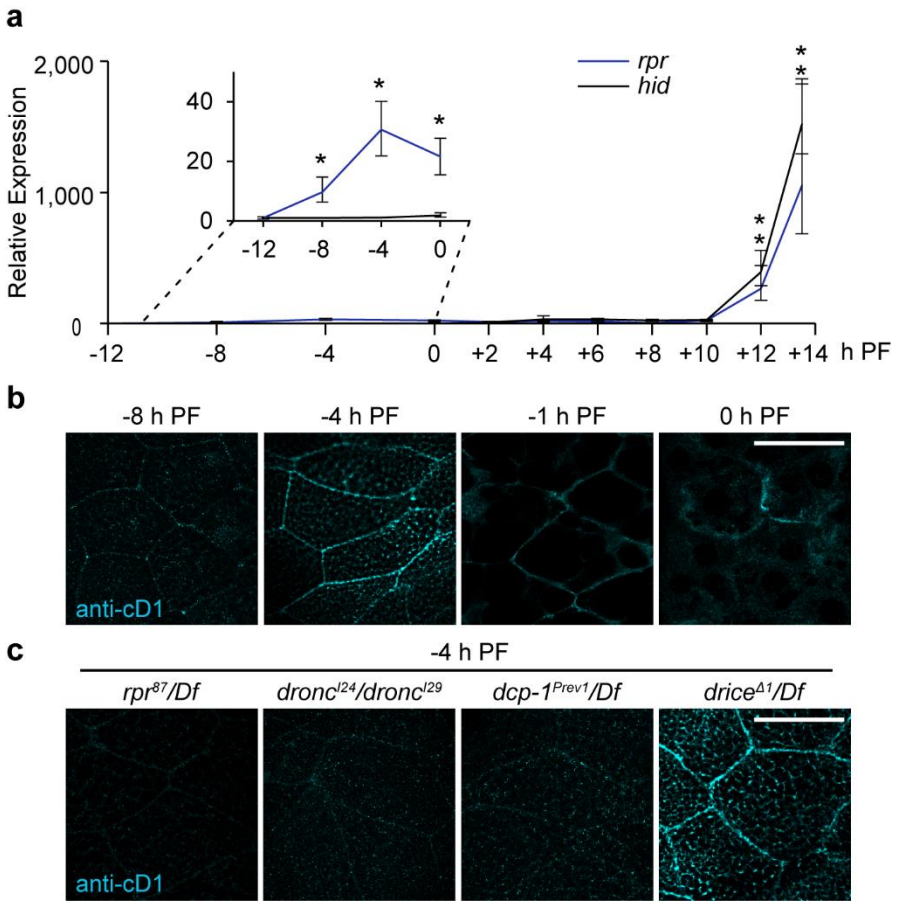

Figure 1. A low amplitude pulse of *reaper* (*rpr*) triggers caspase activation at the cortex of salivary glands. (a) qPCR analysis of *rpr (*blue line) and *head involution defective* (*hid*) (black line) expression in salivary glands at the onset of metamorphosis. Both *rpr* and *hid* are induced >1000-fold at the start of pupal development, while only *rpr* is induced (~30-fold) at the end of larval development. *y*-axis shows relative expression; *x*-axis shows developmental stage in hours relative to the onset of metamorphosis (puparium formation: PF). Expression levels shown relative to the lowest point for each gene and normalized to the reference gene *rp49*. Three biological samples analyzed for each stage; error bars represent standard error determined by REST analysis (see Methods); asterisks indicate *p*-value <0.05 calculated by REST analysis. **(b)** Timecourse

of cleaved-Dcp1 (anti-cD1) antibody staining in salivary glands at the end of larval development. Anti-cD1, in cyan, does not exhibit specific staining at -8 h PF, but stains strongly at the cortex at -4 h PF. Cortical staining of cD1 persists through -1 h PF, but diminishes at 0 h PF. **(c)** Regulation of anti-cD1 cortical staining in salivary glands at -4 h PF. Cortical cD1 staining is absent in *rpr*, *dronc*, and *dcp-1* mutant salivary glands, but present in *drice* mutant salivary glands. Scale bars represent 100μm. PF: Puparium Formation; Df: Deficiency.

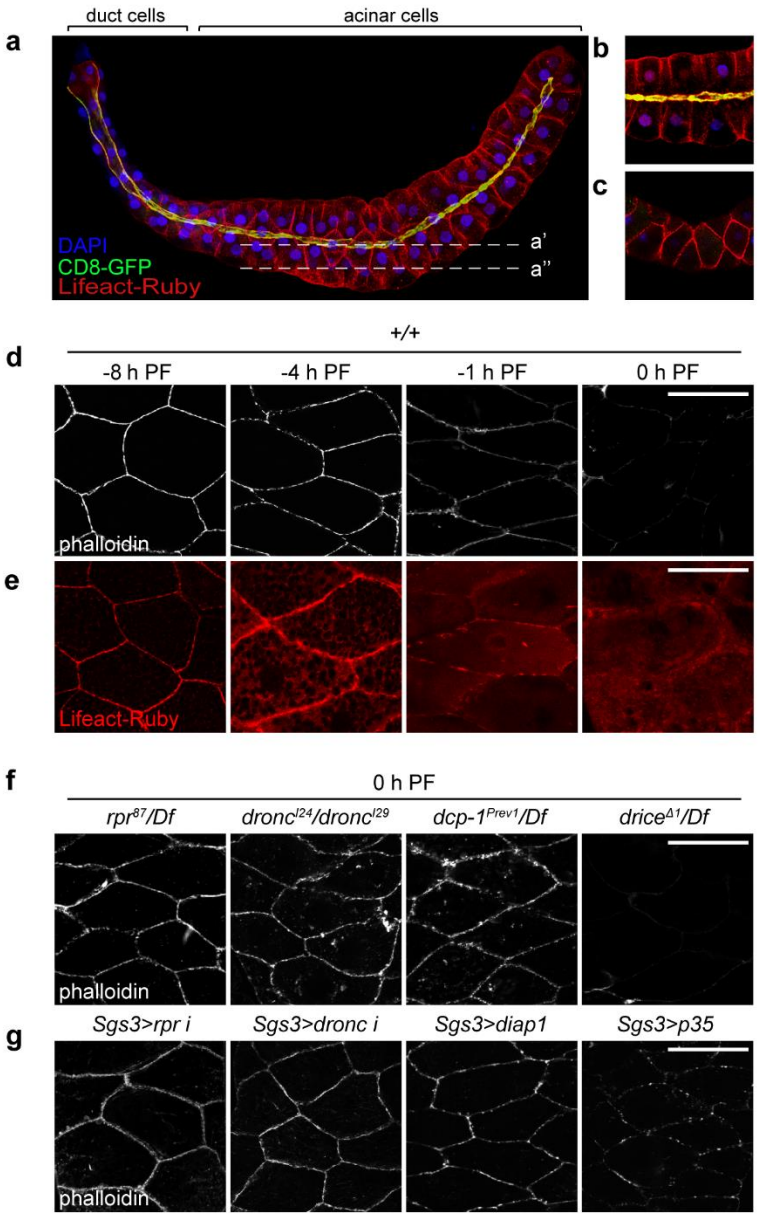

Figure 2. A *rpr*-triggered caspase cascade dismantles the cortical F-actin cytoskeleton in living salivary glands. (a) Maximal intensity projection of a whole salivary gland at -8 h PF expressing the actin-binding peptide Lifeact-Ruby in red and the membrane marker CD8-GFP in green, both under control of the salivary gland driver *fkh-GAL4*. CD8-GFP is enriched at the apical membrane (proximity of Lifeact-Ruby and CD8-GFP at the apical membrane appears yellow); nuclei stained by DAPI in blue. **(b-c)**

Confocal slices through the salivary glands. **(b)** A medial slice shows an apical-basal view of acinar cells, with the lumen in the middle. **(c)** A lateral slice shows a “coronal” view, highlighting the cortical F-actin cytoskeleton. **(d-e)** Cortical F-actin breaks down at the end of larval development. **(d)** Phalloidin staining (white) in salivary glands at -8 h PF reveals tight cortical bundles of F-actin; this structure begins to disintegrate at -4 h PF and -1 h PF, with no phalloidin staining visible by 0 h PF. **(e)** Lifeact-Ruby in salivary glands confirms cortical F-actin breakdown. Lifeact-Ruby reveals that most of the actin in the cell is present at the cortex at -8 h PF. Breakdown of F-actin is reflected by a gradual redistribution of Lifeact-Ruby signal from the cortex to the cytoplasm at -4 h PF and -1 h PF, with only cytoplasmic signal visible at 0 h PF. **(f)** F-actin dismantling requires caspase activity. F-actin breakdown is blocked in *rpr*, *dronc*, and *dcp-1* mutant salivary glands, but not in *drice* mutant salivary glands. **(g)** Caspases regulate F-actin breakdown cell-autonomously. Salivary gland-specific (using *Sgs3-GAL4*) overexpression of *rpr-RNAi*, *dronc-RNAi*, or of the caspase inhibitors *diap1* or *p35* inhibits F-actin breakdown. Scale bars represent 100µm. Df: Deficiency; PF: Puparium Formation.

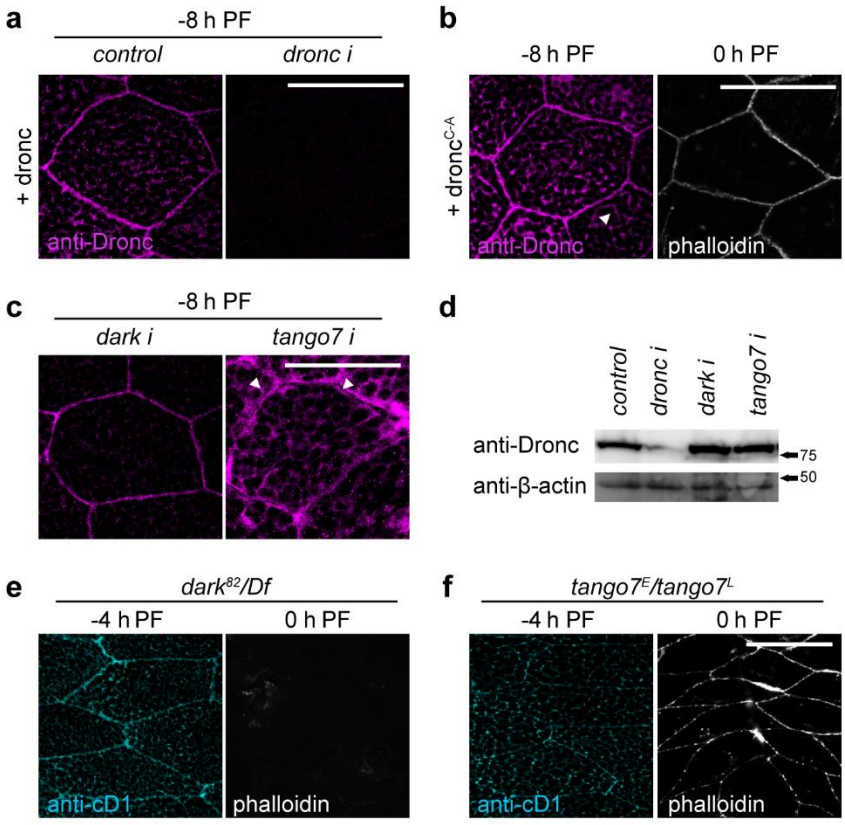

Figure 3. *tango7* is required for cortical localization and activity of Dronc in living salivary glands. (a) Dronc localizes to the cortex of salivary glands at the end of larval development. Immunofluorescent staining using an antibody to detect Dronc protein (anti-Dronc, in magenta) in salivary glands overexpressing *dronc* under control of *Sgs3-GAL4* (+*dronc*) shows that Dronc localizes to the cortex of salivary gland cells at -8 h PF. Co-expression of *dronc-RNAi* abolishes anti-Dronc staining. **(b)** F-actin dismantling requires Dronc catalytic activity. Anti-Dronc staining in salivary glands overexpressing a catalytically-inactive Dronc (+*dronc*$^{C\text{-}A}$, in magenta) under control of *Sgs3-GAL4* reveals that Dronc$^{C\text{-}A}$ still localizes to the cortex at -8 h PF. However, phalloidin staining, in white, shows that F-actin does not break down in these glands at 0 h PF. **(c)** *tango7*, not *dark*, regulates cortical localization of Dronc. Anti-Dronc staining, in magenta, in salivary glands

overexpressing *dronc* under control of *Sgs3-GAL4* shows that Dronc still localizes to the cortex upon co-expression of RNAi against *dark*. In contrast, *tango7* RNAi knockdown causes Dronc to diffuse away from the cortex toward the cytoplasm, with clear gaps lacking anti-Dronc staining visible at the cortex (white arrowheads). The cytoplasm at this stage is filled with secretory granules (black “spots”). **(d)** Dronc levels are not reduced in *tango7*-RNAi salivary glands. Western blot analysis of Dronc protein expression levels in *dronc-RNAi*, *dark-RNAi*, and *tango7-RNAi* salivary glands (under control of *Sgs3-GAL4*) shows that Dronc levels are dramatically reduced upon overexpression of *dronc-RNAi*, but are not decreased upon expression of *dark-RNAi* or *tango7-RNAi*. Salivary glands were dissected at -8 h PF; β-actin used as loading control. **(e-f)** *tango7*, not *dark*, is required for cortical caspase activation and dismantling of F-actin. **(e)** Cortical anti-cD1 staining, in cyan, is not disrupted in *dark* mutant salivary glands at -4 h PF. Phalloidin staining, in white, shows that F-actin breaks down normally in *dark* mutant salivary glands. **(f)** In contrast, cortical anti-cD1 staining is abolished at -4 h PF and F-actin fails to break down at 0 h PF in *tango7* mutant salivary glands. Scale bars represent 100µm. Df: Deficiency; PF: Puparium Formation.

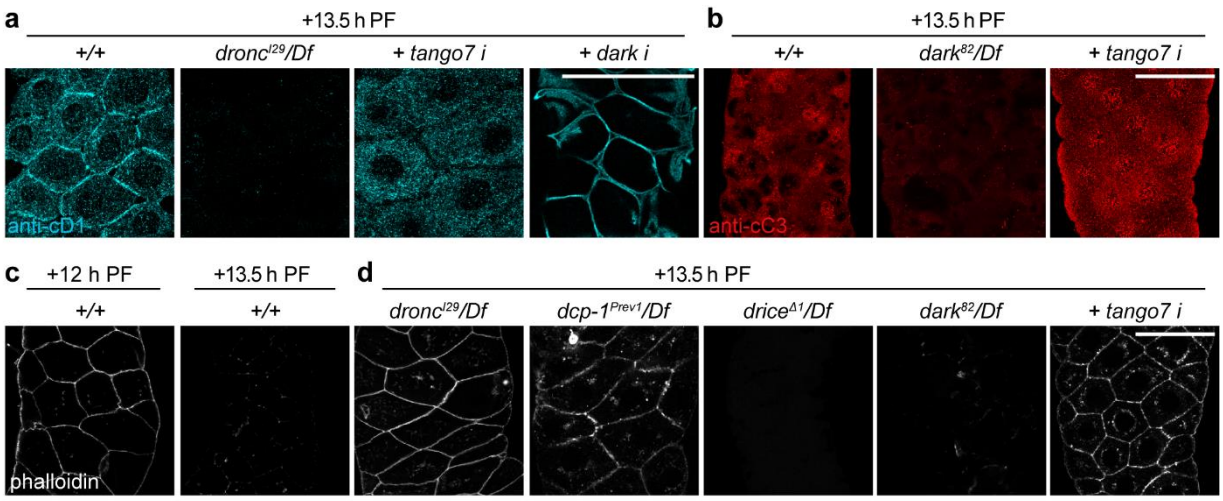

Figure 4. Subcellular domains of caspase activation are independently regulated in dying salivary glands. (a) *tango7* and *dark* regulate mutually-exclusive subcellular domains of caspase activation in dying glands. Anti-cD1 staining, in cyan, is visible at both the cortex and in the cytoplasm of control salivary glands at +13.5 h PF; both cortical and cytoplasmic staining is lost in *dronc* mutant salivary glands. Salivary-gland specific knockdown of *tango7* (with *Sgs3-GAL4*) does not affect cytoplasmic anti-cD1, but disrupts cortical anti-cD1. In contrast, salivary-gland specific knockdown of *dark* (with *fkh-GAL4*) disrupts cytoplasmic anti-cD1 but not cortical anti-cD1. **(b)** Cleaved caspase-3 (anti-cC3, in red), a diagnostic marker of caspase activation and apoptosis, does not require *tango7*. Anti-cC3 staining is visible only in the cytoplasm of control glands at +13.5 h PF; this staining is lost in *dark* mutant animals. However, anti-cC3 staining is unaffected upon salivary gland-specific RNAi knockdown of *tango7* (using *Sgs3-GAL4*). **(c)** Cortical F-actin is dismantled in dying salivary glands. The cortical F-actin cytoskeleton is intact in control salivary glands at +12 h PF, just prior to the death response (phalloidin, in white). However, phalloidin staining shows that F-actin is dismantled at +13.5 h PF. **(d)** F-actin dismantling during the death response requires *dronc*, *dcp-1*, and *tango7*. Phalloidin

staining, in white, indicates that F-actin breakdown is disrupted in *dronc* and *dcp-1* mutant and *tango7-RNAi* (*Sgs3-GAL4*) salivary glands at +13.5 h PF, but F-actin breakdown is unaffected in *drice* and *dark* mutant salivary glands. Scale bars represent 100µm. Df: Deficiency; PF: Puparium Formation.

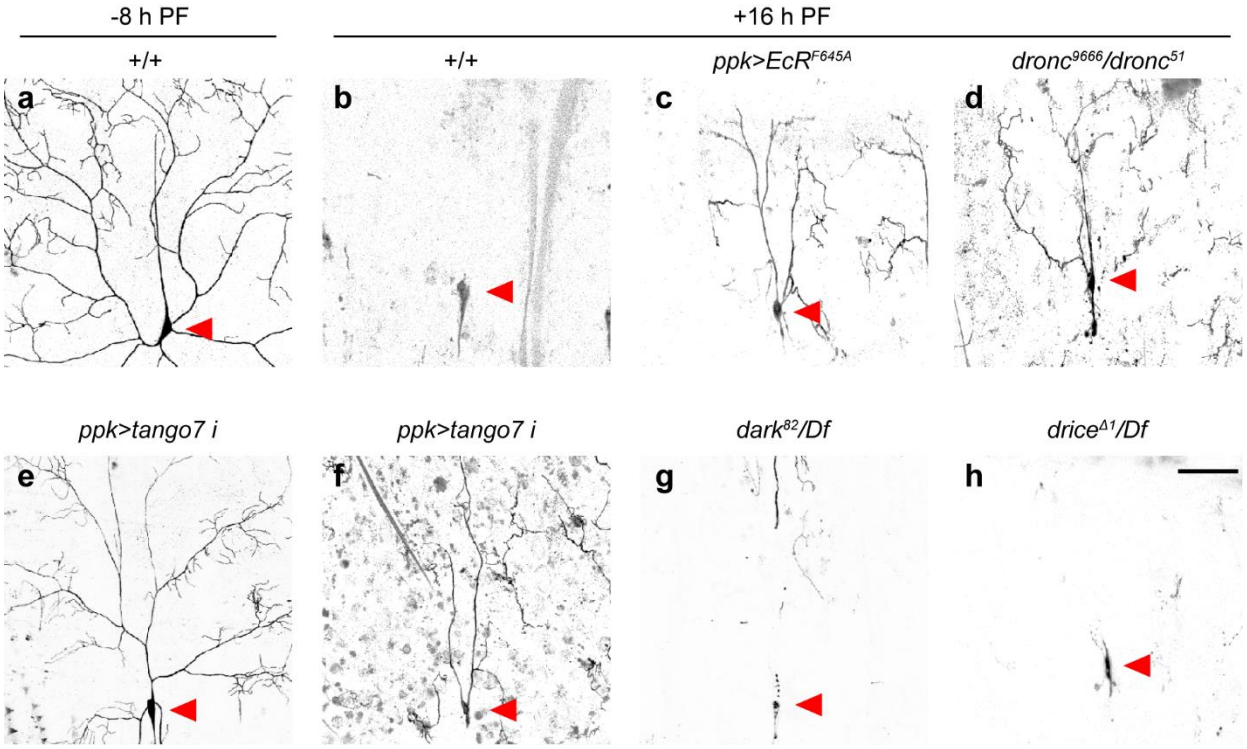

Figure 5. Caspase-dependent pruning of class IV ddaC dendrites during metamorphosis requires *tango7* but not *dark*. (a-b) Dendritic arborizations, visualized by *ppk-GAL4*-driven expression of GFP, are present at -8 h PF **(a)**, but are completely pruned by +16 h PF **(b)**. **(c-d)** Expression of a dominant-negative ecdysone receptor (*EcR*^{F645A}) using *ppk-GAL4* **(c)** or mutation of *dronc* **(d)** disrupts pruning at +16 h PF. **(e-f)** Fewer dendritic arborizations form at -8 h PF upon RNAi knockdown of *tango7* (using *ppk-GAL4*) **(e)**; however, these branches are not properly pruned at +16 h PF **(f)**. **(g-h)** Dendritic pruning occurs normally in *dark* **(g)** or *drice* **(h)** mutant animals. Red arrowheads indicate the soma of ddaC neurons. Scale bars represent 100µm. Df: Deficiency; PF: Puparium Formation.

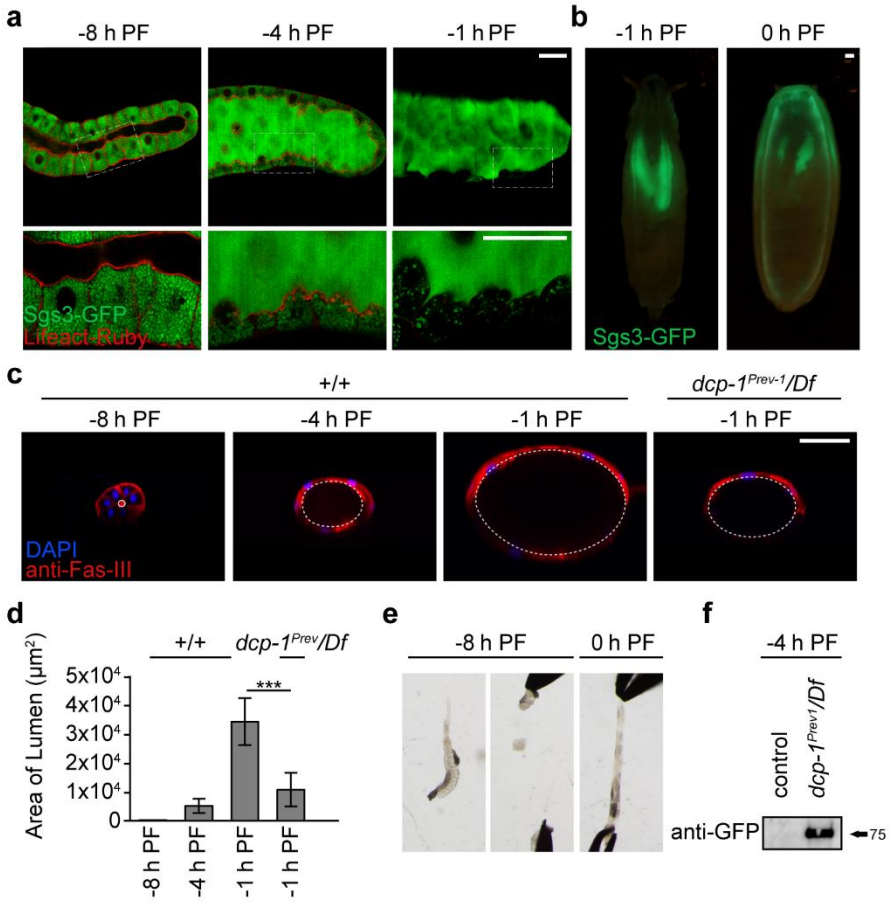

Figure 6. Cortical caspase activation in living salivary glands controls tissue elasticity during expulsion of mucin-like glue proteins. (a) Dismantling of cortical F-actin in acinar cells coincides with secretion of glue proteins; boxed areas imaged at higher magnification below. At -8 h PF, glue proteins (Sgs3-GFP, in green) are present only in the cells of the salivary gland. At -4 h PF, exocytosis of glue proteins from cells into the lumen begins; by -1 h PF, all glue is present in the lumen. Lifeact-Ruby, in red, shows that F-actin begins to break down at -4 h PF, and dismantling is nearly complete by -1 h PF. Salivary glands were imaged live/unfixed. **(b)** Glue proteins present in the lumen at -1 h PF are expelled onto the surface of the animal at 0 h PF. **(c-d)** The lumen increases dramatically in size during glue exocytosis, and luminal expansion requires

caspase activity. **(c)** Transverse view of salivary glands shows luminal expansion during glue secretion. Fasciclin-3 staining (anti-Fas-III, in red) marks septate junctions, nuclei stained with DAPI in blue. At -8 h PF, salivary glands have a narrow lumen; however, as glue exocytosis progresses, the lumen expands dramatically until reaching maximal size at -1 h PF. The lumen of *dcp-1* mutant salivary glands does not expand normally. **(d)** Quantification of luminal area for stages and genotypes shown in c (n=10 per timepoint, error bars indicate s.d., asterisks indicate p<0.01 determined by one-tailed t-test). **(e)** Salivary gland elasticity is developmentally-controlled. At -8 h PF, salivary glands are rigid and tear at the slightest pull. In contrast, 0 h PF salivary glands can be stretched beyond their normal length. Equal force was applied to each stage; n=20 tested per stage. **(f)** Luminal expansion is critical for timely expulsion of glue proteins. Glue expulsion normally occurs after larvae become stationary. Control wandering larvae at -4 h PF do not expel glue, while *dcp-1* mutant larvae precociously expel glue at this stage. Expelled glue proteins (in Sgs3-GFP animals) were collected and measured by western blot with anti-GFP antibodies. Scale bars represent 100μm. Df: Deficiency; PF: Puparium Formation.

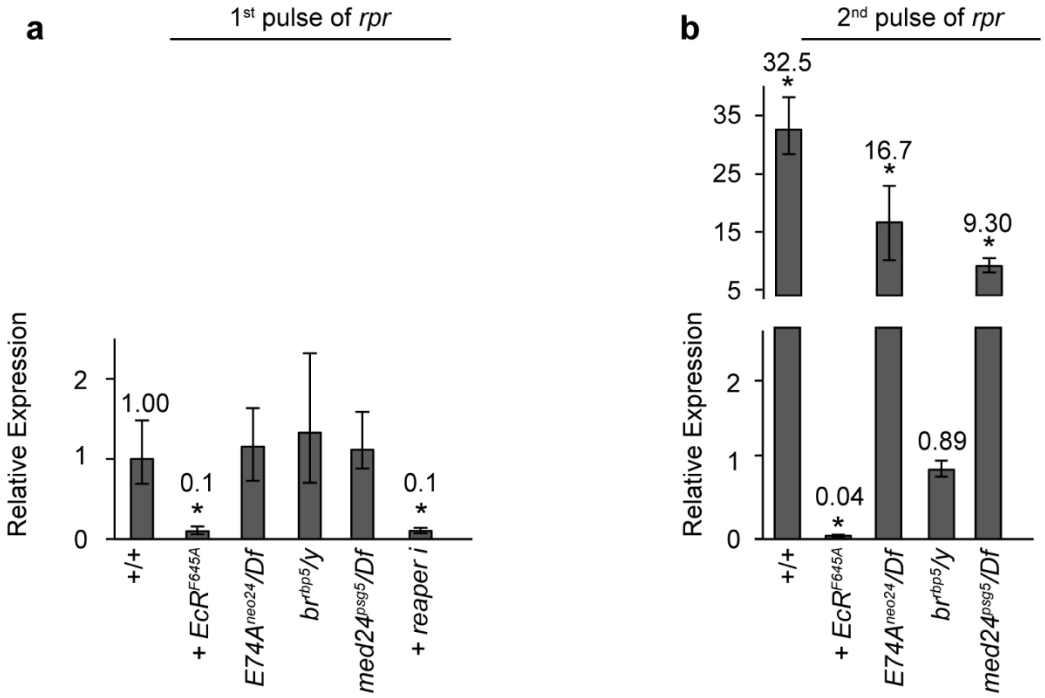

Supplementary Figure 1. Differential amplification of *reaper* (*rpr*) pulses in salivary glands. Genetic control of the two ecdysone-triggered pulses of *rpr* in salivary glands at the onset of metamorphosis. **(a)** The small pulse of *rpr* at the end of larval development depends on ecdysone but is independent of the canonical regulators of ecdysone-triggered transcription. qPCR analysis of *rpr* mRNA levels in salivary glands dissected at 0 h PF and normalized to *rpr* levels in controls. We chose to synchronize the animals at 0 h PF to avoid potential complications with developmental timing in different mutant backgrounds. Expression of either the dominant negative ecdysone receptor (*EcRF645A*) or *rpr-RNAi* (using the salivary gland-specific *Sgs3-GAL4* driver) effectively disrupts the pulse of *rpr*. However, glands dissected from *E74A*, *BR-C*, or *Med24* mutant animals still induce *rpr* at levels comparable to control glands. **(b)** The larger pulse of *rpr* during programmed cell death, at +13.5 h PF, requires the canonical regulators of ecdysone signaling to amplify the transcriptional response. qPCR analysis of *rpr* mRNA expression

from salivary glands dissected at +13.5 h PF. Data was normalized to the small pulse of *rpr* at -4 h PF in wild type glands (*i.e.* the second pulse is 32.5-fold larger than the first one). As with the first pulse, expression of *EcRF645A* effectively disrupts the second pulse of *rpr*. Glands dissected from *E74A*, *BR-C*, and *Med24* mutant animals significantly reduce the induction of *rpr*; however, *rpr* is still induced at, or higher than, the levels of the first pulse (*y*-axis is split to facilitate comparison with the first pulse). *y*-axis shows relative expression; *x*-axis shows genotypes being analyzed. Expression for panel a shown relative to control at 0 h PF; panel b shown relative to -4 h PF; all samples normalized to the reference gene *rp49*. Three biological samples analyzed for each stage; error bars represent standard error determined by REST analysis (see Methods); asterisks indicate *p*-value <0.05 calculated by REST analysis. Df: Deficiency.

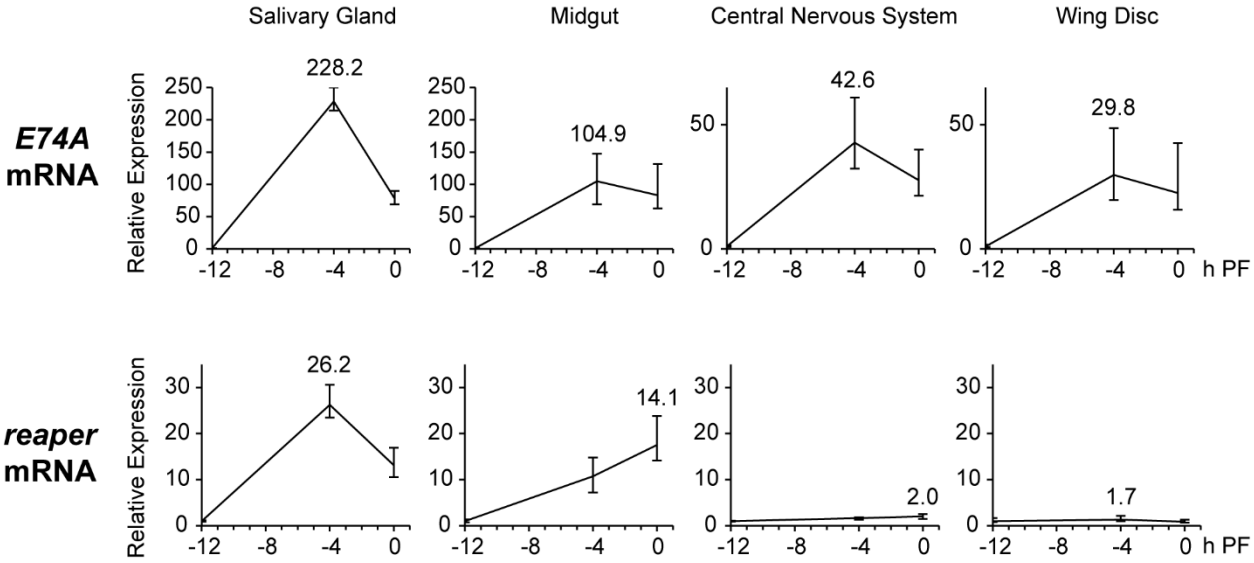

Supplementary Figure 2. Tissue-specific induction of *rpr* at the end of larval development. qPCR analysis of paired tissues (dissected from the same animals) at -12, -4, and 0 h PF. All examined tissues (salivary gland, midgut, central nervous system, wing disc) induce the ecdysone primary response gene *E74A*, indicating a robust ecdysone response. However, only the salivary glands and midgut induce *rpr* expression; no significant change in *rpr* levels is observed in the central nervous system or wing discs. The *y*-axis shows relative expression; the *x*-axis shows developmental stage in hours relative to puparium formation (PF). All samples were normalized to the reference gene *rp49*. Expression shown relative to levels at -12 h PF. Three biological samples analyzed for each stage; error bars represent standard error determined by REST analysis (see Methods). PF: Puparium Formation.

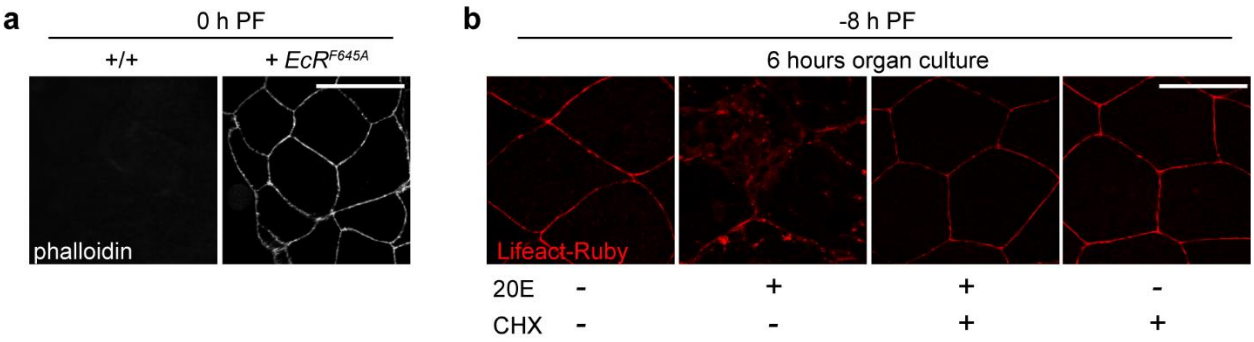

Supplementary Figure 3. Ecdysone is necessary and sufficient for dismantling of cortical F-actin in salivary glands at the end of larval development. (a) Ecdysone signaling is necessary for cortical F-actin breakdown. Phalloidin staining, in white, shows that F-actin is dismantled in control glands at puparium formation (0 h PF), but when ecdysone signaling is blocked by salivary gland-specific (*Sgs3-GAL4*) expression of a dominant negative ecdysone receptor (*EcRF645A*), F-actin does not break down. **(b)** The steroid hormone ecdysone is sufficient to trigger cortical F-actin breakdown in *ex vivo* cultures. Salivary glands dissected at -8 h PF do not dismantle F-actin, shown by the actin marker Lifeact-Ruby in red, after 6 hours in *ex vivo* culture. Under the same conditions, addition of 20-hydroxyecdysone (20E, *a.k.a.* ecdysone) triggers F-actin dismantling. Coculture of 20E with the translational inhibitor cycloheximide (CHX) prevents ecdysone-triggered dismantling of cortical F-actin, indicating that translation of ecdysone-induced transcripts regulates F-actin breakdown. Finally, cycloheximide alone does not dismantle the cortical F-actin cytoskeleton. All samples were cultured simultaneously and repeated in $n>20$; glands were fixed for imaging. Scale bars represent 100μm. PF: Puparium Formation; 20E: 20-hydroxyecdysone/ecdysone; CHX: cycloheximide.

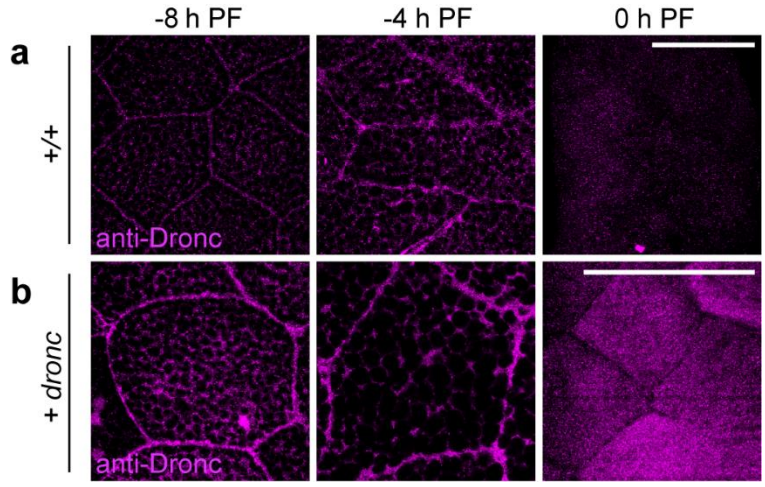

Supplementary Figure 4. Subcellular localization of Dronc in salivary gland cells. **(a)** Immunofluorescent staining for Dronc protein (anti-Dronc, in magenta) in wild type salivary glands shows that endogenous Dronc localizes to the cell cortex at -8 and -4 h PF; however, this cortical localization is lost at 0 h PF. **(b)** Immunofluorescent staining for Dronc protein (anti-Dronc, in magenta) in salivary glands overexpressing Dronc (+*dronc*; with *Sgs3-GAL4* driver) shows similar cortical localization of Dronc protein at -8 and -4 h PF; anti-Dronc staining is lost from the cortex and becomes cytoplasmic at 0 h PF. Scale bars represent 100μm. PF: Puparium Formation.

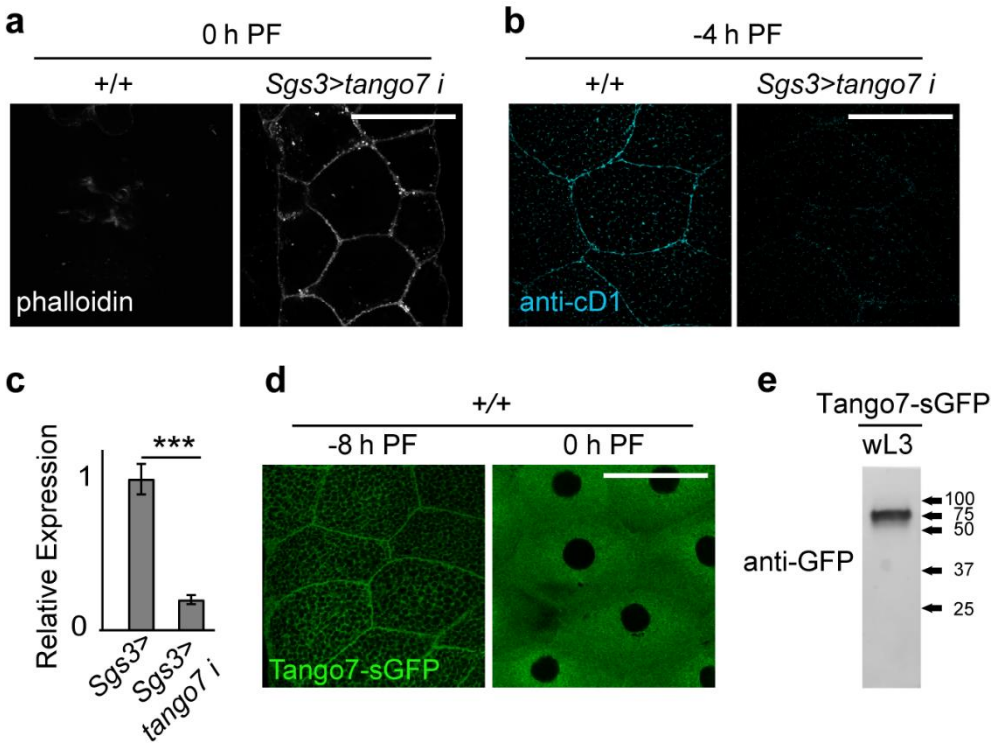

Supplementary Figure 5. *tango7* regulates caspase-dependent F-actin breakdown in salivary glands at the end of larval development. (a) Salivary-gland specific knockdown of *tango7* (using the *Sgs3-GAL4* driver) blocks F-actin dismantling, assayed by staining for phalloidin in white, at 0 h PF. **(b)** *tango7-RNAi* disrupts cortical anti-cD1 staining, in cyan, at -4 h PF. **(c)** qPCR analysis of *tango7* mRNA expression levels in control and *tango7-RNAi* salivary glands at 0 h PF confirms that *tango7* expression levels are significantly reduced upon expression of the RNAi. *y*-axis shows relative expression; *x*-axis shows the genotypes analyzed. Expression levels shown relative to control salivary glands and normalized to the reference gene *rp49*. Three biological samples analyzed for each stage; error bars represent standard error determined by REST analysis (see Methods); asterisks indicate *p*-value <0.05 calculated by REST analysis. **(d)** An endogenously-regulated, superfolder GFP-tagged Tango7 (Tango7-sGFP, in green) shows that Tango7 protein localizes to the salivary gland cell cortex at -8 h PF; this cortical

localization is lost and Tango7-sGFP becomes cytoplasmic at 0 h PF. **(e)** Western blot analysis of Tango7-sGFP (using an anti-GFP antibody) shows a single band at the predicted molecular weight. Scale bars represent 100μm. PF: Puparium Formation.

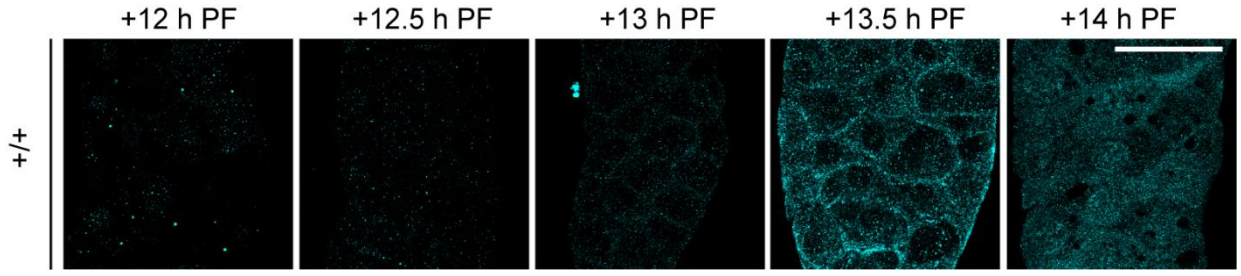

Supplementary Figure 6. Cortical anti-cD1 staining is a transient event during salivary gland cell death. Timecourse showing staining for anti-cD1, in cyan, in salivary glands every 30 min from +12 h PF to +14 h PF. No cortical or cytoplasmic staining is observed in +12, +12.5, or +13 h PF glands; however, +13.5 h PF glands exhibit robust cytoplasmic and cortical anti-cD1 staining. By +14 h PF, however, only cytoplasmic anti-cD1 staining is visible. PF: Puparium Formation.

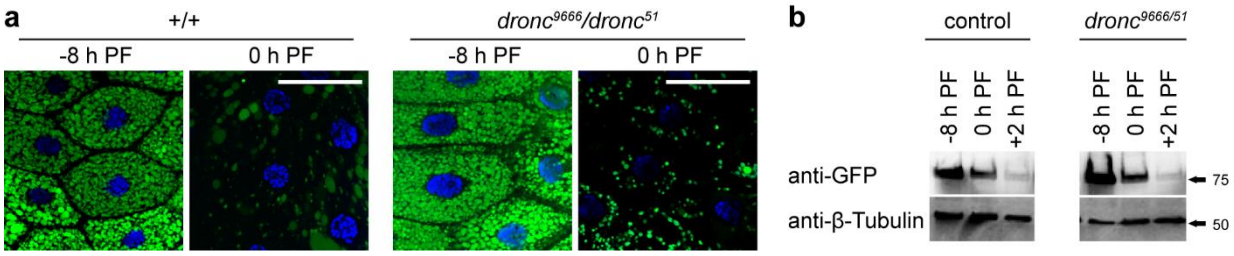

Supplementary Figure 7. *dronc* mutant salivary glands do not disrupt glue protein synthesis or secretion. (a) Live imaging of glue protein granules (visualized with Sgs3-GFP) before and after secretion in salivary glands. At -8 h PF, synthesized glue proteins are sequestered within secretory vesicles. At 0 h PF, when glue proteins are expelled onto the surface of the animal, there is little glue protein remaining inside salivary gland cells. *dronc* mutant glands are indistinguishable from control glands. **(b)** Assay of glue secretion using whole animal western blot analysis. Whole animals of appropriate stages were rinsed and analyzed for remaining glue proteins (western blots probed by anti-GFP and anti-Tubulin antibodies). In control animals, expulsion of glue proteins is completed by +2 h PF. Once again, *dronc* mutant glands are indistinguishable from control glands. All animals carry the *Sgs3-GFP* transgene; DNA stained with DAPI in blue. Scale bars represent 100μm. PF: Puparium Formation.

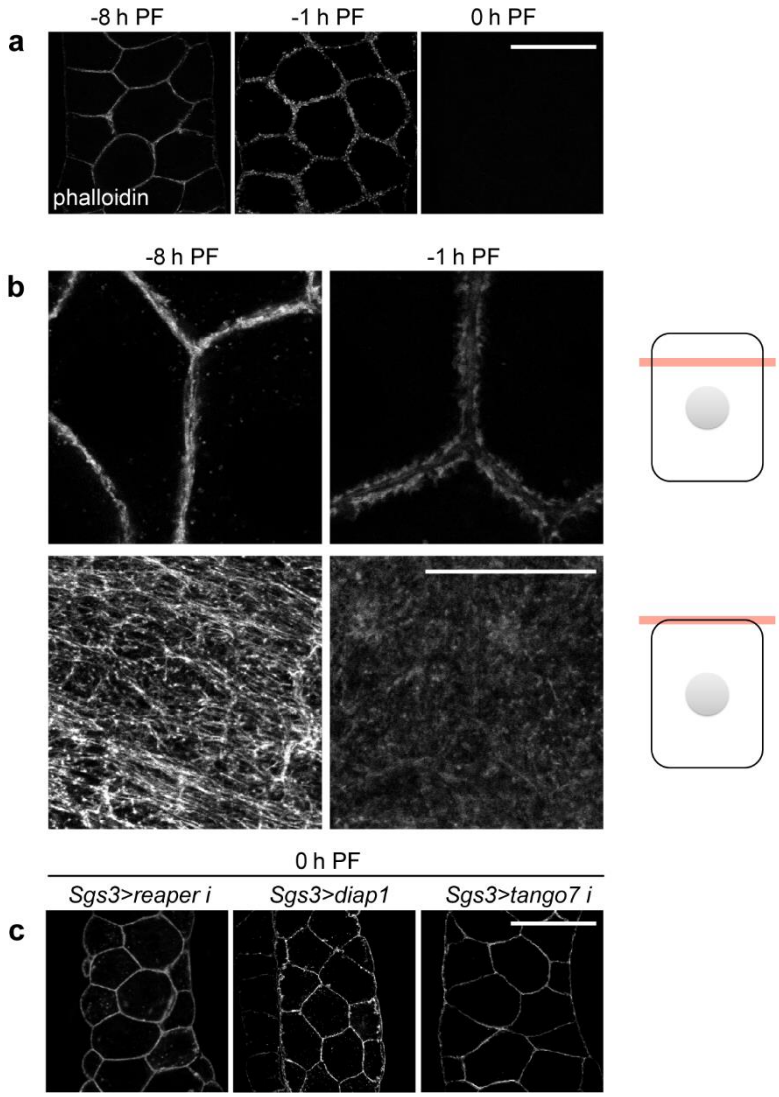

Supplementary Figure 8. Detailed analysis of F-actin breakdown in *rbp5* mutant salivary glands without luminal expansion. *rbp5*, a mutant of the ecdysone primary response gene *BR-C*, synthesizes and secretes very little glue protein; therefore, the lumen does not dramatically expand, enabling high-magnification analysis of F-actin breakdown. **(a)** Analysis of F-actin breakdown in *rbp5* mutant salivary glands. At -8 h PF, phalloidin staining, in white, shows F-actin in tight cortical bundles. By -1 h PF, the F-actin structure has begun to "fray," and by 0 h PF, F-actin is completely broken down. **(b)** High magnification analysis of F-actin structure in *rbp5* mutant salivary glands. At -8 h PF, a

coronal confocal slice shows F-actin tightly bundled at the cortex, while a slice at the surface of the basal membrane shows a clear F-actin meshwork on the surface of the cell. In contrast, at -1 h PF, F-actin has begun to “fray” and fall away from the cortex, and the meshwork has dissolved. Diagrams on right show focal plane being imaged within the cell; gray circle represents the nucleus. **(c)** F-actin breakdown is caspase-dependent in *rbp5* mutant salivary glands. F-actin dismantling is blocked at 0 h PF upon overexpression of *rpr-RNAi*, *diap1*, or *tango7-RNAi* using the *Sgs3-GAL4* driver in the *rbp5* mutant background. All images show phalloidin staining in white. Scale bars represent 100μm. PF: Puparium Formation.

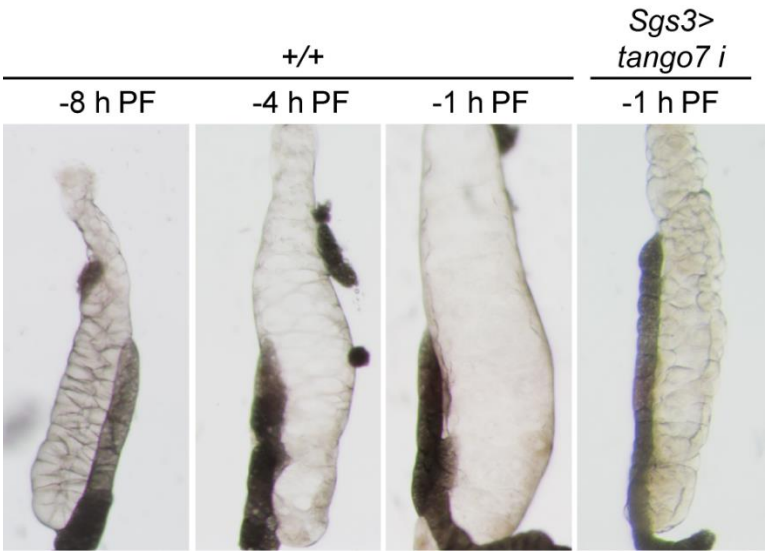

Supplementary Figure 9. Knockdown of *tango7* prevents salivary gland luminal expansion. Light microscope images of whole salivary glands during the end of larval development. Control glands are thin, with no luminal expansion, at -8 h PF. By -4 h PF, when glue exocytosis has begun, the lumen begins to expand, reaching maximal size at -1 h PF. In contrast, salivary glands expressing *tango7-RNAi* do not expand at -1 h PF. PF: Puparium Formation.

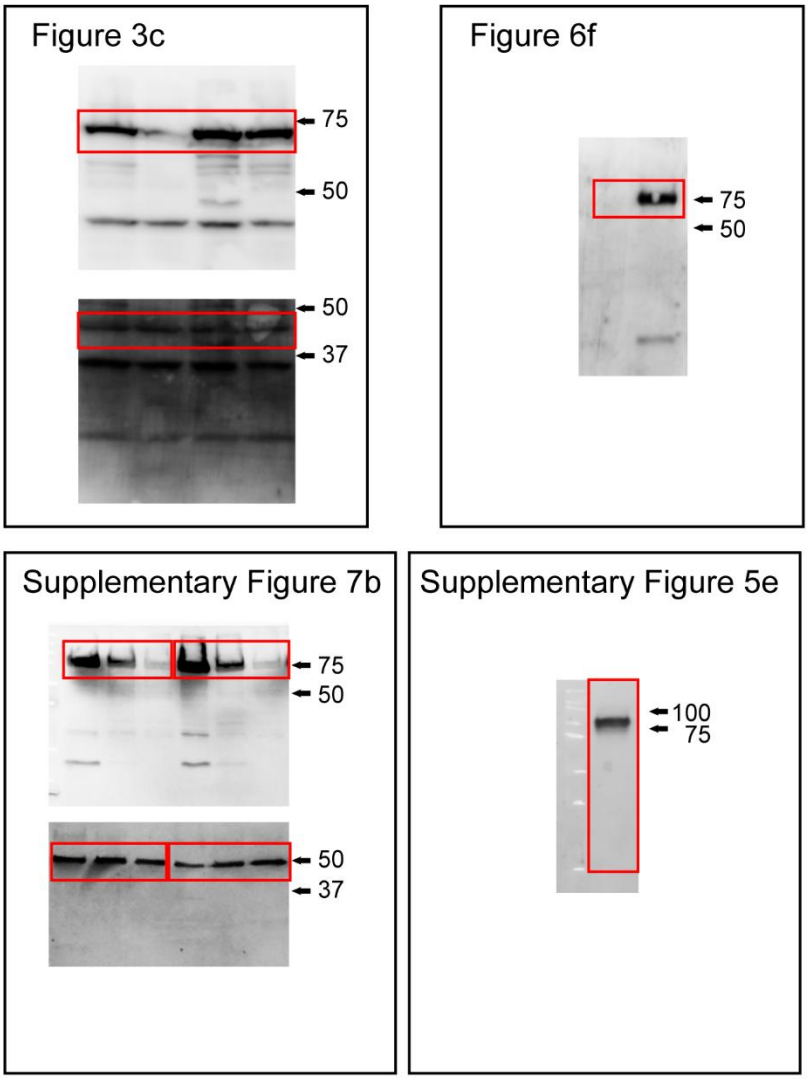

Supplementary Figure 10. Full-length western blots. For each blot, the red box indicates the portion that was cropped and displayed in the indicated figure.

METHODS

Fly strains and genetics

The following strains were obtained from the Bloomington *Drosophila* Stock Center: *Sgs3-GFP, Dronc*^{51}*, UAS-Lifeact-Ruby, Sgs3-Gal4, UAS-tango7-RNAi, E74A*^{neo24}*,* br^{rpb5}*, UAS-EcR*^{F645A}*, UAS-CD8-GFP, fkh-Gal4, ppk-Gal4, Df(3L)Exel6112* (for *med24*)*, Df(3L)81k19* (for *E74A*)*, Df(3R)BSC547* (for *drice*)*, Df(2R)BSC359* (for *dark*)*, Df(2R)BSC785* (for *dcp-1*)*, Df(3L)BSC282* (for *dronc*) *and Df(3L)H99* (for *rpr*)*.* The Vienna *Drosophila* RNAi Center provided *Tango7-sGFP* and the following RNAi lines: *UAS-dronc-RNAi, UAS-dark-RNAi, UAS-rpr-RNAi.* Colleagues in the fly community provided the following stocks: $dronc^{I24}$ and $dronc^{I29}$ [50], $drice^{\Delta 1}$ [51], $dark^{82}$ [42], $dcp\text{-}1^{Prev1}$ [52], $reaper^{87}$ [53], $UAS\text{-}dronc^{C\text{-}A}$ [54], $tango7^{E}$ and $tango7^{L}$ [38], $med24^{psg5}$ [26], *UAS-dronc-GFP*[34]. All crosses were performed at 25ºC in temperature-controlled incubators. Salivary gland-specific overexpression or RNAi-knockdown was performed with the *Sgs3-Gal4* driver unless otherwise noted. Wherever appropriate, control genotypes included an additional UAS transgene (*UAS-GFP*) to facilitate comparisons with experimental genotypes.

Developmental staging

All animals were raised at 25ºC on cornmeal molasses media with granulated yeast. For staging third instar larvae, we combined the standard ‘‘blue food’’ technique[55] with use of the mid-third instar transition-specific reporter, Sgs3-GFP[56]. For -8 h PF larvae, animals with “light blue” guts without glue secretion were collected. For -4 h PF, animals with “clear blue” guts and glue in the lumen were selected. Finally, for -1 h PF, we collected “clear” gut animals that were stationary with everted spiracles and soft cuticles. These staging

methods have been independently tested for timing to PF. For animals after PF, animals were collected at PF and aged for the appropriate time at 25ºC on a dampened filter paper plate. For stages at 12 hours PF or later, we collected animals that were synchronized at head eversion (equivalent to 12 h PF) and aged for the appropriate length of time thereafter.

Quantitative RT-PCR

mRNA expression levels of target genes were measured using quantitative real time PCR (qPCR). RNA was isolated from tissues dissected from appropriately-staged animals using the RNeasy Plus Mini Kit (Qiagen). cDNA was synthesized from 400 ng of total RNA using the SuperScript III First-Strand Synthesis System (Invitrogen). qPCR was performed on a Roche 480 LightCycler using LightCycler 480 SYBR Green I Master Mix (Roche). The target gene primer sequences used in this study were previously validated: *rpr*[57], *hid*[57], *E74A*[58], and *rp49*[59]. In all cases, samples were run simultaneously with three independent biological replicates for each target gene. *rp49* was used as the reference gene. To calculate changes in relative expression and error bars, we used the Relative Expression Software Tool (REST)[60]. REST calculates confidence intervals and *p*-values for relative expression values using integrated bootstrapping and randomization methods. Standard error is calculated based on a confidence interval centered on the median; therefore error bars calculated by REST reflect asymmetrical tendencies in the data.

Immunofluorescent staining and image acquisition

Salivary glands dissected from appropriately-staged animals were fixed for 30 min in PBS with 0.1% Triton X-100 (PBST) and 4% formaldehyde, blocked overnight with PBST/4% BSA, and stained with the appropriate primary and secondary antibodies diluted in PBST/4% BSA. All tissues were fixed and stained using identical conditions, and a wild type control was always done as a base line to detect any antibody signal loss. Identical microscope acquisition settings and image processing parameters were used for each experiment/set of paired samples. All primary antibodies were tested for consistency to reduce variability between lots, and the same lot was used for all experiments whenever possible. Primary antibodies used were: rabbit α-Cleaved Dcp-1 (1:200; Cell Signaling #9578, Lot 1), rabbit α-Dronc (1:200; gift from P. Friesen, University of Wisconsin-Madison), rabbit α-Cleaved Caspase-3 (1:200; Cell Signaling #9661), and mouse anti-Fasciclin-3 (1:50; Developmental Studies Hybridoma Bank 7G10). Secondary antibodies used were AlexaFluor 488 anti-mouse and anti-rabbit (1:200; Invitrogen A11029 and A11034) and anti-rabbit Cy3 (1:200; Jackson Immuno-Research Labs 715-165-150). For DNA staining, DAPI was used (1:1000; Invitrogen). For phalloidin staining, salivary glands were dissected in PBS, fixed with 4% formaldehyde in PBS for 30 min and stained in the dark with a 100nM working solution of 488-conjugated Phalloidin (Life Technologies) for 30 min. Stained tissues were mounted in Vectashield (Vector Laboratories). All images were captured on an Olympus FluoView FV1000 confocal microscope and optimized with FV10-ASW software. Images shown in figures are representative of at least three independent experiments with n≥10 tissues analyzed per experiment. Whenever possible, results were confirmed by an independent lab member who was blinded to the genotype/condition being analyzed. For 3D volume views, stained salivary glands were

mounted in a 35mm glass-bottom dish (MatTek Corporation) in 50ºC 0.8% agarose and imaged immediately using a Z-stack sequence at 3µm intervals on a Nikon A1R confocal microscope. Volume views were optimized using the Nikon NIS Element software, and lumen size quantification was done using ImageJ. Light microscope images of whole salivary glands were taken on an Olympus SZX16 stereomicroscope using an Olympus DP72 digital camera with DP2-BSW software.

Ex vivo salivary gland cultures

Ex vivo cultures were performed using standard methods[61]. Salivary glands were dissected in oxygenated Schneider's insect media (Sigma) and pre-incubated for 30 min in a "lung" with flowing oxygen. Fresh oxygenated media with 5µM of 20-hydroxyecdysone (Sigma) and/or 85µM cycloheximide (Sigma) was added to the appropriate samples. Salivary glands were stained and imaged as described above.

Glue secretion assays

For glue protein imaging, salivary glands from strains carrying the Sgs3-GFP fusion protein were dissected in PBS and immediately imaged live on an Olympus FluoView FV1000 confocal microscope. For glue secretion western blot assays, three appropriately-staged animals carrying Sgs3-GFP were collected, washed with water, and the glue content that had not been expelled was measured. The animals were homogenized in 50µL of hi-salt lysis buffer (25 mM HEPES pH 7.4, 300 mM NaCl, 1.5 mM $MgCl_2$, 1 mM EDTA, 0.5% Triton X-100, 50 mM β-glycero-phosphate, 50 mM NaF, 1 mM Na_3V0_4, 5 mg/ml Pepstatin A, 1 mM DTT, 5 mg/ml Aprotinin, 200 mM PMSF, 10

mg/ml Leupeptin, 4 nM Microsystin). 10µL of each sample was then subjected to a western blot analysis. To monitor premature expulsion, five wandering larvae (at -8 h PF) of the appropriate genotype were placed in small PCR tubes, allowed to wander for 2 hours, and then removed. Only samples lacking animals that had started PF were used; 20uL 2x sample buffer (1.0 M Tris-HCl pH 6.8, 8% SDS, 40% Glycerol, 20% 2-Mercaptoethanol) was added to the small PCR tubes and vortexed vigorously to collect expelled proteins. The samples were heated at 95ºC for 5 minutes and were subjected to a western blot analysis.

Western blot analysis

Protein expression levels were measured by western blot analysis. Primary antibodies used were rabbit anti-GFP (1:2000; Torrey Pines TP401), rabbit anti-Dronc (1:1000; gift from P. Friesen, University of Wisconsin-Madison), mouse anti-β-tubulin (1:1000; Millipore #05-661), and rabbit anti-β-actin (1:1000; Cell Signaling #4967). Secondary antibodies used were alkaline phosphatase-conjugated goat anti-rabbit and anti-mouse IgG (1:30,000; Sigma A3687 and A3438). Membranes were developed for imaging with ECF substrate (GE Healthcare) and were imaged using a Storm 840 Scanner (Amersham Bioscience) and processed with ImageQuant TL software version 7.0 (GE Healthcare). Full-length, uncropped blots are included in Supplementary Figure 10.

Dendrite pruning

Dendritic arborizations of the ddaC neurons on the larval abdomen were imaged by expression of *CD8-GFP* driven by *ppk-Gal4*[46]. For -8 h PF, the larvae were placed in a

drop of PBS and pushed between a coverslip and microscope slide until the animals were immobile but still alive. For 16 h PF, the cuticle of appropriately-staged pupae was carefully removed and the animals were mounted in PBS. All mounted samples were imaged immediately on an Olympus FluoView FV1000 confocal microscope with 10-25 optical sections at 1.5µm intervals. Images were optimized using the FV10-ASW software and inverted using Photoshop CC 2015.

REFERENCES

1. McIlwain, D. R., Berger, T. & Mak, T. W. Caspase functions in cell death and disease. *Cold Spring Harbor Perspectives in Biology* **5,** a008656–a008656 (2013).

2. Taylor, R. C., Cullen, S. P. & Martin, S. J. Apoptosis: controlled demolition at the cellular level. *Nat Rev Mol Cell Biol* **9,** 231–241 (2008).

3. Salvesen, G. S. & Dixit, V. M. Caspase activation: the induced-proximity model. *Proc Natl Acad Sci USA* **96,** 10964–10967 (1999).

4. Riedl, S. J. & Salvesen, G. S. The apoptosome: signalling platform of cell death. *Nat Rev Mol Cell Biol* **8,** 405–413 (2007).

5. Bratton, S. B. & Salvesen, G. S. Regulation of the Apaf-1-caspase-9 apoptosome. *Journal of Cell Science* **123,** 3209–3214 (2010).

6. Stennicke, H. R. *et al.* Pro-caspase-3 is a major physiologic target of caspase-8. *J Biol Chem* **273,** 27084–27090 (1998).

7. Stennicke, H. R. & Salvesen, G. S. Properties of the caspases. *Biochim Biophys Acta* **1387,** 17–31 (1998).

8. Shalini, S., Dorstyn, L., Dawar, S. & Kumar, S. Old, new and emerging functions of caspases. *Cell Death Differ* **22,** 526–539 (2015).

9. Yamaguchi, Y. & Miura, M. Programmed Cell Death and Caspase Functions During Neural Development. *Curr. Top. Dev. Biol.* **114,** 159–184 (2015).

10. Unsain, N. & Barker, P. A. New Views on the Misconstrued: Executioner Caspases and Their Diverse Non-apoptotic Roles. *Neuron* **88,** 461–474 (2015).

11. Nakajima, Y.-I. & Kuranaga, E. Caspase-dependent non-apoptotic processes in development. *Cell Death Differ* (2017). doi:10.1038/cdd.2017.36

12. Solier, S., Fontenay, M., Vainchenker, W., Droin, N. & Solary, E. Non-apoptotic functions of caspases in myeloid cell differentiation. *Cell Death Differ* (2017). doi:10.1038/cdd.2017.19

13. Fogarty, C. E. & Bergmann, A. Killers creating new life: caspases drive apoptosis-induced proliferation in tissue repair and disease. *Cell Death Differ* (2017). doi:10.1038/cdd.2017.47

14. Cusack, C. L., Swahari, V., Hampton Henley, W., Michael Ramsey, J. & Deshmukh, M. Distinct pathways mediate axon degeneration during apoptosis and axon-specific pruning. *Nat Comms* **4,** 1876 (2013).

15. Vesela, B. *et al.* Non-apoptotic role for caspase-7 in hair follicles and the surrounding tissue. *J. Mol. Histol.* **46,** 443–455 (2015).

16. Williams, D. W., Kondo, S., Krzyzanowska, A., Hiromi, Y. & Truman, J. W. Local caspase activity directs engulfment of dendrites during pruning. *Nature Neuroscience* **9,** 1234–1236 (2006).

17. Kuo, C. T., Zhu, S., Younger, S., Jan, L. Y. & Jan, Y.-N. Identification of E2/E3 ubiquitinating enzymes and caspase activity regulating Drosophila sensory neuron dendrite pruning. *Neuron* **51,** 283–290 (2006).

18. Arama, E., Agapite, J. & Steller, H. Caspase activity and a specific cytochrome C are required for sperm differentiation in Drosophila. *Dev Cell* **4,** 687–697 (2003).

19. Arama, E., Bader, M., Srivastava, M., Bergmann, A. & Steller, H. The two Drosophila cytochrome C proteins can function in both respiration and caspase activation. *EMBO J* **25,** 232–243 (2006).

20. Huh, J. R. *et al.* Multiple apoptotic caspase cascades are required in nonapoptotic roles for Drosophila spermatid individualization. *PLoS Biol* **2,** E15 (2004).

21. Vasudevan, D. & Ryoo, H. D. Regulation of Cell Death by IAPs and Their Antagonists. *Curr. Top. Dev. Biol.* **114,** 185–208 (2015).

22. Jiang, C., Baehrecke, E. H. & Thummel, C. S. Steroid regulated programmed cell death during Drosophila metamorphosis. *Development* **124,** 4673–4683 (1997).

23. Jiang, C., Lamblin, A. F., Steller, H. & Thummel, C. S. A steroid-triggered transcriptional hierarchy controls salivary gland cell death during Drosophila metamorphosis. *Molecular Cell* **5,** 445–455 (2000).

24. Warren, J. T. *et al.* Discrete pulses of molting hormone, 20-hydroxyecdysone, during late larval development of Drosophila melanogaster: correlations with changes in gene activity. *Dev Dyn* **235,** 315–326 (2006).

25. Lee, C. Genetic Mechanism for the Stage- and Tissue-Specific Regulation of Steroid Triggered Programmed Cell Death in Drosophila. *Dev Biol* **252,** 138–148 (2002).

26. Ihry, R. J. & Bashirullah, A. Genetic control of specificity to steroid-triggered responses in Drosophila. **196,** 767–780 (2014).

27. Yin, V. P., Thummel, C. S. & Bashirullah, A. Down-regulation of inhibitor of apoptosis levels provides competence for steroid-triggered cell death. *J Cell Biol* **178,** 85–92 (2007).

28. Riedl, J. *et al.* Lifeact: a versatile marker to visualize F-actin. *Nature Methods* **5,** 605–607 (2008).

29. Melak, M., Plessner, M. & Grosse, R. Actin visualization at a glance. *Journal of Cell Science* **130,** 525–530 (2017).

30. Li, J. *et al.* Caspase-11 regulates cell migration by promoting Aip1–Cofilin-mediated actin depolymerization. *Nat Cell Biol* **9,** 276–286 (2007).

31. Kamber Kaya, H. E., Ditzel, M., Meier, P. & Bergmann, A. An inhibitory mono-ubiquitylation of the Drosophila initiator caspase Dronc functions in both apoptotic and non-apoptotic pathways. *PLoS Genet* **13,** e1006438 (2017).

32. Snipas, S. J., Drag, M., Stennicke, H. R. & Salvesen, G. S. Activation mechanism and substrate specificity of the Drosophila initiator caspase DRONC. *Cell Death Differ* **15,** 938–945 (2008).

33. Rodriguez, A. *et al.* Dark is a Drosophila homologue of Apaf-1/CED-4 and functions in an evolutionarily conserved death pathway. *Nat Cell Biol* **1,** 272–279 (1999).

34. Quinn, L. M. *et al.* An essential role for the caspase dronc in developmentally programmed cell death in Drosophila. *J Biol Chem* **275,** 40416–40424 (2000).

35. Gramates, L. S. *et al.* FlyBase at 25: looking to the future. *Nucl Acids Res* **45,** D663–D671 (2017).

36. Guruharsha, K. G. *et al.* A Protein Complex Network of Drosophila melanogaster. *Cell* **147,** 690–703 (2011).

37. Chew, S. K. *et al.* Genome-wide silencing in Drosophila captures conserved apoptotic effectors. *Nature* **460,** 123–127 (2009).

38. D'Brot, A. *et al.* Tango7 directs cellular remodeling by the Drosophila apoptosome. *Genes Dev* **27,** 1650–1655 (2013).

39. Sarov, M. *et al.* A genome-wide resource for the analysis of protein localisation in Drosophila. *eLife Sciences* **5,** e12068 (2016).

40. Daish, T. J., Mills, K. & Kumar, S. Drosophila caspase DRONC is required for specific developmental cell death pathways and stress-induced apoptosis. *Dev Cell* **7,** 909–915 (2004).

41. Martin, D. N. & Baehrecke, E. H. Caspases function in autophagic programmed cell death in Drosophila. *Development* **131,** 275–284 (2004).

42. Akdemir, F. *et al.* Autophagy occurs upstream or parallel to the apoptosome during histolytic cell death. *Development* **133,** 1457–1465 (2006).

43. Fan, Y. & Bergmann, A. The cleaved-Caspase-3 antibody is a marker of Caspase-9-like DRONC activity in Drosophila. *Cell Death Differ* **17,** 534–539 (2010).

44. Williams, D. W. & Truman, J. W. Cellular mechanisms of dendrite pruning in Drosophila: insights from in vivo time-lapse of remodeling dendritic arborizing sensory neurons. *Development* **132,** 3631–3642 (2005).

45. Kuo, C. T., Jan, L. Y. & Jan, Y.-N. Dendrite-specific remodeling of Drosophila sensory neurons requires matrix metalloproteases, ubiquitin-proteasome, and ecdysone signaling. *Proc Natl Acad Sci USA* **102,** 15230–15235 (2005).

46. Kirilly, D. *et al.* A genetic pathway composed of Sox14 and Mical governs severing of dendrites during pruning. *Nature Neuroscience* **12,** 1497–1505 (2009).

47. Rousso, T., Schejter, E. D. & Shilo, B.-Z. Orchestrated content release from Drosophila glue-protein vesicles by a contractile actomyosin network. *Nat Cell Biol* **18,** 181–190 (2016).

48. Tran, D. T., Masedunskas, A., Weigert, R. & Hagen, Ten, K. G. Arp2/3-mediated F-actin formation controls regulated exocytosis in vivo. *Nat Comms* **6,** 10098 (2015).

49. Campbell, D. S. & Okamoto, H. Local caspase activation interacts with Slit-Robo signaling to restrict axonal arborization. *J Cell Biol* **203,** 657–672 (2013).

50. Xu, D., Li, Y., Arcaro, M., Lackey, M. & Bergmann, A. The CARD-carrying caspase Dronc is essential for most, but not all, developmental cell death in Drosophila. *Development* **132,** 2125–2134 (2005).

51. Muro, I. *et al.* The Drosophila caspase Ice is important for many apoptotic cell deaths and for spermatid individualization, a nonapoptotic process. *Development* **133,** 3305–3315 (2006).

52. Laundrie, B. *et al.* Germline cell death is inhibited by P-element insertions disrupting the dcp-1/pita nested gene pair in Drosophila. *Genetics* **165,** 1881–1888 (2003).

53. Moon, N.-S. *et al.* E2F and p53 induce apoptosis independently during Drosophila development but intersect in the context of DNA damage. *PLoS Genet* **4,** e1000153 (2008).

54. Meier, P., Silke, J., Leevers, S. J. & Evan, G. I. The Drosophila caspase DRONC is regulated by DIAP1. *EMBO J* **19,** 598–611 (2000).

55. Andres, A. J. & Thummel, C. S. Methods for quantitative analysis of transcription in

larvae and prepupae. *Methods Cell Biol.* **44,** 565–573 (1994).

56. Biyasheva, A., Do, T. V., Lu, Y., Vaskova, M. & Andres, A. J. Glue secretion in the Drosophila salivary gland: a model for steroid-regulated exocytosis. *Dev Biol* **231,** 234–251 (2001).

57. Ihry, R. J., Sapiro, A. L. & Bashirullah, A. Translational Control by the DEAD Box RNA Helicase belle Regulates Ecdysone-Triggered Transcriptional Cascades. *PLoS Genet* **8,** e1003085 (2012).

58. Caldwell, P. E., Walkiewicz, M. & Stern, M. Ras activity in the Drosophila prothoracic gland regulates body size and developmental rate via ecdysone release. *Curr Biol* **15,** 1785–1795 (2005).

59. Denton, D. *et al.* Autophagy, not apoptosis, is essential for midgut cell death in Drosophila. *Curr Biol* **19,** 1741–1746 (2009).

60. Pfaffl, M. W., Horgan, G. W. & Dempfle, L. Relative expression software tool (REST) for group-wise comparison and statistical analysis of relative expression results in real-time PCR. *Nucl Acids Res* **30,** e36 (2002).

61. Bashirullah, A. *et al.* Coordinate regulation of small temporal RNAs at the onset of Drosophila metamorphosis. *Dev Biol* **259,** 1–8 (2003).

CHAPTER 5

Genetic control of caspase activation in dying larval salivary glands during *Drosophila* metamorphosis

This chapter is in preparation for publication.

Neuman SD*, Kang Y*, Ihry RJ, Bashirullah A. Genetic control of caspase activation in dying larval salivary glands during *Drosophila* metamorphosis. In preparation.

*authors contributed equally to this work

ABSTRACT

Proper control of cell death is critical for both normal development and disease. In *Drosophila*, the larval salivary glands are destroyed during metamorphosis, and this endogenous death response is initiated by the steroid hormone ecdysone. Ecdysone signaling is thought to directly initiate transcription of IAP antagonists, potent death activators that antagonize inhibitor of apoptosis proteins (IAPs) and trigger a caspase cascade. Here we re-examine the mechanisms that regulate caspase activation during the salivary gland death response. We find that salivary glands do not always activate caspases in response to IAP antagonist expression; instead, glands need to acquire competence to activate caspases during metamorphosis. This switch in competence coincides with the timing of transcriptional upregulation of other pro-apoptotic regulators, including the initiator caspase *dronc* and its adaptor protein *dark*. We find that these pro-apoptotic regulators and IAP antagonists are coordinately induced in dying glands, and disruption of either response inhibits caspase activation. Finally, we demonstrate that overexpression of *dronc* and *dark* is sufficient to confer competence to activate caspases in response to IAP antagonist expression. Our results support a model where upregulation of caspase expression levels is necessary to “prime” cells, demonstrating that, unlike previously thought, IAP antagonist expression alone is not sufficient to trigger caspase activation during developmentally-programmed cell death.

INTRODUCTION

Apoptosis is a genetically-controlled process by which unwanted cells are eliminated during normal development, and misregulation of this process leads to both developmental defects and disease (Suzanne and Steller, 2013). Apoptosis is executed by an evolutionarily-conserved group of cysteine proteases (Thornberry, 1998; Yuan et al., 1993). Initiator caspases sit at the top of the cascade, and their activation requires dimerization on a signaling platform called the apoptosome, composed primarily of Apaf-1 homo-oligomers (Li et al., 1997; Zou et al., 1999a). Caspase activity is held in check by inhibitor of apoptosis proteins (IAPs), which bind and inhibit both initiator and effector caspases (Li et al., 2011; Meier et al., 2000; Zaffaroni et al., 2002). Once activated, initiator caspases cleave and thereby activate effector caspases, initiating a rapidly expanding cascade of caspase activation that results in apoptosis (Boatright and Salvesen, 2003; Li et al., 1997; Zou et al., 1999b). Although caspases are expressed in all cells, IAPs inhibit caspase activation, thereby preventing the signaling cascade from starting. Thus, healthy cells are thought to live in a precarious balance between death activators and death inhibitors, where altering the balance determines survival versus death.

During normal development and physiological homeostasis, apoptosis is initiated by removal of IAP-dependent inhibition of caspase activation. In *Drosophila*, regulation of apoptosis converges on the transcription of the IAP antagonists *reaper*, *hid* and/or *grim* (RHG proteins). *Drosophila* IAP 1 (Diap1) is thought to be required to prevent apoptosis in most somatic cells (Wang et al., 1999; Yoo et al., 2002). Consistently, knockdown of Diap1 through RNAi results in apoptosis (Yin and Thummel, 2004), and ectopic

expression of Diap1 blocks both developmental apoptosis and apoptosis induced by overexpression of *reaper* and *hid* (Hay et al., 1995). IAP antagonists bind to Diap1, disrupting its interaction with caspases and triggering caspase activation and apoptosis (Lisi et al., 2000; Meier et al., 2000; Sandu et al., 2010). Elimination of all three death activator genes blocks apoptosis, while ectopic expression of any of them is sufficient to trigger apoptosis (Chen et al., 1996; Grether et al., 1995; White et al., 1994). The mammalian death activators Smac/Diablo and Omi/Htra2 appear to function in a similar manner to RHG proteins by inhibiting IAPs such as Survivin and XIAP, demonstrating that this pathway is conserved through evolution (Du et al., 2000; Shiozaki and Shi, 2004; Srinivasula et al., 2001; Yang et al., 2003).

The destruction of the *Drosophila* larval salivary glands during metamorphosis is one of the most well-characterized models for developmentally-programmed cell death. This endogenous death response is initiated by the prepupal pulse of the steroid hormone 20-hydroxyecdysone, henceforth called ecdysone. Ecdysone functions as a canonical steroid hormone, binding to its heterodimeric nuclear receptor, *EcR/USP* (Koelle et al., 1991; Thomas et al., 1993; Yao et al., 1992). This nuclear receptor complex then induces transcription of a small set of primary target genes; these primary targets in turn induce expression of larger set of secondary target genes. In this manner, ecdysone signaling induces a transcriptional cascade that culminates in the death of the larval salivary glands. Expression of *reaper* and *hid* is directly induced by *EcR/USP* and the ecdysone primary target genes *E74A* and *BR-C* (Jiang et al., 2000). Therefore, the ecdysone-dependent induction of *reaper* and *hid* is thought to be sufficient to initiate salivary gland cell death.

In this report, we identify additional factors beyond IAP antagonists that are critical for caspase activation during the salivary gland death response. We demonstrate that IAP antagonist expression is not always sufficient to trigger caspase activation; competence to activate caspases is regulated in a tissue- and stage-specific manner. Gene expression analysis shows that both IAP antagonists and caspases are coordinately induced in dying glands, and induction of these genes requires the ecdysone-induced transcriptional hierarchy. Furthermore, competence to trigger caspase activation coincides with the timing of induction of the initiator caspase *dronc* and its *Apaf-1* adaptor protein *dark*. Disruption of either *dronc* or *dark* expression is sufficient to inhibit caspase activation, even when IAP antagonists are ectopically expressed. Conversely, raising *dronc* and *dark* expression levels is sufficient to confer competence to activate caspases, indicating that these genes are required to “prime” tissues for apoptosis.

MATERIALS AND METHODS

Fly stocks

The following stocks were obtained from the Bloomington *Drosophila* Stock Center: w^{1118}, *Sgs3-GAL4*, *Df(3R)Exel6149* (*bel Df*), *Df(3R)ED6332* (*hdc Df*), *Df(3R)Exel6178* (*mdh2 Df*), *Df(3L)Exel6112* (*med24 Df*), *Df(3L)Exel6105* (*psg2 Df*), *Df(3L)81k19* (*E74A Df*), *Df(3R)Exel6188* (*E93 Df*), rbp^{5}, $dronc^{51}$, $E74A^{neo24}$. The following stocks were kindly provided by members of the *Drosophila* community: *hs-reaper* (White et al., 1996), $dark^{82}$ and *UAS-dark* (Akdemir et al., 2006), *UAS-dronc* (Quinn et al., 2000), $\beta FTZ\text{-}F1^{ex17}$ and $Df(3L)Cat^{DH104}$ (*βFTZ-F1 Df*) (Broadus et al., 1999). $E93^{psg11}$, bel^{psg9}, hdc^{psg12}, $med24^{psg5}$, pak^{psg4a}, pak^{psg4b}, $mdh2^{psg7a}$, and $psg2^{psg2}$ were generated in an EMS mutagenesis screen (Ihry and Bashirullah, 2014; Wang et al., 2008).

Fly husbandry, developmental staging, and delivery of apoptotic triggers

Flies were grown on standard cornmeal molasses media in uncrowded bottles or vials in a temperature-controlled incubator set to 25°C. To deliver an apoptotic stimulus (*hs-reaper*) to wandering third instar (wL3) larvae, animals of the appropriate genotype were picked from the side of uncrowded bottles and placed on a grape agar plate sealed with Parafilm. Animals were heat-shocked by submerging the sealed grape agar plate in a 37°C water bath for 30 minutes, then allowed to recover for the appropriate time at 25°C until tissue dissection and staining. For *hs-reaper* experiments during prepupal development, animals were picked as newly-formed white prepupae and allowed to age on moist filter paper plates for 6.5 h (for +8 h PF sample), 8.5 h (for +10 h PF sample), or 10.5 h (for +12 h PF sample). Animals were then heat-shocked on Parafilm-sealed grape

agar plates for 30 minutes at 37ºC. After heat-shock, animals were allowed to recover for one hour at 25ºC; tissues were then dissected for staining. For +13.5 h PF samples (control and PSG mutant animals), animals were synchronized at head eversion, then subjected to the *hs-reaper* treatment and recovery protocol described above.

Immunofluorescent staining and image capture

Tissues were dissected from animals of the appropriate developmental stage and genotype and stained using standard methods (Yin et al. 2007). For caspase staining in salivary glands, tissues were dissected and permeabilized with heptane, then fixed in PBS/0.1% Triton X-100 (PBST) with 4% formaldehyde at room temperature for 30 minutes. Samples were then blocked overnight in PBST/4% BSA and stained with the appropriate primary and secondary antibodies diluted in PBST/4% BSA. Primary antibodies used include 1:200 rabbit α-cleaved-caspase-3 (Cell Signaling) and 1:50 mouse α-lamin (Developmental Studies Hybridoma Bank). Secondary antibodies used include 1:200 α-rabbit AlexaFluor 488 (Invitrogen), 1:200 α-rabbit Cy3 (Jackson Immuno-Research Labs), 1:200 α-mouse Cy3 (Jackson Immuno-Research Labs), and 1:200 α-mouse AlexaFluor 488 (Invitrogen). DNA was counterstained with DAPI (1:1000; Invitrogen). Images were taken on an Olympus FluoView FV1000 confocal microscope and optimized using FV10-ASW software. PSG images were captured on an Olympus SXZ16 stereomicroscope coupled to an Olympus DP72 digital camera with DP2-BSW software.

Quantitative RT-PCR (qPCR)

qPCR was performed as previously described (Ihry et al., 2012). For paired tissue samples (Fig. 1 and Fig. S2), the central nervous system, wing discs, and salivary glands were dissected from the same pool of animals, allowing a direct comparison of gene expression patterns between these tissues. For all samples, total RNA was isolated using the Qiagen RNeasy Plus Mini Kit, and reverse transcription was performed using 400 ng total RNA with oligo(dT) primers and SuperScript III reverse transcriptase (Invitrogen). qPCR was performed on a Roche LightCycler 480 with 480 SYBR Green I Master Mix (Roche). Samples were run in biological triplicate and expression was normalized to two reference genes, *rp49* and *ubcd6*, unless otherwise noted. Serial dilutions were used to calculate primer amplification efficiencies. Relative expression was calculated using Relative Expression Software Tool (REST) (Pfaffl et al., 2002). Primer sequences were previously published (Kang and Bashirullah, 2014), with the exception of *ubcd6* (*ubcd6* F: 5’ ACA TAT TGC AGA ACC GCT GG 3’ and *ubcd6* R: 5’ GCT TTC ACA CGC TTC TCG T 3’).

RESULTS

The larval salivary glands are highly resistant to IAP antagonist-induced caspase activation

We previously described the use of a heat-controlled transgene expressing the IAP antagonist *reaper* (*hs-reaper*) to identify restrictive and permissive windows for apoptosis in whole animals during development (Kang and Bashirullah, 2014). These studies revealed that animals at some developmental stages are highly resistant to *reaper* expression, while other stages are highly sensitive. We wanted to extend these studies to see if individual tissues exhibited differences in sensitivity to *reaper* expression, so we tested if tissues within wandering L3 (wL3) animals exhibited any differences in caspase activation after treatment with *hs-reaper*. We first analyzed the wing imaginal discs. The wing discs do not exhibit caspase activation, assayed by staining for cleaved-caspase-3, immediately after *hs-reaper* treatment (Fig. 1A); however, caspase activation is observed at 30 min after heat-shock (AHS) (Fig. 1B), and the intensity of the caspase staining increases at 60 and 90 min AHS (Fig. 1C-D). Similar results are seen in the ventral nerve cord (VNC); caspase activation is not observed at 0 or 30 min AHS (Fig. 1E-F), but is seen at 60 and 90 min AHS (Fig. 1G-H). However, we see very different results in the larval salivary gland. This tissue does not exhibit caspase activation, here assayed by staining for both cleaved-caspase-3 and lamin, a substrate of caspases, at any timepoint (Fig. 1I-L). qPCR analysis confirms that *hs-reaper* treatment does induce *reaper* expression in the glands (Fig. S1A). Importantly, this tissue is not completely resistant to *hs-reaper* treatment; caspase activation is observed when glands are dissected 2 h after an extreme treatment with two copies of the *hs-reaper* transgene (Fig. S1B), consistent

with previously published reports (Yin et al., 2007). Taken together, these results indicate that competence to activate caspases in response to IAP antagonist expression is regulated in a tissue-specific manner.

Our previous studies demonstrated that differences in death gene expression levels played a critical role in defining restrictive and permissive windows for apoptosis in whole animals (Kang and Bashirullah, 2014). To determine if gene expression differences regulate these tissue-specific responses to IAP antagonist expression, we used qPCR to analyze mRNA expression levels of death genes. We dissected paired wing imaginal discs, salivary glands, and central nervous systems from wL3 animals to allow direct comparison of gene expression across these tissues. Interestingly, we observe significant differences in death gene expression levels (Fig. 1M). Salivary glands display significantly lower levels of *dronc*, *dark*, *drice*, and *dcp-1* compared to both wing discs and the central nervous system, while levels of *diap-1* do not change (Fig. 1M). These results suggest that, like our whole animal studies, tissue-specific expression levels of pro-apoptotic regulators may play an important role in competence for IAP antagonist-induced caspase activation.

The timing of competence to trigger caspase activation coincides with transcriptional upregulation of pro-apoptotic regulators

Although the salivary glands do not appear to be competent for caspase activation during the wL3 stage, this tissue is later destroyed during metamorphosis. We wanted to determine when competence for caspase activation is aqcquired. Normally, caspase activation and lamin breakdown are not visible until 13.5 h after puparium formation

(+13.5 h PF) (Fig. 2A-D), signifying the start of the endogenous death response. We then tested if precocious *reaper* expression altered the onset of caspase activation. Surprisingly, *hs-reaper* treatment at +8 h PF or +10 h PF did not result in caspase activation or a decrease in nuclear lamin staining (Fig. 2E-F). However, *hs-reaper* treatment at +12 h PF did result in caspase activation and cleavage of nuclear lamin (Fig. 2G), and this pattern continued at +13.5 h PF (Fig. 2H). These results indicate that salivary glands can only initiate caspase activation in response to IAP antagonist expression beginning at +12 h PF.

We next wanted to understand what regulated this apparent switch in the ability to activate caspases in the salivary glands during metamorphosis. As mentioned before, our previous work showed that expression levels of death genes are important in defining restrictive and permissive windows for apoptosis in whole animals (Kang and Bashirullah, 2014). To test if this was also true in the salivary glands during metamorphosis, we used qPCR to analyze mRNA expression levels of six death genes in salivary glands during a timecourse spanning late larval through early pupal stages (-12 h PF to +13.5 h PF). We normalized our data to two different reference genes, *rp49* and a new reference gene, *ubcd6* (Fig. S2), to enable a more tightly controlled analysis of gene expression levels. Consistent with previous reports (Jiang et al., 1997), we see strong induction of the IAP antagonists *reaper* and *hid* during early pupal stages (Fig. 3A-B). Expression of these genes begins to increase at +12 h PF, and reaches maximal levels by +13.5 h PF. However, IAP antagonists were not the only genes that were upregulated in dying glands. The effector caspases *drice* and *dcp-1* are also induced; *drice* levels begin to rise at +10 h PF, while *dcp-1* begins to increase at +12 h PF, with levels of both genes peaking at

+13.5 h PF (Fig. 3E-F). Additionally, the initiator caspase *dronc* and its adapter protein *dark* are induced. *dronc* expression levels begin to rise at +10 h PF, and continue to increase through +13.5 h PF (Fig. 3C). *dark* levels peak at +10 h PF, then plateau at +12 h PF and +13.5 h PF (Fig. 3D). Taken together, these results indicate that both IAP antagonists and caspases are coordinately induced in dying salivary glands. Furthermore, *dronc* and *dark* expression levels rise early in the death response, immediately before the salivary glands become competent to activate caspases in response to IAP antagonist expression, suggesting that these genes may play an important role in this process.

The ecdysone-triggered transcriptional hierarchy differentially regulates the expression of pro-apoptotic regulators

Thus far, our results show that IAP antagonists and pro-death caspases are coordinately induced in dying glands, and the timing of this induction coincides with competence to activate caspases. We next wanted to determine how expression levels of IAP antagonists and caspases are regulated. We previously reported several mutants that disrupt salivary gland cell death and exhibit a persistent salivary gland (PSG) phenotype (Ihry and Bashirullah, 2014; Wang et al., 2008). Many of these genes function within the ecdysone-induced transcriptional hierarchy (Ihry and Bashirullah, 2014), suggesting that they may play a role in regulating IAP antagonist and caspase expression. We therefore used qPCR to analyze expression of these death genes in our PSG mutants, as well as mutants of other ecdysone primary target genes, in salivary glands at +13.5 h PF. Interestingly, expression of the death genes appears to depend on different ecdysone primary response genes and PSG genes; furthermore, these genes appear to

fall into distinct regulatory groups. *reaper* induction is disrupted in almost all mutant salivary glands, with the exception of *E93*, *hdc* and *mdh2* (Fig. 4A,G). Similarly, *hid* expression is disrupted in all mutant glands except *hdc*, *mdh2*, and *βFTZ-F1* (Fig. 4B,G). *drice* expression requires all the PSG genes except for *E93*, *βFTZ-F1*, and *mdh2* (Fig 4E,G); similarly, *dcp-1* expression requires all genes except *βFTZ-F1* and *mdh2* (Fig. 4F,G). In contrast, expression of *dark* is only disrupted in *βFTZ-F1* mutant glands (Fig. 4D,G), suggesting that this ecdysone target gene may directly regulate *dark* transcription. Finally, *dronc* expression is only disrupted in *BR-C* (*rbp^5*) mutant salivary glands (Fig. 4C,G). Taken together, these results demonstrate that expression of the death genes is differentially regulated by members of the ecdysone-induced transcriptional hierarchy; significantly, *dronc* and *dark* appear to be regulated differently from the other death genes, suggesting that this differential regulation may play a role in the temporal difference in induction of these genes that we observed earlier. Importantly, these results also indicate that IAP antagonist expression cannot be genetically separated from caspase expression, further suggesting that these genes are coordinately induced during the ecdysone-dependent death response.

The ecdysone primary response gene *E93* does not play a role in ecdysone-triggered salivary gland cell death

The ecdysone primary response gene *E93* has previously been reported to play a critical role during salivary gland cell death (Lee et al., 2000). However, a recent study demonstrates that the three alleles of *E93* that were originally described (*$E93^1$*, *$E93^2$*, and *$E93^3$*) do not actually disrupt *E93* function and instead map to *Idh3b*, a critical

mitochondrial enzyme; furthermore, newly-generated loss-of-function *E93* alleles did not disrupt salivary gland cell death (Duncan et al., 2017). These results raise the question of whether *E93* plays any role in salivary gland destruction. We have identified an independent allele of *E93* containing a nonsense mutation early in the coding sequence (Q485X) (Ihry and Bashirullah, 2014) in our PSG collection. However, only homozygous $E93^{psg11}$ animals display a PSG phenotype; the salivary glands are destroyed normally in hemizygous ($E93^{psg11}/Df$) animals (Fig. S3), suggesting that the $E93^{psg11}$ chromosome may contain a second, independent lesion that affects salivary gland destruction. Furthermore, these *E93* hemizygotes only disrupt induction of *hid* (Fig. 4B,G); *reaper* and the pro-apoptotic caspases are induced normally (Fig. 4), indicating that *E93* plays a minor role within the ecdysone hierarchy. Moreover, caspase activation is also observed in $E93^{psg11}/Df$ at +13.5 h PF (Fig. 5E), suggesting that maximal induction of *hid* is dispensable for caspase activation during salivary gland cell death. Taken together, these results suggest that *E93* does not play a central role in cell death or caspase activation in the larval salivary glands during metamorphosis.

Caspase activation during the endogenous salivary gland death response requires coordinate induction of IAP antagonists and pro-death genes

It has previously been thought that induction of the IAP antagonists *reaper* and/or *hid* is sufficient to trigger programmed cell death (Grether et al., 1995; White et al., 1996). Many of our PSG mutants disrupt expression of these genes, but also disrupt expression of the initiator and effector caspases. To determine if expression of IAP antagonists is sufficient to trigger programmed cell death in the glands without expression of the

caspases, we tested if *hs-reaper* treatment in representative PSG mutants could trigger caspase activation. We tested six total mutants that differentially disrupt expression of IAP antagonists and/or caspases. Control salivary glands exhibit massive caspase activation and nuclear lamin breakdown, both with and without *hs-reaper* treatment (Fig. 5A,H). We first tested *βFTZ-F1* mutant salivary glands, which only disrupt expression of *dark* (Fig. 4G), and strikingly, these glands did not exhibit caspase activation with or without *reaper* treatment (Fig. 5B,I). We next tested the *BR-C* mutant rbp^5, which disrupted expression of all IAP antagonists and caspases except *dark* (Fig. 4G). Like *βFTZ-F1*, rbp^5 mutant salivary glands did not exhibit caspase activation without treatment with *hs-reaper* (Fig. 5C); additionally, they failed to activate caspases after treatment with *hs-reaper* (Fig. 5J). *E74A* mutant glands disrupt expression of *reaper*, *hid*, *drice*, and *dcp-1*, but induce *dronc* and *dark* normally (Fig. 4G); these mutant glands also did not exhibit caspase activation with or without *hs-reaper* treatment (Fig. 5D,K). As mentioned earlier, *E93* mutant glands only disrupt *hid* expression (Fig. 4G) and exhibit caspase activation with and without *hs-reaper* induction (Fig. 5E,L), although levels of caspase activation are slightly reduced compared to controls. In contrast, *hdc* mutant glands had decreased levels of only *drice* and *dcp-1* (Fig. 4G). Surprisingly, *hdc* mutant salivary glands exhibited caspase activation without *hs-reaper* treatment, albeit at reduced levels compared to controls (Fig. 5F). These glands exhibited higher levels of caspase activation after treatment with *hs-reaper* (Fig. 5M). This contrast between *BR-C* and *βFTZ-F1* mutant salivary glands, which disrupted expression of either *dronc* or *dark*, and *hdc* mutant salivary glands, which have normal levels of *dronc* and *dark,* suggests that expression levels of these two genes are critically important for caspase activation during salivary

gland cell death. *E74A* mutant glands do not disrupt mRNA expression levels of *dronc* and *dark*, but also do not exhibit caspase activation, suggesting that E74A may be require for translation of Dronc and/or Dark protein. Finally, *mdh2* mutant salivary glands exhibit normal expression levels of all death genes (Fig. 4G), yet did not exhibit caspase activation without *hs-reaper* treatment (Fig. 5G), consistent with previous reports (Wang et al., 2010). Treatment of *mdh2* mutant glands with *hs-reaper* resulted in a small amount of caspase activation that was greatly reduced compared to controls (Fig. 5N). This result suggests that other factors, perhaps involving mitochondria, also play a role in caspase activation during salivary gland cell death. Taken together, these results demonstrate that IAP antagonist expression alone is not sufficient to trigger caspase activation in the absence of caspase expression, particularly *dronc* and *dark*.

Levels of *dronc* and *dark* are necessary and sufficient to confer competence to activate *dark*-dependent caspase activation

We next wanted to directly test if altered expression levels of *dronc* and *dark* affected the ability to activate caspases in dying salivary glands. To do this, we dissected salivary glands from animals that were doubly heterozygous for loss-of-function mutations in *dronc* and *dark* (*dark*^{82}/+*; dronc*^{51}/+) and stained for cleaved-caspase-3 at +13.5 h PF, testing if the endogenous IAP antagonist pulse could trigger caspase activation in these tissues. Strikingly, these double heterozygous glands lacking one copy of *dronc* and *dark* did not exhibit caspase activation in response to the endogenous *reaper* pulse (Fig. 6E-F). These results suggest that expression levels of *dronc* and *dark* are critical for caspase activation during the endogenous death response.

To further analyze the role of *dronc* and *dark* in IAP antagonist-triggered caspase activation, we overexpressed these genes in wandering L3 (wL3) salivary glands and tested if *hs-reaper* treatment triggered caspase activation. As mentioned earlier, the salivary glands are normally highly resistant to IAP antagonist expression; they do not exhibit caspase activation after treatment with *hs-reaper* (Fig. 1I-L). To test if increased levels of *dronc* and *dark* altered the ability to activate caspases, we overexpressed these genes using *Sgs3-GAL4*, which drives *GAL4* expression specifically in the larval salivary glands beginning at the mid-third instar transition. This treatment significantly elevates the expression levels of both genes, assayed by measuring transcript levels using qPCR (Fig. 6E). Importantly, overexpression of both *dronc* and *dark* without *hs-reaper* treatment does not result in caspase activation (Fig. 6A). However, overexpression of both *dronc* and *dark* with ectopic *reaper* expression results in massive caspase activation, lamin degradation, and morphological breakdown of the salivary gland tissue (Fig. 6D). Interestingly, overexpression of either *dronc* or *dark* alone does not result in caspase activation after *reaper* expression (Fig. 6B-C), suggesting that *dronc* and *dark* must be expressed at elevated, proportional levels in order to promote caspase activation, consistent with the known role of *dark* as an adaptor protein for *dronc* activation during apoptosis (Quinn et al., 2000; Rodriguez et al., 1999). Taken together, these results suggest that transcriptional induction of *dronc* and *dark* is critical to “prime” cells for developmentally-regulated apoptosis, allowing them to become competent to activate caspases and execute the death response.

DISCUSSION

Proper control of programmed cell death is critical for both normal development and disease. Here, we use the destruction of the *Drosophila* salivary glands during metamorphosis as a model system to genetically dissect the mechanisms regulating caspase activation during this endogenous death response. Our results demonstrate that IAP antagonists and pro-death caspases are coordinately induced in dying salivary glands, and upregulation of these genes requires the ecdysone-induced transcriptional hierarchy. Expression levels of the initiator caspase *dronc* and the adaptor protein *dark* appear to be critical for caspase activation, as failure to increase expression of these genes inhibits caspase activation even upon ectopic expression of IAP antagonists. Therefore, these results suggest that *dronc* and *dark* “prime” salivary glands for caspase activation during programmed cell death, providing insight into a new layer of regulation during salivary gland endogenous cell death.

The current model for caspase activation during salivary gland cell death hinges on transcriptional induction of the IAP antagonists; expression of these genes is thought to be sufficient to induce programmed cell death (Chen et al., 1996; Grether et al., 1995; Jiang et al., 2000; White et al., 1996). However, our results indicate that caspase activation is a much more tightly regulated process. Although IAP antagonists are induced during the death response, other pro-death genes are also upregulated, suggesting that caspase activation requires coordinate upregulation of both IAP antagonists and pro-death caspases. Indeed, induction of IAP antagonists and caspases appears to be inextricably linked on a genetic level, as mutation of a single protein within the ecdysone hierarchy disrupts expression of both classes of pro-death regulators. These results

highlight the importance of coordinated control of gene expression during an endogenously-regulated death response.

Our results indicate that salivary glands must be primed in order to initiate caspase activation. However, priming is also an important concept in many other developmental and disease contexts, including cancer. A hallmark of cancer cells is the ability to evade apoptosis (Hanahan and Weinberg, 2011, 2000), and in many cases, this ability results from reduced expression levels of pro-apoptotic genes (Adams and Cory, 2007; Lowe et al., 2004). For example, many melanomas display reductions in *Apaf-1* expression levels, making these malignant cells resistant to apoptotic triggers (Dai et al., 2004; Soengas et al., 2001). Some chemotherapeutic agents kill cancer cells by promoting increased expression levels of pro-apoptotic genes, rendering the cells susceptible to programmed cell death (Bolden et al., 2006; West and Johnstone, 2014). Additionally, our results suggest that priming is also developmentally-regulated, even between different tissues at the same developmental stage. This priming mechanism may function to protect cells or tissues that are long-lived, such as mature neurons, which must persist for the lifetime of the organism, while sensitizing tissues that could be prone to oncogenic transformation. However, the precise function of priming, as well as its prevalence, remains unclear within a developmental context.

Although priming clearly plays an important role in IAP antagonist-induced caspase activation, our results suggest that other factors may also play a role in this process. Our *mdh2* mutant induces expression of all death genes normally, yet does not exhibit caspase activation. *mdh2* is a mitochondrial enzyme, and mitochondria are known to play a critical role in apoptosis in mammals (Estaquier et al., 2012). The role of

mitochondrial permeability and cytochrome c release in *Drosophila* apoptosis has remained unclear, however, a recent study implicated the mitochondrial enzyme *Idh3b* in programmed cell death of the larval salivary glands (Duncan et al., 2017), suggesting that there may be a previously unappreciated role for mitochondria in caspase activation during *Drosophila* developmental cell death. Additionally, *E74A* mutant animals induce *dronc* and *dark* expression normally, yet do not exhibit caspase activation after ectopic *reaper* expression. We have previously shown that translational control plays an important role during salivary gland cell death (Ihry et al., 2012), suggesting that *E74A* may play an unknown role in translation of Dronc and/or Dark protein. Future studies will be required to fully characterize the role of these processes during developmentally-programmed caspase activation.

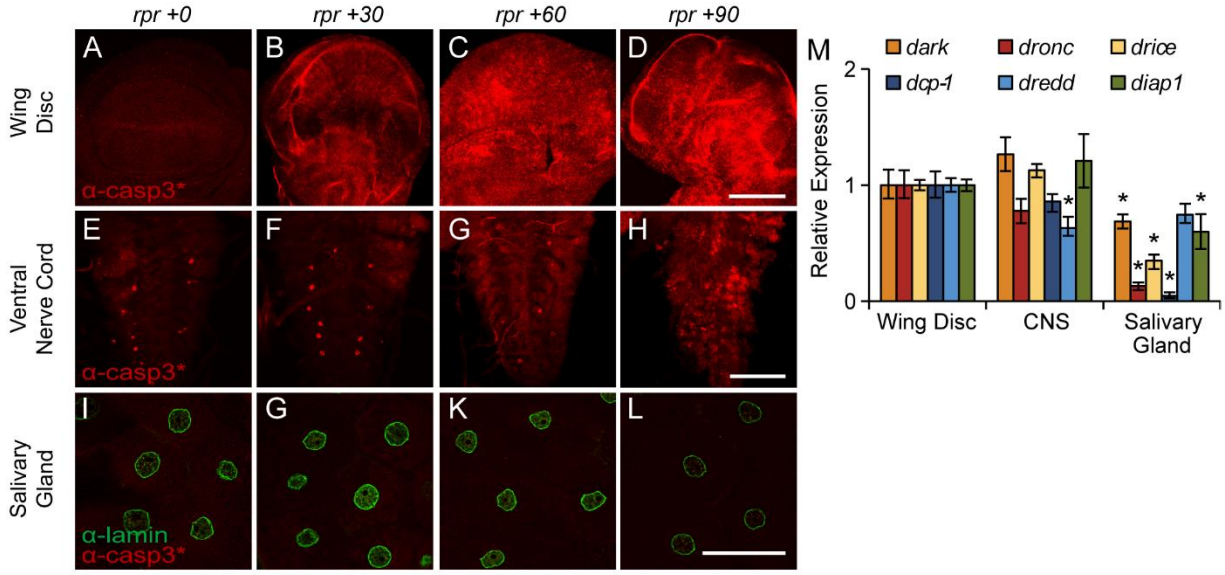

Figure 1. Competence to activate caspases in response to IAP antagonist expression is regulated in a tissue-specific manner in wandering L3 (wL3) larvae. **(A-D)** Analysis of caspase activation, assayed by staining for cleaved-caspase-3 (in red), in the wing imaginal disc after treatment with *hs-reaper*. **(A)** No caspase activation is visible at 0 min after heat-shock. **(B)** Wing discs exhibit ubiquitous caspase activation 30 min after treatment with *hs-reaper*, which intensifies at 60 min **(C)** and 90 min **(D)** after heat-shock. **(E-H)** Analysis of caspse activation in the ventral nerve cord after *hs-reaper* treatment. No caspase activation is visible at 0 min **(E)** or 30 min **(F)** after *hs-reaper*. The few cleaved-caspase-3-positive cells are the vCrz neurons, which undergo developmentally-programmed cell death (Choi et al., 2006). Caspase activation is visible at both 60 min **(G)** and 90 min **(H)** after *reaper* treatment. **(I-L)** Analysis of caspase activation in the larval salivary glands. No caspase activation or breakdown of nuclear lamin (in green) is visible at 0 min **(I)**, 30 min **(J)**, 60 min **(K)**, or 90 min **(L)** after *hs-reaper* treatment. Scale bars are 100μm. **(M)** qPCR analysis of death gene mRNA expression

levels in wL3 paired tissues. All three tissues were dissected from the same pool of animals to enable direct gene expression comparisons. The salivary glands express significantly lower levels of *dronc*, *dark*, *drice*, and *dcp-1* than the wing discs or the central nervous system (CNS). The *y*-axis shows relative expression, the *x*-axis shows the tissue being analyzed. Samples were run in biological triplicate and normalized to the reference gene *rp49*. Error bars represent standard error calculated by REST analysis; asterisks indicate $p<0.05$.

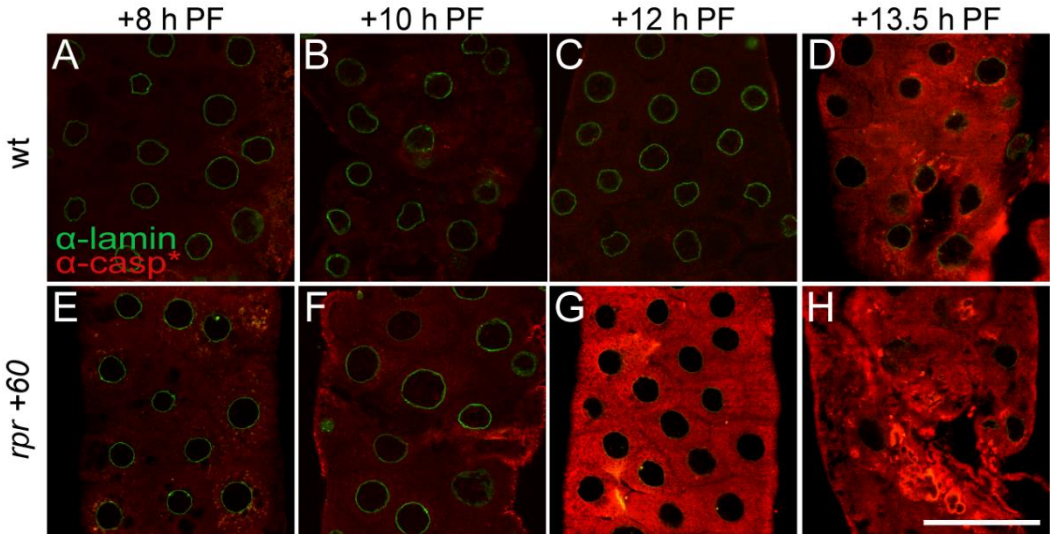

Figure 2. Salivary glands become competent to activate caspases during metamorphosis. (A-D) Timecourse of caspase activation, assayed by staining for cleaved-caspase-3 (red) and nuclear lamin (green) in control salivary glands. Control glands do not exhibit caspase activation at +8 h PF **(A)**, +10 h PF **(B)**, or +12 h PF **(C)**, but do have massive caspase activation and lamin breakdown at +13.5 h PF **(D)**. **(E-H)** Precocious expression of *reaper* from the *hs-reaper* transgene triggers premature caspase activation. Animals were heat-shocked for 30 min 1.5 h prior to the specified developmental timepoint, then allowed to recover for 1 h before tissue dissection (i.e. animals were heat-shocked at 6.5 h PF and dissected at +8 h PF, etc.). Salivary glands treated with *hs-reaper* do not exhibit caspase activation at +8 h PF **(E)** or +10 h PF **(F)**, but do exhibit caspase activation at +12 h PF **(G)**, which intensifies at +13.5 h PF **(H)**. Scale bar 100μm.

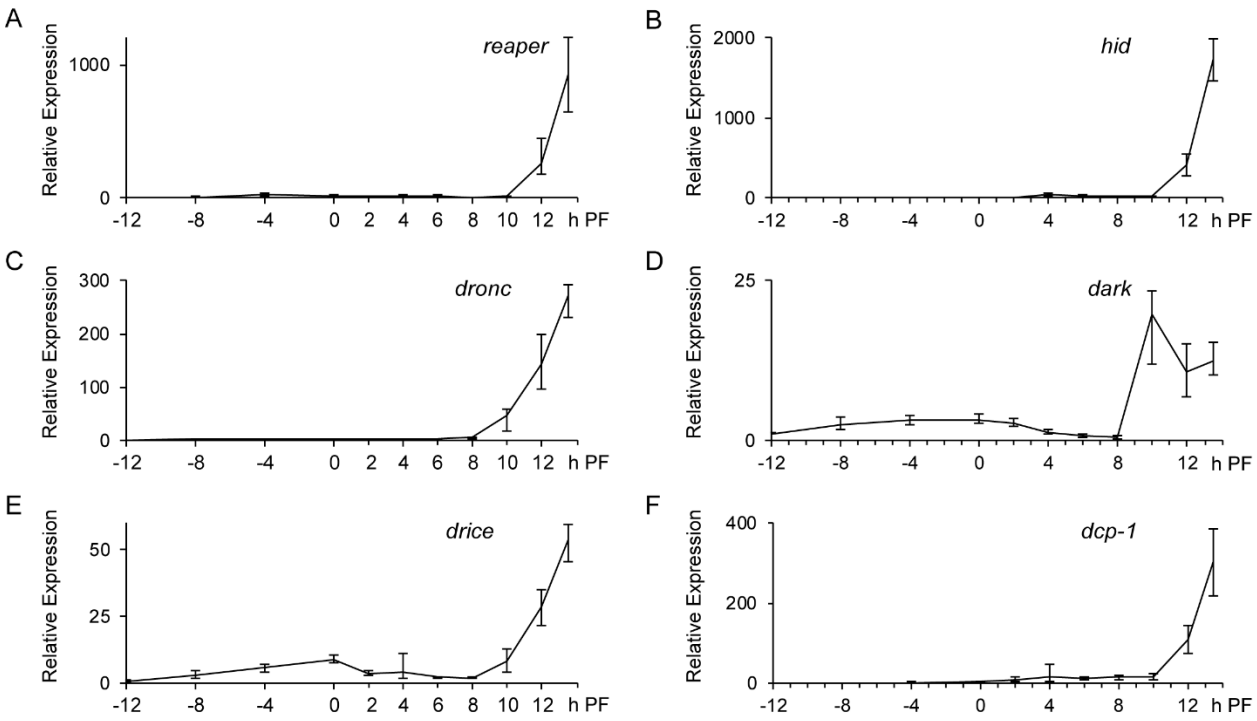

Figure 3. IAP antagonists and pro-death caspases are coordinately upregulated in dying salivary glands. qPCR timecourse analyzing mRNA expression levels of critical pro-apoptotic genes in salivary glands at the onset of metamorphosis. The IAP antagonists *reaper* **(A)** and *hid* **(B)** are both induced at +12 h PF. The initiator caspase *dronc* is induced at +10 h PF **(C)**, as is the adaptor protein *dark* **(D)**. The effector caspases *drice* **(E)** and *dcp-1* **(F)** are also induced in dying glands. In all graphs, the *y*-axis shows relative expression, and the *x*-axis shows the developmental stage in h after puparium formation (h PF). Samples were run in biological triplicate and normalized to *rp49* and *ubcd6*. Expression shown relative to the lowest point in each graph. Error bars represent standard error calculated by REST analysis.

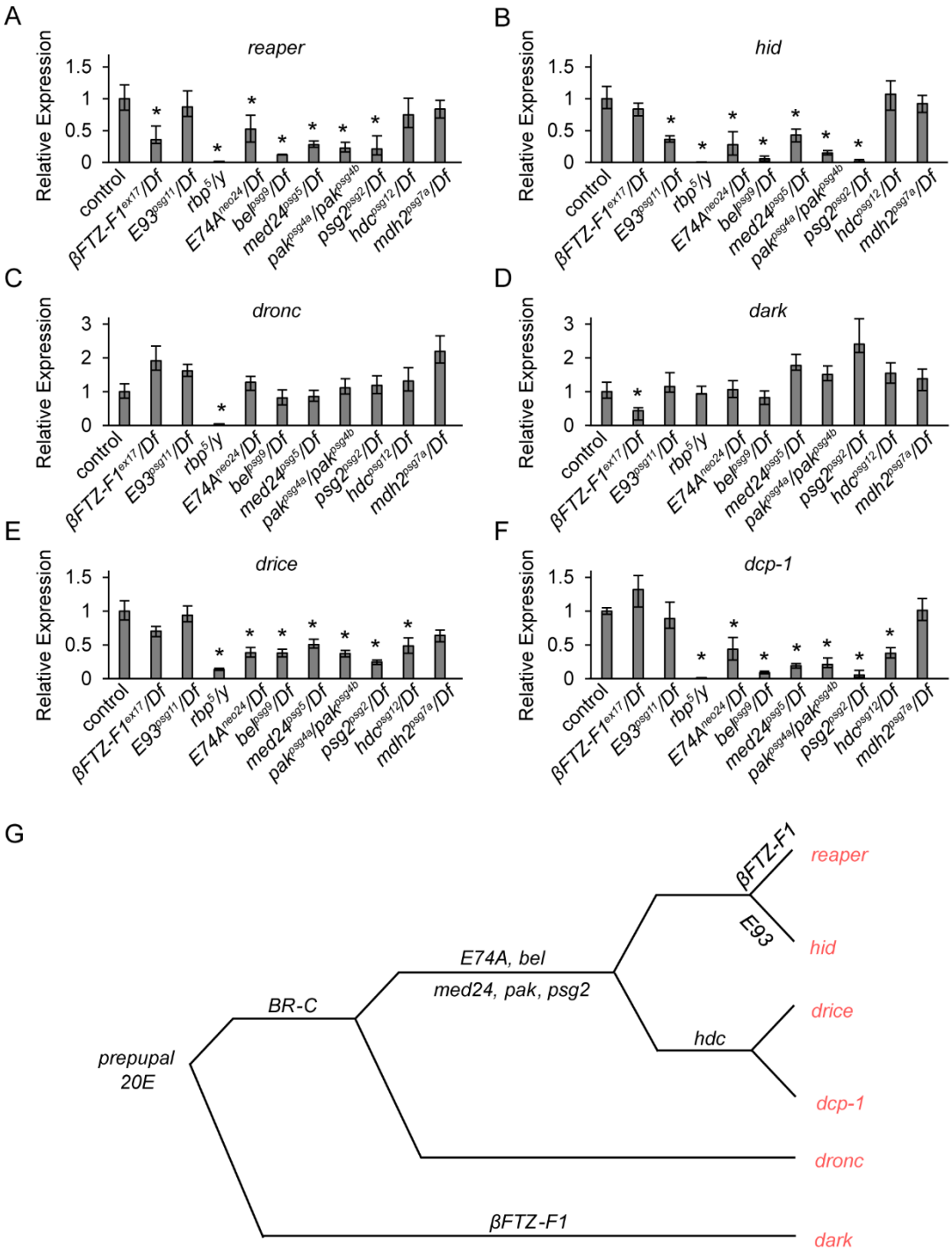

Figure 4. Components of the ecdysone-induced transcriptional hierarchy regulate induction of IAP-antagonists and pro-death caspases during the salivary gland death response. (A-F) qPCR analysis of critical death gene expression levels in control

and PSG mutant salivary glands at +13.5 h PF. All PSG mutant samples were collected from hemizygous or trans-heterozygous (for *pak*) animals; see Materials and Methods for the specific deficiency used for each gene. **(A)** Most PSG mutants disrupt induction of *reaper*, with the exception of $E93^{psg11}$, hdc^{psg12}, and $mdh2^{psg7a}$. **(B)** *hid* induction is disrupted in all mutant salivary glands except $\beta FTZ\text{-}F1^{ex17}$, hdc^{psg12}, and $mdh2^{psg7a}$. **(C)** *dronc* induction is only disrupted in *BR-C* (rbp^{5}) mutant salivary glands. **(D)** Induction of *dark* is only disrupted in $\beta FTZ\text{-}F1^{ex17}$ mutant salivary glands. Most PSG mutants disrupt induction of *drice* **(E)** and *dcp-1* **(F)**, except $\beta FTZ\text{-}F1^{ex17}$, $E93^{psg11}$, and $mdh2^{psg7a}$. **(G)** Graphical summary of data presented in panels **(A-F)**. qPCR samples were run in biological triplicate and expression levels are shown relative to controls. The *y*-axis shows relative expression and the *x*-axis shows the genotypes analyzed. Expression was normalized to *rp49* and *ubcd6*. Error bars represent standard error calculated by REST analysis. Asterisks indicate $p<0.05$.

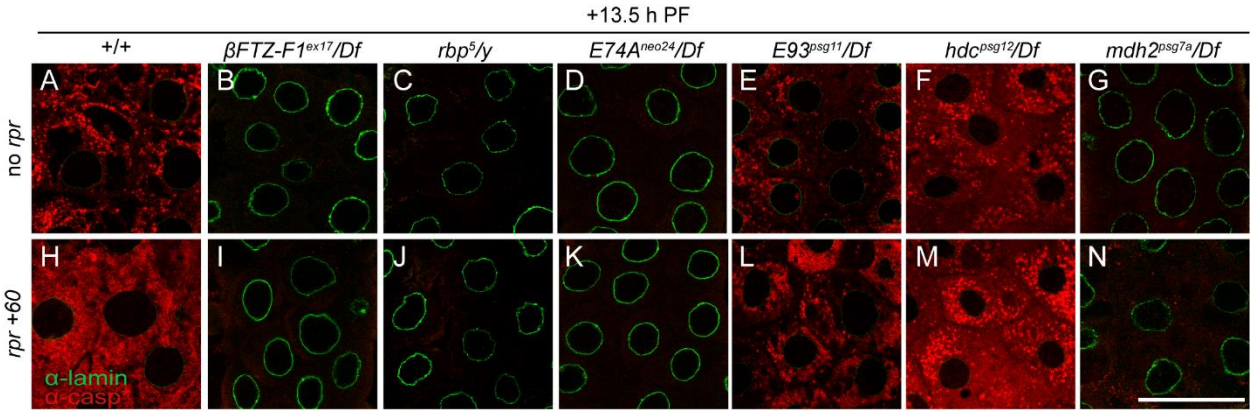

Figure 5. Ectopic IAP antagonist expression is not sufficient for caspase activation in PSG mutant salivary glands with reduced caspase expression levels. (A-G) Staining for cleaved-caspase-3 (in red) and nuclear lamin (in green) in control and PSG mutant salivary glands without *hs-reaper* treatment at +13.5 h PF. Caspase activation and lamin breakdown is observed in controls **(A)**, *E93^{psg11}/Df* **(E)**, and *hdc^{psg12}/Df* **(F)**, but is absent from *βFTZ-F1^{ex17}/Df* **(B)**, *rbp^{5}/y* **(C)**, *E74A^{neo24}/Df* **(D)**, and *mdh2^{psg7a}/Df* **(G)**. **(H-N)** Staining for cleaved-caspase-3 and lamin in salivary glands treated with *hs-reaper* at +13.5 h PF. Animals were heat-shocked at head eversion (+12 h PF) for 30 min, then allowed to recover for 1 h before tissue dissection. Caspase activation and lamin breakdown is observed in controls **(H)**, *E93^{psg11}/Df* **(L)**, and *hdc^{psg12}/Df* **(M)**, but is absent from *βFTZ-F1^{ex17}/Df* **(I)**, *rbp^{5}/y* **(J)**, and *E74A^{neo24}/Df* **(K)**. A small amount of caspase activation is observed in *mdh2^{psg7a}/Df* after *hs-reaper* treatment **(G)**. Scale bar 100μm.

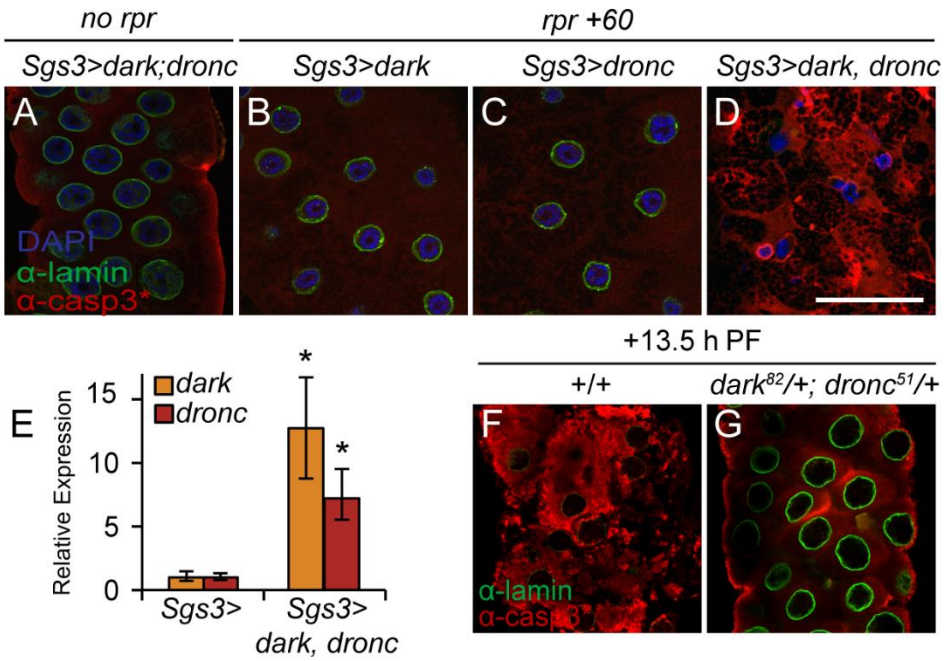

Figure 6. Expression of *dronc* and *dark* is necessary and sufficient to "prime" salivary glands for IAP antagonist-induced caspase activation. (A) Stage- and tissue-specific overexpression of *dark* and *dronc* in wL3 salivary glands with the *Sgs3-GAL4* driver does not result in caspase activation without *reaper* expression. Salivary glands are stained for cleaved-caspase-3, in red, nuclear lamin, in green, and DNA (DAPI), in blue. **(B-C)** Overexpression of *dark* **(B)** or *dronc* **(C)** alone does not result in caspase activation 60 min after treatment with *hs-reaper*; however, overexpression of both *dark* and *dronc* results in massive caspase activation and breakdown of nuclear lamin 60 min after *hs-reaper* induction **(D)**. **(E)** *Sgs3-GAL4*-driven overexpression of *dark* and *dronc* significantly increases expression levels of both genes in the larval salivary glands, as measured by qPCR. qPCR samples were run in biological triplicate and normalized to the reference gene *rp49*. *y*-axis shows relative expression; *x*-axis shows the genotype analyzed. Error bars indicate standard error calculated by REST analysis;

asterisks indicate $p<0.05$. **(F-G)** Reducing expression levels of *dark* and *dronc* inhibits caspase activation in the larval salivary glands during metamorphosis. Control salivary glands exhibit strong cleaved-caspase-3 staining and weak nuclear lamin staining at +13.5 h PF **(F)**, while $dark^{82}$ and $dronc^{51}$ double heterozygous ($dark^{82}$/+; $dronc^{51}$/+) mutant salivary glands do not have caspase activation and exhibit strong nuclear lamin staining **(G)**. Scale bar 100µm.

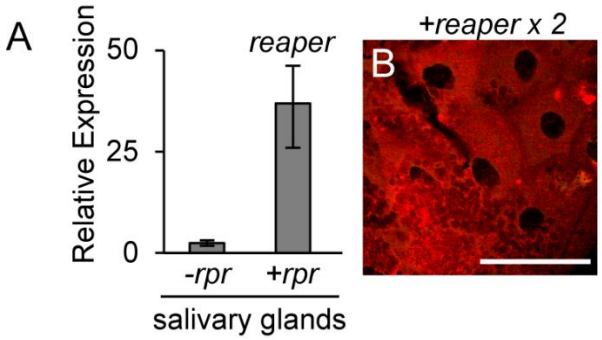

Figure S1. wL3 salivary glands can respond to treatment with *hs-reaper*. (A) qPCR analysis confirms that *hs-reaper* treatment does induce *reaper* expression in wL3 salivary glands. *hs-reaper*-treated glands were collected 1 h after heat-shock. The *y*-axis shows relative expression; the *x*-axis shows the genotypes analyzed. Samples were run in biological triplicate and normalized to *rp49*. Error bars reflect standard error calculated by REST analysis. **(B)** Extreme doses of *reaper* expression can activate caspases in wL3 glands. Animals containing two copies of the *hs-reaper* transgene were heat-shocked for 30 min at 37ºC and dissected 2 h after heat-shock. Cleaved-caspase-3 staining (red) is observed under these conditions. Scale bar 100µm.

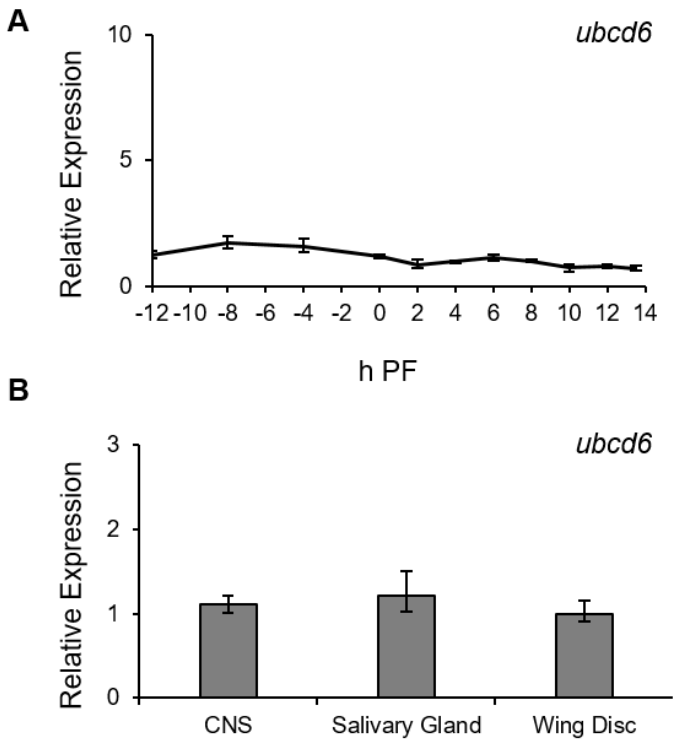

Figure S2. Validation of *ubcd6* as a reference gene. (A) Timecourse of *ubcd6* expression in salivary glands at the onset of metamorphosis. This analysis shows that *ubcd6* expression levels are stable and minimally variable in salivary glands throughout this developmental period. *y-axis* shows relative expression; *x*-axis shows developmental stage in h after puparium formation (PF). **(B)** qPCR analysis of *ubcd6* expression levels in paired tissue samples dissected from wL3 animals. *ubcd6* is expressed at consistent levels in the central nervous system (CNS), salivary gland, and wing disc. *y-axis* shows relative expression, *x*-axis shows the tissue analyzed. In both graphs, samples were run in biological triplicate and normalized to *rp49*. Error bars reflect standard error calculated by REST analysis.

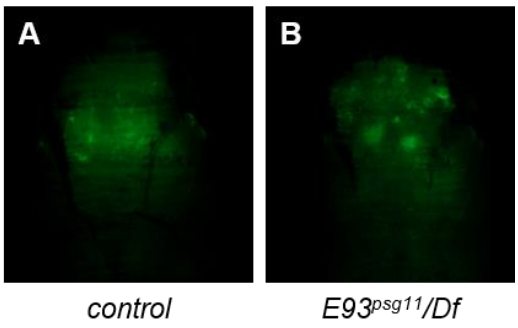

Figure S3. *E93^{psg11}/Df* mutant animals do not exhibit a PSG phenotype. (A) Control animals expressing GFP in the salivary glands (*fkh-GAL4, UAS-GFP*) have diffuse GFP signal at +24 h PF, indicating that the salivary glands have been destroyed. **(B)** *E93^{psg11}/Df* animals expressing GFP in the salivary glands also exhibit diffuse fluorescence at +24 h PF, indicating that the glands have been destroyed and that hemizygous animals do not have a PSG phenotype.

REFERENCES

Adams, J.M., Cory, S., 2007. The Bcl-2 apoptotic switch in cancer development and therapy. Oncogene 26, 1324–37. doi:10.1038/sj.onc.1210220

Akdemir, F., Farkaš, R., Chen, P., Juhasz, G., Medved'ová, L., Sass, M., Wang, L., Wang, X., Chittaranjan, S., Gorski, S.M., Rodriguez, A., Abrams, J.M., 2006. Autophagy occurs upstream or parallel to the apoptosome during histolytic cell death. Development 133.

Boatright, K.M., Salvesen, G.S., 2003. Mechanisms of caspase activation. Curr. Opin. Cell Biol. 15, 725–731. doi:10.1016/j.ceb.2003.10.009

Bolden, J.E., Peart, M.J., Johnstone, R.W., 2006. Anticancer activities of histone deacetylase inhibitors. Nat. Rev. Drug Discov. 5, 769–784. doi:10.1038/nrd2133

Broadus, J., McCabe, J.R., Endrizzi, B., Thummel, C.S., Woodard, C.T., 1999. The Drosophila beta FTZ-F1 orphan nuclear receptor provides competence for stage-specific responses to the steroid hormone ecdysone. Mol. Cell 3, 143–9.

Chen, P., Nordstrom, W., Gish, B., Abrams, J.M., 1996. grim, a novel cell death gene in Drosophila. Genes Dev. 10, 1773–82. doi:10.1101/GAD.10.14.1773

Choi, Y.-J., Lee, G., Park, J.H., 2006. Programmed cell death mechanisms of identifiable peptidergic neurons in Drosophila melanogaster. Development 133.

Dai, D.L., Martinka, M., Bush, J.A., Li, G., 2004. Reduced Apaf-1 expression in human cutaneous melanomas. Br. J. Cancer 91, 1089–95. doi:10.1038/sj.bjc.6602092

Du, C., Fang, M., Li, Y., Li, L., Wang, X., 2000. Smac, a mitochondrial protein that promotes cytochrome c-dependent caspase activation by eliminating IAP inhibition. Cell 102, 33–42.

Duncan, D.M., Kiefel, P., Duncan, I., 2017. Mutants for Drosophila Isocitrate Dehydrogenase 3b Are Defective in Mitochondrial Function and Larval Cell Death. G3 Genes, Genomes, Genet. 7.

Estaquier, J., Vallette, F., Vayssiere, J.-L., Mignotte, B., 2012. The Mitochondrial Pathways of Apoptosis, in: Advances in Experimental Medicine and Biology. pp. 157–183. doi:10.1007/978-94-007-2869-1_7

Grether, M.E., Abrams, J.M., Agapite, J., White, K., Steller, H., 1995. The head involution defective gene of Drosophila melanogaster functions in programmed cell death. Genes Dev. 9, 1694–1708. doi:10.1101/gad.9.14.1694

Hanahan, D., Weinberg, R.A., 2011. Hallmarks of cancer: the next generation. Cell 144, 646–74. doi:10.1016/j.cell.2011.02.013

Hanahan, D., Weinberg, R.A., 2000. The Hallmarks of Cancer. Cell 100, 57–70. doi:10.1016/S0092-8674(00)81683-9

Hay, B. a, Wassarman, D. a, Rubin, G.M., 1995. Drosophila homologs of baculovirus inhibitor of apoptosis proteins function to block cell death. Cell 83, 1253–62.

Ihry, R.J., Bashirullah, A., 2014. Genetic control of specificity to steroid-triggered responses in Drosophila. Genetics 196, 767–80. doi:10.1534/genetics.113.159707

Ihry, R.J., Sapiro, A.L., Bashirullah, A., Akagi, K., Takai, M., 2012. Translational Control by the DEAD Box RNA Helicase belle Regulates Ecdysone-Triggered Transcriptional Cascades. PLoS Genet. 8, e1003085. doi:10.1371/journal.pgen.1003085

Jiang, C., Baehrecke, E.H., Thummel, C.S., 1997. Steroid regulated programmed cell death during Drosophila metamorphosis. Development 124, 4673–83.

Jiang, C., Lamblin, a F., Steller, H., Thummel, C.S., 2000. A steroid-triggered transcriptional hierarchy controls salivary gland cell death during Drosophila metamorphosis. Mol. Cell 5, 445–55.

Kang, Y., Bashirullah, A., 2014. A steroid-controlled global switch in sensitivity to apoptosis during Drosophila development. Dev. Biol. 386, 34–41. doi:10.1016/j.ydbio.2013.12.005

Koelle, M.R., Talbot, W.S., Segraves, W.A., Bender, M.T., Cherbas, P., Hogness, D.S., 1991. The Drosophila EcR gene encodes an ecdysone receptor, a new member of the steroid receptor superfamily. Cell 67, 59–77. doi:10.1016/0092-8674(91)90572-G

Lee, C.-Y., Wendel, D.P., Reid, P., Lam, G., Thummel, C.S., Baehrecke, E.H., 2000. E93 Directs Steroid-Triggered Programmed Cell Death in Drosophila. Mol. Cell 6, 433–443. doi:10.1016/S1097-2765(00)00042-3

Li, P., Nijhawan, D., Budihardjo, I., Srinivasula, S.M., Ahmad, M., Alnemri, E.S., Wang, X., 1997. Cytochrome c and dATP-dependent formation of Apaf-1/caspase-9 complex initiates an apoptotic protease cascade. Cell 91, 479–89.

Li, X., Wang, J., Shi, Y., 2011. Structural mechanisms of DIAP1 auto-inhibition and DIAP1-mediated inhibition of drICE. Nat. Commun. 2, 408. doi:10.1038/ncomms1418

Lisi, S., Mazzon, I., White, K., 2000. Diverse domains of THREAD/DIAP1 are required to inhibit apoptosis induced by REAPER and HID in Drosophila. Genetics 154, 669–78.

Lowe, S.W., Cepero, E., Evan, G., 2004. Intrinsic tumour suppression. Nature 432, 307–315. doi:10.1038/nature03098

Meier, P., Silke, J., Leevers, S.J., Evan, G.I., 2000. The Drosophila caspase DRONC is regulated by DIAP1. EMBO J. 19, 598–611. doi:10.1093/emboj/19.4.598

Pfaffl, M.W., Horgan, G.W., Dempfle, L., 2002. Relative expression software tool (REST) for group-wise comparison and statistical analysis of relative expression results in real-time PCR. Nucleic Acids Res. 30, e36.

Quinn, L.M., Dorstyn, L., Mills, K., Colussi, P.A., Chen, P., Coombe, M., Abrams, J., Kumar, S., Richardson, H., 2000. An essential role for the caspase dronc in developmentally programmed cell death in Drosophila. J. Biol. Chem. 275, 40416–24. doi:10.1074/jbc.M002935200

Rodriguez, A., Oliver, H., Zou, H., Chen, P., Wang, X., Abrams, J.M., 1999. Dark is a Drosophila homologue of Apaf-1/CED-4 and functions in an evolutionarily conserved death pathway. Nat. Cell Biol. 1, 272–9. doi:10.1038/12984

Sandu, C., Ryoo, H.D., Steller, H., 2010. Drosophila IAP antagonists form multimeric complexes to promote cell death. J. Cell Biol. 190.

Shiozaki, E.N., Shi, Y., 2004. Caspases, IAPs and Smac/DIABLO: mechanisms from structural biology. Trends Biochem. Sci. 29, 486–494. doi:10.1016/j.tibs.2004.07.003

Soengas, M.S., Capodieci, P., Polsky, D., Mora, J., Esteller, M., Opitz-Araya, X., McCombie, R., Herman, J.G., Gerald, W.L., Lazebnik, Y.A., Cordón-Cardó, C., Lowe, S.W., 2001. Inactivation of the apoptosis effector Apaf-1 in malignant melanoma. Nature 409, 207–11. doi:10.1038/35051606

Srinivasula, S.M., Hegde, R., Saleh, a, Datta, P., Shiozaki, E., Chai, J., Lee, R. a, Robbins, P.D., Fernandes-Alnemri, T., Shi, Y., Alnemri, E.S., 2001. A conserved XIAP-interaction motif in caspase-9 and Smac/DIABLO regulates caspase activity and apoptosis. Nature 410, 112–6. doi:10.1038/35065125

Suzanne, M., Steller, H., 2013. Shaping organisms with apoptosis. Cell Death Differ. 20, 669–675. doi:10.1038/cdd.2013.11

Thomas, H.E., Stunnenberg, H.G., Stewart, A.F., 1993. Heterodimerization of the Drosophila ecdysone receptor with retinoid X receptor and ultraspiracle. Nature 362, 471–5. doi:10.1038/362471a0

Thornberry, N. a., 1998. Caspases: Enemies Within. Science (80-.). 281, 1312–1316. doi:10.1126/science.281.5381.1312

Wang, L., Evans, J., Andrews, H.K., Beckstead, R.B., Thummel, C.S., Bashirullah, A., 2008. A genetic screen identifies new regulators of steroid-triggered programmed cell death in Drosophila. Genetics 180, 269–81. doi:10.1534/genetics.108.092478

Wang, L., Lam, G., Thummel, C.S., 2010. Med24 and Mdh2 are required for Drosophila larval salivary gland cell death. Dev. Dyn. 239, 954–964. doi:10.1002/dvdy.22213

Wang, S.L., Hawkins, C.J., Yoo, S.J., Müller, H. a, Hay, B. a, 1999. The Drosophila caspase inhibitor DIAP1 is essential for cell survival and is negatively regulated by HID. Cell 98, 453–63.

West, A.C., Johnstone, R.W., 2014. New and emerging HDAC inhibitors for cancer treatment. J. Clin. Invest. 124, 30–9. doi:10.1172/JCI69738

White, K., Tahaoglu, E., Steller, H., 1996. Cell killing by the Drosophila gene reaper. Science 271, 805–7.

Yang, Q.-H., Church-Hajduk, R., Ren, J., Newton, M.L., Du, C., 2003. Omi/HtrA2 catalytic cleavage of inhibitor of apoptosis (IAP) irreversibly inactivates IAPs and facilitates caspase activity in apoptosis. Genes Dev. 17, 1487–96. doi:10.1101/gad.1097903

Yao, T.-P., Segraves, W.A., Oro, A.E., McKeown, M., Evans, R.M., 1992. Drosophila ultraspiracle modulates ecdysone receptor function via heterodimer formation. Cell 71, 63–72. doi:10.1016/0092-8674(92)90266-F

Yin, V.P., Thummel, C.S., 2004. A balance between the diap1 death inhibitor and reaper and hid death inducers controls steroid-triggered cell death in Drosophila. Proc. Natl. Acad. Sci. U. S. A. 101, 8022–7. doi:10.1073/pnas.0402647101

Yin, V.P., Thummel, C.S., Bashirullah, A., 2007. Down-regulation of inhibitor of apoptosis levels provides competence for steroid-triggered cell death. J. Cell Biol. 178, 85–92. doi:10.1083/jcb.200703206

Yoo, S.J., Huh, J.R., Muro, I., Yu, H., Wang, L., Wang, S.L., Feldman, R.M.R., Clem, R.J., Müller, H.-A.J., Hay, B.A., 2002. Hid, Rpr and Grim negatively regulate DIAP1 levels through distinct mechanisms. Nat. Cell Biol. 4, 416–24. doi:10.1038/ncb793

Yuan, J., Shaham, S., Ledoux, S., Ellis, H.M., Horvitz, H.R., 1993. The C. elegans cell death gene ced-3 encodes a protein similar to mammalian interleukin-1 beta-converting enzyme. Cell 75, 641–52.

Zaffaroni, N., Pennati, M., Colella, G., Perego, P., Supino, R., Gatti, L., Pilotti, S., Zunino, F., Daidone, M.G., 2002. Expression of the anti-apoptotic gene survivin correlates with taxol resistance in human ovarian cancer. Cell. Mol. Life Sci. 59, 1406–1412. doi:10.1007/s00018-002-8518-3

Zou, H., Li, Y., Liu, X., Wang, X., 1999a. An APAf-1 · cytochrome C multimeric complex is a functional apoptosome that activates procaspase-9. J. Biol. Chem. doi:10.1074/jbc.274.17.11549

Zou, H., Li, Y., Liu, X., Wang, X., 1999b. An APAF-1 Cytochrome c Multimeric Complex Is a Functional Apoptosome That Activates Procaspase-9 *. Biochemistry 274, 11549–11556.

PART THREE

Developmental timing: a new role for transcriptional repression

CHAPTER 6

INO80-dependent regression of ecdysone-induced transcriptional responses regulates developmental timing in *Drosophila*

This chapter has been published in *Developmental Biology* (with permission)

Neuman SD*, Ihry RJ*, Gruetzmacher KM, Bashirullah A. (2014) INO80-dependent regression of ecdysone-induced transcriptional responses regulates developmental timing in *Drosophila*. *Dev Biol*. Mar 15;387(2):229-39.

*authors contributed equally to this work

ABSTRACT

Sequential pulses of the steroid hormone ecdysone regulate the major developmental transitions in *Drosophila*, and the duration of each developmental stage is determined by the length of time between ecdysone pulses. Ecdysone regulates biological responses by directly initiating target gene transcription. In turn, these transcriptional responses are known to be self-limiting, with mechanisms in place to ensure regression of hormone-dependent transcription. However, the biological significance of these transcriptional repression mechanisms remains unclear. Here we show that the chromatin remodeling protein *ino80* facilitates transcriptional repression of ecdysone-regulated genes during prepupal development. In *ino80* mutant animals, inefficient repression of transcriptional responses to the late larval ecdysone pulse delays the onset of the subsequent prepupal ecdysone pulse, resulting in a significantly longer prepupal stage. Conversely, increased expression of *ino80* is sufficient to shorten the prepupal stage by increasing the rate of transcriptional repression. Furthermore, we demonstrate that enhancing the rate of regression of the mid-prepupal competence factor *βFTZ-F1* is sufficient to determine the timing of head eversion and thus the duration of prepupal development. Although *ino80* is conserved from yeast to humans, this study represents the first characterization of a *bona fide ino80* mutation in any metazoan, raising the possibility that the functions of *ino80* in transcriptional repression and developmental timing are evolutionarily conserved.

INTRODUCTION

In all metazoans, the life cycle is divided into discrete stages, including embryonic development, a juvenile growth phase, sexual maturation, and reproductive adulthood. In *Drosophila*, these stages correspond to embryogenesis, three instars of larval development, metamorphosis with prepupal and pupal stages, and adulthood. The transition between each of these developmental stages is regulated by the steroid hormone 20-hydroxyecdysone (Riddiford, 1993), henceforth referred to as ecdysone. At the onset of each transition, a systemic pulse of ecdysone triggers the appropriate morphological and behavioral changes, causing the animal to progress forward in development toward adulthood. After a developmental transition has occurred, the ecdysone pulse recedes, only to be triggered again when the animal reaches the next developmental transition. Therefore, the duration of each developmental stage is determined by the timing of ecdysone pulses.

At the onset of metamorphosis, two sequential pulses of ecdysone regulate the transformation of a crawling larva into an immature adult. These two pulses outline the boundaries of prepupal development, an intermediate stage during which adult tissues undergo morphogenesis and obsolete larval tissues are destroyed (Robertson, 1936). The first pulse, referred to as the late larval pulse, triggers puparium formation, signaling the transition from larval development to prepupal development. The second pulse, referred to as the prepupal pulse, triggers head eversion, signaling the end of prepupal development and the start of pupal development. The duration of prepupal development is one of the most tightly regulated stages during the fly life cycle, with most animals in a

population completing the stage within an hour of one another (Bainbridge and Bownes, 1981).

Ecdysone, like all steroid hormones, acts through its nuclear receptor to directly regulate transcription of target genes. These transcriptional responses not only initiate stage- and tissue-specific biological responses, but also play a critical role in regulating the onset of the subsequent pulse of ecdysone, particularly during prepupal development (Thummel, 1996). Following the late larval ecdysone pulse, the early gene *E74A* is directly induced by ecdysone (Burtis et al., 1990). The early-late gene *DHR3* is also regulated by ecdysone signaling, but additional factors are required for maximal expression, resulting in delayed induction compared to early genes like *E74A* (Horner et al., 1995; Huet et al., 1995). *DHR3* then induces expression of the mid-prepupal competence factor *βFTZ-F1* (Lam et al., 1999; 1997; White et al., 1997). In turn, *βFTZ-F1* expression is required to initiate the prepupal pulse of ecdysone (Broadus et al., 1999; Woodard et al., 1994), whereupon *E74A* is induced again. In this manner, the late larval pulse of ecdysone initiates a sequential wave of gene activation that determines the timing of the prepupal ecdysone pulse and the duration of prepupal development.

The sequential transcriptional responses during prepupal development are subject to elaborate mechanisms that ensure timely repression of hormone-dependent gene expression. Many of the protein products of these ecdysone-induced genes repress their own transcription. For example, at the prepupal pulse of ecdysone, E74A protein binds the *E74A* genomic locus and inhibits ecdysone-dependent transcription, resulting in a sharp and self-limiting peak of *E74A* mRNA expression (Ihry et al., 2012; Urness and Thummel, 1990). βFTZ-F1 is thought to have a similar auto-inhibitory property (Woodard

et al., 1994). In addition to auto-inhibitory regulation, ecdysone-regulated genes exhibit cross-inhibitory regulation. For example, DHR3 protein represses *E74A* mRNA transcription after the late larval ecdysone pulse (Lam et al., 1997), ensuring that *E74A* levels decrease as DHR3 levels increase. Together, these transcriptional repression mechanisms help generate the sharp peaks and proper sequence of transcription in response to ecdysone pulses. However, despite ample evidence for mechanisms regulating repression of ecdysone-induced transcription, the biological significance of these mechanisms remains unclear.

The INO80 complex is one of the most highly conserved chromatin remodelers (Clapier and Cairns, 2009). The INO80 protein contains two functional domains: an N-terminal helicase-SANT-associated/post-HSA (HSA/PTH) domain and a Snf2 ATPase domain, which is split by a spacer region into N-terminal and C-terminal regions (Watanabe and Peterson, 2010). Each of these domains is required for binding to specific proteins that together comprise the INO80 chromatin remodeling complex, the composition of which is highly conserved from yeast to humans (R. C. Conaway and J. W. Conaway, 2009). INO80, together with its protein partners, facilitates ATP-dependent nucleosome sliding (Jin et al., 2005; Shen et al., 2000). Studies in yeast reveal that *ino80* is required for proper transcriptional regulation of many target genes (Jónsson et al., 2004; Shimada et al., 2008), and *in vitro* biochemical studies in yeast reveal that *ino80* tends to relocate nucleosomes from the edges of DNA fragments toward the center (Shen et al., 2003). Recent biochemical studies in a *Drosophila* cell culture system reveal that *ino80* primarily functions by increasing nucleosome density at its target loci (Moshkin et al., 2012), likely helping to establish repressive chromatin signatures and inhibit

transcription of target genes. Despite a high level of evolutionary conservation, studies of INO80 function have been largely limited to biochemical analysis, as mutant alleles have only been characterized in yeast and *Arabidopsis* (Fritsch et al., 2004; Shen et al., 2000).

Here, we report the identification and characterization of the first metazoan mutant of *ino80*. We demonstrate that *ino*80 function is essential for development, with mutant animals arresting during metamorphosis. This lethality can be rescued by ectopic expression of *ino80* from a transgenic construct. By focusing on prepupal development, we show that mutation of *ino80* results in defects in the timely repression of ecdysone-induced transcription. Importantly, the biological consequence of these repression defects is an extended duration of prepupal development. Moreover, increased expression of *ino80* reduces the duration of prepupal development, suggesting that *ino80*-dependent regression is critical for developmental timing. We also show that the rate of regression of the mid-prepupal competence factor *βFTZ-F1* is critical to determine the timing of head eversion and the duration of prepupal development. These results provide the first characterization of *ino80* function in a metazoan organism, and also provide novel insights linking transcriptional repression mechanisms with regulation of developmental timing.

MATERIALS AND METHODS

Stocks and recombination mapping

The following stocks were obtained from the Bloomington *Drosophila* Stock Center: *Df(3R)ED5942*, *Df(3R)DI-BX12*, *Df(3R)BSC475*, P{EPgy2}*Ino80*^{EY09251}, *Δ2-3 transposase*, *tubulin-Gal4*, *UAS-Dcr-2*, *Sgs3-GFP*. *ino80* RNAi KK102202 was obtained from the Vienna *Drosophila* RNAi Center. The *ino80*^{psg25} mutation was generated in an EMS mutagenesis screen (Wang et al., 2008). C. Thummel (University of Utah, Salt Lake City, UT) kindly provided the *hs-E74A* and *hs-βFTZ-F1* stocks. The dominant marker recombination mapping method used to identify *ino80*^{psg25} is described elsewhere (Sapiro et al., 2013). Experiments with hemizygous *ino80*^{psg25} mutant animals used the *Df(3R)ED5942* chromosomal deficiency.

Developmental staging and lethal phase analysis

Animals were raised on standard cornmeal molasses medium in the presence of yeast in an environmental chamber set to 25^{o}C. For developmental staging during metamorphosis, animals were synchronized either at puparium formation (white prepupa) or pupation (head eversion), placed on grape agar plates, and aged for the appropriate time at 25^{o}C. Staging prior to head eversion was based on the average duration of prepupal development (puparium formation to head eversion) of each respective genotype. Standard "blue food" technique was used to stage late third instar larvae (Andres and Thummel, 1994). Additional developmental stages prior to metamorphosis were aged at 25^{o}C from egg lay. For heat-shock treatments, animals at the appropriate stage were placed on grape agar plates sealed with Parafilm and submerged in a 37.5^{o}C

water bath for 30 minutes. Bainbridge and Bownes staging criteria was used to assign lethal phases: P1-P3 for prepupae (PP), P4-P9 for pupae (P), P10-15 for pharate adults (PA), and eclosed adults (A) (Bainbridge and Bownes, 1981).

Developmental timing analysis

For head eversion timing, white prepupae were placed on grape agar plates and allowed to age for an appropriate time at 25^{o}C. Aging on agar plates allowed for proper control of humidity. Animals were then scored for completed head eversion in 15 minute intervals. For eclosion timing, adult flies of the appropriate genotype were allowed to mate for two days, then transferred to fresh vials each day for three consecutive days. To determine the timing of eclosion, the vials were examined for empty pupal casings every 12 hours until all animals eclosed.

Generation of the *ino80* transgene

The *ino80* sequence was amplified from cDNA clone SD02886 (BDGP) with the following primers: 5' GAAATTAATACGACTCACTATAGGGAGACCGG 3' and 5' CGTCGACGTTAGAATTCGGCTACAAT 3'. The resulting amplicon was digested with *EcoRI*, ligated into *pCASPER-hs*, and sequence-verified. Transgenic flies were generated via standard protocols (Genetic Services, Inc.).

Imprecise excision

To generate excision events within the *ino80* locus, virgin females containing the viable P{EPgy2}*Ino80*^{EY09251} P-element were crossed to males with the *Δ2-3* transposase.

Progeny that lost the mini-white (w^{+mC}) marker on the P-element were selected, indicating that an excision event occurred, and stable stocks were generated from these animals. To identify imprecise excision events, each stock was screened for lethality. Complementation tests were carried out on the lethal excisions with *Df(3R)ED5942* and $ino80^{psg25}$ to identify potential *ino80* alleles. Standard PCR on a genomic DNA template was used to identify the deleted region in $ino80^{ex64}$.

A previously published report characterizes 2 excision alleles generated from mobilization of the same P-element we used (P{EPgy2}$Ino80^{EY09251}$), resulting in a 3 or 4 kilobase deletion, respectively, in the vicinity of the P-element (Bhatia et al., 2010). These alleles, unlike our *ino80* alleles, have a lethal phase early in development. However, these reported excision alleles were not tested for complementation with the *ino80*-containing chromosomal deficiency. Moreover, the specific location of the deletions was not directly characterized. Given that the P-element resides within a ~10 kilobase intron, it is unclear if these excision events disrupt *ino80* coding sequences. Importantly, in our excision scheme, most (27 of 28) of the excision events recovered were generated from a single locus residing outside the *ino80*-containing chromosomal deficiency. Each of the 27 lethal excision events of this complementation group has a lethal phase early in development. Thus, our results suggest that the original stock may have a second P-element, and the majority of lethal excision events affect that currently unidentified locus.

Quantitative PCR

qPCR was performed as previously described (Ihry et al., 2012). RNA was isolated from appropriately-staged whole animals or dissected salivary glands using the RNeasy Plus Mini Kit (Qiagen). cDNA was synthesized from 100-400 ng of total RNA using the SuperScript III First-Strand Synthesis System with oligo(dT)$_{20}$ primers (Invitrogen). qPCR was performed using LightCycler 480 SYBR Green I Master Mix (Roche) on a Roche 480 LightCycler. For each experiment, target genes of interest and the reference gene *rp49* were run simultaneously on three independently-isolated control and experimental biological samples. 3-4 serial dilutions of pooled cDNA derived from samples spanning development were used to determine the amplification efficiency of the primers in each experiment. Roche LightCycler 480 Software (Version 1.5) was used to calculate cycle threshold values and melting curves for each reaction. Relative expression and standard error were calculated using Relative Expression Software Tool (REST) (Pfaffl et al., 2002). Standard error calculated by REST reflects asymmetrical tendencies in the data. Primer sequences are listed in Table S1. Primers were designed with A plasmid Editor (ApE), GenScript Real-time PCR Primer Design tool, or QuantPrime (Arvidsson et al., 2008).

Immunofluorescence and image capture

Salivary glands from appropriately-staged animals were dissected, fixed, and immunostained using standard techniques (Yin et al., 2007). Primary antibodies used were rabbit α-cleaved caspase-3 (1:200; Cell Signaling) to detect activity of the caspase *Nc* (Fan and Bergmann, 2010) and mouse α-Lamin (1:50; Developmental Studies Hybridoma Bank) to detect breakdown of a target of caspases. Secondary antibodies

used were α-rabbit Cy3 (1:200; Jackson Immuno-Research Labs) and α-mouse AlexaFluor 488 (1:200; Invitrogen). DAPI was used to counterstain DNA (1:1,000; Invitrogen). Stained tissues were mounted on slides in Vectashield (Vector Laboratories). Immunofluorescence images were captured using an Olympus FLUOVIEW FV1000 confocal microscope with FV10-ASW software. Persistent salivary gland and lethal phase images were captured using an Olympus SZX16 stereomicroscope coupled to an Olympus DP72 camera with Olympus DPX2-BSW software.

Western blotting

Western blots were performed using standard methods as previously described (Ihry et al., 2012). 10 whole animals at the appropriate stage were homogenized in 75 µl of hi-salt lysis buffer, and total protein concentration was calculated using the Bradford assay. Transferred membranes were blocked with 5% BSA in PBST and then incubated with properly diluted primary antibodies overnight at 4^{o}C. Primary antibodies used were mouse α-E74A (1:2,000; a gift from C. Thummel) and rabbit α-β-actin (1:1,000; Cell Signaling Technologies). Secondary antibodies used were α-rabbit IgG alkaline phosphatase-linked antibody (1:30,000; GE Healthcare) and α-mouse IgG alkaline phosphatase-linked antibody (1:30,000; Sigma). Membranes were developed for imaging with ECF substrate (GE Healthcare) and were imaged using a Storm 840 Scanner (Amersham Bioscience) with ImageQuant TL software version 7.0 (GE Healthcare).

RESULTS

Identification of the first metazoan *ino80* mutant

To gain new insights into the mechanisms regulating ecdysone signaling during development, we previously conducted an EMS-based mutagenesis screen for mutations that disrupt the ecdysone-triggered destruction of the larval salivary glands during metamorphosis (Wang et al., 2008). Here, we characterize one of the mutations identified in this screen: *psg25*. Recombination mapping with pairs of dominant markers, followed by complementation tests with chromosomal deficiencies, was used to identify the region containing the *psg25* mutation (Sapiro et al., 2013). Additional complementation tests with deficiencies mapped *psg25* to a small region containing 20 genes (Fig. S1). *psg25* complemented all available lethals within the region; however, Sanger sequencing of *psg25* revealed a point mutation disrupting a donor splice site in the chromatin remodeler, *ino80.* Sanger sequencing of *psg25* cDNA confirmed that disruption of the donor splice site after the fourth exon results in the retention of a 26 base pair intron fragment, causing a frameshift leading to a nonsense mutation (Fig. 1A). When translated, *psg25* mRNA would produce a truncated INO80 protein, with loss of the C-terminal region of the Snf2 ATPase domain (Fig. 1B).

We also generated an independent allele of *ino80* via imprecise excision. We mobilized the P{EPgy2}*Ino80*^{EY09251} P-element, located in the 12th intron of the *ino80* locus. After mobilization of the P-element, 163 flies with excision events were identified by loss of the mini-white marker (w^{+mC}) on the transposable element; of these, 28 generated a lethal mutation on the excision chromosome (Fig. S2A). Of the 28 lethal mutations, only one failed to complement the *ino80*-containing chromosomal deficiency

and resulted in sterile progeny when crossed to *psg25*. This allele, designated as *ino80*^{ex64}, contains a large deletion to the right of the P-element (~20 kilobases), excising most of the Snf2 ATPase domain and leaving a short stretch of P-element sequence within the *ino80* locus (Fig. S2B). The excision event also deletes several other genes located within the introns of *ino80*. The remaining 27 lethal excisions comprise a single complementation group that has a lethal phase early in development, unlike *ino80*^{ex64} and *ino80*^{psg25}, which arrest during metamorphosis (Fig. 2B,S2C). Additionally, the 27 early lethal mutations complement *ino80*^{psg25}, *ino80*^{ex64}, and the chromosomal deficiency that deletes the entire *ino80* locus.

To confirm the gene identification of the *ino80*^{psg25} and *ino80*^{ex64} alleles, we conducted a rescue experiment. We generated a transgenic construct containing *ino80* cDNA under control of the heat-shock promoter (*hs-ino80*), and placed this construct in the *ino80*^{psg25} mutant background. *ino80*^{psg25} hemizygous (*ino80*^{psg25}*/Df*) and homozygous animals exhibit semi-lethality, with about 15% of the expected flies eclosing as viable, but sterile, adults (Fig. 1C). However, ubiquitous, leaky expression of *ino80* from the *hs-ino80* construct is able to rescue both the lethality and sterility observed in *ino80*^{psg25} hemizygous and homozygous animals. Additionally, *hs-ino80* also rescues the lethality observed in hemizygous and homozygous *ino80*^{ex64}, suggesting that the other genes disrupted by the excision event in *ino80*^{ex64} are not essential for viability. These results, together with the identical lethal phases of homozygous and hemizygous mutant animals (Fig. 2B, S2C), suggest that *ino80*^{psg25} and *ino80*^{ex64} are loss-of-function alleles of *ino80*. However, because *ino80*^{ex64} disrupts additional genes, we chose to continue our analysis of INO80 function with the EMS-induced *ino80*^{psg25} allele.

ino80 is primarily required at the onset of metamorphosis

To gain insights into the function of *ino80*, we first used quantitative reverse transcription real-time PCR (qPCR) to analyze the developmental profile of *ino80* mRNA expression. RNA was isolated from whole animals spanning embryogenesis through metamorphosis, and qPCR was used to quantify *ino80* mRNA levels in each developmental stage. *ino80* mRNA is expressed at low levels throughout development; however, the highest levels are observed during metamorphosis, with a peak of expression from puparium formation to two days after puparium formation (Fig. 2A).

We next determined when $ino80^{psg25}$ mutants arrest during development. Interestingly, all hemizygous mutant animals survive to enter metamorphosis, as the predicted percentage of expected progeny (one-third) is observed on the sides of vials when compared to balancer-containing siblings (33.4%, n=692). However, only a small percentage of these animals survive to reach adulthood. Most homozygous and hemizygous $ino80^{psg25}$ mutant animals arrest during pupal or pharate adult stages (Fig. 2B), and the few that do eclose are sterile (Fig. 1C). A similar lethal phase is observed in hemizygous $ino80^{ex64}$ mutant animals and in animals ubiquitously expressing *ino80-RNAi* (Fig. S2C). Although $ino80^{psg25}$ mutant animals arrest during metamorphosis, they form normal pupae or pharate adults without visible abnormalities, demonstrating that morphogenetic processes are not disrupted by mutation of *ino80* (Fig. 2C,D). Overall, the expression profile and mutant lethal phase suggest that *ino80* plays a critical role during metamorphosis.

Initiation of the ecdysone-dependent death response is delayed in *ino80^{psg25}* mutant salivary glands

To gain insights into the role of *ino80* during metamorphosis, we first analyzed the function of this gene in the ecdysone-dependent destruction of the larval salivary glands. *ino80^{psg25}* mutant animals (*ino80^{psg25}/Df(3R)ED5942*, unless otherwise indicated) exhibit a highly penetrant persistent salivary gland (PSG) phenotype (85.2%, n=54) at 24 h after puparium formation (APF) (Fig. S3A, B). The PSG phenotype is also observed in *ino80^{ex64}* hemizygous animals (83.7% PSG, n=37) (Fig. S3C). Importantly, other ecdysone-dependent processes, such as Sgs3 glue protein synthesis and secretion, occur normally (Fig. S3D-H), indicating that *ino80^{psg25}* mutant salivary glands have the ability to respond to ecdysone signals. To understand how *ino80^{psg25}* disrupts salivary gland destruction, we first analyzed induction of the death activators *reaper* (*rpr*) and *hid involution defective* (*hid*), which represents a point-of-no-return during the death response (Grether et al., 1995; White et al., 1996). We dissected salivary glands from control and *ino80^{psg25}* mutant animals staged relative to head eversion and analyzed their gene expression profiles using qPCR. As expected, control animals exhibit strong induction of both *rpr* and *hid* by 1.5 h after head eversion (AHE)(black line, Fig. 3A). In contrast, *ino80^{psg25}* salivary glands do not have maximal induction of *rpr* and *hid* until 3 AHE (blue line, Fig. 3A). Consistent with the observed delay in induction of *rpr* and *hid*, *ino80^{psg25}* salivary glands show a delay in caspase activation. At 1.5 AHE, control salivary glands have bright staining for cleaved-caspase-3 and dim staining for nuclear lamin, a substrate of caspases (Fig. 3B). In contrast, *ino80^{psg25}* mutant salivary glands at the same stage do not have staining for caspase activity and have bright staining for nuclear lamin (Fig. 3C). However, at 3 AHE,

ino80^{psg25} mutant salivary glands exhibit caspase activity similar to that seen in control glands at 1.5 AHE (Fig. 3D). Overall, these results suggest that *ino80*^{psg25} delays, rather than disrupts, the ecdysone-triggered death response.

Because the death response in salivary glands is triggered by the prepupal pulse of ecdysone (Jiang et al., 1997; 2000), we next used qPCR to measure expression of ecdysone response genes in *ino80*^{psg25} mutant salivary glands. The prepupal ecdysone pulse occurs two hours prior to head eversion, and, as expected, control glands exhibit strong induction of *E74A*, an early gene that is directly induced by ecdysone, at this timepoint (black line, Fig. 3A). However, at the same stage in *ino80*^{psg25} mutant salivary glands, *E74A* has yet to be induced (blue line, Fig. 3A), suggesting a delayed onset of the prepupal ecdysone pulse. Consistent with these results, expression of *E74B*, which is repressed by high ecdysone titers, shows a corresponding delayed repression in *ino80*^{psg25} mutant salivary glands (Fig. 3A). Taken together, these results suggest that the timing of the prepupal ecdysone pulse is likely delayed in *ino80*^{psg25} mutant animals.

Regression of transcriptional responses is delayed during *ino80*^{psg25} prepupal development

To determine why the prepupal pulse of ecdysone is delayed in *ino80*^{psg25} mutant animals, we analyzed the sequence of expression of ecdysone-regulated genes during prepupal development. We collected control and *ino80*^{psg25} mutant whole animals staged relative to puparium formation and analyzed the expression profiles of ecdysone-regulated genes using qPCR. The samples collected span two pulses of ecdysone: the late larval pulse, which triggers puparium formation, and the prepupal pulse, which

triggers head eversion and pupation. In *ino80*^{psg25} mutant animals, induction of ecdysone-target genes in response to the late larval pulse occurs normally (Fig. 4A). The early gene *E74A* is induced to maximal levels at -4 APF, followed by induction of the early-late gene *DHR3*, which peaks at 2 APF. *βFTZ-F1* also reaches maximal expression levels on time, with a transcriptional peak at 8 APF. All of these genes are induced at the proper time, intensity, and sequence following the late larval pulse of ecdysone in *ino80*^{psg25} mutant animals, indicating that induction of target genes is unaffected by mutation of *ino80*.

In contrast, regression of these ecdysone-regulated genes does not occur in a timely manner following the late larval pulse of ecdysone in *ino80*^{psg25} mutant animals (Fig. 4A). In control animals, *E74A* transcription is shut off by 4 APF, while *E74A* expression is maintained until 6 APF in *ino80*^{psg25} mutant animals. Similarly, *DHR3* and *βFTZ-F1* expression persists about two hours longer in *ino80*^{psg25} compared to controls. Therefore, transcriptional responses to the late larval pulse of ecdysone are induced on time but regress two hours late in *ino80*^{psg25} mutant animals. These regression defects appear to affect only a subset of genes during prepupal development. For example, the ecdysone biosynthetic genes *phantom* (*phm*), *spookier* (*spok*), *shadow* (*sad*), and *disembodied* (*dib*) are properly induced prior to the late larval pulse of ecdysone, and are properly repressed at the end of the pulse in *ino80*^{psg25}, although *sad* exhibits a subtle delay in repression (Fig. 4A, S4A). Additionally, *Cyp18a1*, a cytochrome P450 responsible for degradation of ecdysone, is also properly induced and repressed in *ino80*^{psg25} mutant animals (Fig. 4A).

In addition, *ino80*^{psg25} mutant animals also exhibit a delay in the onset of the responses to the prepupal ecdysone pulse. *E74A* expression is induced at high ecdysone

titers and reflects the peak of the prepupal ecdysone pulse. In control animals, *E74A* is maximally induced by the prepupal ecdysone pulse at 10 APF, while *E74A* is not induced until 12 APF in *ino80^{psg25}* mutant animals (Fig. 4A), two hours later than controls. Additionally, *E74B*, which is induced at low ecdysone titers and repressed at high ecdysone titers, shows a normal expression profile in *ino80^{psg25}* mutant animals after the late larval pulse of ecdysone, but exhibits delayed induction during prepupal development (Fig. 4A), suggesting that *ino80^{psg25}* does not affect the titer of the prepupal ecdysone pulse, only when it is induced. Our data thus far suggests that delayed repression of ecdysone-induced transcription after the late larval ecdysone pulse results in delayed onset of the prepupal ecdysone pulse.

Auto-inhibition of ecdysone-induced genes is inefficient in *ino80^{psg25}* mutant animals

To understand the nature of the regression defects, we examined the efficiency of auto-inhibitory mechanisms in *ino80^{psg25}* mutant animals. Although the hyper-induction and prolonged expression of *E74A* mRNA observed in *ino80^{psg25}* is also observed in mutants that disrupt E74A protein translation (Ihry et al., 2012), western blots with an E74A antibody show that both control and *ino80^{psg25}* mutant animals have robust expression of E74A protein (Fig. S4B). We then tested the possibility that *ino80* is required to facilitate the auto-inhibitory activity of E74A protein. Precocious expression of E74A protein from a heterologous transgenic construct (*hs-E74A*) results in strong repression of the hormone-dependent transcription of endogenous *E74A* after the prepupal ecdysone pulse (Fig. 4B,C). In contrast, precocious expression of E74A protein in

ino80^{psg25} mutant animals results in incomplete repression of ecdysone-dependent transcription of *E74A*. Similarly, precocious expression of βFTZ-F1 protein results in incomplete repression of endogenous *βFTZ-F1* transcription in *ino80*^{psg25} mutant animals compared to control animals (Fig. 4B,C). Taken together, these results show that *ino80* is required for the efficient auto-inhibitory activity of the E74A and βFTZ-F1 proteins, suggesting that the transcriptional regression defects during prepupal development are due to defects in auto-inhibition.

Loss of *ino80* extends the duration of prepupal development

Our data thus far indicates that regression defects during *ino80*^{psg25} prepupal development result in delayed induction of the prepupal ecdysone pulse. Given that the prepupal ecdysone pulse triggers head eversion, we tested if the timing of head eversion was affected in *ino80*^{psg25} mutant animals. Control and *ino80*^{psg25} mutant animals were synchronized at puparium formation, then allowed to age until head eversion. Control animals begin to head evert at about 10.75 APF, and all animals complete head eversion by 12.5 APF, with about 50% of animals head everting by 11.5 APF (HE_{50}~11.5 APF, n=156)(black line, Fig. 5A). Control animals exhibit little variance in the duration of prepupal development, with nearly 90% of animals completing head eversion within a one-hour interval. The synchrony of this process is evident in the steep slope of the head eversion timing curve. *ino80*^{psg25} mutant animals do not begin head everting until about 12.5 APF, and all animals complete head eversion by 14.25 APF (HE_{50}~13.25 APF, n=152)(blue line, Fig. 5A), demonstrating that *ino80*^{psg25} animals head evert nearly two hours later than controls. A similar head eversion delay is observed in *ino80*^{ex64}

(HE_{50}~13.5 APF, n=11). Despite a significant delay in the timing of head eversion, the *ino80*^{psg25} timing curve still exhibits a steep upward slope, suggesting that *ino80*^{psg25} does not disrupt the mechanisms that execute head eversion. The two hour delay in head eversion, coupled with the two hour delay in the onset of the prepupal ecdysone pulse shown above, suggest that the prolonged prepupal stage is likely a consequence of the regression defects in *ino80*^{psg25} mutant animals.

Increased levels of *ino80* shorten the duration of prepupal development through acceleration of transcriptional regression

To demonstrate a causal relationship between INO80-dependent transcriptional repression mechanisms and the duration of prepupal development, we first tested whether increased expression of *ino80* could accelerate transcriptional repression and/or developmental timing. Strikingly, increased expression of *ino80* does both. We collected control and *hs-ino80* animals staged relative to puparium formation and used qPCR for gene expression analysis, using a one-hour sampling rate during prepupal development in order to detect smaller shifts in gene expression. Leaky expression of *ino80* from the heat-inducible transgenic construct (*hs-ino80*) results in about a 20-fold increase in *ino80* mRNA levels at 25^{o}C. In *hs-ino80* animals, transcription of *E74A* and *DHR3* in response to the late larval pulse appears to regress normally (Fig. 5B). However, *βFTZ-F1* regresses faster in *hs-ino80* animals, with significantly lower levels at 9 APF compared to controls. This accelerated regression coincides with precocious induction of *E74A* at the prepupal ecdysone pulse, one hour earlier than in controls. These results indicate that increased expression of *ino80* is sufficient to accelerate regression of *βFTZ-F1*.

Importantly, *hs-ino80* animals head evert faster than control animals. Animals overexpressing *ino80* have an HE_{50} of ~10.75 APF (n=151, purple line, Fig. 5A), about 45 minutes faster than control animals. Similar results were obtained with an independent insertion of the *hs-ino80* transgene (HE_{50} ~10.75 APF, n=85). These effects on developmental timing were not limited to prepupal development. Control animals begin to eclose at 9.5 days after egg deposition (AED), and over 50% eclose by 11 days AED (E_{50}~10.75 AED, n=624) (black box, Fig. 5C). In contrast, increased expression of *ino80* results in nearly a one day acceleration of overall development (E_{50}~10 AED, n=906) (purple box, Fig. 5C). Although only a few *ino80^{psg25}* animals eclose, those that do survive to adulthood eclose about one day later than controls (E_{50}~11.75 AED, n=19) (solid blue box, Fig. 5C), demonstrating that *ino80^{psg25}* mutants exhibit developmental delays throughout the entire life cycle. Importantly, this delay in *ino80^{psg25}* is fully rescued by leaky expression of *ino80* from the *hs-ino80* transgene (*hs-ino80/+; ino80^{psg25}/Df*, E_{50}~10.75 AED, n=224) (dashed blue box, Fig. 5C).

Accelerated transcriptional repression of *βFTZ-F1* is sufficient to shorten the duration of prepupal development

To confirm a causal relationship between transcriptional repression mechanisms and the duration of prepupal development, we focused on independently modifying the rate of regression of *βFTZ-F1*. To do this, we exploited the auto-inhibition assay described earlier (Fig. 4B). When βFTZ-F1 protein is expressed from a heterologous promoter prior to initiation of endogenous *βFTZ-F1* transcription, the endogenous transcriptional response is ablated (Woodard et al., 1994). However, we show that when βFTZ-F1

protein is expressed immediately after the start of endogenous transcription, it does not block induction of *βFTZ-F1*; instead it appears to accelerate regression of *βFTZ-F1* transcription. Animals were heat-shocked at 6 APF, at the start of endogenous *βFTZ-F1* expression, then collected at one-hour intervals following the heat-shock. In this assay, the endogenous transcriptional response does occur, as *βFTZ-F1* transcript levels are equal in both control and *hs-βFTZ-F1*-treated animals at 0.5 hrs after heat-shock (AHS) (Fig. 6A). However, in *hs-βFTZ-F1*-treated animals, endogenous *βFTZ-F1* transcription regresses significantly faster, with transcription shut off by 3.5 AHS, while endogenous *βFTZ-F1* transcription is still detectable at 4.5 AHS in control animals (*cf.* solid and dashed black lines, Fig. 6A). These results demonstrate that increased expression of βFTZ-F1 protein, delivered at the proper time, is sufficient to accelerate the rate of *βFTZ-F1* transcriptional regression. Importantly, this faster regression results in a dramatically shorter prepupal stage (HE_{50} ~10.75 APF, n=101), accelerating the timing of head eversion by almost 2 hours compared to comparably-treated controls (*cf.* solid and dashed black lines, Fig. 6B).

Given that auto-inhibition of *βFTZ-F1* appears to be inefficient in *ino80*^{psg25} (Fig. 4C), we next analyzed the effects of ectopic βFTZ-F1 expression in the *ino80*^{psg25} mutant background. Endogenous *βFTZ-F1* expression starts about one hour later in *ino80*^{psg25} mutant animals compared to controls (Fig. S5A); therefore, as expected, heat-shock-induced expression of βFTZ-F1 at 6 APF abolishes the endogenous *βFTZ-F1* transcriptional response (blue dashed line, Fig. S5B) and results in prepupal lethality. These effects of precocious expression of βFTZ-F1 on survival are consistent with similar experiments in control animals (Yamada et al., 2000). However, *hs-βFTZ-F1* treatment in

ino80^{psg25} mutant animals at 7 APF, when *βFTZ-F1* transcripts are at a comparable level to controls at 6 APF (Fig. S5A), allows the endogenous *βFTZ-F1* transcriptional response to occur (Fig. 6A). Addition of βFTZ-F1 protein accelerates regression of endogenous *βFTZ-F1* in *ino80*^{psg25} mutant animals (blue dashed line, Fig. 6A). Strikingly, this regression occurs slightly faster than in control animals lacking the *hs-βFTZ-F1* transgene (*cf.* blue dashed and black solid lines, Fig. 6A). As a result, head eversion in these *hs-βFTZ-F1*-treated *ino80*^{psg25} mutant animals occurs nearly two hours faster (HE_{50}~12.25 APF, n=99) than comparably treated *ino80*^{psg25} animals lacking the transgene (HE_{50}~14.25 APF, n=97) (*cf.* blue dashed and blue solid lines, Fig. 6B), effectively rescuing the timing of head eversion to that of control animals. Taken together, these results demonstrate that *ino80*-dependent repression of transcriptional responses, particularly those of *βFTZ-F1*, determines the duration of prepupal development.

DISCUSSION

The duration of the *Drosophila* life cycle is determined by the timing of ecdysone pulses that regulate each developmental transition. Here, we demonstrate the importance of regression of ecdysone-induced transcriptional responses in the regulation of developmental timing. The chromatin remodeling protein *ino80* is required for efficient repression of ecdysone-induced genes. *ino80*^{psg25} mutant animals fail to shut off ecdysone-induced transcription in a timely manner, resulting in delayed onset of head eversion and prolonged prepupal development. Furthermore, accelerating regression of the mid-prepupal competence factor *βFTZ-F1* through overexpression of *ino80* or enhancement of the auto-inhibitory activity of βFTZ-F1 protein is sufficient to accelerate the timing of head eversion and shorten the duration of prepupal development. Therefore, INO80 function is required for timely regression of target genes, revealing a critical role for transcriptional regression in the timing of prepupal development.

The role of *ino80* in efficient repression of ecdysone-regulated transcriptional responses is consistent with the previously-described biochemical functions of this chromatin remodeler. Although loss of INO80 changes expression levels of a significant fraction of the yeast genome (Jónsson et al., 2004; Shimada et al., 2008), the function of INO80 in transcription appears to be primarily in modulating the kinetics of gene expression (Barbaric et al., 2007). These effects on transcription are mediated by the ability of the INO80 complex to promote ATP-dependent nucleosome sliding (Shen et al., 2000). This sliding activity results in nucleosome eviction at some sites while increasing nucleosome density at others (Morrison and Shen, 2009), raising the question of whether the primary role of INO80 in transcription is in activation or repression of its target genes.

Our data suggests that *ino80* plays a more critical role in repression of target genes in *Drosophila*. Consistent with our data, studies in a *Drosophila* cell culture system indicate that INO80 tends to increase nucleosome density at target loci (Moshkin et al., 2012).

All of the genes that show *ino80*-dependent regression defects--*E74A, DHR3,* and *βFTZ-F1*--were originally identified as ecdysone-induced "puffs" on *Drosophila* polytene chromosomes (Ashburner et al., 1974). In other words, the expression of these genes occurs on such a large scale that they elicit visible "puffs" of open chromatin on the polytene chromosomes of the larval salivary glands. Given that INO80 also appears to regulate repair and resolution of complex DNA rearrangements (R. C. Conaway and J. W. Conaway, 2009; Morrison and Shen, 2009), it is possible that INO80 is required to restore normal chromatin structure to chromosomal puffs following ecdysone-induced transcription, thereby facilitating regression of these hormone-dependent responses. Genomic studies show that INO80 binds many, but not all, loci in the genome (Moshkin et al., 2012); however, it is unclear whether there is a direct correlation between INO80 binding and target gene expression levels. Moreover, given that INO80 does not directly bind DNA *in vivo*, how INO80 selects its target genes remains unclear. One possibility is that Ying-Yang 1 (YY1), or Pleiohomeotic (Pho) in *Drosophila*, a zinc finger transcription factor that is part of the INO80 complex in all metazoans (Cai et al., 2005; Jin et al., 2005; Klymenko et al., 2006), may play that role. In fact, in human cells, YY1 plays a role in localizing the INO80 complex to some target genes (Cai et al., 2007), raising the possibility that this transcription factor aids in recognition of INO80-target genes in *Drosophila*.

Our results indicate that *βFTZ-F1* is a biologically-relevant target of *ino80*-dependent transcriptional repression. Under all experimental conditions tested, head eversion does not begin until *βFTZ-F1* transcription is shut off, showing a direct correlation between the rate of regression of *βFTZ-F1* and the onset of head eversion. Additionally, the timing of shut-off of *βFTZ-F1* directly correlates with the onset of *E74A*, raising the possibility that regression of *βFTZ-F1* serves as a temporal checkpoint for initiation of the prepupal ecdysone pulse. The mechanism by which *βFTZ-F1* regulates the prepupal ecdysone pulse has yet to be determined, although ectopic expression of βFTZ-F1 protein is sufficient to amplify early-gene expression in response to ecdysone (Woodard et al., 1994). Given that *βFTZ-F1* expression is critical at various stages of development, it is possible that the developmental delays observed in *ino80* mutant animals are mediated by its effects on repression of genes, like *βFTZ-F1*, that play a critical role in temporal checkpoints during development.

Our *ino80* data highlights a novel class of developmental timing phenotypes. Many developmental timing phenotypes disrupt the order of developmental programs. For example, heterochronic genes in *C. elegans* specify temporal cell fate decisions during development, thereby regulating the proper sequence of developmental events (Ambros, 2000; Thummel, 2001). Another class of timing phenotypes affects the ability to progress from one developmental program to the next. For example, an inability to remove ecdysone during prepupal development prevents the transition to pupal development (Rewitz et al., 2010). Our *ino80* mutations highlight the subtle but essential role of the timely progression through development. Although the progression and order of developmental programs do not appear to be disrupted in *ino80* mutant animals, most

animals fail to complete development, highlighting the importance of proper control of the timing of events during development.

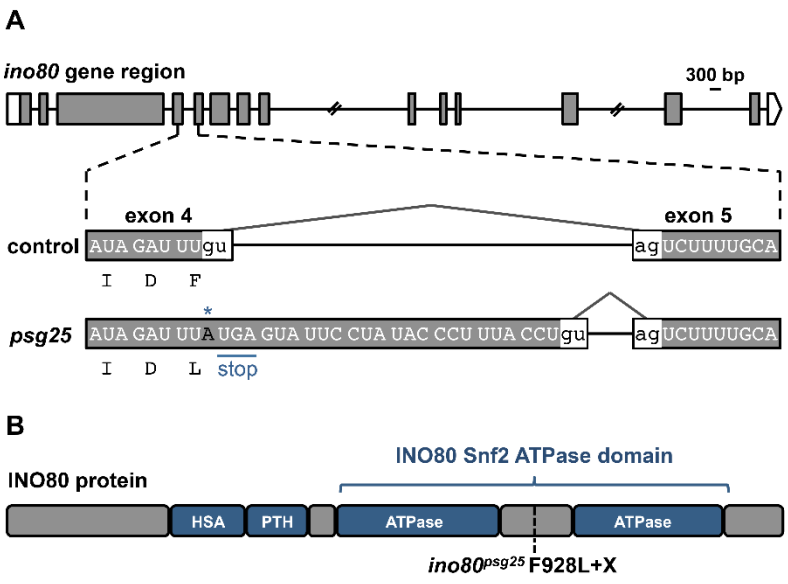

C

genotype	*hs-ino80*	eclosed / expected (%)	sterility
ino80^{psg25}/Df(3R)ED5942	-	14.9% (n=141)	sterile
	+	84.5% (n=174)	fertile
ino80^{psg25}/*ino80*^{psg25}	-	19.1% (n=173)	sterile
	+	81.6% (n=114)	fertile
ino80^{ex64}/Df(3R)ED5942	-	0% (n=77)	n/a
	+	35.4% (n=161)	fertile
ino80^{ex64}/*ino80*^{ex64}	-	0% (n=133)	n/a
	+	83.5% (n=273)	fertile

Figure 1. Identification of a novel allele of *ino80*. (A) Schematic describing the *psg25* lesion in the *ino80* locus. *psg25* has a point mutation (G to A) that disrupts the donor splice site after the fourth exon, resulting in retention of an intron fragment and an in-frame stop codon immediately following the mutated donor splice site. Retention of the intron also changes a phenylalanine immediately before the donor splice site to a leucine. Boxes represent exons and shaded regions highlight coding sequences. Diagram to scale, except for two large introns, marked with slashes. Scale bar=300 base pairs (bp). **(B)** Schematic of the domains of the INO80 protein and the location of the *psg25* nonsense mutation, indicated by the dotted line. **(C)** Leaky expression of *ino80* from a *hs-*

ino80 transgene rescues *ino80*^{psg25} and *ino80*^{ex64} lethality. Percentage of mutant animals surviving to adulthood in the presence (+) or absence (-) of one copy of the *hs-ino80* transgene. Presence of the *hs-ino80* transgene also rescues the fertility of eclosing animals. Eclosion percentages expressed as observed eclosion percentage divided by expected eclosion percentage (33%).

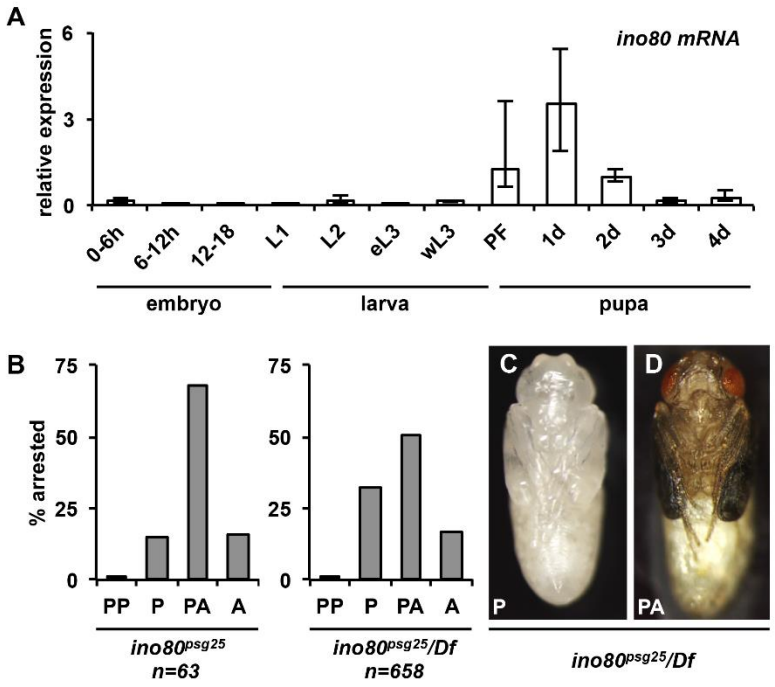

Figure 2. *ino80* is required for viability during metamorphosis. (A) qPCR analysis of *ino80* mRNA expression throughout development. The highest expression levels are observed at the onset of metamorphosis, from puparium formation to 2 days after puparium formation (APF). Animals staged from egg lay for embryonic (0-6, 6-12 and 12-18 hours after egg lay (AEL)) and larval stages (L1: 30-42 AEL, L2: 54-66 AEL, eL3: 76-88 AEL). wL3 identified by robust expression of Sgs3-GFP. Stages during metamorphosis were synchronized at puparium formation (PF) and collected in 24-hour intervals. *y*-axis plots relative expression compared to 2 days APF; *x*-axis denotes the developmental stage analyzed. Three independently-isolated whole animal samples were run for each time point and target genes were normalized to *rp49*. **(B)** Lethal phase analysis of homozygous and hemizygous *ino80*^{psg25} mutant animals. Most homozygous and hemizygous *ino80*^{psg25} mutant animals die after head eversion, as either pupae or pharate

adults. A smaller fraction eclose as adults. **(C-D)** Hemizygous *ino80*^{psg25} mutant animals that arrest as pupae (C) or pharate adults (D) have normal morphology, with head eversion and extension of wings and legs. Animals were dissected out of their pupal cases and imaged at their respective terminal stages. PF=puparium formation, PP=prepupa, P=pupa, PA=pharate adult, A=eclosed adult.

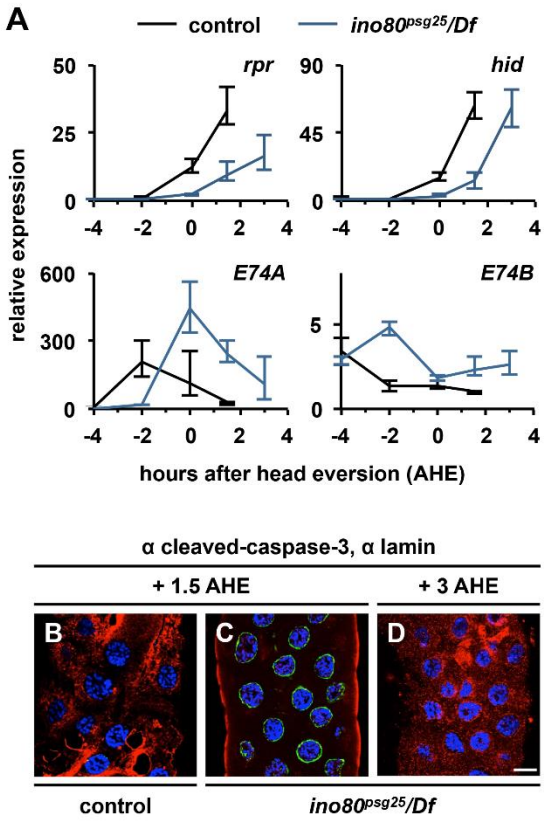

Figure 3. Destruction of the larval salivary glands is delayed in *ino80*^{psg25} mutant animals. (A) qPCR analysis of target gene expression in control (black lines) and *ino80*^{psg25} (blue lines) mutant salivary glands staged relative to head eversion. Control glands have strong induction of *rpr* and *hid* by 1.5 h after head eversion (AHE), while *ino80*^{psg25} glands do not have maximal induction of *rpr* and *hid* until 3 AHE. Induction and regression of *E74A* and *E74B* is also delayed in *ino80*^{psg25} mutant salivary glands. *y*-axis represents relative expression compared to the lowest point in control animals; *x*-axis represents developmental stage relative to head eversion. Three independently-isolated samples were run for each timepoint; relative expression calculated by normalizing to *rp49*. **(B-D)** Activation of caspases detected by staining for cleaved-caspase-3 (red) and nuclear lamin (green) in control and *ino80*^{psg25} mutant salivary glands. DNA labeled with

DAPI shown in blue. Control glands have ubiquitous caspase activation and strong loss of nuclear lamin staining by 1.5 AHE (B). In contrast, *ino80*^{psg25} glands have caspase activation similar to controls by 3AHE (D), but not at 1.5 AHE (C). Scale bar is 20µm. AHE= after head eversion.

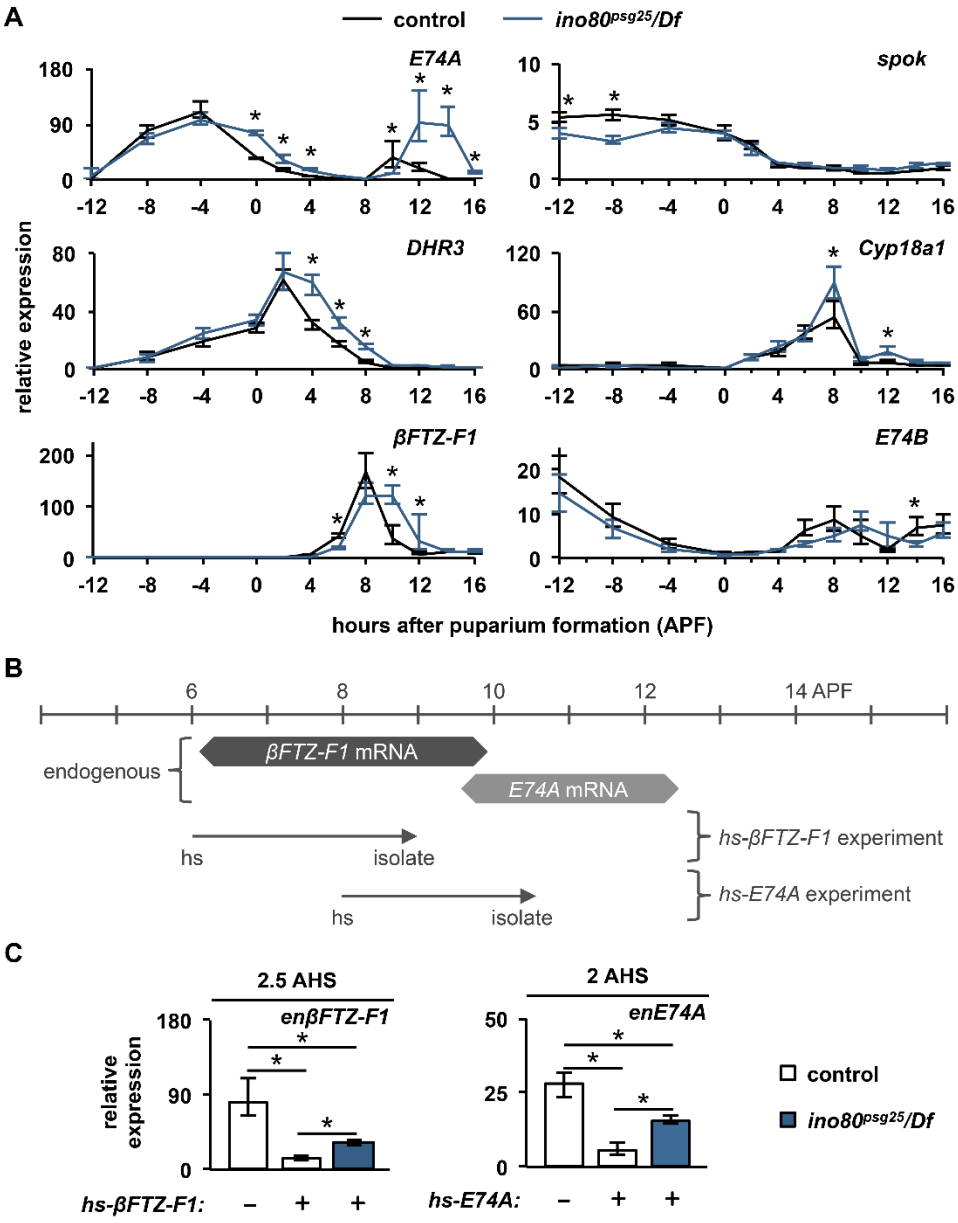

Figure 4. *ino80* is required for efficient regression of ecdysone-regulated genes during prepupal development. (A) qPCR analysis of target genes during prepupal development in control (black lines) and *ino80*^{psg25} (blue lines) mutant whole animals. The ecdysone-regulated genes *E74A*, *DHR3*, and *βFTZ-F1* are induced in the proper sequence in *ino80*^{psg25} mutant animals following the late larval ecdysone pulse; however,

ino80^{psg25} mutant animals exhibit significant delays in repression of all three of these genes. In contrast, the ecdysone biosynthetic gene *spok*, the ecdysone turnover gene *Cyp18a1*, and the ecdysone concentration-dependent target *E74B* are unaffected in *ino80*^{psg25} mutant animals. *y*-axis represents relative expression compared to the lowest point in control animals; *x*-axis represents developmental stage relative to puparium formation. Three independently-isolated whole animal samples were run for each timepoint and normalized to *rp49*. **(B)** Experimental paradigm to test efficiency of auto-inhibition by ectopic expression of the βFTZ-F1 and E74A proteins. Control and *ino80*^{psg25} animals were heat-shocked two hours prior to the endogenous peak of *βFTZ-F1* (dark gray) or *E74A* (light gray) expression in each respective genotype, then allowed to recover for about 2 hours before isolation of total RNA. Timescale shows hours after puparium formation (APF). Arrows indicate time of heat-shock and isolation. **(C)** Auto-inhibition of βFTZ-F1 and E74A occurs inefficiently in *ino80*^{psg25} mutant animals. On left, expression of βFTZ-F1 protein from the *hs-βFTZ-F1* transgene is sufficient to repress endogenous *βFTZ-F1* transcription in control animals (white bars). The same treatment in *ino80*^{psg25} mutant animals results in incomplete repression of endogenous *βFTZ-F1* transcription (blue bar). On right, similar results are obtained in a comparable experiment with ectopic expression of E74A. *y*-axis represents relative expression compared to the lowest point in each developmental profile; *x*-axis denotes heat-shock treatment. Asterisks denote significant differences between control and mutant samples ($p<0.05$).

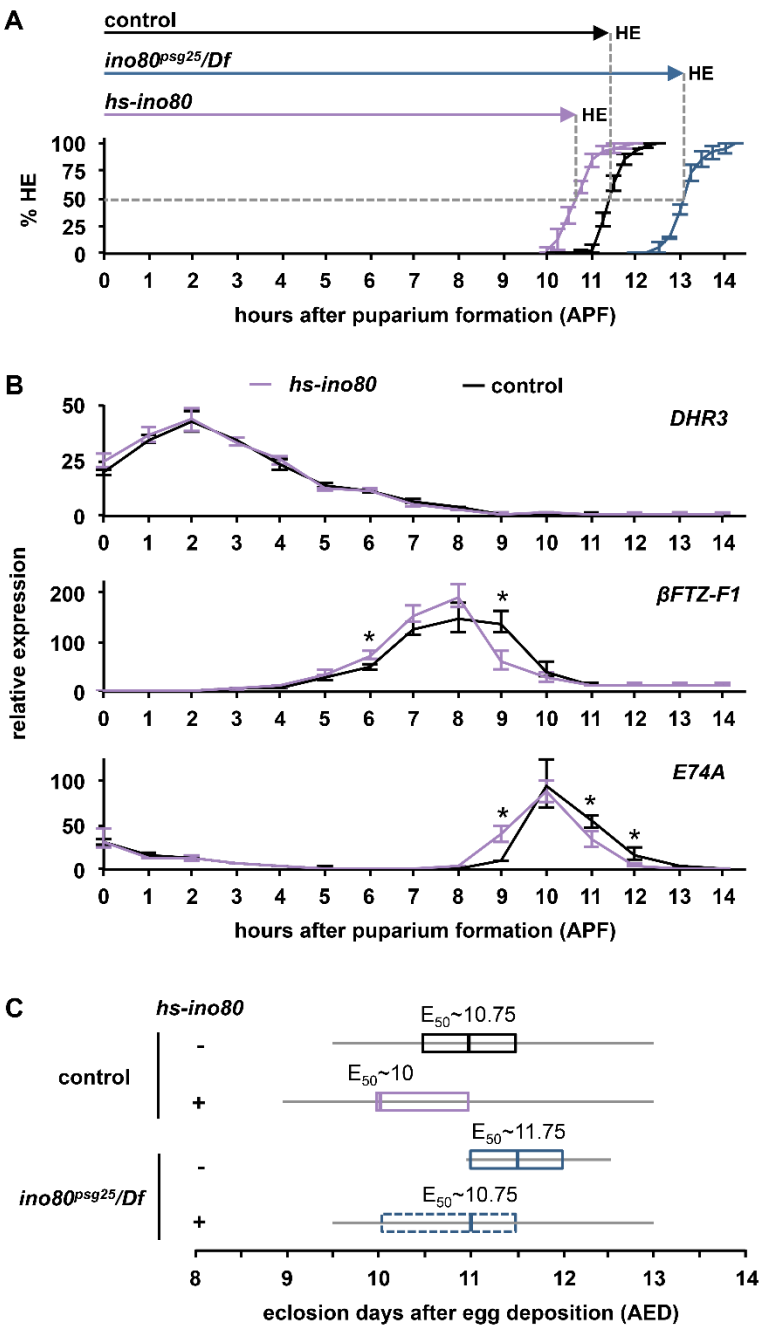

Figure 5. *ino80* regulates the duration of development. (A) Head eversion timing in control (black line), *ino80*^{psg25} (blue line), and *hs-ino80* (purple line) animals. 50% of control animals head evert by 11.5 APF (HE_{50}~11.5, total n=156). *ino80*^{psg25} mutant animals have delayed head eversion, with 50% of the animals head everting by 13.25

APF (HE_{50}~13.25, total n=152). *hs-ino80* accelerates head eversion, with 50% of animals head everting by 10.75 APF (HE_{50}~10.75, total n=151). *y*-axis plots the percentage of animals completing head eversion; *x*-axis plots time in hours relative to puparium formation (APF). Three independent samples of n~50 animals were analyzed for each genotype; error bars represent plus or minus one standard deviation. **(B)** qPCR analysis of ecdysone-regulated transcription in control (black line) and *hs-ino80* (purple line) whole animals staged relative to puparium formation. The *DHR3* expression profile is nearly identical in control and *hs-ino80* animals. In contrast, *βFTZ-F1* regresses significantly faster in *hs-ino80* animals compared to controls. *E74A* also displays a significant acceleration in onset and repression in *hs-ino80*. *y*-axis plots relative expression compared to the lowest point in controls; *x*-axis represents stages relative to puparium formation. Three independently-isolated whole animal samples were run for each timepoint and normalized to *rp49*. Asterisks denote significant differences between control and mutant samples ($p<0.05$). **(C)** Box plot of eclosion time in control and $ino80^{psg25}$ mutant animals with or without the *hs-ino80* transgene. Control animals (black box) begin to eclose at 9.5 days AED, and 50% eclose by 10.75 AED (n=624). Few $ino80^{psg25}$ animals eclose (blue box), but those that do begin to eclose at 11 days AED, and 50% eclose by 11.75 AED (n=19). Increased expression of *ino80* from the *hs-ino80* transgene (purple box) accelerates eclosion timing, with animals beginning to eclose before 9 days AED (E_{50}~10 AED, n=906). Leaky expression of *ino80* from the *hs-ino80* transgene (dotted blue box) is sufficient to rescue the eclosion delay observed in $ino80^{psg25}$ mutant animals, as *hs-ino80/+;* $ino80^{psg25}$*/Df* animals begin to eclose at 9.5 days AED (E_{50}~10.75 AED, n=224). For each genotype, the gray horizontal lines

(whiskers) represent the range for all animals analyzed, the boxes outline the middle two quartiles, and vertical lines within the boxes denote the median. *x*-axis represents time to eclosion in days after egg deposition (AED); *y*-axis shows each respective genotype plus (+) or minus (-) the *hs-ino80* transgene. The time when 50% of animals eclose (E_{50}) is listed for each respective genotype.

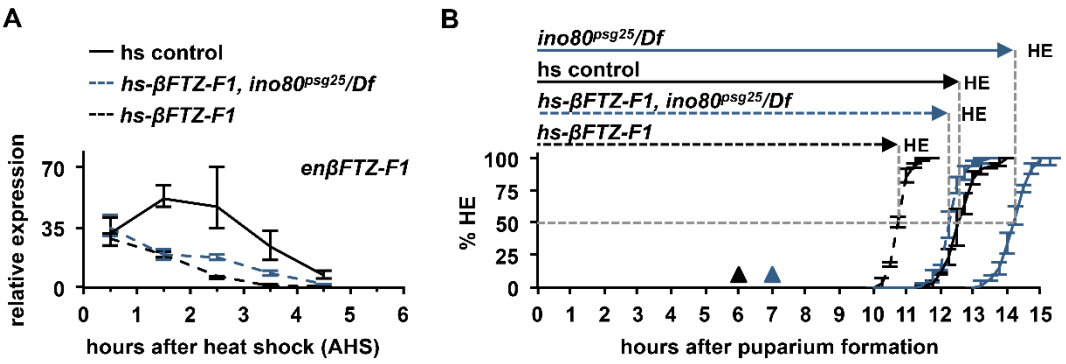

Figure 6. Precocious transcriptional repression of endogenous *βFTZ-F1* is sufficient to accelerate developmental timing. (A) Endogenous *βFTZ-F1* regresses significantly faster after expression of βFTZ-F1 protein from a heterologous promoter (*hs-βFTZ-F1*). All genotypes have similar levels of induction of endogenous *βFTZ-F1* at 0.5 hrs after heat shock (AHS). Ectopic βFTZ-F1 protein shuts off endogenous *βFTZ-F1* transcription by 3.5 AHS in control animals (dashed black line), but it takes longer in *ino80*^{psg25} mutant animals (dashed blue line). *y*-axis plots relative expression compared the lowest point in the developmental profile; *x*-axis represents hours after heat-shock (AHS). Three independently-isolated whole animal samples were run for each timepoint and normalized to *rp49*. **(B)** Accelerated repression of *βFTZ-F1* is sufficient to decrease the duration of prepupal development. 50% of heat-shocked control animals head evert by 12.75 APF (HE_{50}~12.5 APF, total n=104). However, additional βFTZ-F1 protein accelerates the timing of head eversion by 2 hours (dashed black line, HE_{50}~10.75 APF, total n=101). 50% of heat-shocked *ino80*^{psg25} mutants head evert by 14.25 APF (solid blue line, HE_{50}~14.25 APF, total n=97), but ectopic expression of βFTZ-F1 protein in the *ino80*^{psg25} mutant background accelerates the timing of head eversion by about 2 hours (dashed blue line, HE_{50}~12.25 APF, total n=99). *x*-axis represents hours after puparium

formation (APF); *y*-axis represents the percentage of animals head everted. Three independent samples of n~33 animals were analyzed for each genotype; error bars represent plus or minus one standard deviation. Triangles denote time of heat-shock in each genotype (black=control; blue=*ino80*^{psg25}*/Df*).

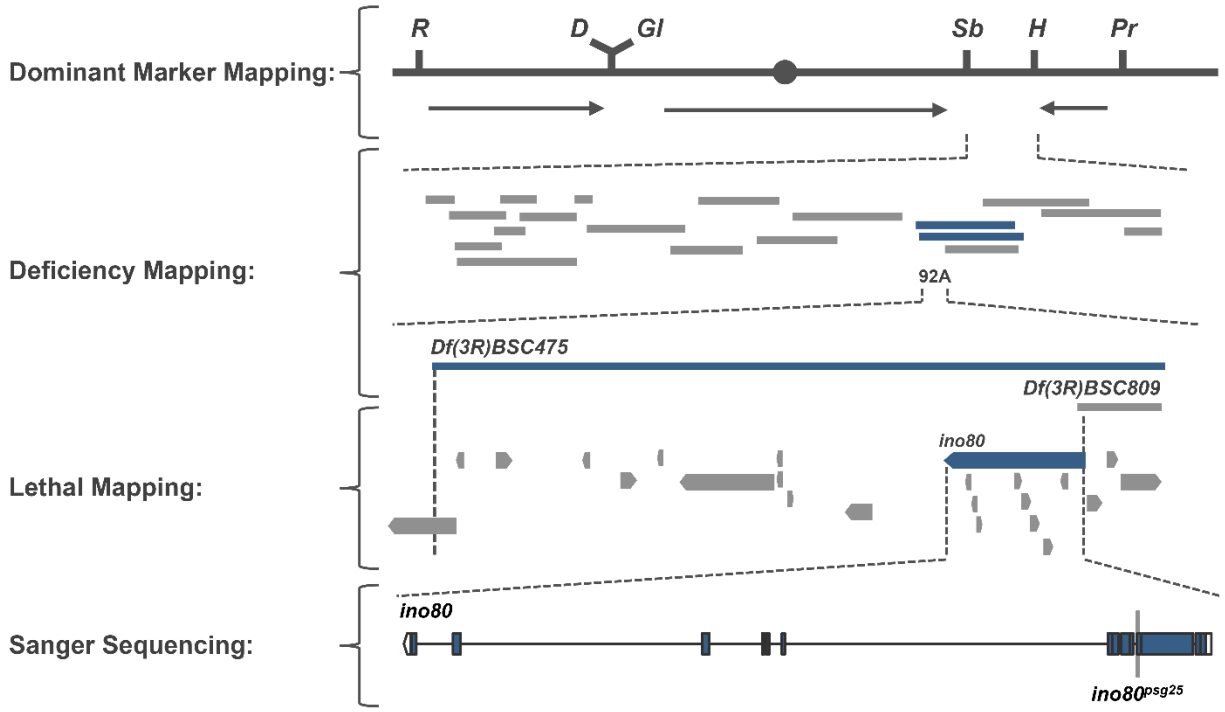

Figure S1. Mapping of the *psg25* mutation. *psg25* was mapped by dominant marker recombination, complementation tests, and Sanger sequencing. Recombination mapping with pairs of dominant markers placed *psg25* in the *Stubble* (*Sb*), *Hairless* (*H*) region, right of the *Roughened* (*R*), *Dichaete* (*D*) and *Glued* (*Gl*), *Stubble* (*Sb*) regions and left of the *Hairless* (*H*), *Prickly* (*Pr*) region (see arrows, method described in Sapiro *et al.* 2013). *psg25* failed to complement two overlapping chromosomal deficiencies, but complemented all available lethals in the region. Sanger sequencing of candidate genes identified a lesion disrupting the donor splice site after the fourth exon of *ino80*. The entire *ino80* locus encompasses over 34 kilobases.

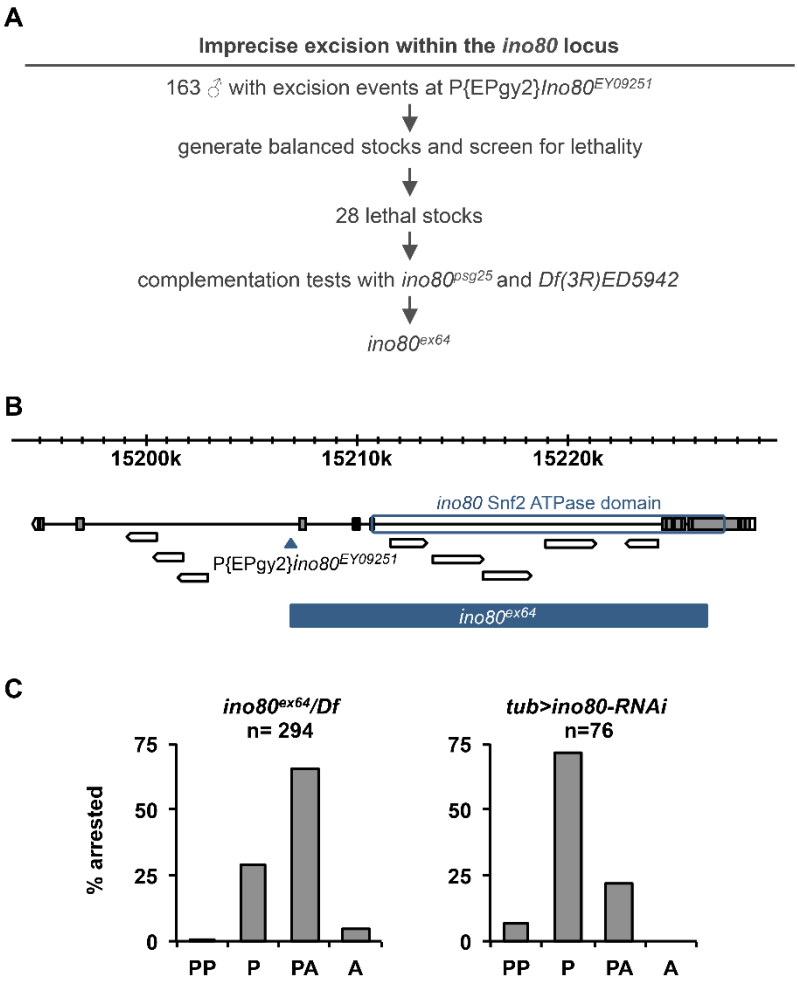

Figure S2. Generation of a second *ino80* allele via imprecise excision. (A) Diagram of crosses used to generate imprecise excision stocks. Of 163 excision events tested, only one excision, *ex64*, failed to complement the *ino80*-containing chromosomal deficiency. **(B)** Characterization of the molecular lesion in $ino80^{ex64}$. PCR analysis identified a large deletion within the *ino80* locus, removing most of the Snf2 ATPase domain and leaving a region of P-element sequence behind. **(C)** Lethal phase analysis of $ino80^{ex64}/Df$ and ubiquitous expression of *ino80-RNAi* (*uas-ino80-RNAi/UAS-Dcr-2; tubulin-Gal4*). Most $ino80^{ex64}$ and *ino80-RNAi* animals arrest after head eversion, as pupae or pharate adults.

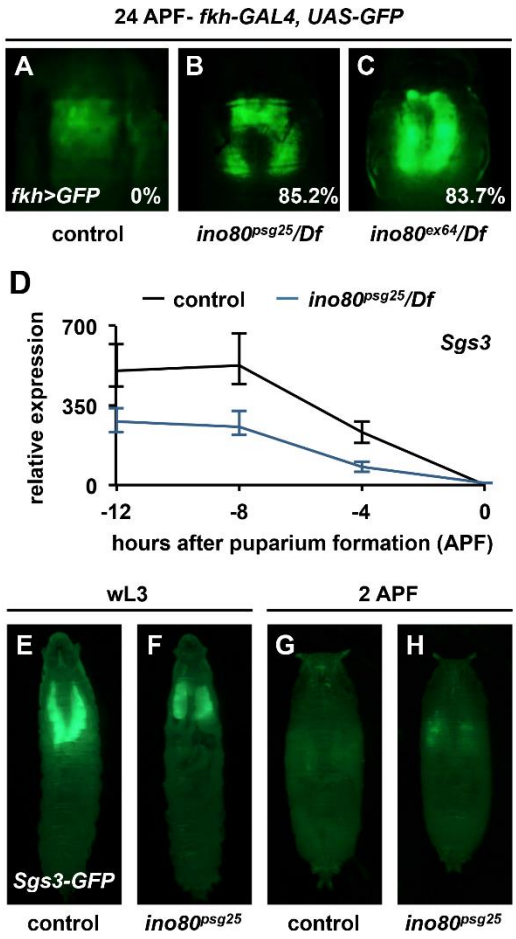

Figure S3. Analysis of ecdysone-dependent responses in *ino80^{psg25}* mutant salivary glands. (A-C) *fkh-Gal4, UAS-GFP* expression in control (A), *ino80^{psg25}/Df* (B), and *ino80^{ex64}/Df* (C) mutant animals at 24 h after puparium formation (APF). (A) Control glands have diffuse GFP expression, indicating the glands have been eliminated via programmed cell death. (B-C) *ino80^{psg25}* and *ino80^{ex64}* mutant animals have strong expression of GFP at 24 APF, indicative a persistent salivary gland phenotype (85.2%, n=54 and 83.7%, n=37, respectively). **(D)** qPCR analysis of *Sgs3* mRNA expression in control (black line) and *ino80^{psg25}* (blue line) mutant whole animals. *Sgs3* transcription is induced and repressed properly in *ino80^{psg25}*. y-axis represents relative expression

compared to the lowest point in control animals; x-axis represents developmental stage relative to puparium formation (APF). Three independently-isolated samples were run for each timepoint; relative expression calculated by normalizing to *rp49*. **(E-H)** Sgs3-GFP expression in control (E,G) and *ino80*^{psg25} (F,H) mutant animals. (E,F) Both genotypes robustly express Sgs3-GFP in wL3, indicating that *ino80*^{psg25} does not disrupt glue protein synthesis. (G,H) Sgs3-GFP is no longer present in salivary glands of either genotype at 2 APF, indicating that *ino80*^{psg25} does not disrupt glue protein secretion.

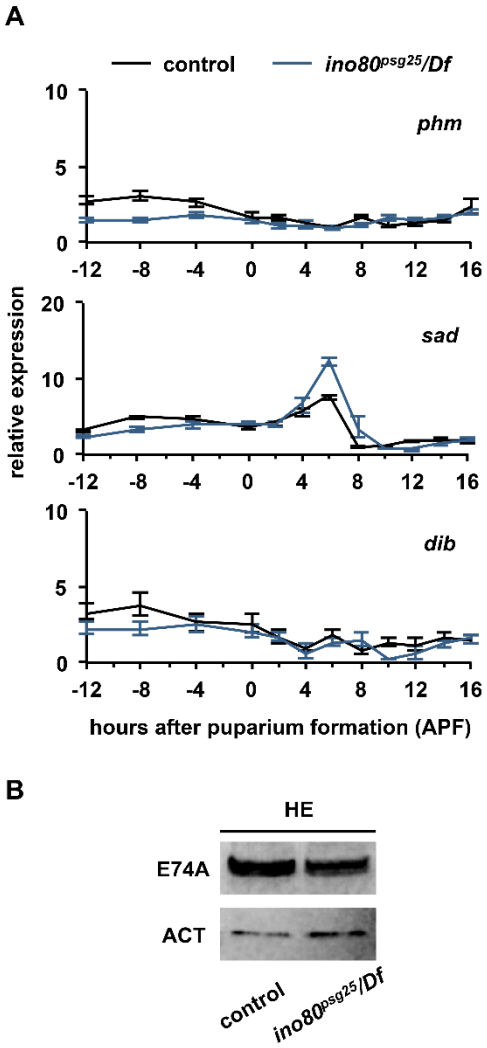

Figure S4. *ino80* is not required for repression of all genes during prepupal development. (A) qPCR analysis of ecdysone biosynthesis genes in whole animals staged relative to puparium formation. *ino80*^{psg25} (blue line) does not disrupt expression of *phantom (phm)*, *shadow* (*shd*), or *disembodied* (*dib*) when compared to controls (black line). y-axis represents relative expression compared to the lowest point in control animals; x-axis represents developmental stage relative to puparium formation (APF). Three independently-isolated samples were run for each timepoint; relative expression calculated by normalizing to *rp49*. **(B)** Western blot for E74A protein in control and

ino80^{psg25} mutant whole animals at head eversion. E74A is robustly translated in both control and *ino80*^{psg25} animals. β-actin used as a loading control.

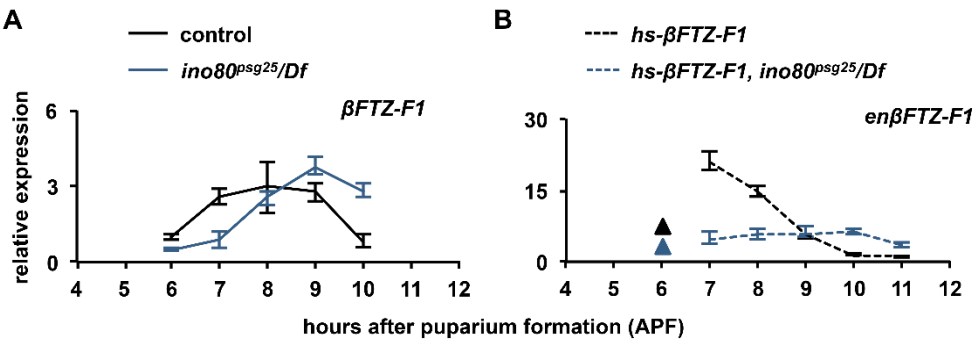

Figure S5. Regulation of *βFTZ-F1* expression in control and *ino80^{psg25}* mutant animals. (A) qPCR analysis of *βFTZ-F1* expression in control (black line) and *ino80^{psg25}* mutant (blue line) animals in one-hour increments. *βFTZ-F1* induction is delayed by about 1 hour in *ino80^{psg25}*. y-axis plots relative expression compared to the lowest point in controls; x-axis represents hours relative to puparium formation. Three independently-isolated whole animal samples were run for each timepoint and normalized to *rp49*. **(B)** Expression of βFTZ-F1 protein at 6 APF abolishes endogenous *βFTZ-F1* transcription in *ino80^{psg25}* mutant animals. qPCR analysis of endogenous *βFTZ-F1* expression after heat-treatment with *hs-βFTZ-F1* at 6 APF in control (dashed black line) and *ino80^{psg25}* mutant (dashed blue line) animals. y-axis plots relative expression compared to the lowest point in controls; x-axis represents stages relative to puparium formation. Three independently-isolated whole animal samples were run for each timepoint and normalized to *rp49*. Triangles denote the time of heat-shock (black=control, blue=*ino80^{psg25}*).

Table S1 Primer sequences for qPCR

Gene	Primer Sequence	Source
Cyp18a1 F	TCTTCGATGGCAAGAATCACGAG	This Study
Cyp18a1 R	TATCCACAGCAGGGTGGTCTTG	
DHR3 F	GGCAGGAGCTGGAAACGAATC	This Study
DHR3 R	GGTCCTGCTGCGAATCTATCG	
dib F	GTGACCAAGGAGTTCATTAGATTTC	(Deng and Kerppola, 2013)
dib R	CCAAAGGTAAGCAAACAGGTTAAT	
E74A F	GTTGCCGGAACATTATGGATATA	(Caldwell et al., 2005)
E74A R	GCCCTATGTCGGCTTGCT	
E74B F	ATCGGCGGCCTACAAGAAG	(Caldwell et al., 2005)
E74B R	TCGATTGCTTGACAATAGGAATTTC	
FTZ-F1 F	TGGACTACACCCTCACCTGC	(Ihry et al., 2012)
FTZ-F1 R	CACGTTCTCCCGGCCTCTAT	
enβFTZ-F1 F	TGCATGCACCGAATACAATA	This Study
enβFTZ-F1 R	GCTGTTCTGCTGGTGTGG	
hid F	ATCCAGTCTGCCATACCGATAG	(Ihry et al., 2012)
hid R	AACAGTTGGCCAAGTGAAGCTC	
ino80 F	GTTAAGGTGACGACGCTGCTG	This Study
ino80 R	CCTGGCTATTCTCACACTGATTG	
phm F	TTTCGGCGCGATGTGATGACTG	This Study
phm R	GCGCAGATGATGCCAAATCCAC	
rp49 F	CCAGTCGGATCGATATGCTAA	(Denton et al., 2009)
rp49 R	ACGTTGTGCACCAGGAACTT	
rpr F	ATCCGAAGACCGGAAGAAAG	(Ihry et al., 2012)
rpr R	GTGGCTCTGTGTCCTTGACTG	
sad F	GATGTGCCAGGCGATATGAT	(Deng and Kerppola, 2013)
sad R	ACTGCTGAATGCGGTCGT	
Sgs3 F	CTACCGCCCTAGCGAGCAT	(Chiang and Kurnit, 2003)
Sgs3 R	GCATCCACAATCGCAACAGT	
spok F	GCGGTGATCGAAACAACTC	(Deng and Kerppola, 2013)
spok R	CGAGCTAAATTTCTCCGCTTT	

REFERENCES

Ambros, V., 2000. Control of developmental timing in Caenorhabditis elegans. Current Opinion in Genetics & Development 10, 428–433.

Andres, A.J., Thummel, C.S., 1994. Methods for quantitative analysis of transcription in larvae and prepupae. Methods Cell Biol. 44, 565–573.

Arvidsson, S., Kwasniewski, M., Riaño-Pachón, D.M., Mueller-Roeber, B., 2008. QuantPrime--a flexible tool for reliable high-throughput primer design for quantitative PCR. BMC Bioinformatics 9, 465.

Ashburner, M., Chihara, C., Meltzer, P., Richards, G., 1974. Temporal control of puffing activity in polytene chromosomes. Cold Spring Harb. Symp. Quant. Biol. 38, 655–662.

Bainbridge, S.P., Bownes, M., 1981. Staging the metamorphosis of Drosophila melanogaster. Journal of embryology and experimental morphology 66, 57–80.

Barbaric, S., Luckenbach, T., Schmid, A., Blaschke, D., Hörz, W., Korber, P., 2007. Redundancy of chromatin remodeling pathways for the induction of the yeast PHO5 promoter in vivo. J Biol Chem 282, 27610–27621.

Bhatia, S., Pawar, H., Dasari, V., Mishra, R.K., Chandrashekaran, S., Brahmachari, V., 2010. Chromatin remodeling protein INO80 has a role in regulation of homeotic gene expression in Drosophila. Genes to Cells.

Broadus, J., McCabe, J.R., Endrizzi, B., Thummel, C.S., Woodard, C.T., 1999. The Drosophila beta FTZ-F1 orphan nuclear receptor provides competence for stage-specific responses to the steroid hormone ecdysone. Molecular Cell 3, 143–149.

Burtis, K.C., Thummel, C.S., Jones, C.W., Karim, F.D., Hogness, D.S., 1990. The Drosophila 74EF early puff contains E74, a complex ecdysone-inducible gene that encodes two ets-related proteins. Cell 61, 85–99.

Cai, Y., Jin, J., Florens, L., Swanson, S.K., Kusch, T., Li, B., Workman, J.L., Washburn, M.P., Conaway, R.C., Conaway, J.W., 2005. The mammalian YL1 protein is a shared subunit of the TRRAP/TIP60 histone acetyltransferase and SRCAP complexes. J Biol Chem 280, 13665–13670.

Cai, Y., Jin, J., Yao, T., Gottschalk, A.J., Swanson, S.K., Wu, S., Shi, Y., Washburn, M.P., Florens, L., Conaway, R.C., Conaway, J.W., 2007. YY1 functions with INO80 to activate transcription. Nature Structural & Molecular Biology 14, 872–874.

Caldwell, P.E., Walkiewicz, M., Stern, M., 2005. Ras activity in the Drosophila prothoracic gland regulates body size and developmental rate via ecdysone release. Curr Biol 15, 1785–1795.

Chiang, P.-W., Kurnit, D.M., 2003. Study of dosage compensation in Drosophila. Genetics 165, 1167–1181.

Clapier, C.R., Cairns, B.R., 2009. The biology of chromatin remodeling complexes. Annu. Rev. Biochem. 78, 273–304.

Conaway, R.C., Conaway, J.W., 2009. The INO80 chromatin remodeling complex in transcription, replication and repair. Trends Biochem Sci 34, 71–77.

Deng, H., Kerppola, T.K., 2013. Regulation of Drosophila metamorphosis by xenobiotic response regulators. PLoS Genet 9, e1003263.

Denton, D., Shravage, B., Simin, R., Mills, K., Berry, D.L., Baehrecke, E.H., Kumar, S., 2009. Autophagy, not apoptosis, is essential for midgut cell death in Drosophila. Curr Biol 19, 1741–1746.

Fan, Y., Bergmann, A., 2010. The cleaved-Caspase-3 antibody is a marker of Caspase-9-like DRONC activity in Drosophila. Cell Death Differ 17, 534–539.

Fritsch, O., Benvenuto, G., Bowler, C., Molinier, J., Hohn, B., 2004. The INO80 protein controls homologous recombination in Arabidopsis thaliana. Molecular Cell 16, 479–485.

Grether, M.E., Abrams, J.M., Agapite, J., White, K., Steller, H., 1995. The head involution defective gene of Drosophila melanogaster functions in programmed cell death. Genes Dev 9, 1694–1708.

Horner, M.A., Chen, T., Thummel, C.S., 1995. Ecdysteroid regulation and DNA binding properties of Drosophila nuclear hormone receptor superfamily members. Dev Biol 168, 490–502.

Huet, F., Ruiz, C., Richards, G., 1995. Sequential gene activation by ecdysone in Drosophila melanogaster: the hierarchical equivalence of early and early late genes. Development 121, 1195–1204.

Ihry, R.J., Sapiro, A.L., Bashirullah, A., 2012. Translational Control by the DEAD Box RNA Helicase belle Regulates Ecdysone-Triggered Transcriptional Cascades. PLoS Genet 8, e1003085.

Jiang, C., Baehrecke, E.H., Thummel, C.S., 1997. Steroid regulated programmed cell death during Drosophila metamorphosis. Development 124, 4673–4683.

Jiang, C., Lamblin, A.F., Steller, H., Thummel, C.S., 2000. A steroid-triggered transcriptional hierarchy controls salivary gland cell death during Drosophila metamorphosis. Molecular Cell 5, 445–455.

Jin, J., Cai, Y., Yao, T., Gottschalk, A.J., Florens, L., Swanson, S.K., Gutiérrez, J.L., Coleman, M.K., Workman, J.L., Mushegian, A., Washburn, M.P., Conaway, R.C., Conaway, J.W., 2005. A mammalian chromatin remodeling complex with similarities to the yeast INO80 complex. J Biol Chem 280, 41207–41212.

Jónsson, Z.O., Jha, S., Wohlschlegel, J.A., Dutta, A., 2004. Rvb1p/Rvb2p recruit Arp5p and assemble a functional Ino80 chromatin remodeling complex. Molecular Cell 16, 465–477.

Klymenko, T., Papp, B., Fischle, W., Köcher, T., Schelder, M., Fritsch, C., Wild, B., Wilm, M., Müller, J., 2006. A Polycomb group protein complex with sequence-specific DNA-binding and selective methyl-lysine-binding activities. Genes Dev 20, 1110–1122.

Lam, G., Hall, B.L., Bender, M., Thummel, C.S., 1999. DHR3 is required for the prepupal-pupal transition and differentiation of adult structures during Drosophila metamorphosis. Dev Biol 212, 204–216.

Lam, G.T., Jiang, C., Thummel, C.S., 1997. Coordination of larval and prepupal gene expression by the DHR3 orphan receptor during Drosophila metamorphosis. Development 124, 1757–1769.

Morrison, A., Shen, X., 2009. Chromatin remodelling beyond transcription: the INO80 and SWR1 complexes. Nat Rev Mol Cell Biol.

Moshkin, Y.M., Chalkley, G.E., Kan, T.W., Reddy, B.A., Ozgur, Z., van Ijcken, W.F.J., Dekkers, D.H.W., Demmers, J.A., Travers, A.A., Verrijzer, C.P., 2012. Remodelers organize cellular chromatin by counteracting intrinsic histone-DNA sequence preferences in a class-specific manner. Mol Cell Biol 32, 675–688.

Pfaffl, M.W., Horgan, G.W., Dempfle, L., 2002. Relative expression software tool (REST) for group-wise comparison and statistical analysis of relative expression results in real-time PCR. Nucl Acids Res 30, e36.

Rewitz, K.F., Yamanaka, N., O'connor, M.B., 2010. Steroid hormone inactivation is required during the juvenile-adult transition in Drosophila. Dev Cell 19, 895–902.

Riddiford, L., 1993. Hormones and Drosophila development, in: Bate, M., Martinez-Arias, A. (Eds.), The Development of Drosophila Melanogaster. The development of Drosophila melanogaster., pp. 899–939.

Robertson, C.W., 1936. The metamorphosis of Drosophila melanogaster, including an accurately timed account of the principal morphological changes. Journal of morphology 59, 351–399.

Sapiro, A.L., Ihry, R.J., Buhr, D.L., Konieczko, K.M., Ives, S.M., Engstrom, A.K., Wleklinski, N.P., Kopish, K.J., Bashirullah, A., 2013. Rapid Recombination Mapping for High-Throughput Genetic Screens in Drosophila. G3 (Bethesda) 3, 2313-2319.

Shen, X., Mizuguchi, G., Hamiche, A., Wu, C., 2000. A chromatin remodelling complex involved in transcription and DNA processing. Nature 406, 541–544.

Shen, X., Ranallo, R., Choi, E., Wu, C., 2003. Involvement of actin-related proteins in ATP-dependent chromatin remodeling. Molecular Cell 12, 147–155.

Shimada, K., Oma, Y., Schleker, T., Kugou, K., Ohta, K., Harata, M., Gasser, S.M., 2008. Ino80 chromatin remodeling complex promotes recovery of stalled replication forks. Curr Biol 18, 566–575.

Thummel, C.S., 1996. Flies on steroids--Drosophila metamorphosis and the mechanisms of steroid hormone action. Trends Genet 12, 306–310.

Thummel, C.S., 2001. Molecular mechanisms of developmental timing in C. elegans and Drosophila. Dev Cell 1, 453–465.

Urness, L.D., Thummel, C.S., 1990. Molecular interactions within the ecdysone regulatory hierarchy: DNA binding properties of the Drosophila ecdysone-inducible E74A protein. Cell 63, 47–61.

Wang, L., Evans, J., Andrews, H.K., Beckstead, R.B., Thummel, C.S., Bashirullah, A., 2008. A genetic screen identifies new regulators of steroid-triggered programmed cell death in Drosophila. Genetics 180, 269–281.

Watanabe, S., Peterson, C.L., 2010. The INO80 family of chromatin-remodeling enzymes: regulators of histone variant dynamics. Cold Spring Harb. Symp. Quant. Biol. 75, 35–42.

White, K., Tahaoglu, E., Steller, H., 1996. Cell killing by the Drosophila gene reaper. Science 271, 805–807.

White, K.P., Hurban, P., Watanabe, T., Hogness, D.S., 1997. Coordination of Drosophila metamorphosis by two ecdysone-induced nuclear receptors. Science 276, 114–117.

Woodard, C.T., Baehrecke, E.H., Thummel, C.S., 1994. A molecular mechanism for the stage specificity of the Drosophila prepupal genetic response to ecdysone. Cell 79, 607–615.

Yamada, M., Murata, T., Hirose, S., Lavorgna, G., Suzuki, E., Ueda, H., 2000. Temporally restricted expression of transcription factor betaFTZ-F1: significance for embryogenesis, molting and metamorphosis in Drosophila melanogaster. Development 127, 5083–5092.

Yin, V.P., Thummel, C.S., Bashirullah, A., 2007. Down-regulation of inhibitor of apoptosis levels provides competence for steroid-triggered cell death. J Cell Biol 178, 85–9.

APPENDICES

Analysis of *Drosophila* compound eye development

APPENDIX 1

Retinal expression of the *Drosophila eyes absent* gene is controlled by several cooperatively acting *cis*-regulatory elements

This chapter has been published in *PLoS Genetics*

Weasner BM, Weasner BP, Neuman SD, Bashirullah A, Kumar JP. (2016) Retinal expression of the *Drosophila eyes absent* gene is controlled by several cooperatively acting *cis*-regulatory elements. *PLoS Genet*. Dec 8;12(12): e1006462.

ABSTRACT

The *eyes absent* (*eya*) gene of the fruit fly, *Drosophila melanogaster*, is a member of an evolutionarily conserved gene regulatory network that controls eye formation in all seeing animals. The loss of *eya* leads to the complete elimination of the compound eye while forced expression of *eya* in non-retinal tissues is sufficient to induce ectopic eye formation. Within the developing retina, *eya* is expressed in a dynamic pattern and is involved in tissue specification/determination, cell proliferation, apoptosis, and cell fate choice. In this report, we explore the mechanisms by which *eya* expression is spatially and temporally governed in the developing eye. We demonstrate that multiple *cis*-regulatory elements function cooperatively to control *eya* transcription and that spacing between a pair of enhancer elements is important for maintaining correct gene expression. Lastly, we show that the loss of *eya* expression in *sine oculis* (*so*) mutants is the result of massive cell death and a progressive homeotic transformation of retinal progenitor cells into head epidermis.

INTRODUCTION

Construction of a properly functioning organ or tissue is dependent upon the activity of hundreds of genes that can be conceptually organized into a gene regulatory network (GRN) [1–4]. These genes control the specification/determination, patterning, differentiation, and physiology of all cell types within the developing and adult organ. The development of the retina in the fruit fly, *Drosophila melanogaster*, is controlled in part by an evolutionarily conserved gene regulatory network called the retinal determination (RD) network [5]. The core members are two PAX6 genes, *twin of eyeless* (*toy*) and *eyeless* (*ey*), the SIX gene *sine oculis* (*so*), the EYA family member *eyes absent* (*eya*), and the SKI/SNO proto-oncogene *dachshund* (*dac*) [6–11]. In addition to these core members, the fly version of this network contains an additional nine genes, of which some are functionally conserved within the vertebrate eye [5]. Mutations in the fly RD genes lead to drastic reductions in the compound eyes, while forced expression in non-ocular tissues such as the wings, antennas, and legs leads to the formation of structurally complete ectopic eyes. These observations suggest that these factors occupy the highest positions within the larger eye/lens gene regulatory network. In addition to the eye, the core members are used reiteratively during development to also determine the fate of many non-ocular tissues, such as the musculature, skeletal system, nose, ear, pancreas, and kidney [12–14]. Studies of the RD network can therefore provide invaluable insights into the specification and patterning of a wide range of tissues and organs beyond the eye.

The RD network has been best studied in *Drosophila*, with a quarter century of investigation having identified a wealth of genetic, biochemical, and molecular interactions amongst the different members. Numerous review articles over the years have summarized these findings in static circuit maps [5,12,15–17]. While these

interaction diagrams have been helpful in understanding the relationship amongst network members, they can be misleading since the network genes are expressed in dynamic patterns that change both spatially and temporally [18]. In addition, individual genes initiate expression at different times in development [6,8,9,11,17,19], are co-expressed with other network genes in some cells but not in others [18], and appear to interact differently depending upon the exact spatial, temporal, and developmental context [20,21]. As a result, the static maps of regulatory interactions do not necessarily reflect the reality of what is happening throughout the eye in either space or time. In this report, we have focused on understanding how, at the level of *cis*-regulatory elements, the *eya* gene is regulated temporally and spatially in the developing retina. We then use this information to evaluate one tenant of the RD circuit map–namely we test the potential regulation of *eya* by the So transcription factor.

The Eya protein functions as a transcriptional co-activator and protein tyrosine phosphatase [22–24], although the latter activity appears dispensable for eye development in *Drosophila* [25]. Within the nucleus, Eya interacts with members of the SIX/So family of homeodomain containing DNA binding proteins [22]. Together, SIX-EYA complexes function as bipartite transcription factors to activate targets necessary for the specification, differentiation, and growth of the retina [22,23,26]. Recent reports indicate that these complexes also function as transcriptional repressors, although the exact mechanism underlying this activity has yet to be determined [19,20,27,28]. Both genes are expressed in nearly identical spatial patterns within the developing eye [10,11]. Expression of both genes is lost in both *eya* and *so* mutants [29]. These properties have led to the proposal that the So-Eya complex regulates the expression of both genes.

In the wild type eye *eya* expression is temporally and spatially dynamic [11]. This expression is completely eliminated from the retina of eya^{2} mutants, which are viable but completely lack the adult compound eyes [11]. These flies harbor a 322bp deletion, which lies 576bp upstream of the transcriptional start site [11]. When multimerized, this 322bp fragment drives expression of a transcriptional reporter in a pattern that approximates the wild type gene [30,31]. It also contains sufficient activity to partially restore eye development to eya^{2} mutants when driving expression of a rescuing transgene [30,31]. Based on this evidence, this enhancer, for many years, was thought to be the sole *cis*-regulatory element controlling *eya* expression within the developing eye. Sequence analysis identified the presence of a canonical So binding site within this enhancer, thereby raising the possibility that *eya* expression in the eye is controlled by So [31,32]. More recently, several studies of the *eya* locus have identified two additional retinal enhancers, the presence of additional So binding sites, and multiple genomic positions where So appears to bind in eye-antennal discs [33–35]. Together these data have been used to support the premise that the initiation and maintenance of *eya* expression is under the control of So.

In this paper, we report the identification of several *cis*-regulatory elements within the *eya* locus that contribute to its expression in the developing eye. Three of these enhancers lie adjacent to each other, and we demonstrate that they function cooperatively to regulate the temporal and spatial expression pattern of *eya* during eye development. We also show that the spacing between two of these enhancers is important for the activity of each cis-regulatory element. And finally, we show that each of the retinal enhancers (those identified in this and other studies) remain active in *so* loss-of-function

mutants. This is at odds with the model in which *eya* is regulated by So. We show that the loss of *eya* expression in *so* mutants is actually the result of cell death and a progressive fate transformation of the retina into head epidermis. Our findings do not support a role for So in the initiation of *eya* expression. However, we do not rule out the possibility that So functions to maintain *eya* transcription in the retina.

MATERIALS AND METHODS

Fly Strains

The following fly strains were used in this study: (1) *eya*^{1}, (2) *eya*^{2}, (3) *so*^{1}, (4) *FRT42D so*^{3}*/CyO*, (5) *FRT42D Ubi-GFP/CyO*, (6) *y w eyflp*, (7) *w*^{1118}, (8) *w;; ey-GAL4*, (9) *UAS-so*^{VP16}, (10) *y*^{1} *M(vas-int.Dm))* [2] *ZH-2A w*; PBac(y*$^{+}$*-attP-3B)VK00033—BL24871*, (11) *y*^{1} *M(vas-int.Dm)ZH-2A w*; PBac(y*$^{+}$*-attP-9A)VK00019—BL24866*, (12) *so*^{1}*, UAS-p35*, (13) *w*^{1118}*; eya composite enhancer-GAL4*. Loss-of-function clones were generated with the following genotype: *y w eyflp; FRT42D so*^{3}*/FRT42D Ubi-GFP*. All crosses were conducted at 25°C. BL = Bloomington *Drosophila* Stock Center

Antibodies, Dissections, and Microscopy

The following antibodies were used: (1) mouse anti-Eya (1:5, DSHB), (2) mouse anti-β-galactosidase (1:250, Promega), (3) chicken anti-β-galactosidase (1:800, Promega), (4) rat anti-Elav (1:100, DSHB). (5) rabbit anti-Dcp-1 (1:100, Cell Signaling Technologies). DSHB = Developmental Studies Hybridoma Bank. Fluorophore-conjugated secondary antibodies and phalloidin-fluorophore conjugates were obtained from Jackson Immuno Research Laboratories and Life Technologies. Imaginal discs were prepared as described previously in [47]. For dissections performed at specific time intervals, adult flies were placed in egg laying chambers and allowed to lay for 30–60 minutes on agar plates. Individual embryos were then transferred to microcentrifuge tubes with approximately 200µl of standard fly media. The tubes were then placed at 25°C and aged for the appropriate amount of time. Eye-antennal discs were photographed on a Zeiss Axioplan II compound microscope. For scanning electron microscopy, adult flies were

serially incubated in 25% ethanol, 50% ethanol, 75% ethanol, 100% ethanol, 50% ethanol: 50% hexamethyldisilazane (HMDS), and then 100% HMDS, coated with gold-palladium, and viewed with a JEOL 5800LV SEM. For light microscopy of adult heads, flies were photographed on a Zeiss Discovery Microscope.

Luciferase Reporter Activation Assays

3mL of Drosophila Kc167 cells (approximately $1X10^7$ cells/mL) were transfected with a total of 400ng of plasmid DNA using the Qiagen Effectene Transfection Reagent (Cat. No. 301427). For each transfection, *mt-GAL4* (136ng) was transfected along with the indicated UAS responder plasmids (64ng each) and ARE-luciferase (132ng). *UAS-renilla* (0.26ng) was also included in the transfection mix as a control for transfection efficiency. The plasmids were diluted in 98μL of Buffer EC, then 3.2μL of the Enhancer Solution was added to the dilution. The solution was incubated at room temperature for 5min. 10μL of Effectene Transfection Reagent was added to the dilution and the solution was incubated at room temperature for an additional 10min. The transfection solution was mixed with 600μL of Hyclone SFX Insect Culture Media (Cat. No. SH30278.02) and added drop-wise to the plated cells.

Following transfection, the cells were incubated at 25°C for 20hr. Protein production was then induced by the addition of 1mM $CuSO_4$. Following induction, cells were incubated at 25°C for an additional 24hr before harvesting for determination of luciferase activity. The luciferase activity was assayed using the Promega Dual Luciferase Reporter Assay System (Cat. No. E1910) and a Promega GloMAX 20/20 Luminometer (Model No.

E5311). Cells were collected by centrifugation at 500g for 2min. The supernatant was removed and the pellet was re-suspended in 500μL of Passive Lysis Buffer (PLB) at the working concentration. The cells were lysed in the PLB for 20min at room temperature. 20μL of cell lysis solution was added to 100μL of Luciferase Assay Reagent II and mixed by pipetting for 10sec. The light output of the solution was measured in the luminometer once a second for 10s and the average output over the time period was recorded. This was the activity of the luciferase enzyme—the experimental result. 100μL of Stop and Glo Reagent was then added to the tube and mixed briefly by vortexing. The light output of the solution was once again measured, and the results were recorded as the output from Renilla enzyme—the transfection efficiency control. These two measurements were performed for each of three separate plates of independently transfected cells for each plasmid combination. The Relative Luciferase Units (RLUs) for each combination of plasmids were calculated by dividing the experimental light output (Luciferase) by the transfection efficiency control (Renilla) for each of the three independent transfections. Error bars in Fig. 1 represent standard deviation

The target sequence for So and So-VP16 consists of five copies of the ARE element (GGT GTC AGG TTG CTC GAG) that is reported in [23,48] placed upstream of the luciferase gene within the pGL3 vector (Promega, catalog #E1751).

LacZ transcriptional reporters

For lacZ reporter analysis, individual genomic fragments illustrated in Fig. 2 were amplified from w^{1118} genomic DNA and cloned into either p-lacZ.attB or pg-lacZ.attB

plasmids (Konrad Basler, University of Zurich, Switzerland). Genomic fragment sequences are provided in S1 Table. Cloning strategies and primer sequences are listed in S2 Table. RED refers to standard restriction enzyme digestion and ligation into a multiple cloning site. Gateway refers to the Life Technologies Gateway Recombination Cloning system.

eya RB cDNA rescue plasmid

For the cDNA enhancer fusion rescue assay, a pg-*eya* RB+3'UTR cDNA.attB plasmid was created by modifying an existing pg-RFP.attB plasmid (derived from pg-lacZ.attB). The *eya* RB+3'UTR cDNA was first amplified by PCR from an existing pUAS-*eya* RB+3'UTR plasmid as an *EcoRI-NdeI* fragment and cloned into a pg-RFP.attB plasmid. Portions of the Gateway cloning cassette and hsp70 minimal promoter were then amplified from pg-RFP.attB as an *EcoRI* fragment and cloned ahead of the *eya*RB+3'UTR cDNA. Primer sequences are listed in S2 Table.

Enhancer *eya* cDNA fusion rescue constructs

Putative enhancers (Fig 2A) were amplified from the appropriate p.lacZ.attB plasmid and cloned into the new pg-*eya* RB+3'UTR cDNA.attB plasmid using Gateway recombination cloning (Life Technologies). Gateway 5' att primer sequence: 5'-GGG GAC AAG TTT GTA CAA AAA AGC AGG CTC AAC-3' and Gateway 3' att primer sequence: 5'-GGG GAC CAC TTT GTA CAA GAA AGC TGG GTC CTA-3.'

Integrated DNA Technologies (IDT) synthesized constructs

Enhancer 2 minimal fragment and enhancer 1+5bp+2 fragment were synthesized by IDT and flanked by Gateway att sequences for recombination into the pg-lacZ.attB and pg-*eya* RB+3'UTR cDNA plasmids.

Enhancer 1+2 lacZ transcriptional reporter and cDNA fusion constructs

Enhancer 1 was amplified from the p-*eya*-enhancer 1.lacZ.attB plasmid with the following primers: 5'primer: 5'-ATA ATA AAG CTT ACT ACA CCT CGT ACC AAA TTC TCG G-3'and 3'primer: 5'-CCT GCT CAA CTC AAA TGG CCA GTT TCG TCT CC-3' Enhancer 2 was amplified from the p-*eya* enhancer 3.lacZ.attB plasmid using the following primers: 5' primer: 5'-GGA GAC GAA ACT GGC CAT TTG AGT TGA GCA GG-3'and 3' primer: 5'-ATA ATA GGT ACC TCA ACT GAT TCG ACT TGG TCG-3' PCR products were combined together using Gibson Assembly (New England Biolabs). Gateway recombination sequences were then added to the 5'and 3' ends of the product using the following primers: 5' primer: 5'-GGG GAC AAG TTT GTA CAA AAA AGC AGG CTC AAC ACT ACA CCT CGT ACC AAA TTC TCG G-3' and 3' primer: 5'-GGG GAC CAC TTT GTA CAA GAA AGC TGG GTC CTA TCA ACT GAT TCG ACT TGG TCG AAA AGC-3.' The resulting fragment (enhancer 1+2) was cloned into the pDONR201 plasmid and shuttled into pg-lacZ.attB and pg-*eya*RB+3'UTR cDNA.attB plasmids using Gateway recombination cloning (Life Technologies).

Enhancer 1+spacer+2 lacZ transcriptional reporter

Enhancer 1 minimal fragment was amplified from the pg-*eya* enhancer 1 minimal.lacZ.attB plasmid using the following primers: 5' primer: 5'-AAA TAT TTG GAT ATG TGG GGG AAA GGG-3' and 3' primer: 5'-ATA ATA GAA TTC GGC CAG TTT CGT CTC CTC TTT TGC-3' (adds an *EcoRI* site). The spacer fragment was amplified from the pg-*eya* intron 1-1.lacZ.attB plasmid using the following primers: 5' primer: 5'-ATA ATA GAA TTC TGA AAG ATC TCA ATT AGC TAA CCG-3' (adds an *EcoRI* site) and 3' primer: 5'-ATA ATA TCT AGA CAA CTG CTA CCA TTT TGG CCA TTT C-3' (adds a *XbaI* site). Enhancer 2 was amplified from the p-*eya* enhancer #2.lacZ.attB plasmid using the following primers: 5' primer: 5'-ATA ATA TCT AGA ATT TGA GTT GAG CAG GTC AGT TAA TAT TAC-3' (adds a *XbaI* site) and 3' primer: 5'-TCA ACT GAT TCG ACT TGG TCG-3.' The three fragments were ligated together to generate 1+spacer+2. The following primers were then used to amplify this product, which was then cloned into the p-lacZ.attB plasmid as a *HindIII-KpnI* fragment. 5' primer: 5'-ATA ATA AAG CTT AAA TAT TTG GAT ATG TGG GGG AAA GGG-3' (adds a *HindIII* site) and 3' primer: 5'-ATA ATA GGT ACC TCA ACT GAT TCG ACT TGG TCG-3' (adds a *KpnI* site).

Enhancer 1+spacer+2 *eya* RB cDNA fusion

The pg-*eya* RB cDNA+3'UTR.attB plasmid (see above) was digested with *HindIII* and *KpnI* resulting in a plasmid missing the Gateway cassette, hsp70 promoter and a portion of the *eya* RB cDNA. Into this plasmid was cloned the 1+spacer+2 region (see above) as a *HindIII-KpnI* fragment resulting in a p-*eya* 1+spacer+2 *eya* RB cDNA+ 3'UTR(partial). attB plasmid that is still missing the hsp70 minimal promoter and a portion of the *eya* RB cDNA. These pieces were amplified as a single fragment from pg-*eya* RB

cDNA+3'UTR.attB using the following primers: 5' primer: 5'-TCG AAT CAG TTG AGG TAC CTC TAG AGC-3' (adds a *KpnI* site) and 3' primer: 5'-CCA GAG CCG GCG GTA CCC ACA CTG-3' (adds a *KpnI* site). This fragment was cloned into p-*eya* 1+spacer+2 *eya*RB cDNA+3'UTR (partial).attB as a *KpnI* fragment to yield the final p-*eya* 1+spacer+2 *eya*RB cDNA+3' UTR.attB plasmid.

Cloning of enhancers into the promoterless pg-lacZ.attB vector

Enhancer 2 and the composite enhancer were amplified from the p-*eya* enhancer 2.lacZ.attB and p-*eya* composite enhancer.lacZ.attB plasmids respectively (primer sequences are listed in S2 Table). The 3' primer adds 40bp of genomic sequence downstream of enhancer 2 and the transcriptional start site to ensure the entire endogenous promoter region was included. These 40bp were omitted from the above plasmids since a hsp70 minimal promoter is included within the plasmid. Gateway recombination sequences were added to the ends of each construct and the fragments were cloned into the pg-lacZ.attB plasmid that lacks a hsp70 promoter (Konrad Basler, University of Zurich, Switzerland) using standard Gateway Recombination Cloning.

Generation of transgenic fly strains

All lacZ reporter and cDNA fusion constructs were stably integrated into the *pBAC(y*$^{+}$*-attP-3B)VK00033* third chromosome landing site using PhiC31-mediated integration. Proper site-specific integration was confirmed by PCR with attP/attB primers and the correct sequence of the construct was confirmed. The composite enhancer-lacZ construct

was also inserted into a second landing site on the third chromosome for comparison: *PBac(y^{+}-attP-9A)VK00019*.

Molecular analysis of the *eya^{1}* deletion

The genomic region surrounding the *eya^{1}* deletion [31] was amplified from genomic DNA of the *eya^{1}* stock (BL-3631). Genomic DNA from the same region was amplified from *w^{1118}*. The following primers were used to amplify the area surrounding the deletion: 5' primer: 5'-TTC CCG CTG GTG ACT TAC TG-3' and 3' primer: 5'-GTT GTG AGG GAG CTG TCT GG-3' The 5' primer sits 2683 bp upstream of the *eya* RB transcriptional start site and the 3' primer sits 702bp into the first intron. Q5 high-fidelity DNA polymerase (New England Biolabs) was used for the amplification. The PCR product was purified using GeneJet PCR Purification Kit (Thermo-Fisher #K0701). The amplified region from *w^{1118}* is approximately 4kb, while it is just over 2kb in the *eya^{1}* mutant stock. Twelve sequencing primers were used to sequence the amplified genomic region in both directions. Primer sequences are listed within S3 Table. The *eya^{1}* deletion is 1826bp in size: it begins 581bp upstream of the 5' start of the *eya^{2}* deletion and extends 344bp into the 5' UTR of the *eya*RB transcript. There are an additional 11bp that do not correspond to the published genomic region. BL = Bloomington *Drosophila* Stock Center

qPCR

qPCR was performed as previously described [49]. For each experiment, three biological replicates were analyzed once. For each biological replicate, approximately 50 eye-antennal imaginal discs from wandering 3rd instar larvae were dissected in PBS and

immediately placed into a microcentrifuge tube containing 200µl of RLT buffer with β-mercaptoethanol (Qiagen #79216). The tissue was disrupted with a pestle for 1 minute. After disruption, an additional 150µl of RLT buffer with β-mercaptoethanol was added to the tube and the sample was homogenized using a QIAshredder column (Qiagen #79654). After homogenization, total RNA was isolated using the Qiagen RNeasy Mini Kit (Qiagen #74101). 100-200ng of total RNA was reverse transcribed to cDNA using the SuperScript III First Strand Synthesis System with oligo(dT) primers (Invitrogen). qPCR was performed on a Roche LightCycler 480 using SYBR Green I Master Mix (Roche). For each experiment, target genes were analyzed on biological triplicate samples and normalized to *rp49*. 3–4 serial dilutions of pooled cDNA were used to determine primer amplification efficiencies for each target gene. In eya^{1} and eya^{2} rescue experiments, primers specific to the endogenous *eya* RA and *eya* RB transcripts were used. Roche LightCycler 480 Software (Version 1.5) was used to calculate cycle threshold values and melting curves for each reaction. Relative expression and standard error was calculated using Relative Expression Software Tool (REST) [50]. Error bars generated by REST analysis reflect standard error determined by a confidence interval centered on the median, allowing representation of asymmetric tendencies in the data. Primers were designed using A plasmid Editor (ApE) or Fly Primer Bank [51]. Primer sequences are listed in S4 Table.

So binding site sequence analysis

Examination of the *eya* locus (both strands) for predicted So binding sties was performed using the following reported sequences: GTAANYNGANAYC [52], GTAANYNGANAYG

[52], GGTATCA [53], GATATCA [53], TGATAC [54], TGATAC [32], CGATAC [32], ATTGATATCAAT [55], and TTGATATCAA [55].

Acknowledgments

The authors would like to thank Konrad Basler, Nancy Bonini, Tiffany Cook, Georg Halder, Francesca Pignoni, the Bloomington *Drosophila* Stock Center (BDSC), and the Developmental Studies Hybridoma Bank (DSHB) for fly stocks and antibodies. We would also like to thank Jinjin Zhu for technical help with images.

RESULTS

So-VP16 partially restores *eya* expression and rescues *eya*^{2} mutants

In third larval instar retinas, *eya* is expressed in a small stripe of cells ahead of the advancing morphogenetic furrow, in differentiating photoreceptor, cone, and pigment cells, and in the developing ocelli (Fig 1A and 1B) [11]. In the *eya*^{2} mutant, *eya* expression is completely lost from the eye field (Fig 1C and 1D). We first set out to determine if the So consensus sites and regions of So ChIP peaks that are found outside of the original 322bp enhancer are functional. To do this, we attempted to rescue the *eya*^{2} mutant by forcibly expressing a So-VP16 chimeric construct in the developing eye with an *ey-GAL4* driver. This protein is capable of fully restoring eye development to *so*^{1} mutants [27] and activates a luciferase reporter at levels that are 20-fold higher than So alone and 5-fold higher than the So-Eya complex (Fig 1G). Based on these data, we reasoned that So-VP16 serves as a strong transcriptional activator and therefore is a suitable substitute for the So-Eya complex (So-VP16 = So-Eya). Expression of So-VP16 partially restores both *eya* expression and eye development to 62% of the 57 animals that we examined (Fig 1E and 1F; S1A–S1C Fig). Consistent with being a very weak activator, expression of wild type So alone is insufficient to restore either *eya* expression or eye development to *eya*^{2} mutants (Fig 1G; S1D and S1E Fig) [27]. These results led us to initially conclude that additional So-responsive enhancer element(s) are present within the *eya* locus.

Newly-identified regulatory elements are dynamically regulated during larval eye development

In order to identify regulatory elements that are responsive to the So-Eya complex, we used the *osm-6* gene and a CTSF insulator site to define the 5' and 3' boundaries, respectively, of the *eya* locus, and then cloned fragments of DNA between these two genomic markers ahead of a minimal hsp70 promoter and a lacZ reporter (Fig 2A). These constructs were inserted into the same genomic coordinates (*attP-3BVK00033*—cytological position 65B2) using the PhiC31 integrase system to maintain similar expression levels across reporters. Wandering third instar eye-antennal imaginal discs were then examined for lacZ reporter expression. We identified six genomic fragments that are capable of driving expression of the reporter in portions of the endogenous *eya* pattern (Fig 2B–2G). Three of these fragments (PSE, 1, and E) have been previously identified as enhancers controlling *eya* expression in the retina [30,31,35]. The PSE, which stands for photoreceptor-specific enhancer, drives expression solely in cells behind the morphogenetic furrow (Fig 2A and 2B) [35], while fragment 1 (also called IAM for immediately anterior to the morphogenetic furrow) drives expression ahead of the advancing morphogenetic furrow and in differentiating cells (Fig 2A and 2C) [35]. Fragment E (for extant) is the enhancer that is deleted in eya^{2} mutants (Fig 2A and 2D) [30,31]. Our sequence analysis indicates that the fragment is 319bp in length (and not 322bp as originally reported). Fragments 2, 3 and 4 are three new retinal enhancers that control *eya* expression in the developing eye (Fig 2A and 2E–2G).

We next determined the temporal and spatial expression patterns of each individual fragment and compared these patterns to endogenous *eya* expression. Eya protein is present in the wild type eye disc as early as 48hrs AEL (early 2nd instar, Fig 3A) and continues to be expressed broadly at 72hrs AEL (early 3rd instar, Fig 3B). By the

late third larval instar stage, *eya* expression is restricted to a narrow band of cells ahead of the morphogenetic furrow and to all differentiating photoreceptor and cone cells (Fig 3C). No single individual fragment fully recapitulates the endogenous *eya* expression pattern. For example, reporter expression driven by fragment 1 is temporally and spatially delayed compared to wild type *eya* expression, meaning that although it is activated in a few *eya* expressing cells early in development, it is not until late third instar that expression starts to coincide with the spatial pattern of endogenous *eya* (Fig 3D–3F, Table 1). In contrast, while reporter expression driven by fragment E coincides with early endogenous *eya*, its late expression is weak in intensity and appears mottled (Fig 3G–3I, Table 1). Lastly, the bulk of fragment 2-driven expression within younger discs is in *eya* negative cells, while in later discs, reporter expression does coincide with the endogenous *eya* gene (Fig 3J–3L, Table 1).

Since each of these three fragments (1,E,2) does mimic a specific temporal and/or spatial aspect of *eya* expression, we hypothesized that these enhancers, which lie adjacent to each other, might function cooperatively to control all temporal and spatial aspects of *eya* expression. To test this model, we generated a single 1181bp fragment consisting of fragments 1, E, and 2, and as predicted, this composite enhancer fully recapitulates the temporal and spatial expression pattern of *eya* within the developing eye (Fig 3M–3O, Table 1). To rule out position-dependent effects, we inserted this construct into a second genomic landing site (*attP-9A VK00019*—cytological position 68D2) and observe that the expression pattern of this insertion is identical to the original insertion and recapitulates endogenous *eya* expression (S2 Fig). It appears that the temporal expression of the composite enhancer is the sum or addition of the individual elements.

And interestingly, recreating the genomic organization of these three *cis*-regulatory elements eliminates the ectopic expression from the eye-antennal disc (Fig 3J–3O, Table 1). Since the composite enhancer recapitulates the entire *eya* expression pattern, it is possible that fragments 3, 4, and PSE are functionally redundant. Consistent with this model, the expression patterns controlled by these fragments are fully covered by the composite enhancer (Fig 3P–3U, Table 1).

The composite *eya* enhancer can fully rescue eye development in *eya*^{1} and *eya*^{2} mutants

We then set out to test if the composite enhancer is sufficient to fully rescue the no-eye phenotypes of *eya*^{2} and *eya*^{1} mutants. The original characterization of the *eya*^{1} mutant indicated that two chromosomal aberrations are associated with this mutation. First, a chromosomal re-arrangement completely inverts the orientation of the *eya* locus within the left arm of the second chromosome. This is not thought to interfere with normal *eya* expression. Second, an approximately 1.5kb deletion was detected at the 5' end of the gene. The 319bp deletion in *eya*^{2} lies within the larger ~1.5kb deletion in *eya*^{1}. Thus, the no-eye phenotype of *eya*^{1} and *eya*^{2} is thought to result from the disruption of the same regulatory sites [11,31]. To precisely determine the breakpoints of the *eya*^{1} deletion in relation to the composite enhancer, we isolated and re-sequenced the region around the transcriptional start site and determined that the deletion is actually 1826bp in length, with the deletion extending 581bp upstream of the *eya*^{2} deletion and 344bp downstream of the transcriptional start site. This deletion completely deletes the composite enhancer, the transcriptional start site, and a large portion of the *eya* RB transcript 5'UTR (Fig 2A).

Using qRT-PCR, we confirmed that the RB transcript is completely eliminated in *eya*^{1} mutants and drastically reduced in *eya*^{2} mutants (Fig 4A). The RA transcript is also greatly reduced, but not eliminated, in both mutant alleles, suggesting that the composite enhancer regulates both *eya* promoters (Figs 2A and 4A).

To test whether fragments 1, E, and 2 are sufficient to rescue the two *eya* mutants, each enhancer element, as well as the full composite enhancer, was cloned upstream of a minimal hsp70 promoter and the *eya* RB cDNA. Using the PhiC31 integrase system, these constructs were inserted into the same genomic location that we used for the original lacZ reporter expression analysis (*attP-3BVK00033*—cytological location 65B2). For all rescue experiments, at least 100 adult flies were initially assayed qualitatively for the restoration of eye development. For the rescue quantification in Table 1 the number of ommatidia in adult right eyes from 2–3 individual female flies were counted and compared to wild type. The number of ommatidia per rescue is presented as an average of the 2–3 individuals. A wild type eye from a female fly is defined as having between 750 and 800 ommatidia [36].

Both fragments 1 and E are capable of partially restoring eye development in 100% of *eya*^{2} and *eya*^{1} mutants. Fragment 1 restores eye size to approximately 38% of wild type in *eya*^{2} and 25% in *eya*^{1} (Fig 4B and 4I, Table 1). Enhancer E restores eye size to approximately 49% of wild type in *eya*^{2}, but less than 1% in *eya*^{1} (Fig 4C and 4J, Table 1). Expression from fragment 2, on its own, fails to rescue either mutant (Fig 4D and 4K, Table 1). Consistent with our expression analysis, the full composite enhancer fully restores eye development to 100% of both *eya* mutants (Fig 4E and 4L, Table 1). And finally, neither fragment 3 nor 4 are capable of rescuing the no-eye phenotype of either

mutant (Fig 4G, 4H, 4N and 4O, Table 1). The majority of fragment 3 driven expression is outside of the endogenous *eya* expression pattern and would therefore not be predicted to restore eye development to *eya* mutants (Fig 3P–3R, Table 1). The inability of fragment 4 to rescue eye development stems from the fact that it is normally expressed only in differentiating cells posterior to the morphogenetic furrow (Fig 3S–3U, Table 1). Neither the furrow nor differentiated photoreceptor cells are present in either eya^{1} or eya^{2} mutants [11].

The lack of any discernable rescue by fragment 2 and its inappropriate expression pattern initially indicated that it may not function as an enhancer. Instead, its proximity to the transcriptional start site of *eya* RB suggested that it might serve as a basal core promoter. To test this idea, we placed fragment 2 and the composite enhancer into a plasmid that contains a lacZ reporter but lacks a minimal promoter. Under these conditions, fragment 2 is still capable of driving lacZ expression in the developing eye but only in developing photoreceptors (S3A and S3B Fig). In contrast, lacZ reporter expression driven by the composite enhancer is identical to the construct that contained the minimal hsp70 promoter fragment (S3C and S3D Fig). These data support the proposal that fragment 2 functions, in part, as a basal promoter. As such we then tested the model that all pertinent regulatory information may reside only in fragments 1 and E. We first examined lacZ reporter expression with a fragment that contained segments 1 and E only and, as expected, this construct fully recapitulates endogenous *eya* expression (S3E and S3F Fig). We next attempted to rescue both eya^{1} and eya^{2} mutants with this shorter fragment. While we observed rescue in 100% of animals, it only restores eye size to 82% of wild type in eya^{2} and 44% in eya^{1} mutants (Fig 4E, 4F, 4L and 4M,

Table 1). This is unlike the composite enhancer, which completely restores eye size to the both *eya* mutants. This suggests that, in addition to functioning as a basal core promoter, fragment 2 does indeed contain regulatory information that is necessary for robust *eya* expression.

We were intrigued by the differences in rescue efficiency of our constructs in eya^{1} and eya^{2} mutants. Since the endogenous transcriptional start site for the RB transcript is intact in the eya^{2} mutant but is deleted in the eya^{1} mutant, we hypothesized that the higher degree of rescue in the eya^{2} mutant is due to a reactivation of the endogenous *eya* gene. Using qRT-PCR, we measured *eya* RB transcript levels within *eya* mutants that have been rescued by expression from enhancer E. This enhancer was chosen since it showed the most dramatic difference in rescue efficiency. As predicted, we observe that expression of the *eya* RB cDNA initiates a positive feedback loop on the endogenous locus and reactivates *eya* expression in eya^{2} but not eya^{1} (Fig 4A, 4C and 4J). In the eya^{2} mutant, fragments 1 (IAM), 2, 3, 4, and PSE are present, and one or more of these could be targets of the auto-regulatory loop. To test this possibility, we brought combinations of rescue constructs together within a single eya^{1} animal and asked if the degree of rescue could mimic that of the extant enhancer rescue of eya^{2}. We combined the extant enhancer (E, Fig 5A) with each of the other enhancer elements (Fig 5B–5F) and observed a synergistic increase in the quality of rescue only with enhancer 1 (Fig 5G). The quality of eye restoration did not improve by combining the other elements with the extant enhancer (Fig 5H–5K). These data, when combined with the reporter expression and rescue results, suggest that enhancer 1 mediates the Eya-dependent auto-regulatory loop.

The no-eye phenotype of *eya*^{2} mutants results from disrupting neighboring enhancers

The ability of enhancer 1 to partially restore eye development to *eya*^{1} and *eya*^{2} mutants was of particular interest to us since eye development is completely blocked in the *eya*^{2} mutant despite the continued presence of enhancer 1. We hypothesized that the loss of eye development is due to the combined loss of enhancer E and a disruption of enhancer 1 activity. To test this model, we recapitulated the genomic organization of the *eya*^{2} mutant by fusing enhancers 1 and 2 together. When the enhancers are placed in this configuration, expression of the lacZ reporter is lost throughout young eye discs and ahead of the furrow in third instar discs. Expression of the reporter only remains in some differentiating cells posterior to the furrow (Fig 6A–6C, Table 1). Consistent with the loss of expression in undifferentiated cells, this construct drives reporter expression in a very small number of cells in the *eya*^{2} mutant (Fig 6D). The loss of expression in undifferentiated cells prevents this construct from rescuing the *eya*^{2} mutant (Fig 6E, Table 1).

The inability of this construct to properly drive lacZ and *eya* cDNA expression could be due either to the unintended creation of a synthetic binding site for a transcriptional repressor at the junction where enhancers 1 and 2 meet, or there might be a need for some amount of genomic space between the two enhancers. To test the first possibility, we placed a *BamHI* restriction site between enhancers #1 and #2. Addition of this 5bp spacer restores expression to some cells in wild type discs and to a few cells in *eya*^{2} mutant discs (Fig 6F–6I, Table 1). The expression pattern in wild type discs resembles that of enhancer 2, suggesting that insertion of the 5bps failed to allow for the early

activation of enhancer 1. Consistent with this construct behaving similar to enhancer 2, we did not see any rescue of the *eya*^{2} mutant (Fig 6J, Table 1). Since this construct failed to restore *eya* expression and eye development, we can rule out the possibility that a synthetically-created repressor site is the underlying reason for the loss of *eya* expression in *eya*^{2} mutants.

To test the latter hypothesis that a certain amount of genomic space is required between enhancers 1 and 2, we inserted a 319bp fragment of DNA (the size of enhancer E) between the two fragments in an effort to reinstate normal spacing. On its own this neutral sequence, which comes from intron 1 of the *eya* locus, does not direct expression of lacZ or rescue the *eya*^{2} mutant (Figs 2A and 6Q–6S, Table 1). At 48hrs and 72hrs AEL, the majority, but not all, of the reporter expression of 1+spacer+2 was still seen in non-*eya* expressing cells (Fig 6K and 6L, Table 1). However, by the late third larval instar, reporter expression is now seen in the majority of Eya positive cells (Fig 6M, Table 1). Overall early reporter expression of 1+spacer+2 is similar to that of enhancer 2 alone, while late reporter expression is comparable to enhancer 1 alone (compare to Fig 3D–3F and 3J–3L, Table 1). This construct can drive expression in and partially rescue both *eya*^{1} and *eya*^{2} mutants, demonstrating that the reconstitution of spacing was sufficient to restore limited function to enhancers 1 and 2 (Fig 6O and 6P, Table 1). The restoration of eye size in *eya*^{2} and *eya*^{1} is approximately 64% and 58% of wild type respectively, compared to 100% for the composite (1+E+2) enhancer, suggesting that in addition to providing critical space between enhancers #1 and #2, enhancer E must also contain regulatory information necessary for robust *eya* expression (Table 1).

Activation of the composite enhancer is not So-dependent

Since we are able to partially restore *eya* expression and eye development to *eya*^{2} mutants through expression of the So-VP16 chimeric protein (Fig 1F and 1G), we reasoned that one or more of the newly-discovered enhancers might be regulated by So. Three enhancers contain canonical So binding sites, and So ChIP peaks are present within two other enhancers (Fig 2A) [33,34]. We first tested whether the So-VP16 chimeric protein is capable of activating the composite (1+E+2) enhancer. When forcibly expressed in the antennal disc under the control of the *dpp-GAL4* driver, So-VP16 is surprisingly unable to activate the composite enhancer (S4A–S4D Fig, rose arrow). In contrast, forced Ey does activate the reporter, suggesting that Ey, but not So, regulates the *eya* locus during eye development (S4E–S4H Fig, yellow arrow). To further test whether activation of any of the enhancers is So-dependent, we placed each of the lacZ reporter constructs into the *so*^{1} mutant background and assayed for lacZ expression. *so*^{1} mutants are viable, lack compound eyes, have a small eye disc, and have drastically reduced levels of *so* expression (S5 Fig) [10,37]. Any So-dependent element should remain silent in this mutant background. However, all of the elements with the exception of enhancer 4 remain activated in *so*^{1} mutant eye discs (Fig 7A–7F). Enhancer 4 drives expression exclusively in differentiating cells; thus, the lack of activation from this enhancer is most likely due to the fact that *so*^{1} mutants lack photoreceptor, cone, and pigment cells. It is striking that the composite enhancer remains strongly activated in *so*^{1} mutants (Fig 7D). To ensure that this is not due to residual So protein, we examined lacZ expression driven by the composite enhancer in *so*^{3} null mutant clones. We again find that the composite enhancer is strongly activated in clones both ahead and behind the

morphogenetic furrow (Fig 7G–7J). Thus, despite the presence of a So binding site and the apparent binding of So, the composite enhancer (which contains all regulatory information for proper *eya* expression) is not activated by So.

So is not required for the initiation of *eya* expression but may be required for its maintenance

When we examined the potential activation of the composite enhancer in so^{3} null clones, we were quite surprised to see clones that contain Eya protein (Fig 7H). This clearly suggests that activation of reporters in *so* mutants is not due the persistence of lacZ protein, although we cannot entirely rule that out. However, this result certainly was inconsistent with what we observed in late third instar whole mutant so^{1} discs, where Eya protein was completely missing in the eye portion of the disc. These data were also inconsistent with qRT-PCR data, which showed a dramatic reduction of *eya* transcript levels in so^{1} mutants (S4 Fig). A possible explanation for these apparently contradictory observations could be that Eya protein expression is lost over the course of larval eye development. This could be the result of a requirement for So in the maintenance of *eya* expression, retinal progenitor cell death, a fate transformation, or a combination of all three [28,38]. Retinal progenitors have previously been defined as those proliferating in the most anterior regions of the eye disc that express Ey but lack So and Eya. Retinal precursors are defined as cells anterior to the morphogenetic furrow which express all three genes [39]. Support for the model that *eya* expression is lost over developmental time comes from three previously published observations: (1) *eya* expression is lost within the retinal field in roughly 50% of mid-late second larval instar so^{1} eye-antennal discs

[29]; (2) *so*^{1} mutants undergo a significant wave of cell death that eliminates retinal progenitors in the growing eye field [10]; and (3) retinal progenitors within *so* and *eya* mutants undergo a fate transformation into head epidermis [28,38].

To test our hypothesis that loss of Eya in *so*^{1} mutants is progressive, we first re-examined *eya* expression in *so*^{1} mutants over the course of larval eye development. Beginning at 72hrs AEL, we found that 100% of *so*^{1} mutant discs had strong Eya expression throughout the eye disc, thereby demonstrating that So is not required for the initiation of *eya* expression (Fig 8A; S6 Fig). By 96hrs AEL, *eya* expression weakens, is expressed in fewer discs, and is found in smaller and smaller populations of cells over time (Fig 8B–8D; S6 Fig). By 168hrs AEL, the overwhelming majority of *so*^{1} discs have completely lost *eya* expression within the retinal field (Fig 8E; S6 Fig). This analysis confirms that Eya protein is indeed lost over the course of larval eye development.

To determine whether the loss of Eya protein could be due to increased cell death in retinal progenitors, as suggested by previous studies, we conducted a temporal examination of cell death in *so*^{1} mutants and find that retinal progenitors undergo significant cell death over the course of larval eye development (Fig 8F–8J). Using an antibody against Dcp-1, a marker of cell death, we observed increased cell death at 72hrs AEL in a large swathe of cells in the anterior-most portions of the eye disc. At this point cell death seems restricted mostly to retinal progenitors outside the endogenous Eya expression domain, as indicated by the expression of Ey but not Eya (Fig 8F and 8K). By 96hrs AEL, the wave of cell death becomes broader and extends to the posterior margins of the disc to include both retinal progenitors and retinal precursors, as indicated by the presence of both Ey and Eya expression (Fig 8G and 8L). It is important to note that 96hrs

AEL is the first time point in which we see decreases in the expression of Eya protein. Finally, as development proceeds, the amount of cell death decreases and becomes restricted to the ventral-most portions of the disc (Fig 8H–8J and 8M–8O). Although some Eya positive cells do appear to remain outside the population of dying cells, it is clear that the majority of Eya expressing cells have been removed by these later time points, consistent with the idea that retinal progenitors, and by default retinal precursors, have been cleared by cell death. These data also corroborate the qRT-PCR data from late *so*^{1} mutant discs.

If the loss of Eya expression in *so*^{1} mutants was solely the result of cell death of retinal progenitors, then it follows that blocking cell death should restore *eya* expression to a subset of cells in late *so*^{1} mutant discs, as those cells would be saved earlier in larval eye development and then proceed to differentiate into retinal precursors and express *eya*. To test this hypothesis, we blocked cell death by expressing p35, a well-known inhibitor of caspase-dependent cell death, with an *eya composite enhancer-GAL4* driver. We saw no increase in *eya* expression at 120hrs AEL, suggesting that the loss of *eya* in *so*^{1} mutants is not simply the result of a clearing of retinal progenitors (Fig 8Q). However, we do see a significant number of cells still expressing *ey*, indicating the continued presence of retinal progenitors that are not proceeding to differentiate into retinal precursors (Fig 8P).

We have previously shown that retinal progenitors within *so* and *eya* mutants undergo a cell fate transformation into head epidermis [28,38]. It is possible that after the wave of cell death the continued loss of *eya* expression in *so*^{1} mutants may be the indirect result of this homeotic transformation. The non-ocular bristle and antennal selector gene

cut (*ct*) and the head capsule selector gene *orthodenticle* (*otd*) have previously been shown to be de-repressed in eye to head epidermis transformations in *eya*^{2} mutants [28]. We therefore examined expression of both genes in *so*^{1} mutants. Concomitant with the decrease in *eya* expression, we saw a de-repression and expansion of both *ct* and *otd* throughout the entire eye disc (Fig 9A–9L). The de-repression of both genes initiates at 72hrs AEL in just a few cells of the eye disc but is more pronounced by 96hrs AEL (Fig 9D, 9E, 9G, 9H, 9J and 9K). Most striking is that starting at 120hrs AEL, when we first begin to see discs without any *eya* expression in the retinal field, *ct* and *otd* expression have expanded to cover the entire eye field (Fig 9F, 9I and 9L). Based on the continued presence of *ey* expression within the same portion of the eye disc, it appears that the surviving retinal progenitor cells have undergone a transformation to head epidermis (Fig 8H). Furthermore, when we block cell death in the mutants, *ct* and *otd* are still expressed in the majority of cells within the disc, again supporting the idea that these cells have undergone a cell fate transformation (Fig 9M). We believe it is this ongoing cell fate transformation that is blocking the continued expression of *eya* resulting in a loss of Eya protein in late stage *so*^{1} mutant discs. However, additional studies are needed to fully determine if, and possibly to what extent, So might be required for the maintenance of *eya* expression later in larval eye development.

Finally, to ensure that the Eya protein we observed in *so*^{1} mutants is not the result of residual levels of So protein activity, we examined *eya* expression in *so*^{3} null mutant clones. Consistent with the analysis of *so*^{1} discs, we found multiple *so*^{3} null clones in which Eya protein was still present (Fig 10A–10H, yellow arrows). We did, however, observe that the majority of large clones spanning the middle of the eye field contained

no Eya protein (Fig 10A–10H, green arrows). The adult retinas of these animals often contain large patches of head epidermis protruding through the middle of the eye field (Fig 10I–10L, green arrows). We predict that these patches of head cuticle correspond to the clones in the disc that lack *eya* expression and thus are the result of a cell fate transformation.

Together, our lacZ reporter and cDNA rescue analyses suggest that a single 1181bp genomic fragment composed of three *cis*-regulatory elements is capable of controlling all *eya* expression in the developing retina. Furthermore, our combinatorial rescue analysis in eya^{1} mutants suggests that although enhancer elements 1 and E sit adjacent to each other within the *eya* locus, these two elements are functioning as independent *cis*-regulatory elements. Additionally, we find that spacing between elements within the composite enhancer is critical for proper function. When fragments 1 and 2 are located adjacent to each other, as is the case in eya^{2} mutant animals, these enhancers can no longer function to provide *eya* expression early in larval development, leading to an adult no-eye phenotype. Finally, we find that loss of *eya* expression in *so* loss-of-function mutants is progressive and likely the result of increased cell death and a cell fate transformation. Although our data cannot rule out the possibility that So is required for the maintenance of *eya* expression during larval eye development, it is clearly not required for its initiation. Given our identification of multiple independently functioning *cis*-regulatory elements within the *eya* locus and the potential differential requirement for So in its activation at later stages of eye development, *eya* regulation over the course of eye development is likely to be dynamic and require the input of different combinations of RD

members and signaling pathways at different times and in different cell types for overall proper temporal and spatial expression.

DISCUSSION

Members of the retinal determination network play crucial roles in specification, pattern formation, cell fate choice and proliferation during *Drosophila* compound eye development. As such, their regulation and gene expression is often highly temporally and spatially dynamic, allowing for the proper differentiation of the multiple cell types necessary for the proper function of the compound eye [40]. *eyes absent* is a core member of this network and provides a key example of this type of complex gene expression. In this report, we have identified several enhancers that cooperate to regulate temporal and spatial expression of *eya* in the developing retina (Figs 2 and 11). It is not uncommon for a single expression pattern to be controlled by multiple enhancers [39–44]. We find that a single enhancer module, comprised of three distinct and separable *cis*-regulatory elements, is responsible for the correct temporal and spatial expression of *eya* (Figs 3 and 4). Furthermore, the three elements (1+E+2) that comprise the composite enhancer regulate *eya* at specific times during retinal development (Figs 3 and 11). For example, enhancer E controls early *eya* expression, while enhancer 1 is responsible for the bulk of late *eya* transcription (Fig 3). Having separate cis-regulatory elements control *eya* expression at different times during development is consistent with the idea that RD genes are dynamically regulated temporally and spatially to ensure distinct expression patterns necessary for the differentiation of specific retinal cell types over the course of eye development [40].

In the context of temporal expression, we propose that these enhancers function additively (Figs 3,5 and 11). Additive control of gene expression levels has been described in many organisms, including *Drosophila*. In the *Drosophila* embryo, a set of

proximal and distal enhancers controls the expression patterns of the *hunchback* (*hb*) and *knirps* (*kni*) gap genes [41–44]. The expression level of each of these two genes appears to be the sum of the levels that are driven by the individual enhancers [45]. Although additional experimentation to measure the specific contribution of each of the elements in terms of transcriptional output of *eya* is required, the results of our cDNA fusion rescue experiments support a model for these elements functioning additively, as the overall size of the eye increases when enhancers #1 and E are combined and complete rescue occurs when all three elements (#1+E+2) are placed together (Figs 4 and 5).

It has been shown that deleting enhancer E leads to a loss of *eya* expression early in development when it is normally needed to promote tissue specification and cell proliferation. We find that this early loss of *eya* expression is a major, but not the sole, contributor to the complete loss of the compound eye in eya^{2} mutants. Our results indicate that spacing is critical for the proper function of two *cis*-regulatory elements within the composite enhancer (Figs 4 and 6). Specifically, we find that the primary cause for the loss of *eya* expression in eya^{2} mutants is the direct juxtaposition of two flanking *cis*-regulatory elements (1 and 2) rather than the deletion of the intervening regulatory element (E). Placement of a neutral sequence between these two elements recapitulates normal spacing in the genome, restores their ability to drive a transcriptional reporter, and rescues the no-eye phenotype of eya^{2} mutants (Fig 6). The *eve* locus provides a parallel example to what we observe in the eye with *eya*. The *eve* stripe 2 and stripe 3 enhancers are separated by 1.7kb of neutral genomic sequence. When these enhancers are placed directly adjacent to each other, the expression pattern driven by both enhancers is altered. Normal expression is restored when a short 160bp sequence is inserted between

the two enhancers, suggesting that without correct spacing improper short-range interactions between *cis*-regulatory elements can lead to abnormal expression patterns [46]. In the *eya*^{2} mutant, enhancers 1 and 2 are directly juxtaposed to each other. Since expression of *eya* is lost in all undifferentiated cells, we propose that inappropriate short-range repression between the two enhancers is likely inactivating both elements. We have not investigated the minimal spacing requirements for the *eya* retinal enhancers but based on the results from [46], the distance is likely to be relatively short.

It has been widely assumed that So plays a role in regulating *eya* in cells undergoing eye specification. This was based in part on the loss of *eya* expression in *so* loss-of-function mutants [29], as well as the presence of So binding sites within the *eya* locus (including enhancer E) and the ability of So to bind to the *eya* locus [11,33,34]. In fact, it is the presence of predicted So binding sites which first led us to explore which DNA elements are controlling *eya* expression in the developing retina. When placed within *so* mutant backgrounds, we found, however, that the *eya* enhancers were still active (Fig 7). This led us to re-examine Eya protein expression in *so* loss-of-function mutants, and we find that Eya expression is lost progressively over the course of larval eye development (Fig 8). Although these results clearly demonstrate that So is not required for the initiation of *eya* expression, they do not rule out a role for So in the maintenance of its expression.

The progressive loss of *eya* could be the consequence of a requirement for So in the regulation of *eya* later in larval eye development. Our initial analyses of the *eya* enhancers would partially support this model of regulation. Enhancer 2, which is bound by So, functions within photoreceptors late in eye development and therefore would be a

promising candidate for regulation by So (Figs 3 and 11). Conversely, enhancer E, which contains a predicted So binding site, is the *cis*-regulatory element responsible for the bulk of early, not late, *eya* expression (Figs 3 and 11). It seems unlikely that So is regulating *eya* through this enhancer, given that So is not required for the initiation of *eya* expression. Two additional enhancers (PSE and enhancer 4), which we find to function redundantly to the composite enhancer, both contain predicted So binding sites and a larger DNA fragment containing the PSE was found to be bound by So. Like enhancer 2, both of these enhancers function in photoreceptors and cone cells later in eye development and as such might be good candidates for the maintenance of *eya* by So (Figs 3 and 11). In our assays, these elements seem to function redundantly to the composite enhancer; therefore, it is likely that if these enhancers are regulated by So, it is in a manner more similar to that of a shadow enhancer [44] to ensure robust *eya* expression. Interestingly, bioinformatic conservation analysis on these enhancer elements would suggest that a requirement for So in the regulation of *eya* might not be conserved across *Drosophila* species. Analysis of the composite enhancer shows that the bulk of conservation lies only within enhancers 1 and E (S7A Fig). There is no sequence conservation within enhancer 2, and the So binding sites in enhancers E, PSE, and 4 are also not conserved (S7A-S7C Fig). However, a stretch of sequence conservation in the PSE is present immediately adjacent to the predicted So binding site (S7B Fig).

Previous studies on so^{1} and eya^{2} mutants support an alternative model in which the loss of *eya* in so mutants could be the result of a combination of increased cell death of retinal progenitors [17,18] and a progressive cell fate transformation from retinal progenitor to head epidermis [35,38]. And indeed, we observe both phenomena occurring

simultaneously in *so* loss-of-function mutants (Figs 8–10). Our re-examination of the *so* mutants showed *eya* expression slowly terminates as the tissue is gradually altering its fate (Fig 8). The state of the cell and/or tissue is an underappreciated idea that needs to be considered when attempting to establish regulatory relationships between transcription factors and putative downstream targets. A wealth of expression data and evidence of molecular interactions may not be sufficient, in all cases, to conclude that a gene is under the control of the DNA binding protein in question.

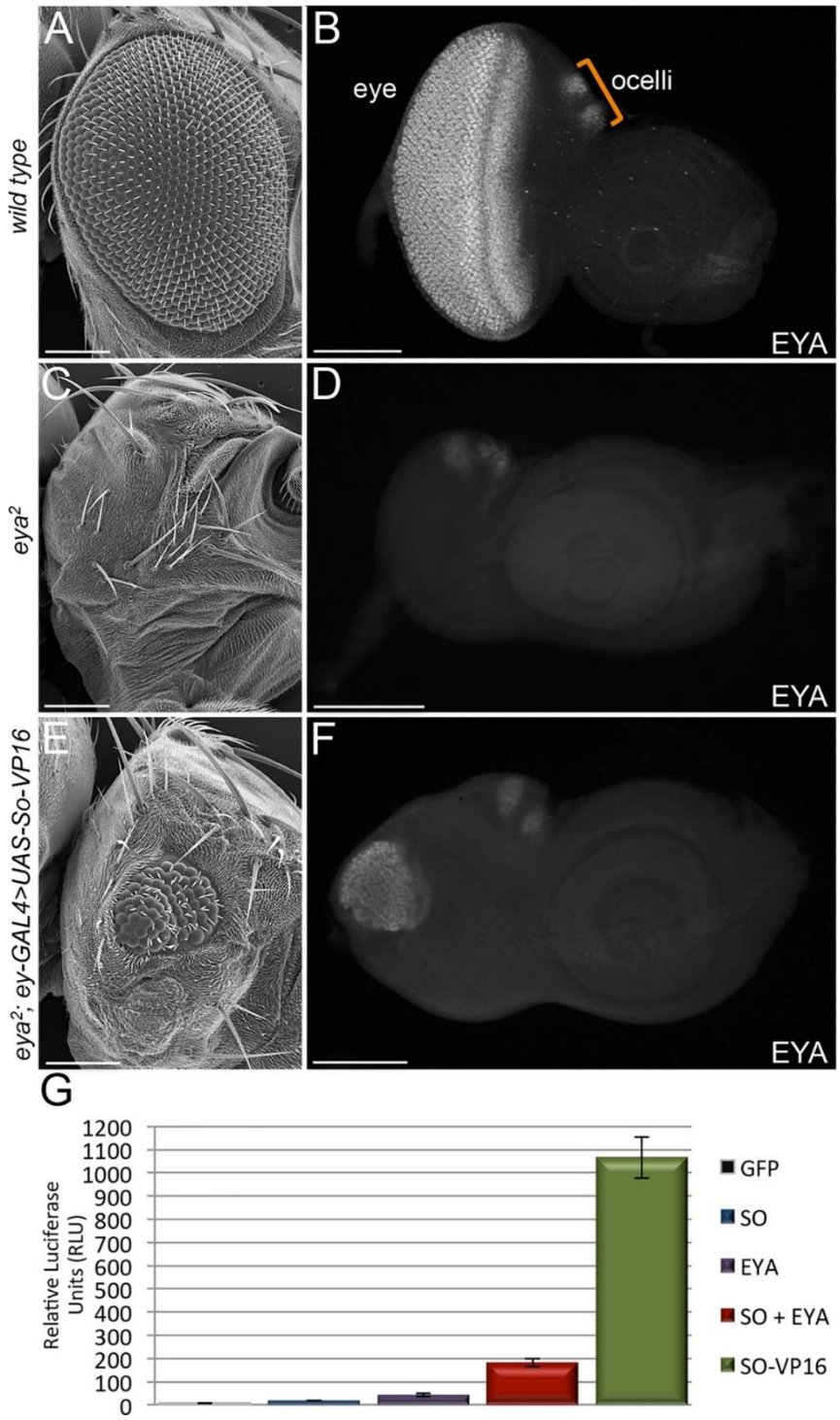

Figure 1. So-VP16 reactivates *eya* expression in the retina of *eya*^{2} mutants. (A,C,E) SEM images of adult female *Drosophila* compound eyes and heads. **(A)** wild type. **(C)** *eya*^{2}. **(E)** *eya*^{2} mutants in which expression of UAS-So-VP16 partially restores eye

development. **(B,D,F)** Light microscope images of third instar eye-antennal discs—*eya* expression is detected by antibody staining against Eya protein. **(B)** Wild type expression of *eya* in the compound eye and ocelli. **(D)** Loss of *eya* expression in the eye portion of disc in eya^{2} mutants. Expression with the ocelli is maintained in the mutant. **(F)** Partial restoration of *eya* expression in the eye portion of disc upon expression of UAS-So-VP16. Anterior is to the right in adult head and imaginal disc images. At least 30 adult flies and developing imaginal discs were examined for each genotype with 57 adult eya^{2}*; ey-GAL4, UAS-So-VP16* flies being scored for rescue of eye structure **(G)** Luciferase assay quantifying activation strength of So-VP16. *y*-axis is relative luciferase units (RLU). Three biological replicates were conducted for each experiment. Error bars in panel G represent standard deviation. Scale bar, 100μm.

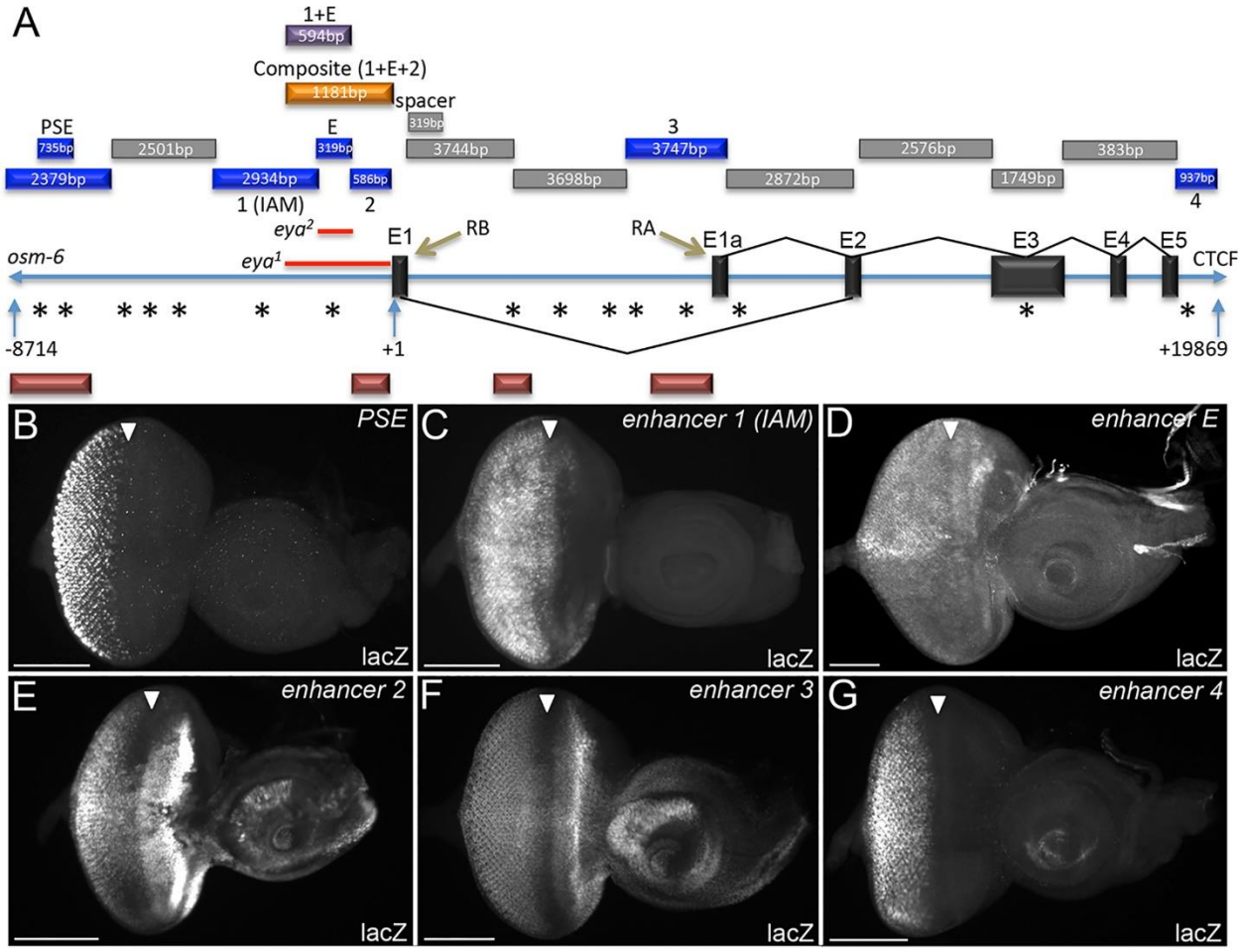

Figure 2. Multiple enhancers control expression of *eya* in the developing eye. (A) Illustration of the genomic map of the *eya* locus—representation is not to scale. Sequences and genomic location of each fragment are provided in supplementary materials and methods S1-3. Size of each fragment (bp) is indicated within each bar. Blue bars=individual retinal enhancers. PSE=photoreceptor specific enhancer previously identified and named by Graeme Mardon's group in [20]. E=319bp extant enhancer previously identified in [11]. Enhancer 1 (IAM)=immediately ahead of morphogenetic furrow enhancer was previously identified and named by Graeme Mardon's group in [20]. We refer to this enhancer as 1 as it shows a different expression pattern than previously reported. 2–4 represent newly identified enhancer elements. Orange bar=composite

enhancer, purple bar=enhancer 1+E, grey bars indicate regions that do not drive expression in the retina including the fragment used as the 319bp spacer, asterisks=So binding sites, red bars=regions of So ChIP peaks. *eya*^{1} and *eya*^{2} deletions are indicated by red lines immediately ahead of exon 1 **(B-G)** Light microscope images of third instar eye-antennal discs. All images represent lacZ reporter expression in a wild type genetic background. LacZ reporter activation is indicated by antibody staining against β-galactosidase. White arrowheads mark the position of the morphogenetic furrow. **(B)** The PSE enhancer drives expression of the reporter only in cells that lie posterior to the morphogenetic furrow. **(C)** Enhancer 1 (also called IAM) drives expression in cells ahead and behind the morphogenetic furrow. **(D)** The 319bp extant enhancer drives weak reporter expression in cells ahead and posterior to the morphogenetic furrow. **(E)** Enhancer 2 drives expression of the reporter in cells anterior and posterior to furrow. **(F)** Enhancer 3 drives expression in cells ahead and behind the morphogenetic furrow. **(G)** Enhancer 4 drives expression only in cells posterior to the morphogenetic furrow. No single enhancer element fully recapitulates endogenous Eya expression. Anterior is to the right in imaginal disc images. At least 30 imaginal discs were examined for each genotype. Scale bar, 100μm.

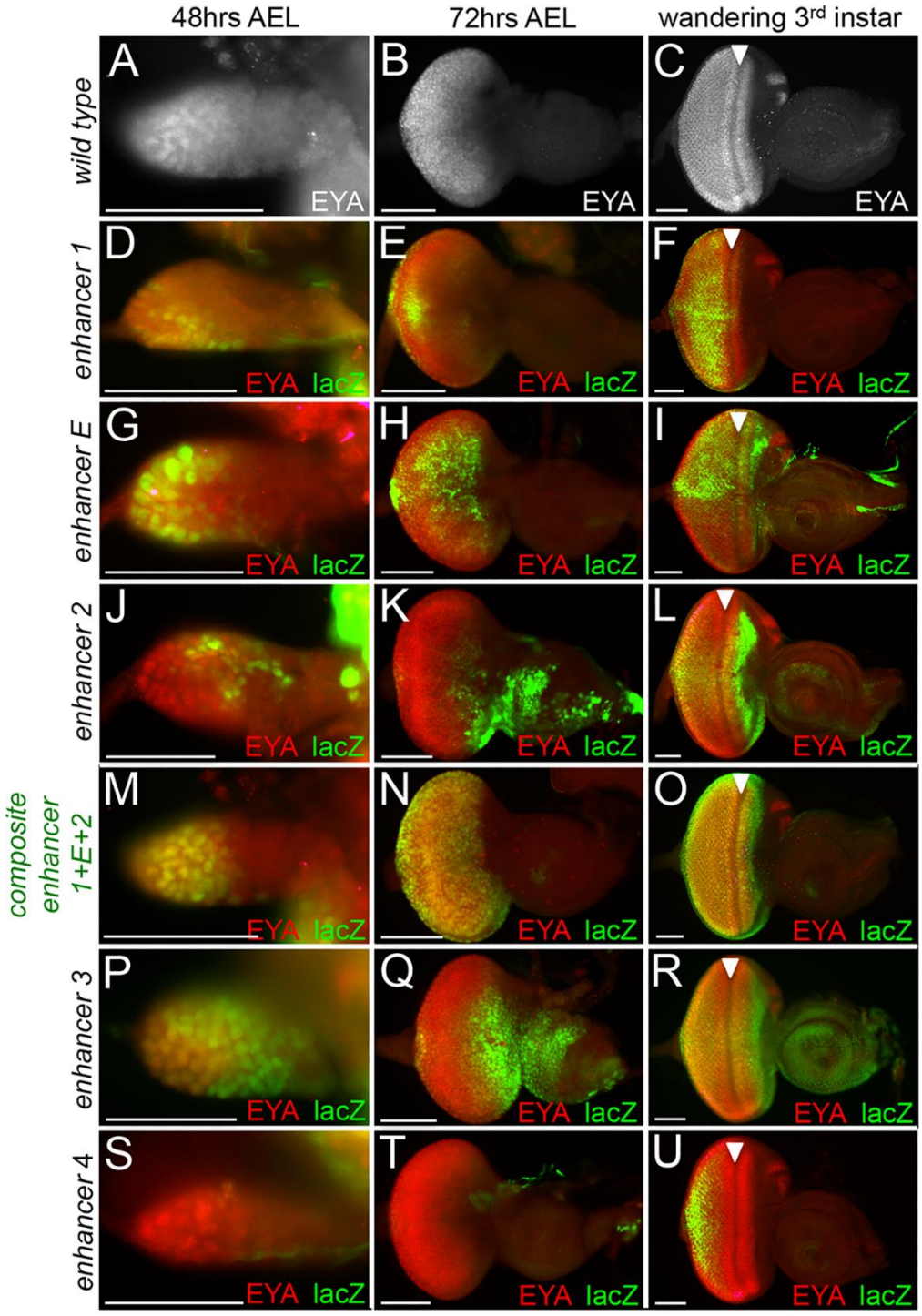

Figure 3. The composite enhancer controls all *eya* expression within the developing eye. (A-U) Light microscope images of developing eye-antennal discs. Images of imaginal discs at 48hrs and 72hrs AEL were taken at 20x while images of wandering third instar larvae were taken at 10x. AEL=after egg laying. Red=Eya protein,

green=β-galactosidase, yellow=positions of co-localization between Eya and β-galactosidase. Arrowhead marks the position of the morphogenetic furrow. All enhancer-lacZ reporters are placed in a wild type genetic background. **(A-C)** Localization of Eya protein in developing wild type retinas at different developmental time points. **(D-F)** Enhancer 1 dependent expression is activated in a few Eya expressing cells early in development and co-localizes with Eya posterior to the morphogenetic furrow late in development. **(G-I)** Extant enhancer dependent expression co-localizes with Eya and is robust early in development but becomes weaker and sparse as development proceeds. **(J-L)** Enhancer 2-dependent expression is largely present in non-*eya* expressing cells early in development. Co-localization with Eya can be seen in cells anterior and posterior to the furrow later in development but a significant portion of reporter expression still present in non-*eya* expressing cells. **(M-O)** Composite enhancer-dependent expression shows co-localization with Eya protein throughout all stages of larval eye development. This is the only construct to fully recapitulate temporal and spatial *eya* expression. **(P-R)** Enhancer 3-dependent expression is largely present in non-*eya* expressing cells throughout development. Some co-localization with Eya protein is seen at later stages in cells anterior and posterior to the furrow. **(S-U)** Enhancer 4-dependent expression co-localizes with a few Eya expressing cells posterior to the furrow late in development. Anterior is to the right in imaginal disc images. At least 30 imaginal discs were examined for each genotype and developmental time point. Scale bar, 50μm.

Enhancer	LacZ Reporter Expression			cDNA Rescue Average # of ommatidia	
	48hrs AEL	72hrs AEL	Late 3rd Instar	*eya*^{1}	*eya*^{2}
Enhancer 1	-	†	‡	189 ± 47	284 ± 54
Enhancer E	‡	‡	†	37 ± 2	364 ± 7
Enhancer 2	†	†	†	-	-
Enhancer 1+E+2	‡	‡	‡	761 ± 31	804 ± 40
Enhancer 1+E	‡	‡	‡	333 ± 40	618± 30
Enhancer 1+2	-	-	†	-	-
Spacer alone	N/A	N/A	-	N/A	-
Enhancer 1+spacer+2	†	†	‡†	432 ± 1	482 ± 64
Enhancer 1+5bp+2	†	†	‡†	-	-
Enhancer 3	†	†	†	-	-
Enhancer 4	-	-	†	-	-

- No expression or rescue
‡ Recapitulates eya expression
† Expresses in non-eya+ cells or only in a few Eya+ cells

doi:10.1371/journal.pgen.1006462.t001

Table 1. Enhancer Expression and Rescue. For each rescue experiment two-three female eyes were photographed with a scanning electron micrograph. We manually counted the number of ommatidia for each eye and calculated both averages and standard deviations (listed within table). The raw ommatidia counts for the rescue experiments are as follows: *eya*^{1}*; enhancer 1—eya RB cDNA* (141, 235, 190), *eya*^{2}*; enhancer 1—eya RB cDNA* (322, 245), *eya*^{1}*; enhancer E—eya RB cDNA* (39, 38, 35), *eya*^{2}*; enhancer E—eya RB cDNA* (358, 372, 362), *eya*^{1}*; enhancer 1+E+2—eya RB cDNA* (792, 730, 762), *eya*^{2}*; enhancer 1+E+2—eya RB cDNA* (757, 825, 829), *eya*^{1}*; enhancer 1+E—eya RB cDNA* (376, 324, 298), *eya*^{2}*; enhancer 1+E—eya RB cDNA* (635, 584, 636), *eya*^{1}*; enhancer 1+spacer+2—eya RB cDNA* (433, 433, 432), *eya*^{2}*; enhancer 1+spacer+2—eya RB cDNA* (443, 448, 556).

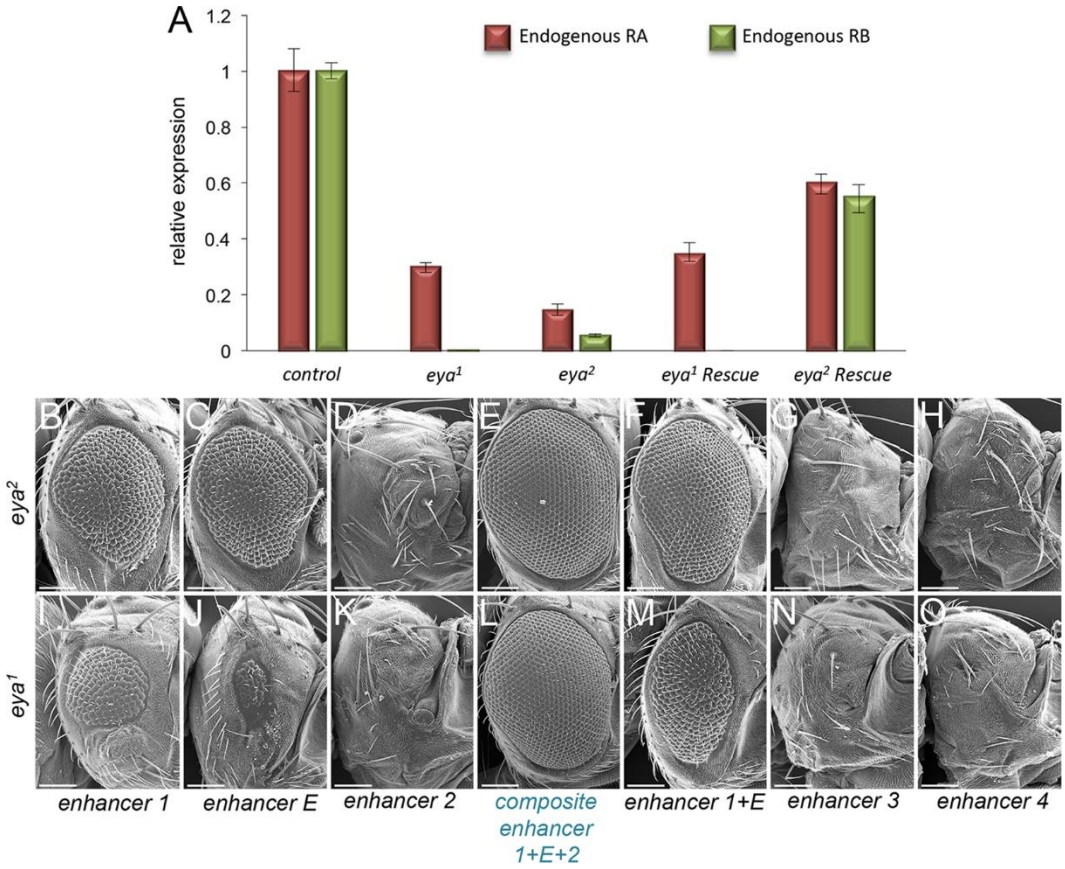

Figure 4. The composite enhancer fully restores eye development to *eya[1]* and *eya[2]* mutants. (A) qRT-PCR quantification of *eya* RA and RB transcript levels in eye-antennal discs. *y*-axis measures the relative expression levels of each transcript. Raw data from single runs from three biological replicates were used to generate the graph. Error bars represent standard error. **(B-O)** SEM images of adult *Drosophila* compound eyes and heads from enhancer cDNA fusion rescue experiments. Each enhancer is driving expression of the *eya* RB isoform within the developing eye of *eya[1]* and *eya[2]* mutants. **(B,I)** *Enhancer 1—eya RB cDNA* fusion partially rescues 100% of animals examined. **(C,J)** *Enhancer E—eya RB cDNA* fusion partially rescues 100% of animals examined. Rescue efficiency is significantly reduced in *eya[1]* background. **(D,K)** *Enhancer 2—eya RB cDNA* fusion does not rescue either *eya[1]* or *eya[2]* mutants. **(E,L)** *Composite enhancer—eya cDNA* fusion fully rescues 100% of animals examined to wild type eye

size. **(F,M)** *Enhancer 1+E—eya cDNA* fusion partially rescues 100% of animals examined. **(G,N)** *Enhancer 3—eya cDNA* fusion does not rescue *eya*^{1} or *eya*^{2} mutants. **(H,O)** *Enhancer 4—eya cDNA* fusion does not rescue *eya*^{1} or *eya*^{2} mutants. Anterior is to the right in all adult head images. At least 100 adult flies were examined qualitatively for each genotype. Quantification of rescue (assayed by number of ommatidia) of a subset of adults is provided in Table 1. Scale bar, 100μm.

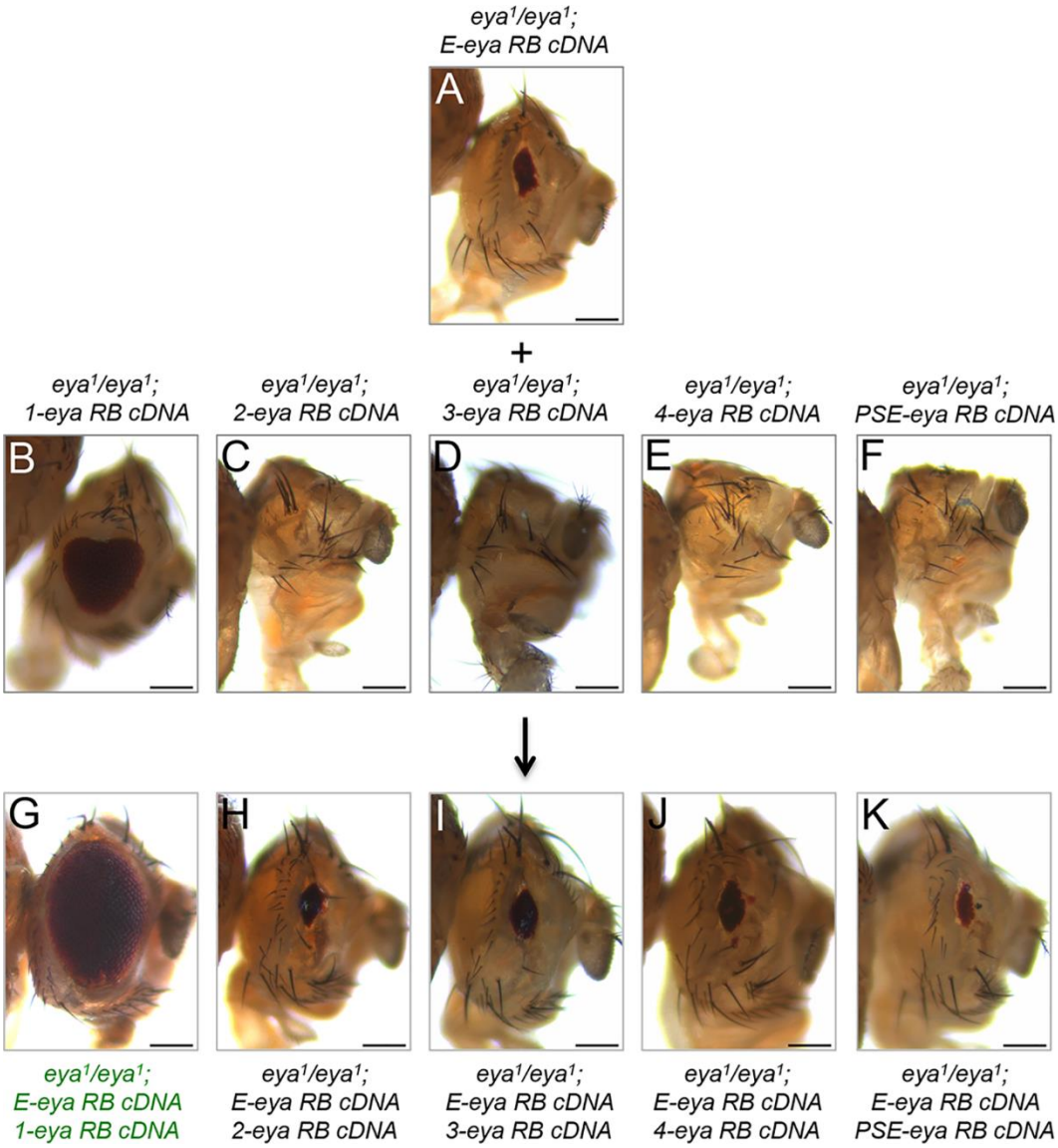

Figure 5. Cooperative interactions between enhancers 1 and E drive eye development. (A-K) Light microscope images of adult *Drosophila* compound eyes and heads from single and combination enhancer—*eya* RB cDNA fusion rescue experiments. Each enhancer is driving expression of the *eya* RB isoform within the developing eye of *eya*^{1} mutants. **(A)** *eya*^{1}*/eya*^{1}*; extant enhancer E—eya RB cDNA*. Expression of the *eya* RB cDNA driven by the extant enhancer alone weakly rescues 100% of animals examined. **(B)** *eya*^{1}*/eya*^{1}*; enhancer 1—eya RB cDNA*. Expression of the *eya* RB cDNA

driven by enhancer 1 alone partially rescues 100% of animals examined. **(C)** *eya^{1}/eya^{1}; enhancer 2—eya RB cDNA*. Expression of the *eya* RB cDNA driven by enhancer 2 alone does not rescue the no-eye phenotype. **(D)** *eya^{1}/eya^{1}; enhancer 3—eya RB cDNA*. Expression of the *eya* RB cDNA driven by enhancer 3 alone does not rescue the no-eye phenotype. **(E)** *eya^{1}/eya^{1}; enhancer 4—eya RB cDNA*. Expression of the *eya* cDNA driven by enhancer 4 alone does not rescue the no-eye phenotype. **(F)** *eya^{1}/eya^{1}; enhancer PSE—eya RB cDNA*. Expression of the *eya* RB cDNA driven by the PSE enhancer alone does not rescue the no-eye phenotype. **(G)** *eya^{1}/eya^{1}; enhancer 1—eya RB cDNA/extant enhancer E—eya RB cDNA*. Combining *enhancer 1—eya RB cDNA and enhancer E—eya RB cDNA* constructs increases the quality of rescue as demonstrated by the larger eye size in 100% of animals examined. **(H)** *eya^{1}/eya^{1}; enhancer 2—eya RB cDNA/extant enhancer E—eya RB cDNA*. Combining *enhancer 2—eya RB cDNA* and *enhancer E—eya RB cDNA* constructs does not increase the quality of rescue over the extant enhancer alone. **(I)** *eya^{1}/eya^{1}; enhancer 3—eya RB cDNA/extant enhancer E—eya RB cDNA*. Combining *enhancer 3—eya RB cDNA* and *enhancer E—eya RB cDNA* constructs does not increase the quality of rescue over the extant enhancer alone. **(J)** *eya^{1}/eya^{1}; enhancer 4—eya RB cDNA/extant enhancer E—eya RB cDNA*. Combining *enhancer 4—eya RB cDNA* and *enhancer E—eya RB cDNA* constructs does not increase the quality of rescue over the extant enhancer alone. **(K)** *eya^{1}/eya^{1}; enhancer PSE—eya RB cDNA/extant enhancer E—eya RB cDNA*. Combining enhancer *PSE—eya RB cDNA* and *enhancer E—eya RB cDNA* constructs does not increase the quality of rescue over the extant enhancer alone. Anterior is to the right in adult head images. At least 100 adult flies were examined for each genotype. Scale bar, 100μm.

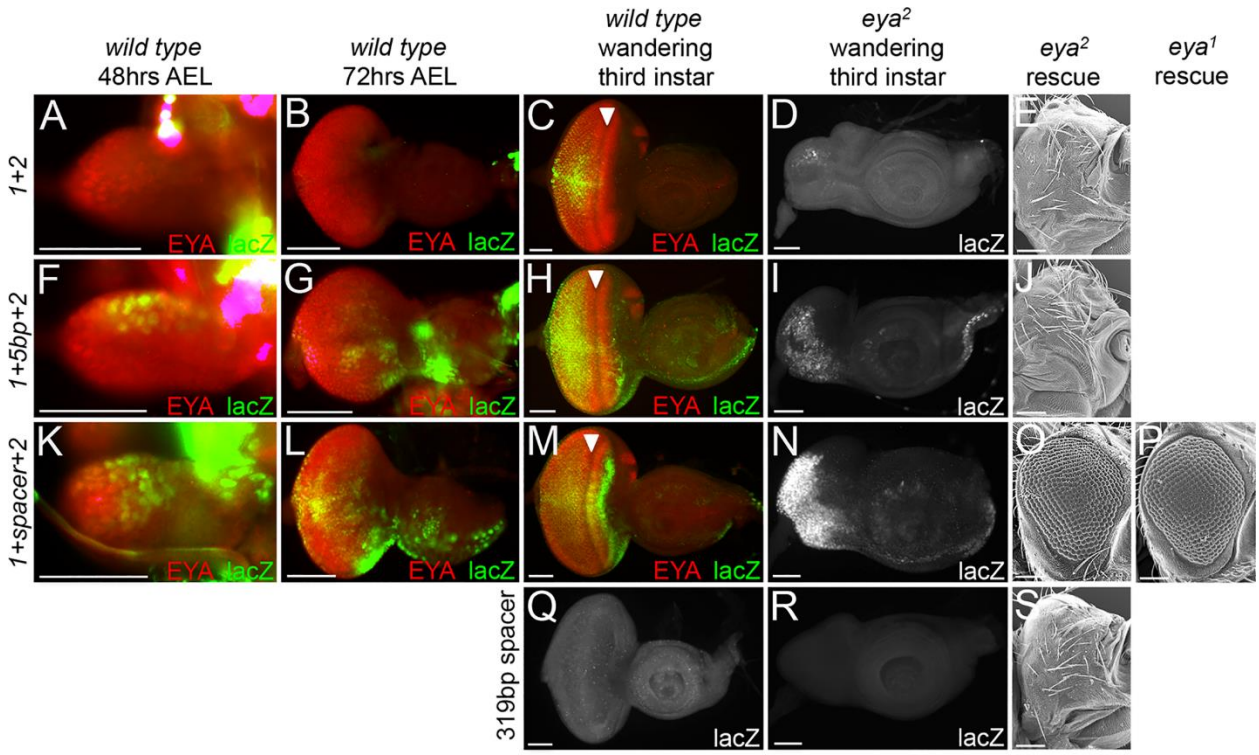

Figure 6. Spacing between enhancers is required for *eya* expression and function. **(A-D, F-I, K-N, Q, R)** Light microscope images of developing eye-antennal discs. Images of imaginal discs at 48hrs and 72hrs AEL were taken at 20x while images of wandering third instar larvae were taken at 10x. Red=Eya, green=β-galactosidase, yellow=regions where Eya and β-galactosidase co-localize. White arrowheads mark the position of the morphogenetic furrow. Each enhancer is driving expression of lacZ within wild type eye-antennal discs. AEL=after egg laying. **(E,J,O,S)** SEM images of adult *Drosophila* compound eyes and heads from enhancer—*eya* RB cDNA rescue experiments. Each enhancer is driving expression of the *eya* RB isoform within the developing eye of either eya^1 or eya^2 mutants. (P) SEM image of adult *Drosophila* compound eyes and heads from *enhancer 1+spacer+2—eya RB cDNA* rescue experiments of eya^1 mutants. **(A-C)** Expression driven by enhancer 1+2 is only activated late in eye development in some *eya*

expressing cells posterior to the furrow. **(D)** Expression driven by enhancer 1+2 is activated in very few cells in *eya*^{2} mutant discs. **(E)** The *enhancer 1+2—eya RB cDNA* does not rescue *eya*^{2} mutants. **(F-H)** Expression driven by enhancer 1+5bp+2 is activated mostly in non-*eya* expressing cells early in development while later activation is seen in *eya* expressing cells both anterior and posterior to the furrow. **(I)** Expression driven by enhancer 1+5bp+2 is activated weakly throughout the eye disc of *eya*^{2} mutants. **(J)** The *enhancer 1+5bp+2—eya RB cDNA* does not rescue *eya*^{2} mutants. **(K-M)** Expression driven by enhancer 1+spacer+2 restores some early expression in *eya* expressing cells but does not fully recapitulate *eya* expression at all stages of development. **(N)** Expression driven by enhancer 1+spacer+2 is strongly activated throughout the eye disc of *eya*^{2} mutants. **(O)** *Enhancer 1+spacer+2—eya RB cDNA* partially rescues 100% of *eya*^{2} mutants suggesting a restoration of function. **(P)** *Enhancer 1+spacer+2—eya RB cDNA* partially rescues 100% of *eya*^{1} mutants suggesting a restoration of function. **(Q-R)** The neutral 319bp of DNA that was used to construct 1+spacer+2 does not drive reporter activation on its own in either wild type or *eya*^{2} discs. **(S)** The 319bp spacer does not rescue *eya*^{2} mutants. Anterior is to the right in adult head and imaginal disc images. At least 100 adult flies and 30 imaginal discs were qualitatively examined for each genotype and at each developmental time point. Panel A-D, F-I, K-N, Q-R Scale bar, 50μm. Panel E,J,O,P,S Scale bar, 100μm.

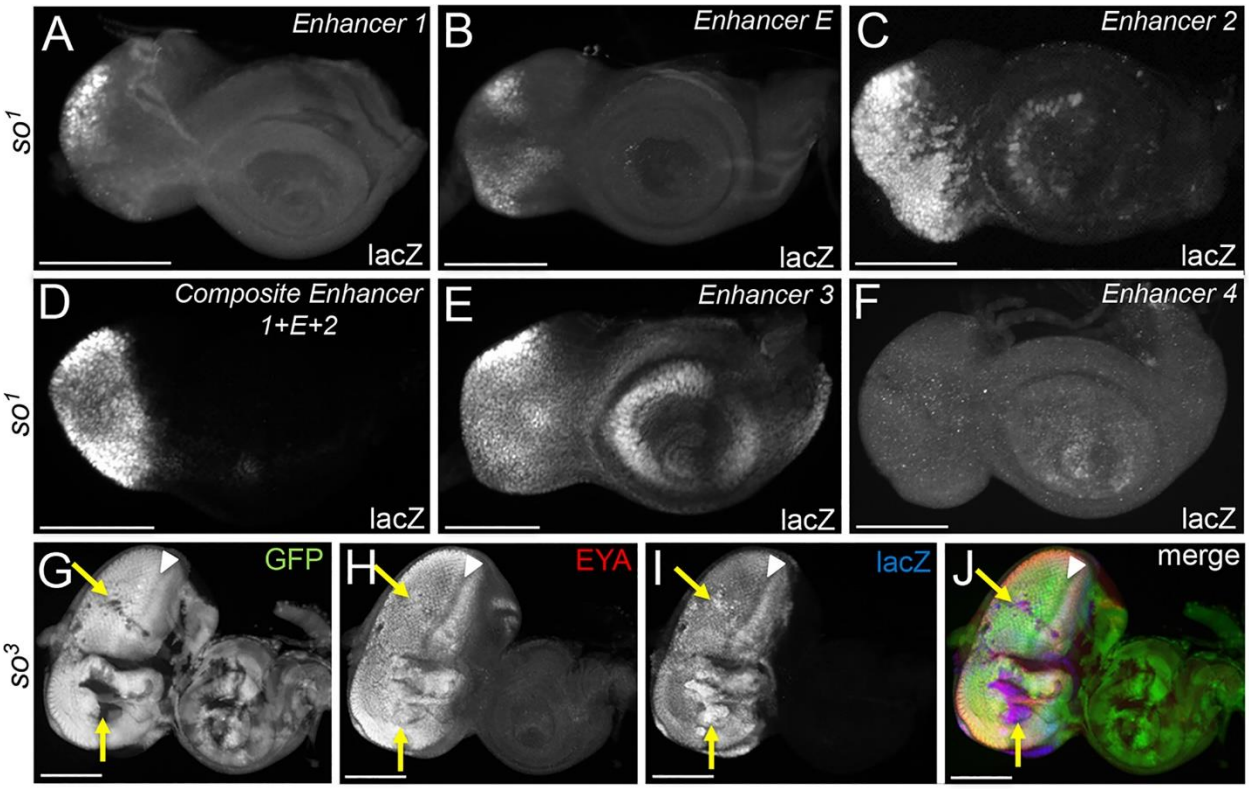

Figure 7. *eya* retinal enhancers remain transcriptionally active in *so* mutants. (A-F) Light microscope images of wandering third instar *so*^{1} mutant eye-antennal discs. Each enhancer is driving expression of lacZ within *so*^{1} eye-antennal discs. LacZ reporter activation is detected with an antibody that recognizes the β-galactosidase enzyme. **(A)** *so*^{1}*; enhancer 1—lacZ*. Reporter expression driven by enhancer 1 is activated only in cells at the far posterior edge of the eye disc. **(B)** *so*^{1}*; enhancer E–lacZ*. Reporter expression driven by the extant enhancer E is weakly activated throughout the eye disc. **(C)** *so*^{1}*; enhancer 2–lacZ*. Reporter expression driven by enhancer 2 is strongly activated throughout the remaining eye disc. **(D)** *so*^{1}*; enhancer 1+E+2 –lacZ*. Reporter expression driven by the composite enhancer is strongly activated throughout the eye disc. **(E)** *so*^{1}*; enhancer 3–lacZ*. Reporter expression driven by enhancer 3 is activated broadly throughout the entire eye-antennal disc. **(F)** *so*^{1}*; enhancer 4 –lacZ*. Reporter expression

driven by enhancer 4 is not activated in the eye disc. **(G-J)** Light microscope images of wandering third instar eye antennal discs in which *so*^{3} null clones have been generated. The absence of GFP marks the position of clones lacking *so*. Green=GFP, red=Eya protein, blue=lacZ. Yellow arrows mark the position of *so*^{3} mutant clones in which Eya protein is present and the composite enhancer lacZ reporter is activated. White arrowheads mark the position of the morphogenetic furrow. Anterior is to the right in all imaginal disc images. At least 30 discs were examined for each genotype. Scale bar, 100μm.

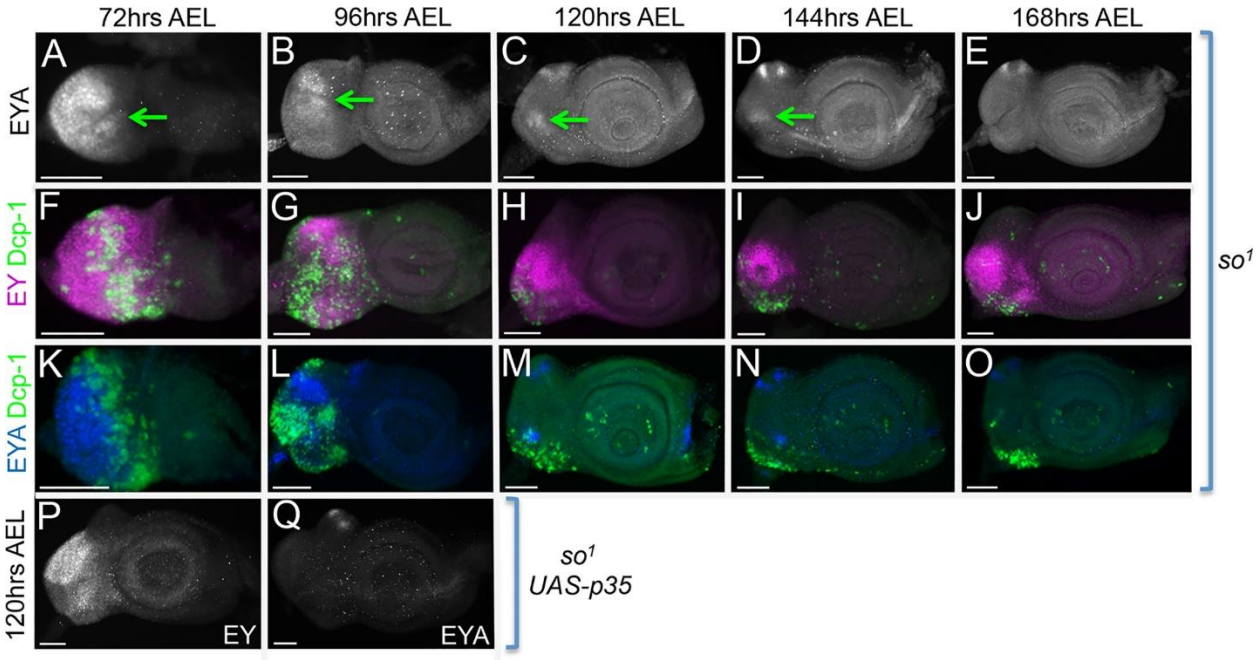

Figure 8. Eya expression is lost progressively in *so*^{1} mutants as a result of increased cell death in retinal progenitors. (A-O) Light microscope images of developing *so*^{1} mutant eye discs. **(A-E)** Green arrows indicate regions containing Eya protein. The amount of Eya protein is progressively lost in *so* mutant retinas. **(F-O)** Light microscope images of developing *so*^{1} mutant eye discs showing positions of dying cells. Cell death (green) is marked by Dcp-1, Ey (magenta) marks the position of progenitor cells, and Eya (blue) marks the position of precursor cells. Cell death in *so*^{1} mutants is elevated in both progenitor and precursor cells. **(P-Q)** Light microscope images of developing *so*^{1}, *eya composite enhancer GAL4, UAS-p35*. Cell death has been blocked in the eye disc of *so*^{1} mutants by expression of the caspase inhibitor p35. Blocking death does not prevent the loss of *eya* expression in late third instar *so*^{1} mutant discs. AEL=after egg laying. Anterior is to the right in all imaginal disc images. At least 30 discs were examined for each genotype and at each developmental time point. Scale bar, 50μm.

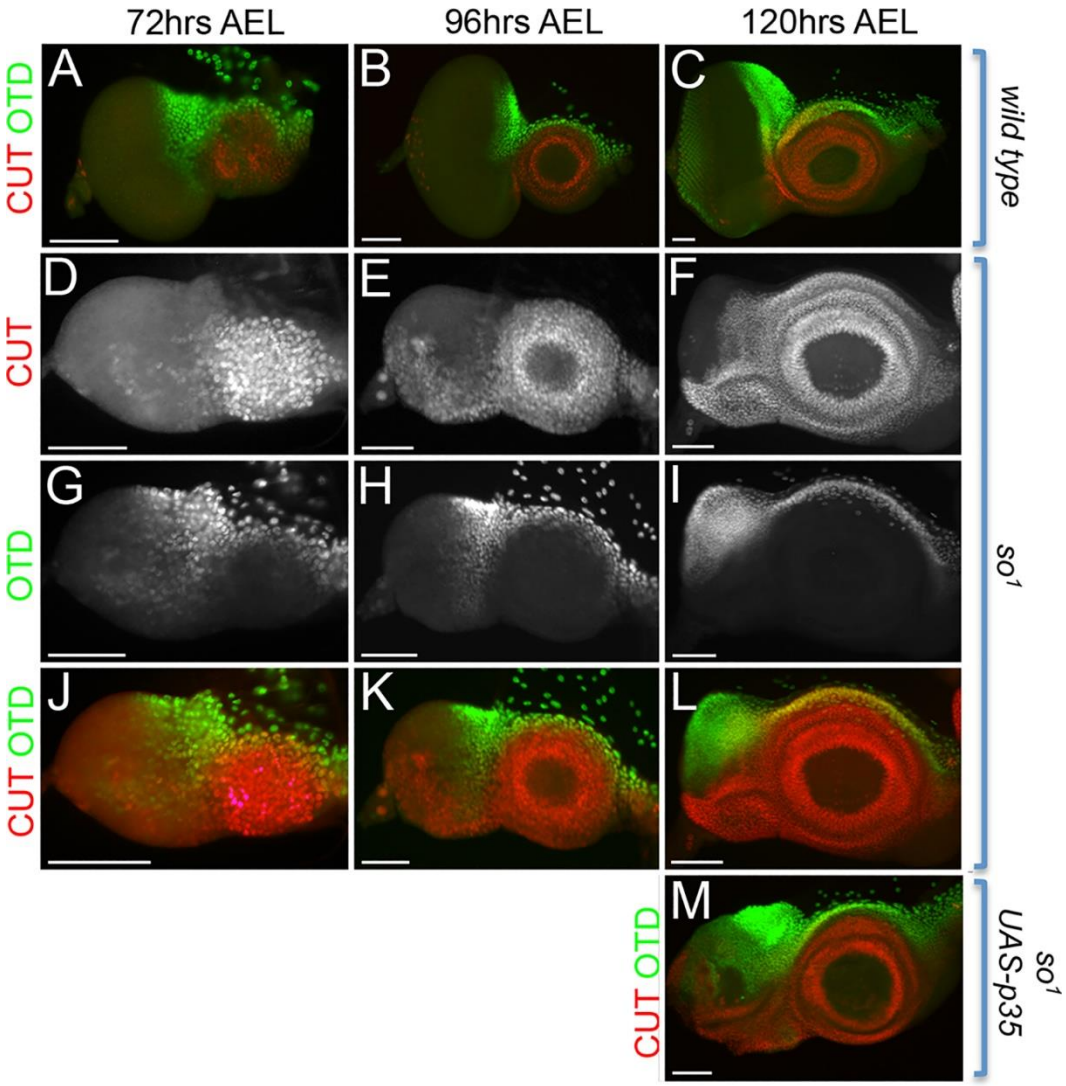

Figure 9. Retinal progenitors within *so*^{1} mutants progressively transform into head epidermis. (A-M) Light microscope images of developing wild type, *so*^{1}, and *so*^{1}*, eya composite enhancer GAL4, UAS-p35* eye-antennal discs. Green=Otd and red=Cut. Expression of both *otd* and *cut* is de-repressed within the eye field of *so*^{1} mutant discs over the course of larval eye development. Although cell death has been blocked in the eye disc of *so*^{1} mutants by the caspase inhibitor p35, expression of *otd* and *cut* is still de-repressed in retinal progenitors. AEL=after egg laying. Anterior is to the right in all disc images. At least 30 discs were examined for each genotype at each developmental time point. Scale bar, 50μm.

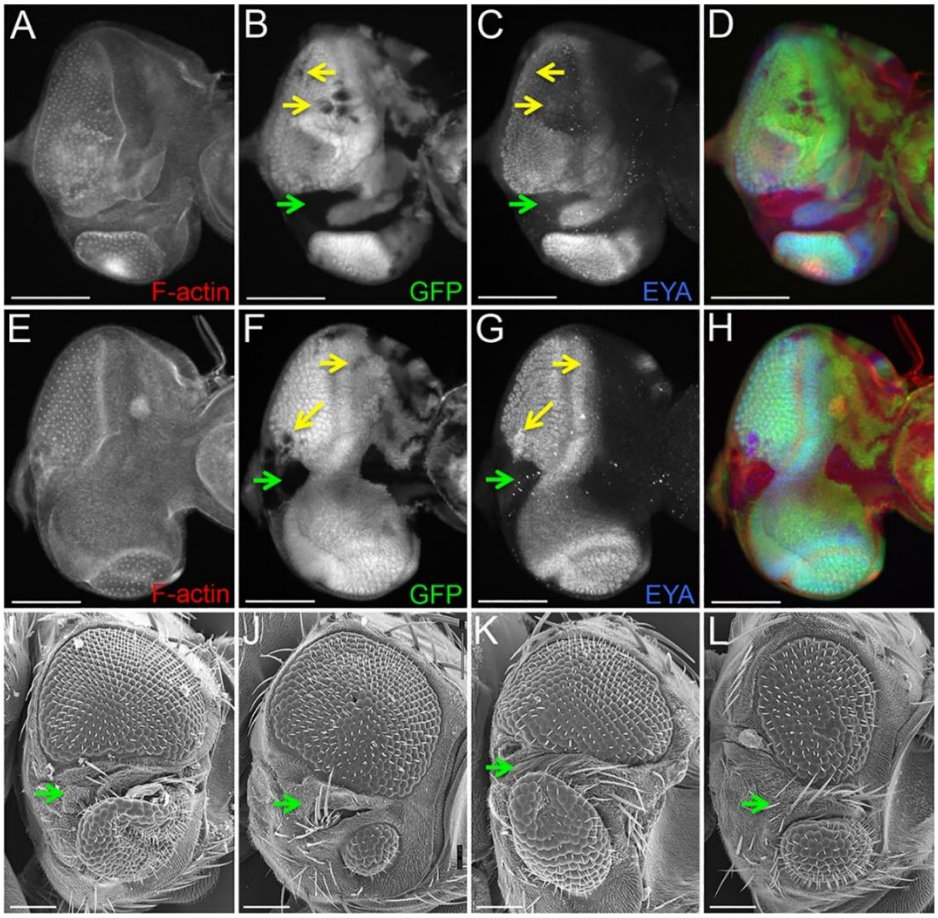

Figure 10. Eya protein is detected in non-transformed *so³* mutant clones. (A-L) Eye discs and adult heads of the genotype: *eyflp; FRT42D so³ /FRT42D Ubi-GFP* that contain *so³* mutant clones. **(A-H)** Light microscope images of developing eye-antennal discs. Yellow arrows identify *so³* clones that have not transformed into head epidermis and still express *eya*. Green arrows demarcate large *so³* clones that are transforming into head epidermis and lack Eya protein. Red=F-actin, green=GFP, blue=Eya. **(I-L)** SEM images of adult *Drosophila* compound eyes and heads. Green arrows indicate regions of the compound eye that has transformed into head epidermis. Green arrows in panels I-L indicated regions of head epidermis bifurcating the retinal field. Anterior is to the right in all adult head and imaginal disc images. At least 30 adult eyes and imaginal discs containing *so³* clones were examined. Scale bar, 100μm.

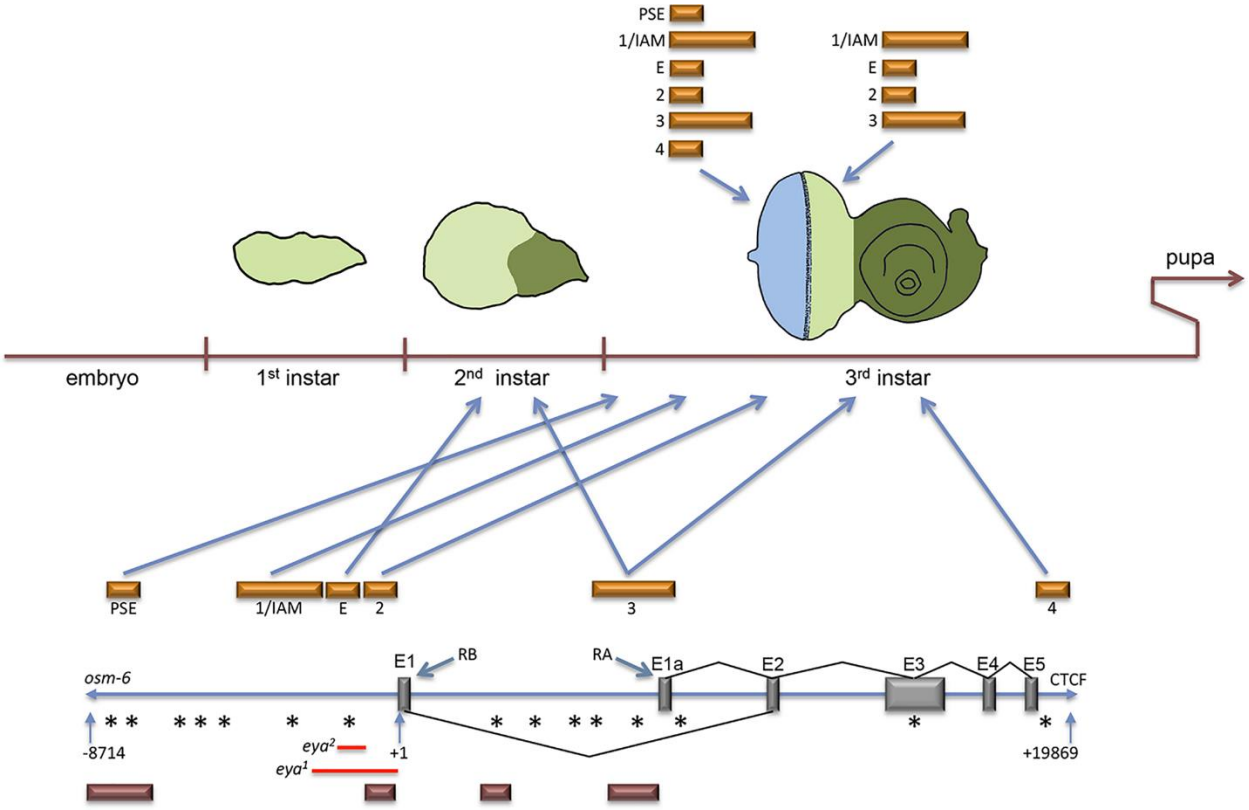

Figure 11. Summary of *cis*-regulatory control of the *eya* locus in the developing eye. This summary diagram depicts spatial and temporal control that *cis*-regulatory elements exert on the expression of *eya* in the developing retina. Orange bars=*eya cis*-regulatory elements, red bars=So ChIP binding peaks, red lines=regions deleted in eya^{1} and eya^{2} mutants, grey bars=exonic sequences, asterisks=position of So consensus binding sites, and RA/RB refer to two predicted isoforms of Eya. The *osm-6* gene and a CTSF insulator site were used to define the *eya* locus. Eya expression is initiated during the second instar stage with enhancers E and 3 driving expression in undifferentiated cells (light green) that are normally positive for Eya protein. At the onset of the third larval instar, the morphogenetic furrow initiates and begins the process of converting the undifferentiated cells into an ordered array (light blue) of differentiating photoreceptors, cone, and pigment cells. At this stage, all six enhancers are expressed in differentiating

cells. However, only four of the enhancers drive expression in the undifferentiated cells. During development, the antennal disc (dark green) does not show Eya protein. However, the individual enhancers can drive ectopic expression in this zone (see Fig 3). The spurious expression in the antenna is eliminated when enhancers 1, E, and 2 are fused together (composite enhancer) to mimic their organization in the genome (see Fig 3). Anterior is to the right.

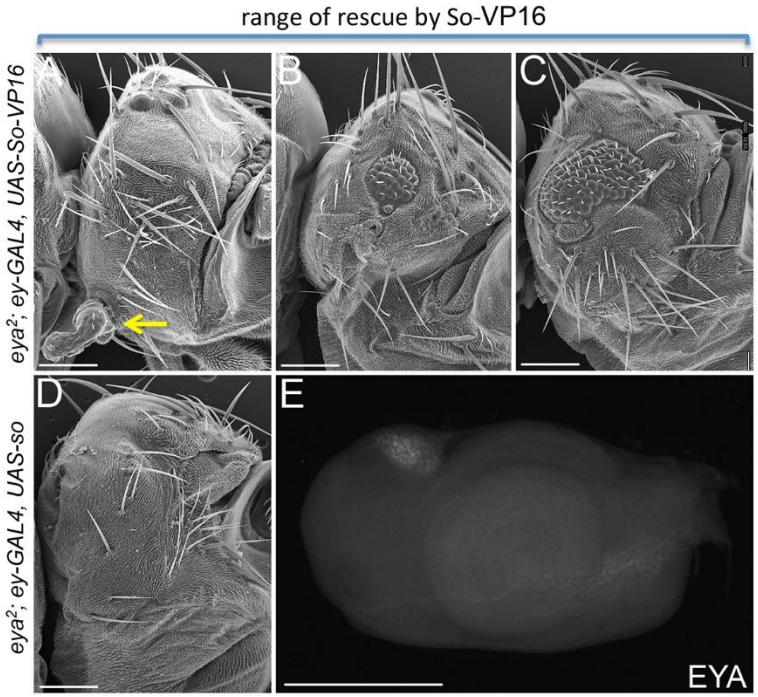

S1 Figure. Expression of So-VP16 (but not So) rescues the *eya*^{2} mutant. (A-C) SEM images of adult *Drosophila* compound eyes and heads from *eya*^{2}*; ey-GAL4, UAS-So-VP16* animals. These panels show the range of rescue phenotypes produced by over-expression of the So-VP16 chimeric protein. Yellow arrow in panel A shows a stalk eye. (D) SEM image of adult *Drosophila* compound eye and head from *eya*^{2}*; ey-GAL4, UAS-so* animals. Over-expression of So does not rescue the *eya*^{2} mutant. (E) Light microscope image of a developing eye-antennal disc from *eya*^{2}*; ey-GAL4, UAS-so* animals. Over-expression of So does not restore Eya expression to the eye disc of *eya*^{2} mutants. Anterior is to the right in all adult head and imaginal disc images. At least 100 adult heads and 30 imaginal discs were examined for each genotype. Scale bar, 100μm.

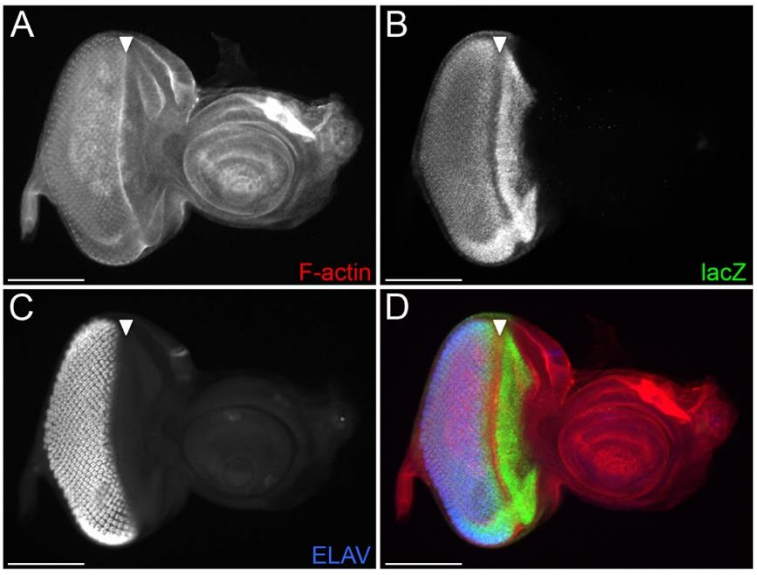

S2 Figure. The expression pattern of the composite enhancer is not altered by changes in its genomic location. (A-D) Light microscope images of developing eye-antennal discs demonstrating that placement of the composite enhancer-lacZ in a second genomic position (*PBac(y^{+}-attP-9A)VK00019*) does not alter the expression of the construct. Red=F-actin, green=lacZ, blue=Elav. Anterior is to the right. At least 30 imaginal discs were examined. Scale bar, 100μm.

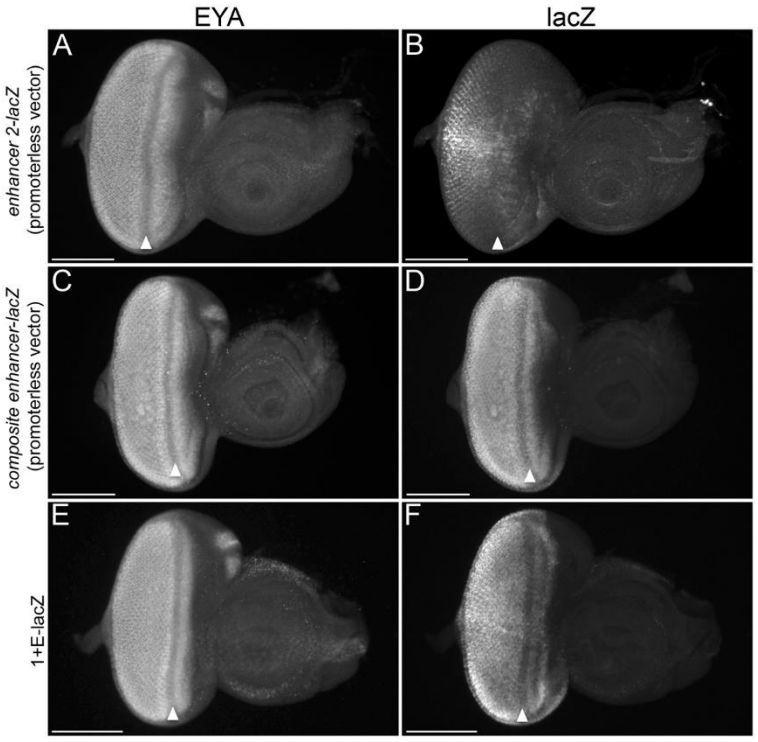

S3 Figure. Enhancer 2 also contains the core promoter of *eya*. (A-F) Light microscope images of wild type eye-antennal discs containing enhancer-lacZ constructs. White arrowheads mark the position of the morphogenetic furrow. **(A-B)** *Enhancer 2—lacZ* reporter in a vector lacking a promoter shows expression mostly in photoreceptors. Ectopic expression in the antenna and ahead of furrow is lost. **(C-D)** The *composite enhancer lacZ* reporter in the vector lacking a promoter shows identical expression to that of a vector containing a minimal hsp70 promoter. Therefore, enhancer 2 contains the core promoter of *eya*. **(E-F)** The *enhancer 1+E—lacZ* reporter construct fully recapitulates Eya expression. Anterior is to the right. 30 imaginal discs were examined for each genotype. Scale bar, 100μm.

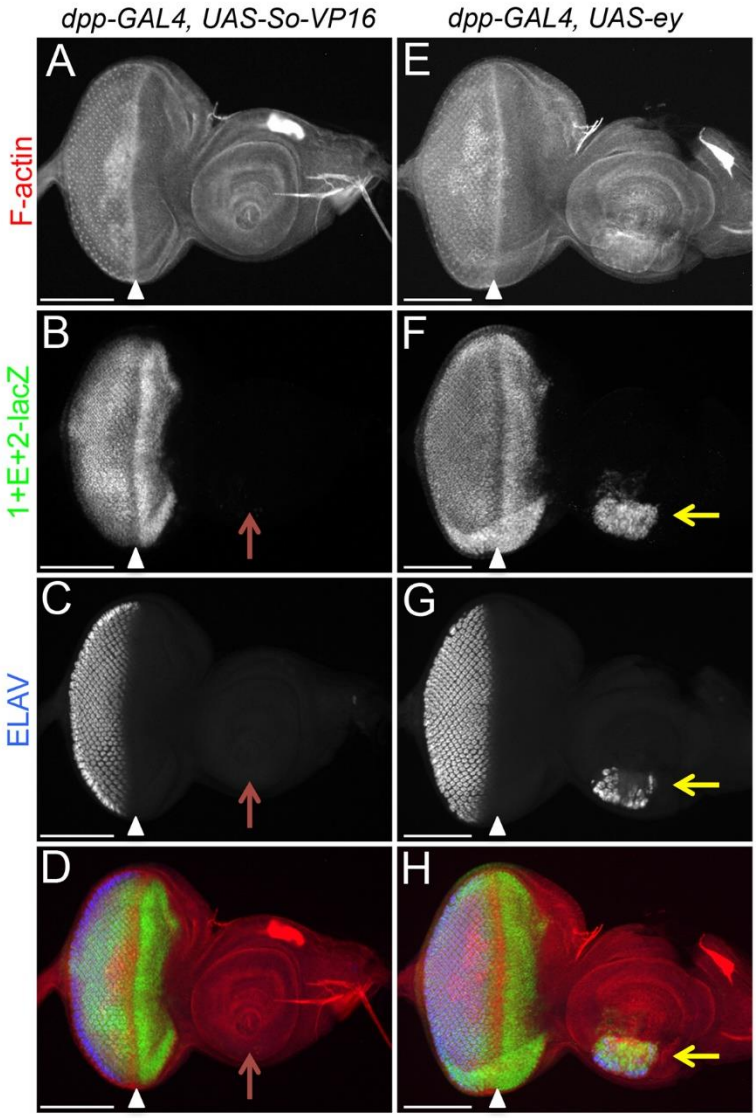

S4 Figure. The composite enhancer is not responsive to So-VP16. (A-D) Light microscope images of developing eye-antennal discs from *dpp-GAL4, UAS-So-VP16* animals. The rose-colored arrows in panels B-D point to cells that fail to activate the composite enhancer even in the presence of So-VP16. **(E-H)** Light microscope images of developing eye-antennal discs from *dpp-GAL4, UAS-ey* animals. The yellow colored arrows in panels F-H mark the activation of the composite enhancer by forced expression of Ey. Red=F-actin, green=lacZ, blue=Elav (photoreceptors). Anterior is to the right. At least 30 imaginal discs were examined for each genotype. Scale bar, 100μm.

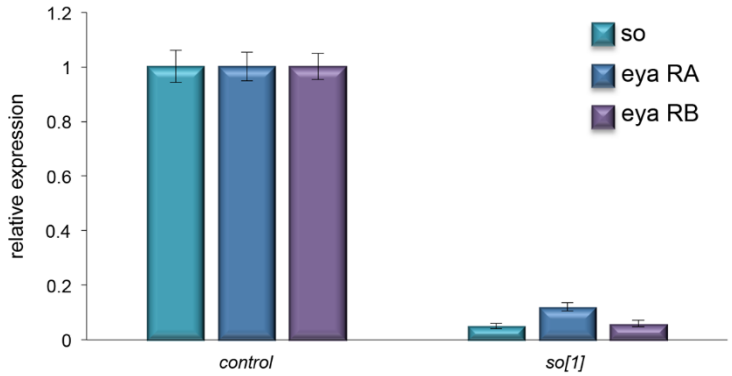

S5 Figure. Transcription of *eya* is dramatically reduced in *so*^{1} mutants. qRT-PCR quantification of *so* and both *eya* RA and RB transcript levels in wild type and *so*^{1} eye-antennal discs. Raw data from single runs of three biological replicates were used to generate the graph. The *y*-axis is the relative expression levels of each transcript. Error bars indicate standard error.

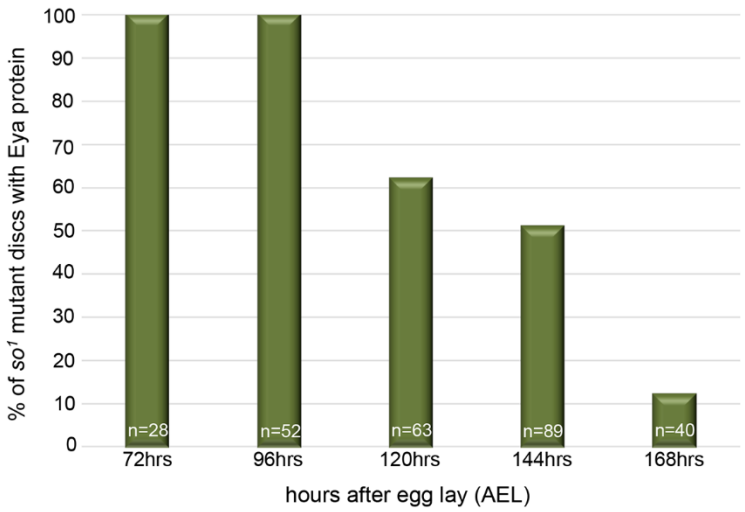

S6 Figure. *eya* expression weakens and is eliminated from progressively older *so*^{1} mutant eye-antennal discs. A graph quantifying the number of discs that have Eya protein within the eye field at different developmental stages. 28 discs were examined at 72hrs, 52 discs at 96hrs, 63 discs at 120hrs, 89 discs at 144hrs and 40 discs at 168hrs. AEL=after egg laying.

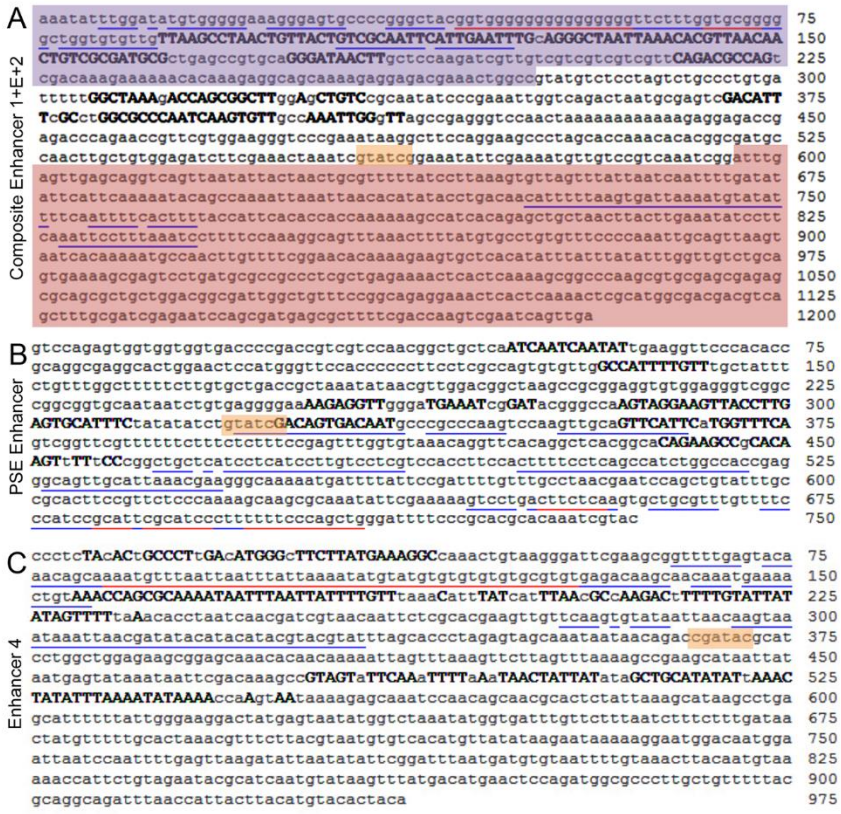

S7 Figure. Conservation analysis of *eya* composite, PSE and 4 enhancers. (A-C) Evoprinter conservation analysis of *eya* enhancers. Black letters represent bases in the *D. melanogaster* reference sequence that are conserved in the *D. sechellia*, *D. simulans*, *D. yakuba*, *D. erecta*, *D. ananassae*, *D. persimilis*, *D. pseudoobscura*, *D. virilis*, *D. willistoni*, and *D. grimshawi* orthologous genomic regions. Blue underlining indicates single-copy repeats and red underlining identifies multi-copy repeats. **(A)** Conservation analysis of *eya* composite enhancer. Purple outline is enhancer 1, rose outline is enhancer 2, orange outline is so binding site described in [32]. **(B)** Conservation analysis of *eya* PSE enhancer. Orange outline is *so* binding site described in [32]. **(C)** Conservation analysis of *eya* enhancer 4. Orange outline is *so* binding site described in [32].

S1 Table. Sequence of *eya* genomic fragments that were fused to lacZ and used to search for new retinal enhancers. Sequences labeled in red failed to drive expression of the reporter within the retina while sequences listed in green represent regions containing *eya* retinal *cis*-regulatory elements.

Fragment Sequences

-8714 to -6333 (2379bp)

GTAAACATGTTGGCGACTCGAATTCAAACATGGCCGGCAAGCCAGCGAAAGAACGCTCCTCCGTTTTTCGTGCAGGGCTCCCGAGTTGAATTACACC
GCAGGCGATTTTTGGAGTGCGGGAAACACAAGACCTGTGGGAAGTAAAGCTATATAGCTGCACTTATGCGCGGCTCAGCCATCGTTTAGTACGAAAA
TTGGTTACTTAACACAATTAATTATTTGTATTAATATTTCCCCGTACGCCAAGGGGTGCCTCCGCGCCACGCAAATCTCCCAAGGGAAATCCTGAGT
AGCTGTTCTGTTTTTAGGTGTCAACGATTTGCTTCCGCTTTTCCGGAGGGGGCGACTCCTGCTATCTCCCTGCTAATTGGGATGAGAACTAGGGTGT
GGGAGTATCTAGTGTGTGAGAAACCACTAGTTAATGCTTGTCACAACAAATAGTGTCATAAATCTGGACTCCCAAGGGGGATGCAATTCCAGGGAGT
GGAGTCCTGTAAAAAATACTTCTCCACAACTGGCGGTTGTAAATTTTTTAGGTTTTCTTTTGGAGAGAAAATGTTTCCCTGGAGTGCGTGGATCCTT
GGGACATGTTTGGGACTGGGACTTTTACCTGAAGACCAGTTGTTGACAACAAGATAAGTTTTAAATTAAGTTTTAACTTGCTCATATTTTATTCATT
CTCATTTCAATAAATTTCCATTCCAAATGGACATCTTTTAGTTAGTTACAGAAATTCGGAATATTATCCAAAATATTACACTATATTATGGATTATT
TACAAAATGTTCCTGTTTTGAAGTCATTTCACCCCGAATCCCCACTTCGAACCGTCCAGAGTGGTGGTGGTGACCCCGACCGTCGTCCAACGGCTGC
TCAATCAATCAATATTGAAGGTTCCCACACCGCAGGCGAGGCACTGGAACTCCATGGGTTCCACCCCCCTTCCTCGCCAGTGTGTTGGCCATTTTGT
TTGCTATTTCTGTTTGGCTTTTTCTTGTGCTGACCGCTAAATATAACGTTGGACGGCTAGGCCGCGGAGGTGTGGAGGGTCGACCGGCGGTGCAATA
ATCTGTGAGGGGAAAAGAGGTTGGGATGAAATCGGATACGGGCCAAGTAGGAAGTTACCTTGAGTGCATTTCTATATATCTGTATCGACAGTGACAA
TGCCCGCCCAAGTCCAAGTTGCAGTTCATTCATGGTTTCAGTCGGTTCGTTTTTTCGTTCTCTTTCCGAGTTTGGTGTAAACAGGTTCACAGGCTCA
CGGCACAGAAGCCGCACAAGTTTTTCCCGGCTGCTCATCCTCATCCTCGTCCTCGTCCACCTTCCACTTTTCCTCAGCCATCTGGCCACCGAGGGCA
GTTGCATTAAACGAAGGGCAAAAATGATTTTATTCCGATTTTGTTTGCCGAACGAATCCAGCTGTATTTGCCGCACTTCCGTTCTCCCCAAAAGCAAG
CGCAAATATTCGAAAAAGTCCTGACTTCTCAAGTGCTGCGTTTGTTTTCCCATCCGCATTCGCATCCCTTTTTTCCCAGCTGGGATTTTCCCGCACA
CAAATCGTACTTTATATATTAGTCACTTTTCCGAACTGTCCACCATTTCTCACCTGTATGAAGCTCGCCAGTGGGGTGGGGGGGGTGCTGAAATTCC
GGGAAAACCCTCATGGAGCACGCCGCGATCGTGATGCGGGTCGTGGCGACATCGTTTTAATTAAATTACAGCCACCAAAACGTGCGACACTATAATC
ATTTTTATTCATTGTCAAAAATGGGCAATCATAAAAAACAACACGTCTGCATCGCAGCTGGCGAAGGTGGAGTTCTAAGTTAATCCGTGGTGGGGGT
TAATCCCACGGAGTGTGGGGCAAGCTGTCCGGACACAGCCACCAACATAAACAGCCATTCGCTCGCACAAGGGGAATGTAACAATCAATTAACAGGC
CAGATAGGTTCAGATCGGAGATTCCAGTTAACCCTTGGGGAGCATCACTTTTTGGCTTCATTTCAGGTCGTAATTTTAACGAGCTATAGGTACTGGG
ATTATGCAGTTTTAAGTAAAATAACTTATCATAAATTTGTATGTCATGTCATCATTAAAGCTTTAAATGATTGTCATGATCTTAGGATTTATTTTTG
TCTGCATAGCCTCTTGAGTGAATGAGTGGTGTGATGGGAACCCTCTTGCCCATGAAAGGGTTAAAGCAGCCGTTGACCCAAGATTGTCATGGCACGC
TTCTTCGTCCGCTGGACTCTCTGTCTTTGTCTTTGTCTCCGTGGATGTCGCTCCACTCGTGTTGTTGTTGTTTCTGTCTGCTGGCGGGGACATGTGG
TTGTTGTTGCCATCGCTGTGGGGCCCAATGTCAATGTCTATATGGCCATC

-6332 to -3831 (2501bp)

ATCGGAATAGAAAGCGTGTCTTTTATGTTGTGGCATTGTTATTAATCTATCATTAGGTCGCTGTTGTACAACAGGCTCTAATGATGCGTGTAAATGC
TAAACAAATCACACATTCTGCCCAAAAAAAAAACTATATAAAAATAAAATACACCAAATCCAAATCGAATATCTCTGCGCAGCGAAACGAGGGAAAA
ATGCTCGAAGCGCGTGTACAATTTAAAATGAAATAAAATCAGACTGCGCAGCTTTCGAAATTTTATGAGCTTGTTGTGCTTATTAGTCGCCCCACGA
GAAATGGCGACAGGCCACAACATCACCAACAACATCACCAACAACACCACCGAAACAACAACACCAATGAGAACAACCAGAACGGTAACAACAACAA
CAACAACAACAATCACAACACGCATTGCCACGGCTAATTTTTCACGCGCACTCCGAATGCAGCTTCACCTCCAGCTCCATACCTGCTCCACCTCCAT
ACCAGCTCCAGCTCCAACTCCATCTCCATTCCGACAGCGACAGCTCCTGACCAGGCTATCACTTGCCGCAGTCCCAGCAAGGGTATCATTGCTATCC
TGTAGCCTTTGTGCTAGTACTGGTCTCGATTTTGATTTAGCGTTAGTTGTGCAGTATTCAATGATGCAAGTGAAGTTTTCCCAATGGAAAACTAATT
CAACGGGGATTTAATGTATAGCAAAGGCATTGAGTGAAATGGAAAATCGAAATATATGGGTGCATACTTTTGGACAGCTTCATAATAGTATCAGTTT
ACGATGTTCGAACTGCCTGACGCATAATTACAATCATTTCTTTGTTTTTCACTTATTATATTGATAGCATTAGAATAAACTTCGATAATTTAATTAT
TGATATGATATATGTACATAATATGTAGTTCAACCAGCATTCGATGATCTTCAATTGGCTGCTTGAGGTTCCTTGTGCTTTATTTTTATACTTTTTG
GCACGCCAGACACGCACGAGAAATTCCAAGAGATAAGGATCGTGTACGACAAGGTGTATTATGGACCCCCAATCCAGGGACCCCAACCCCGGCAGCC
AAATGCCCAGTGTCCCCCAGTCGGAGTTGTGCCGTCGAGTGCCATACTGTTGACTCTGTTAAATTGCCAATATTTATGGTCTTGCCCGCACGGGTTG
ACTTGTTAAATGGGTGTTCCTTCCAGCAGCCTTTCGTTGGATGCCATCACCAGTTCCGTGGCCGGAGGATAGGGACTCCTGCCCGACAGTTGGTAGC
TGTAAAACGTTTAAGGACAAAACGTGTTCGGCCCGATAAGAGGCAGCTGGCCAAGACGATGGGCTACGGCCATCAGCATCAGTTTGACGTATGCCCG
TCAATGGTTTTAATGGCCCAGCTAGCCATTTTGAAAGTGCCAAGATTCAGTTTCTATGTGCAGCTAAGCAGAAATGCGCAATGTCGTCGCCGCTGAA
GCTATAAAAATGTCAAAACATGCAACAAATAATGGCAGAATTATAAAGAAATCTAGCGGTAGCGAAAATAAATAAATAAAAAAAAGCGCGTCATTCA
GTTCGTTCAGTGCAGTAAGCCAGTTGTTTGCGGCTTATTCCCTACAAATTAATTCGGTAGCTTGATTTCTGGAAATCTTATAATAACGAGTGCATAC
TGTACTTATTTATTACTTAGTTAAGTGAGAAGCATGCTACCAAATACGCCATTTTAATAAGAAATTTCAAACTCAATAAATATTAATATATAAACTT
AATAGGATTTCAGAGCATTTATACTTCTTGCAGACCGAATTTATTCCCCATCACCGCCCTTATCTCACTGGATGTGTAATTGACAAAAAACGAAAAA
ATGAGTTTCCTCTGGCTTGTTTCCAGGTTGATACGGCGCTGATCTTGCGGTTTTGCTGGTTTTATATCGCATTTATGCCATTTTCCATGGTAGTTTT
TTTTTTTAGTTTATTTCGGCGAGGAGCCGCACGCGAATCTGCCATGATGCTGACATTTCGAAATCACCCGAATCCCTTCTGAAACCGTAGATGTGTG
AGAGAGGAAAGCCCAGTCTTATCTCGATCCGAATGATCGTCACCTTAAATGCTATAAGTCACACCTAGCCATTTGTCACATTTTCTAGCCGCCCACG
GGGCCAAACCAATGGGCATGGGGCATCGGACATCGGGGATTGGGATCGGAGATTGAGACTTGTTTCATAAATCAAATCGGTGCACGTTACATTTGAG
GCGCATAAAAATGCAAATTGTATGCATAAAGTATAATTTTTATAACTTAATTAACTGAGCTTTGCGGCGAAGTGGGCTTGGGGCACCTGCTGTGTTT
GTCGCTTTTTCCTCATTAGGCTGGCGCCAAGTTTGAGATTGATTTTGGTCGCATTTACATGACAAAGCTGCTGCGGATGCTGTAGGAGTTGTCTTGG
GTCGATTTGGTTGTGATAAGCTCATCAGGGCACCACCACTGGTAGCTGCAGCTCCTCGGGAATCAGCCAGGCCAAG

-3830 to -897 (2934bp) Enhancer 1 Large Fragment

ACTACACCTCGTACCAAATTCTCGGAAGAGCTGCAGATAAGCCGAGTGCCCCAGACGAACATTAAATAATCTGCCTCTAATTTGGGTGTCGTTTACA
CGTGCCAAGATCTCTTGACTCCACTCCACTTCACTTCACTGCCGACTCCCTGACACTGATGAGGCCCATCAAGATGATGATGGGTCGAGTGTTGGGT
CCCCGGCAGGGTCATTAAACACCTGGCATTATCGCTTCATCTCGGAATGTGCCTGATATGCGATTCGAGGGGGTGGCGTTGTGTCGAACTGGCGGAA
TGTCAAAGTTTACATATTTGATTGGATTTTATGGGAATTTCCAAGGTATGTTTGTGTTTGACGATCCTCTGAAAAAGCAATGCTCCCTAAAATAGTA
TAGCCAAGGATTACACCTATCATAATACCCGTAATTAACCACTACGTAAGCCATCCTTAGCCTTTTATGCCTTCAGACAGAGTTTATTTTGTTTATT
TATATTGTGTAATTTGTTATTTCTTCTACCTCTCCTTTGTGGGCCCTGTTTCTCTGCTGGCTGACACTTGACCCTTTTAGAAAATAACCAGTTGTGT
GTGTGTGTGTGCGACGATGGGGTGAATGTTGGTGACTGTCTCGAAATCGAAATCTGGCGCCGTTTACATTGCCCGCGGCTAAACAAAAAAGAAACAT
CAGCCAAATCCACAATCGAGAATGTCTATACAAAAGTCAATAAACTTCAGTGCGATAGGTATGTGGACAACAGCCACAATCACAAGGGCAGCAAAAT
CACAAACAATGGTCACGACAACGGGGGGCGTTCGTCTGGAAGGGATCAGCCAAGGGGTTTCCCATGGAGGTGGTTACAAGCAACAGGTGCAATGGGG
CAGCACACTACTTATTTCTAGCCACAAGTTGAATTAAATCACTTATCTAAATATGATCTTATAGTGAATCGCTTTGGTTTAGTCATTAAACTGAACT
GGGTATCTCCTCCTGCTGTTTCCTAAGAGACAAAAGCAATGTGTTCCATATCAGAGTACTTTAAACTTTGCCTTAGCTTTTCCACTGAACAGCTCAC
TCCACTCCACCCGATGGGTGAAGCCTTGAAAACCCACCACCTTCCAGTGCTGACTCATCCGGGCAGCTGGCTGTGGGCTCTTCCCGCTGGTGACTTA
CTGTCAACTGGCGCTTGGGCCGAACTCGTTGGTCATAAATTATCCGAAAGGAGGACCCTTTGCCTGCGCATCCCAATTGGGGACCAGCTCCTACTTC
TTCTCCAGCTCCTCCTCCAGCTCACTGTCGCCAGCTCGGATGCCAAGTGATTTTTTTTTCTTAGCGCGCCCAGCGGGCGCTCATTGTACGGGCAGTT
AAACAAGACGCTTTTCAGCTCGTAAAACAAGCTGGCTGGCTGTTTGTTTTTGTATAATAAAGTTATTGATTTGTGTTTAAGTGCCGTGGGTGACCCG
CTTGGAAACCCAACGGCGATTTGGGGTACGAGAAGAAAGCCTTTCCCCCAGCAGATTAATGCGTTGCATTCGGGGCCAACAATCGCTGGCATTTATC
AGCTTATTTGCTTTATTAAACGCTAAGCTGAGCCGTTTAAGGCCCAAAGCTGACGCCTGTCAATTGCGACATGAGCAAAGTCACTCCCCTCCAGAAA
TCGCTGCCCACCACTGCTCGATGCTCGACTCCTGATCTTTGGGCTGTGGACAGCGGACTGTGGGCGGCGCACTTAAGTAGCTTAAACAGACGCGGGG
TGGTCCGCGACATAACTTTGTCTAATGACTCGGAAATCCGTCACTAATAATAAGAGCCATGGCCATAAAGAGGCAGCGAGCATTTGAGACCCTCAGT
CGGTCAGCGACTGCCGATGCATTTCTGCACTTAACTGGAATCGGTCAACTTCCAGCTTCAGATGGGAGCTTCCATCTTGGAGCTACAGATGGTAGAG
GCCGAAGCCTCTGACACTGAGCACGTGTGTGTGCTTCTGGCATAATCCTATTACCCAGCCGACGTTGCTCGAGTTTTATGAATGAAAATATTCCTAC
GACCGCAGCAGGCAAACAAATGGTTGTTGAAAAATAAGAGTAAATCCAATTGAAGGCAATCGATGGAGTAGTTGGGCAGGTTGATAGGCAAATGCCA
TGGATTGGGTTGGAAAATCAATAATAGACTACTTTATAACTTCATCGATTGCAACTCAAAGTGAGGTTTAAGTGAGTTACGTGAGTGATTTAAAAAA
AAAAATAATTATATAAGTTATACTATTTAAGGGAGCTAAGTATTTAAGTCCCTGTTCTCAGCATTCAGCATTTCTTAGTTTATATATGTTTTTGCAT
TATACTAATGATTTCCTTTTGCTGTAACTTGCGTATCGTGCCGATCCCATCTTATCTGACTCATTAAAGGAAGCTATGCCTCCGCCCCGCCAAACCA
GGAAACCAATTTAAAGCCACACTGTAGTTTATGGCTTAAAGTCGGATGGAATTAGGAAAACGCCCCCTTCTCCATTCGCCCCATTGTAGCACCATTC
CATCCCTTCAATCCCAATTCCACACCTACAAGAGTCAACATTGAGTGCTTTTCCGCGCGCATGCGTTCGATCCTCGTCTGCCGACGGGGGAGGATTC
CATGTCCTCGGAGCACCAGGACAATTCAAAATGGCTGCACAAATATTTGGATATGTGGGGGAAAGGGAGTGCCCCGGGCTACGGTGGGGGGGGGGGG
GGGTTCTTTGGTGCGGGGGCTGGTGTGTTGTTAAGCCTAACTGTTACTGTCGCAATTCATTGAATTTGCAGGGCTAATTAAACACGTTAACAACTGT
CGCGATGCGCTGAGCCGTGCAGGGATAACTTGCTCCAAGATCGTTGTCGTCGTCGTCGTCCAGACGCCAGTCGACAAAGAAAAAACACAAAGAGGCA
GCAAAAGAGGAGACGAAACTGGCC

-1171 to -897 (275bp) Enhancer 1 Minimal Fragment

AAATATTTGGATATGTGGGGGAAAGGGAGTGCCCCGGGCTACGGTGGGGGGGGGGGGGGGGTTCTTTGGTGCGGGGGCTGGTGTGTTGTTAAGCCTAA
CTGTTACTGTCGCAATTCATTGAATTTGCAGGGCTAATTAAACACGTTAACAACTGTCGCGATGCGCTGAGCCGTGCAGGGATAACTTGCTCCAAGA
TCGTTGTCGTCGTCGTCGTCCAGACGCCAGTCGACAAAGAAAAAACACAAAGAGGCAGCAAAAGAGGAGACGAAACTGGCC

-896 to -577 (320bp) Extant Enhancer

GTATGTCTCCTAGTCTGCCCTGTGATTTTTGGCTAAAGACCAGCGGCTTGGAGCTGTCCGCAATATCCCGAAATTGGTCAGACTAATGCGAGTCGAC
ATTTCGCCTGGCGCCCAATCAAGTGTTGCCAAATTGGGTTAGCCGAGGGTCCAACTAAAAAAAAAAAAGAGGAGACCGAGACCCAGAACCGTTCGTG
GAAGGGTCCCGAAATAAGGCTTCCAGGAAGCCCTAGCACCAAACACACGGCGATGCCAACTTGCTGTGGAGATCTTCGAAACTAAATCGTATCGGAA
ATATTCGAAAATGTTGTCCGTCAAATCGG

-576 to +10 (586bp) Enhancer 2 Large Fragment

ATTTGAGTTGAGCAGGTCAGTTAATATTACTAACTGCGATTTTATCCTTAAAGTGTTAGTTTATTAATCAATTTTGATATATTCATTCAAAAATACA
GCCAAAATTAAATTAACTCATATACCTGACAACATGTTTAAGTGATTAAAATGTATATTTTCAATTTTCACTTTTACCATTCACACCACCAAAAAAG
CCATCACAGAGCTGCTAACTTACTTGAAATATCCTTCAAATTCCTTTAAATCCTTTTCCAAAGGCAGTTTAAACTTTTATGTGCCTGTGTTTCCCCA
AATTGCAGTTAAGTAATCACAAAAATGCCAACTTGTTTTCGGAACACAAAAGAAGTGCTCACATATTTATTTATATTTGGTTGTCTGCAGTGAAAAG
CGAGTCCTGATGCGCCGCCCTCGCTGAGAAAACTCACTCAAAAGCGGCCCAAGCGTGCGAGCGAGAGCGCAGCGCTGCTGGACGGCGATTGGCTGTT
TCCGGCAGAGGAAACTCACTCAAAACTCGCATGGCGACGACGTCAGCTTTGCGATCGAGAATCCAGCGATGAGCGCTTTTCGACCAAGTCGAATCAG
TTGA

-282 to +10 (292bp) Enhancer 2 Minimal Fragment

TGCAGTTAAGTAATCACAAAAATGCCAACTTGTTTTCGGAACACAAAAGAAGTGCTCACATATTTATTTATATTTGGTTGTCTGCAGTGAAAAGCGA
GTCCTGATGCGCCGCCCTCGCTGAGAAAACTCACTCAAAAGCGGCCCAAGCGTGCGAGCGAGAGCGCAGCGCTGCTGGACGGCGATTGGCTGTTTCC
GGCAGAGGAAACTCACTCAAAACTCGCATGGCGACGACGTCAGCTTTGCGATCGAGAATCCAGCGATGAGCGCTTTTCGACCAAGTCGAATCAGTTG
A

-3830 to -897 + -576 to +10 (3520bp) Enhancer 1+2

ACTACACCTCGTACCAAATTCTCGGAAGAGCTGCAGATAAGCCGAGTGCCCCAGACGAACATTAAATAATCTGCCTCTAATTTGGGTGTCGTTTACA
CGTGCCAAGATCTCTTGACTCCACTCCACTTCACTTCACTGCCGACTCCCTGACACTGATGAGGCCCATCAAGATGATGATGGGTCGAGTGTTGGGT
CCCCGGCAGGGTCATTAAACACCTGGCATTATCGCTTCATCTCGGAATGTGCCTGATATGCGATTCGAGGGGGTGGCGTTGTGTCGAACTGGCGGAA
TGTCAAAGTTTACATATTTGATTGGATTTTATGGGAATTTCCAAGGTATGTTTGTGTTTGACGATCCTCTGAAAAAGCAATGCTCCCTAAAATAGTA
TAGCCAAGGATTACACCTATCATAATACCCGTAATTAACCACTACGTAAGCCATCCTTAGCCTTTTATGCCTTCAGACAGAGTTTATTTTGTTTATT
TATATTGTGTAATTTGTTATTTCTTCTACCTCTCCTTTGTGGGCCCTGTTTCTCTGCTGGCTGACACTTGACCCTTTTAGAAAATAACCAGTTGTGT
GTGTGTGTGTGCGACGATGGGGTGAATGTTGGTGACTGTCTCGAAATCGAAATCTGGCGCCGTTTACATTGCCCGCGGCTAAACAAAAAAGAAACAT
CAGCCAAATCCACAATCGAGAATGTCTATACAAAAGTCAATAAACTTCAGTGCGATAGGTATGTGGACAACAGCCACAATCACAAGGGCAGCAAAAT
CACAAACAATGGTCACGACAACGGGGGGCGTTCGTCTGGAAGGGATCAGCCAAGGGGTTTCCCATGGAGGTGGTTACAAGCAACAGGTGCAATGGGG

CAGCACACTACTTATTTCTAGCCACAAGTTGAATTAAATCACTTATCTAAATATGATCTTATAGTGAATCGCTTTGGTTTAGTCATTAAACTGAACT
GGGTATCTCCTCCTGCTGTTTCCTAAGAGACAAAAGCAATGTGTTCCATATCAGAGTACTTTAAACTTTGCCTTAGCTTTTCCACTGAACAGCTCAC
TCCACTCCACCCGATGGGTGAAGCCTTGAAAACCCACCACCTTCCAGTGCTGACTCATCCGGGCAGCTGGCTGTGGGCTCTTCCCGCTGGTGACTTA
CTGTCAACTGGCGCTTGGGCCGAACTCGTTGGTCATAAATTATCCGAAAGGAGGACCCTTTGCCTGCGCATCCCAATTGGGGACCAGCTCCTACTTC
TTCTCCAGCTCCTCCTCCAGCTCACTGTCGCCAGCTCGGATGCCAAGTGATTTTTTTTTCTTAGCGCGCCCAGCGGGCGCTCATTGTACGGGCAGTT
AAACAAGACGCTTTTCAGCTCGTAAAACAAGCTGGCTGGCTGTTTGTTTTTGTATAATAAAGTTATTGATTTGTGTTTAAGTGCCGTGGGTGACCCG
CTTGGAAACCCAACGGCGATTTGGGGTACGAGAAGAAAGCCTTTCCCCCAGCAGATTAATGCGTTGCATTCGGGGCCAACAATCGCTGGCATTTATC
AGCTTATTTGCTTTATTAAACGCTAAGCTGAGCCGTTTAAGGCCCAAAGCTGACGCCTGTCAATTGCGACATGAGCAAAGTCACTCCCCTCCAGAAA
TCGCTGCCCACCACTGCTCGATGCTCGACTCCTGATCTTTGGGCTGTGGACAGCGGACTGTGGGCGGCGCACTTAAGTAGCTTAAACAGACGCGGGG
TGGTCCGCGACATAACTTTGTCTAATGACTCGGAAATCCGTCACTAATAATAAGAGCCATGGCCATAAAGAGGCAGCGAGCATTTGAGACCCTCAGT
CGGTCAGCGACTGCCGATGCATTTCTGCACTTAACTGGAATCGGTCAACTTCCAGCTTCAGATGGGAGCTTCCATCTTGGAGCTACAGATGGTAGAG
GCCGAAGCCTCTGACACTGAGCACGTGTGTGTGCTTCTGGCATAATCCTATTACCCAGCCGACGTTGCTCGAGTTTTATGAATGAAAATATTCCTAC
GACCGCAGCAGGCAAACAAATGGTTGTTGAAAAATAAGAGTAAATCCAATTGAAGGCAATCGATGGAGTAGTTGGGCAGGTTGATAGGCAAATGCCA
TGGATTGGGTTGGAAAATCAATAATAGACTACTTTATAACTTCATCGATTGCAACTCAAAGTGAGGTTTAAGTGAGTTACGTGAGTGATTTAAAAAA
AAAAATAATTATATAAGTTATACTATTTAAGGGAGCTAAGTATTTAAGTCCCTGTTCTCAGCATTCAGCATTTCTTAGTTTATATATGTTTTTGCAT
TATACTAATGATTTCCTTTTGCTGTAACTTGCGTATCGTGCCGATCCCATCTTATCTGACTCATTAAAGGAAGCTATGCCTCCGCCCCGCCAAACCA
GGAAACCAATTTAAAGCCACACTGTAGTTTATGGCTTAAAGTCGGATGGAATTAGGAAAACGCCCCCTTCTCCATTCGCCCCATTGTAGCACCATTC
CATCCCTTCAATCCCAATTCCACACCTACAAGAGTCAACATTGAGTGCTTTTCCGCGCGCATGCGTTCGATCCTCGTCTGCCGACGGGGGAGGATTC
CATGTCCTCGGAGCACCAGGACAATTCAAAATGGCTGCACAAATATTTGGATATGTGGGGGAAAGGGAGTGCCCCGGGCTACGGTGGGGGGGGGGGG
GGGTTCTTTGGTGCGGGGGCTGGTGTGTTGTTAAGCCTAACTGTTACTGTCGCAATTCATTGAATTTGCAGGGCTAATTAAACACGTTAACAACTGT
CGCGATGCGCTGAGCCGTGCAGGGATAACTTGCTCCAAGATCGTTGTCGTCGTCGTCGTCCAGACGCCAGTCGACAAAGAAAAAACACAAAGAGGCA
GCAAAAGAGGAGACGAAACTGGCCATTTGAGTTGAGCAGGTCAGTTAATATTACTAACTGCGATTTTATCCTTAAAGTGTTAGTTTATTAATCAATT
TTGATATATTCATTCAAAAATACAGCCAAAATTAAATTAACTCATATACCTGACAACATGTTTAAGTGATTAAAATGTATATTTTCAATTTTCACTT
TTACCATTCACACCACCAAAAAAGCCATCACAGAGCTGCTAACTTACTTGAAATATCCTTCAAATTCCTTTAAATCCTTTTCCAAAGGCAGTTTAAA
CTTTTATGTGCCTGTGTTTCCCCAAATTGCAGTTAAGTAATCACAAAAATGCCAACTTGTTTTCGGAACACAAAAGAAGTGCTCACATATTTATTTA
TATTTGGTTGTCTGCAGTGAAAAGCGAGTCCTGATGCGCCGCCCTCGCTGAGAAAACTCACTCAAAAGCGGCCCAAGCGTGCGAGCGAGAGCGCAGC
GCTGCTGGACGGCGATTGGCTGTTTCCGGCAGAGGAAACTCACTCAAAACTCGCATGGCGACGACGTCAGCTTTGCGATCGAGAATCCAGCGATGAG
CGCTTTTCGACCAAGTCGAATCAGTTGA

Enhancer 1+5bp+2 (878bp)

AAGCTTAAATATTTGGATATGTGGGGGAAAGGGAGTGCCCCGGGCTACGGTGGGGGGGGGGGGGGGTTCTTTGGTGCGGGGGCTGGTGTGTTGTTAA
GCCTAACTGTTACTGTCGCAATTCATTGAATTTGCAGGGCTAATTAAACACGTTAACAACTGTCGCGATGCGCTGAGCCGTGCAGGGATAACTTGCT
CCAAGATCGTTGTCGTCGTCGTCCAGACGCCAGTCGACAAAGAAAAAACACAAAGAGGCAGCAAAAGAGGAGACGAAACTGGCCCTAGGATTTG
AGTTGAGCAGGTCAGTTAATATTACTAACTGCGATTTTATCCTTAAAGTGTTAGTTTATTAATCAATTTTGATATATTCATTCAAAAATACAGCCAA
AATTAAATTAACTCATATACCTGACAACATGTTTAAGTGATTAAAATGTATATTTTCAATTTTCACTTTTACCATTCACACCACCAAAAAAGCCATC
ACAGAGCTGCTAACTTACTTGAAATATCCTTCAAATTCCTTTAAATCCTTTTCCAAAGGCAGTTTAAACTTTTATGTGCCTGTGTTTCCCCAAATTG
CAGTTAAGTAATCACAAAAATGCCAACTTGTTTTCGGAACACAAAAGAAGTGCTCACATATTTATTTATATTTGGTTGTCTGCAGTGAAAAGCGAGT
CCTGATGCGCCGCCCTCGCTGAGAAAACTCACTCAAAAGCGGCCCAAGCGTGCGAGCGAGAGCGCAGCGCTGCTGGACGGCGATTGGCTGTTTCCGG
CAGAGGAAACTCACTCAAAACTCGCATGGCGACGACGTCAGCTTTGCGATCGAGAATCCAGCGATGAGCGCTTTTCGACCAAGTCGAATCAGTTGAG
GTACC

-576 to +50 (626bp) Enhancer 2 Minimal Fragment in Promoterless Vector

ATTTGAGTTGAGCAGGTCAGTTAATATTACTAACTGCGATTTTATCCTTAAAGTGTTAGTTTATTAATCAATTTTGATATATTCATTCAAAAATACA
GCCAAAATTAAATTAACTCATATACCTGACAACATGTTTAAGTGATTAAAATGTATATTTTCAATTTTCACTTTTACCATTCACACCACCAAAAAAG
CCATCACAGAGCTGCTAACTTACTTGAAATATCCTTCAAATTCCTTTAAATCCTTTTCCAAAGGCAGTTTAAACTTTTATGTGCCTGTGTTTCCCCA
AATTGCAGTTAAGTAATCACAAAAATGCCAACTTGTTTTCGGAACACAAAAGAAGTGCTCACATATTTATTTATATTTGGTTGTCTGCAGTGAAAAG
CGAGTCCTGATGCGCCGCCCTCGCTGAGAAAACTCACTCAAAAGCGGCCCAAGCGTGCGAGCGAGAGCGCAGCGCTGCTGGACGGCGATTGGCTGTT
TCCGGCAGAGGAAACTCACTCAAAACTCGCATGGCGACGACGTCAGCTTTGCGATCGAGAATCCAGCGATGAGCGCTTTTCGACCAAGTCGAATCAG
TTGACACGCAGCTTTATGTGACATTCGTGGCGAAAGCGGACCAC

-1171 to +10 (1181bp) Composite Enhancer

AAATATTTGGATATGTGGGGGAAAGGGAGTGCCCCGGGCTACGGTGGGGGGGGGGGGGGGGTTCTTTGGTGCGGGGGCTGGTGTGTTGTTAAGCCTAA
CTGTTACTGTCGCAATTCATTGAATTTGCAGGGCTAATTAAACACGTTAACAACTGTCGCGATGCGCTGAGCCGTGCAGGGATAACTTGCTCCAAGA
TCGTTGTCGTCGTCGTCGTTCAGACGCCAGTCGACAAAGAAAAAACACAAAGAGGCAGCAAAAGAGGAGACGAAACTGGCCGTATGTCTCCTAGTCT
GCCCTGTGATTTTTGGCTAAAGACCAGCGGCTTGGAGCTGTCCGCAATATCCCGAAATTGGTCAGACTAATGCGAGTCGACATTTCGCCTGGCGCCC
AATCAAGTGTTGCCAAATTGGGTTAGCCGAGGGTCCAACTAAAAAAAAAAAAAGAGGAGACCGAGACCCAGAACCGTTCGTGGAAGGGTCCCGAAATA
AGGCTTCCAGGAAGCCCTAGCACCAAACACACGGCGATGCCAACTTGCTGTGGAGATCTTCGAAACTAAATCGTATCGGAAATATTCGAAAATGTTG
TCCGTCAAATCGGATTTGAGTTGAGCAGGTCAGTTAATATTACTAACTGCGTTTTTATCCTTAAAGTGTTAGTTTATTAATCAATTTTGATATATTC
ATTCAAAAATACAGCCAAAATTAAATTAACACATATACCTGACAACATTTTTAAGTGATTAAAATGTATATTTTCAATTTTCACTTTTACCATTCAC
ACCACCAAAAAAGCCATCACAGAGCTGCTAACTTACTTGAAATATCCTTCAAATTCCTTTAAATCCTTTTCCAAAGGCAGTTTAAACTTTTATGTGC
CTGTGTTTCCCCAAATTGCAGTTAAGTAATCACAAAAATGCCAACTTGTTTTCGGAACACAAAAGAAGTGCTCACATATTTATTTATATTTGGTTGT
CTGCAGTGAAAAGCGAGTCCTGATGCGCCGCCCTCGCTGAGAAAACTCACTCAAAAGCGGCCCAAGCGTGCGAGCGAGAGCGCAGCGCTGCTGGACG
GCGATTGGCTGTTTCCGGCAGAGGAAACTCACTCAAAACTCGCATGGCGACGACGTCAGCTTTGCGATCGAGAATCCAGCGATGAGCGCTTTTCGAC
CAAGTCGAATCAGTTGA

-1171 to +50 (1221bp) Composite Enhancer in Promoterless Vector

AAATATTTGGATATGTGGGGGAAAGGGAGTGCCCCGGGCTACGGTGGGGGGGGGGGGGGGTTCTTTGGTGCGGGGGCTGGTGTGTTGTTAAGCCTAA
CTGTTACTGTCGCAATTCATTGAATTTGCAGGGCTAATTAAACACGTTAACAACTGTCGCGATGCGCTGAGCCGTGCAGGGATAACTTGCTCCAAGA
TCGTTGTCGTCGTCGTCGTTCAGACGCCAGTCGACAAAGAAAAAACACAAAGAGGCAGCAAAAGAGGAGACGAAACTGGCCGTATGTCTCCTAGTCT

GCCCTGTGATTTTTGGCTAAAGACCAGCGGCTTGGAGCTGTCCGCAATATCCCGAAATTGGTCAGACTAATGCGAGTCGACATTTCGCCTGGCGCCC
AATCAAGTGTTGCCAAATTGGGTTAGCCGAGGGTCCAACTAAAAAAAAAAAAAGAGGAGACCGAGACCCAGAACCGTTCGTGGAAGGGTCCCGAAATA
AGGCTTCCAGGAAGCCCTAGCACCAAACACACGGCGATGCCAACTTGCTGTGGAGATCTTCGAAACTAAATCGTATCGGAAATATTCGAAAATGTTG
TCCGTCAAATCGGATTTGAGTTGAGCAGGTCAGTTAATATTACTAACTGCGTTTTTATCCTTAAAGTGTTAGTTTATTAATCAATTTTGATATATTC
ATTCAAAAATACAGCCAAAATTAAATTAACACATATACCTGACAACATTTTTAAGTGATTAAAATGTATATTTTCAATTTTCACTTTTACCATTCAC
ACCACCAAAAAAGCCATCACAGAGCTGCTAACTTACTTGAAATATCCTTCAAATTCCTTTAAATCCTTTTCCAAAGGCAGTTTAAACTTTTATGTGC
CTGTGTTTCCCCAAATTGCAGTTAAGTAATCACAAAAATGCCAACTTGTTTTCGGAACACAAAAGAAGTGCTCACATATTTATTTATATTTGGTTGT
CTGCAGTGAAAAGCGAGTCCTGATGCGCCGCCCTCGCTGAGAAAACTCACTCAAAAGCGGCCCAAGCGTGCGAGCGAGAGCGCAGCGCTGCTGGACG
GCGATTGGCTGTTTCCGGCAGAGGAAACTCACTCAAAACTCGCATGGCGACGACGTCAGCTTTGCGATCGAGAATCCAGCGATGAGCGCTTTTCGAC
CAAGTCGAATCAGTTGACACGCAGCTTTATGTGACATTCGTGGCGAAAGCGGACCAC

+529 to +4272 (3744bp) Intron 1-1

GTAAGTTGAAAGATCTCAATTAGCTAACCGAATATCTGTGGAAGTTTTAGTATGTTGGGTTTTGAATGGATGTATATCTCATGTATTTACGGCAGCT
ACAAATTCCTGGACCACACGCATATTGCATAACTCGCACAAAGTATATTTCACCTCAAATTAAAACCCGAAGAAAGAAGCAAAATCCTAGTCAATTC
CTAGAGCTATTCAAACCTGACTCCTGGTGCTCTCAATCATATTTTCCACATCAAGTGCGCATAATTGCTATCCTTTAATGCGTTCCTCTAGCTCCGA
AATGGCCAAAATGGTAGCAGTTGATCGTGAGAGATAAGCTCACTGTACAGTGAACTGTAAGAAATCAAAGATGCTACTACGCATTTGCCCAGTGCTG
ATCCTTTAAATGCAGGACACAATGCAGACAGTAGTCAAAAGGGAATTTTCAGCTTAAGTGCGCACAAAGGGCCACAGTCAGATATCCAGATATCCTG
TCGATCGAGAAGGAATCATTTGACCAGAAATAAAACCGCAAAAAGGATCAGTTTGAGAAGGCACTAGGTCAAGGGCTGTAACTCAATGGAAGGTAGA
GATCTTTAGATCGGAATTTCTGCTGAATCCCGCTTTGATTGACAGTTGTACGCTCATTTCCTATCCTTCTCTGCTTCTCTGTTAAGTGAGTTCCATT
CCACATAATCGTGCCCTCGTTGCCAGACAGCTCCCTCACAACTCCGGCGTAACTTGAGCAAACTTTTCGGGCAAAGCAATTTGCGATGTGTTTGTCT
CGTTGCCAAGGCAAACAGAACACGGCTTTTTCCTGCCAGCGGCCATCCAAAATGGCTACCGTCGATGGCGGCCGGAAGGAAGAAGCAGAAGAAGGCA
GAAAGCCAAAAACGTCAGAGATACAAAAGCGTCAACTGCCGCCATTTTTTTTCCGGGTATCTATTTGACAGCATCGGAGACAACACGAAAATCTCAT
AAATGGGAATGCAAAAAAGGACGAGCCATTAGCAAATAATTTCAGCGAAAAACATTTTATTCGGCATTGTTTGGCGAGCTGGAGGGAAAAAGACGGC
TACACACGGTGAGTGAGTGAGAGAGAGAGAGAGAGAGGGAGAGGACAGGCAAATGCCGTGAGGATAATTTCATTGAAATTTGAGTAGTCAGAAAGGA
GCAGCAGAGAATGTACAAAAGGACAACGCCGTGCAGATGCCTTGCGCTTTTCGTTTTGCCATTAAAACAACAAACAATGCAGGCAGGAGCGGGACAG
GATCAGGGGTTTCAACTGGGGGTCCTTCAGCACCTCATCCCCCTCATCACCGTTTCGGGATTTTGCGCTACCCGCAGGACTTCTCGCTCTGCGGGTT
CCCAACGATAGCTAGCATTTCAATTCGTTTCTCGTTTGTGGCCGGGCTGCTCCATTTCAGCCACGCCCTGGGAATGTCCCAAAAATTAAAATTAAAT
GCAAGGGGGTGGCCTATTCGCTTGAAGCTCATCACATTATTTCCCCAGGCTCAAATGCCTGGCGACATTTTTACAAAATAATCTGTGAATCTGTGAG
TCCAGGCATTACATCTCTCATCTCCCAGCTCTTAATCCGCATTGTCCTTCGGCTTAAATGGCAAATGTTTGTCTGGGGCGTGGCACAGGAAGTGCAA
CCATCTCTGTCTGGAAGGGATATACATACACCTACATACCTGTTCCCGTTCGAAGTCGAGGAATTTATTTGGGTTTCTGCCACTTCAACAAATGAAC
TTGTTTGTTTGTTTACTCAAAAGTTTCGCCAGCGCTGAGTTGGGCGCGATTTCAGTAGCCATGGTCGAGACAAAGTCAATAAACAAACTTGAAGCTC
GAATTGGAAACTCTTCTTTGGATACTGGCACGAGTTCAATTCGATGATGATCTGCTTGATCATTTCGATTTATTGTACGGGGATTTATGGTGATATA
GAATACTGTAGAAGAATAAGTTTCCTTTTCCAAATCAACTTAGCTATATATAGCTAAGCTATATTATATTATTATTATATTATATTAGCTAT
ATCACTTCCTGTAGTTTTTGTCAAAATTAATTTAAAAACTTGCTCATGCTTATCGCTCGCCTTTCGCCTGACATAATTCCATTGACATCAGCCGTGA
GTCCTTGCTGTGACGTCATATCCGAAGTCTAAACCGCAGAATGTATGGCATAAATTTGCATGCATCATTCTTGAATTACAGCACTGGAAAAAGGGCG
AGAAATGGAGAGGGTAGGAGGAGGAGGAGGCGGTTTATCCCTTAGGCTCCTGCTCGAAGGACCTGCTTTTTGTTCCAGTTTCACCAGAGGCTCGCAT
AATCCGCTCAACTGGCGACGCTGCTTAGTCCTTTTATCCTGTTTTATGTCGCCTGTCAGCAGATGAAGACGTGGAACGGAAAATTAGAGCAACCTGC
CTGATGGATGGATAAATGTCCCTTCCTTTCCGCTGGATTCCGATCCTAATGCCCTCTAATGATTACAAATATTTGTACCTTGCTGTGGCCATTTTAA
GAGGGATTTGCTTTGTCTGCTCTCTCCAGCCTTGTGACTCATTGTTGTCTCCTGGTCTAAATTTGAATGGTGGCAGATACAGAAATAGCCCAGTCAA
ATGCGAAACGTCTGTACGCAATCAATTGTCACTTTCGACAGCATATTTTGAGCCAACGTGCGTCTATAGATAGCCATCACTACACTAAATATAGTGC
CCAACTCTTTCCTGGCCACCAATTTGGTGAATAATTTGGAATAGATCACCAAAACATTGACAGTGGGGCAACATCTAATGGTTGTCAATTAGAGCTA
AACATCATTGTTGAATAAGTAAAATGAATTACAAGGGGATTTGCCAATAAAAACGGTTTAGCTTAACTTTAAACTATGACAAACTATTTGTCTCAAA
TCCCCCTTTTCAAATTCACAGCTTACTTTTGAGAAGCTTCTTGAAAGCGTCTTTCAGCCCGTTTGTGGCTAAATCGAGAAGTATTATTCGTAGAACC
ACCATGTGATGGAGCAATACACCTCAGTAGCGACACGGACACGCATCTGTCACATCAAAAGCCGCGGGCATCTTACAACGCTCCGGTAATTGGTGGG
GCCGGATCCGGGTCTGAGTCTTTTTCCGTGGCTGCCTTCGCTTACAGGAATTCTTGGTAAAATCGAAGGGAAAAATAGATGCGAACGGGAGCCAAAC
AAATGAGCGAAAGTGCGACGAAATGAACTTGTCATAATTATTTGACAGTCAGGGTAAGTGGGATGCTGACTCTGCCCAGCGGCACATTAACCAAAAA
TTGATGTAAAACATTTTGCCGATGGGAAAGGGGTGCCATCGCCATTGGCATCGGCATCGGATTCGGTTCACTTTGATTCCACGTTTCGGTGTCACTG
CCAGCGGGTTGCGGGGTCAAGTGGTCGCAGCCTGTGAAAACAAAACTTGCGCCTCATTTCCGGTTCAATCAAGTGGCAGACAGCTTGGAGCATGATA
AGACTCCTGCCGGCGACTGTGACTCTCTGCGCCCGGTTTACTTAGGTGTGGCTGTTGTCAGTCAAAGGCGCAGACAGCCAGCTGCCCTCCTTGTAAC
CCCATCCCATTCCAAGCGATCCCATCCCACCCAAAGCCCCTACCAATTAAGCGGTTTTTTCCGAGACAAATTTGTGCGACCTTTGACTTTACGGAGC
GAAATGAGAGGAACGGGGATAGCATTACTCGTTAGCAGTCGTGACAGTTTTTCTTAGA

+3957 to +7672 (3698bp) Intron 1-2

GTGAAAACAAAACTTGCGCCTCATTTCCGGTTCAATCAAGTGGCAGACAGCTTGGAGCATGATAAGACTCCTGCCGGCGACTGTGACTCTCCGCGCC
CGGTTTACTTAGGTGTGGCTGTTGTCAGTCAAAGGCGCAGACAGCCAGCTGCCCTCCTTGTAACCCCATCCCATTCCAAGCGATCCCATCCCACCCA
AAGCCCCTACCAATTAAGCGGTTTTTTCCGAGACAAATTTGTGCGACCTTTGACTTTACGGAGCGAAATGAGAGGAACGGGGATAGCATTACTCGTT
AGCAGTCGTGACAGTTTTTCTTAGATTTTTTCATAATTTTACCACGAATTTTTTCCTCGCCTGGTCTCGTCCCCAGCAATTTTCCAGGCAGTCTCAC
ACAAAAAAAAAAAAAATATGAAAAAAAAATATCAGATTTCCTCGTTGCACATTTTTTCCATCCATTCTTCGGGGCTTGGGAAAGTGCAGCAGCAGTAG
CAGCCTCCGAAATCCGGACAATTGGCAGCCAAAATGCCAACAAACAAATCATTCACATTTCGTCCATTGATTGGCGAGGCGGTAAAGCGAAATTCGA
TATTCGGGATCGTCTGGATGGTCCGGAGGGAGGGAGGAGAGAGGTGGTAGATGAAAGTGCTGGCAGGGATGCAGCGGCAAGGGTCCAGGGGCTTAGA
TCCCGGCACCATCCTCCGATTTCCATAGGGTTTCCGCACCGATTCCGGTTCGATTCCCAGTGACGAGCGCACCTGTTCCTCCACCGTCGCGAAAGTT
GTCCCATCAACAGTTGGTCGCACAATTCAGCTTTACGCTCTTCCAACCAAACGGGTAATACTATACGTATTTCCCTCAATTCGGTCCGGCCTTGCCG
CTCTATTTTCGACGTTATTAAGTTTAACGGAAATAATCAACTATTTGCCATTTTTTATACCCATTTATAATAGTTAGAATTTCCACAATTGTCGAAC
GGCTGCCGCGCAAAAGTTACAATAAATGTGGCCAAGGTCTGAGTGATGAAAATGATACGCGGCAACTTTAGGGCTGCCACATATGGTGTAAGTGTAA
CTGGTAGTTCAGCAGGGTATTCGGTTGCCGTTTACCATTTTACCAGATACCAGTTGCCCAAGTCCAAGTGTTGCACAGTTGGCACAGTTTGCGGTGC
GCCATCAGCCGCAGTGTGGAATCTCTGCCTTAAACTCGGTAGATTCATCGCAGAATTAACTTAAAGATTATTTTATTAAGGGATGAAATAGAAAGGC
TAACAATACTGAGAAAAAAAAAGAGTTATTCATTTATTTTCCCAAAAGTACCCTGTAATCCGAAAGACATCGTTAGCGCTCGCCCAATCTCAACTCAA
CTTTATAATTTACAATACTGTCTTTCCTTCAACTTAATTATTACAAGAATGAAAGGGTTGAAGCGCAACTCAAAGGGTTAACAAGCAACTTCTTCAG
CAGATAAACTCAAAGGGTTAGCAAGGCGAACTTCTTTAAGGGTTGTTCTTCGCCTAGCAATCAAAAGTTTTTAATTAACAAACAATGCAACCGATTT
TCCGAAAAAGTAGTGTAAATAATTTGCAATGATTTTTTAACCCAAAAGGAAGTTTTCATTGAACCCGATCCGTGACATCTTGAGAATAGGTCAACAT

TGTTGTTTAATTAGAAGACAATAGCTGTCAATAGCTTATTCCGGACAGTCAGGATTCCGGCTCACCATGAAGGGAGTTGGGCCGGAGTCAAAGGTTG
TTGGCTAATTGCAAGGCGGGGTTCTTGTTCTTGCTTTTTTTTTCGTTTGGCGAGGGGTTGGCGAATGTACTGGCTGGTACCAACGGCAGGACAGCCA
GCTGTGGAAAAATCTTATCCACACTCGATCTTAATGACTACTTAAACAGCGACAAAGCCAACGCCCAACCCCGCTCAACCCCCGGGTTGCAACCCCC
TGTTCCGGGATCCAGATCGGCTCAAGTGCGGCACTTGAGGCAGCTGTTTGGCACTCGGGATGACTTTAATTTAAGCCCTGGGGTGCCATATATATGG
AAACCTCAACATTAATAAGTGTTAATAATTGTGCGTAAGCGTGTGTGTGTGTTTTTTTTTCCAACTGCGTTGACACGCCCCCAACCGCCCGAAAG
CAAGTCTATAATTTCACATCACTTTCGCCACTGTTTTTGTGGGGGAGTGATGGGCGGCTGGTTGGGAGGACAGAACCGAGCCGGCGAACTGAGACCG
AGTTAGAAAGTCCGTCCAGAGGAGCGTAACATGGATAGGGCATGGGTATTGGATTACCAGCGTCCCATGGCATTCGCATCCACCTCCGTGTCGGGCG
GCGTCGTCCTCCTCCTCCTGCTGACTCCGGAATCCGGATGGTTATGGCAACGGACGGATCAGCAACCGAAACAGCATCCCTGGGGGTCTCCAATGAT
TTGTTGTTGCCCGCGGACAAGTTTACAAATTCAATTTGTCAGCGATGCCTCAATGTTGTTGTTTTCCGGACGGGGCGAGTGGTTGCAAGCACCATTT
CATAGGCCTGGCAACGGTTAACCCAAGAAACAACGCAGCCAAATTGGCGGAAAGTGCGAAGGGCGTCGACTACAGCATACCCAGTAAGCTGGATTCT
GTGATCCCTAGGGCATCATACAAAAGACGAACTTATCTAGTACATAAATAAAAGATTTAAGAACGCATTTGATTTAATTTGAGAGTTTCAGAAGATT
ATCATATACCCTGGAGCTTACTAACAATACTTTTTTAGTTTATAATTTATAATTCAATTCAATATATCAACAGGAAGAAATCTGTCACTACTTATCT
GCCTTGGGTACCATTGTAAAATGCTAGCGATTTTGTGCTGGCATTCCAAAGCCACCCCTAGTCGAGCACACCCTCTTACCCGATACCCTGTGTTACC
CACCCGGTAAAAGCATATGTTTCCATTGCATACTTGAGGGCGCATTTGATTAGAGCCCACCGAGGCGTGAGTATTTAATTTTGTTGTTCGTTGTTGG
GTCGCTGCGCGTTTTGACACGCGTTAGTCGAGAGCACGTAATTAAATTAATTAGAGAGCCGTTCCCACAGGTAAACCTCCACATCCACCCACTCACC
CATCCAACACAATTCGCTTTGGTCCAATCCAATCCATTCTGCCACCATTCTGCTGTTCTGTAGTTCTGCCGTTCTGCGGCAGTTTTGATGCTCATTC
GCAGTGACAGGCGACACACTTCGCTCGGTGGGTGGCCCAGTCGGCGGCAGGTTGATGGGTGGTTGGCTGGGTGGCGTTGTGCGCCGGTTGCCAGGAG
AACACACACATAGAAGCTGCTCGGCTTTGGGCTTCGGCTTTACCTTTTAATGAAATTCCTAACCAATGTTTGCTTCGCCTCGGTCACTATGGCGATT
CACATCCTTTCTCCACCTCCTCCTGACCCCCATCAGATGTGCATACTTATGTACATATACGTATCAGTCGGAGATCGGCACGTGCCTGGAACTGAAA
CACAGGTTCCGCATAATTTTTCCCAAGAATGAAAGCATAAACGAACCGTTTCTCGCCGACCCTGGTGGCCATAATAATCGGCTCAATCATAATGAAC
TGGATGCCTCATTCTGGTGCAAGTGCAATTCCCGACTCAGTTTATTTTTGTATTCATTGTTTTTTTGTTTTGCTTTTTATCGGGTGTATCAAGACCC
AGCCAAACGCCC

+7330 to +11076 (3747bp) Enhancer 3 Large Fragment

TTTGCTTCGCCTCGGTCACTATGGCGATTCACATCCTACTCCGTTCCATTCTCCACCTCCTCCTGACCCCCATCAGATGTGCATACTTATGTACATA
TACGTATCAGTCGGAGATCGGCACGTGCCTGGAACTGAAACACAGGTTCCGCATAATTTTTCCCAAGAATGAAAGCATAAACGAACCGTTTCTCGCC
GACCCTGGTGGCCATAATAATCGGCTCAATCATAATGAACTGGATGCCTCATTCTGGTGCAAGTGCAATTCCCGACTCGGTTTATTTTTGTATTCAT
TGTTTTTTTGTTTTGCTTTTTATCGGGTGTATCAAGACCCAGCCAAACGCCCACATACTCGTAGACCACTGACCAAGTCTTTGTTTAGCTTTGCCAT
CCGATCGACGGCTCCCTCTGGCCTTGTTGATTTATAAAATCCAAGTTTATGTTCATATTTTTTATAGAGCCAGCACAGTAGTTCGTTTTAATGATCT
TCGACCCATAAAATGGCCTGTCAAAATTATATATTCGGCTAATGCGCCTTGTGCTCAGTTGTATAGGAAACACGATTTTTGTGTGATTTACGATCGA
TTTGAGGCGAGTCGATTCGATTGATATGGGATCCCTGCTGCAACAGCTGATCGTCTGGAGTTACCCTATAAATATTTGTACAAGTGGGAAATGTGTT
TTCCATAGGAAATGCAATACCTTCAGATTGGCTGTTGACTTTTCCATTTATTTCGCAAGTTTCTGTGGAAATAAACGAGTGACAAGCGGACCAAGGA
AAGTTCAGTGCGCTTTTGTCTATGAAGCGTTTTAATTACCAAGCCGTTTCATTCAAGATTTTTAGGAATTGAAATCCCATGTGCAGTTCCCCTTCGG
AAGACCAGCTACAAAACGAAAAAACCCCAATCCAGAAATCTGCATACCAAACCTCTTCTGGGCATTACTTCATGCAAATATCGCTGCAATTTTTAGC
TCCATGGCCTGCGCTTTTTATCGTTTTGTTCTCTATTTTATAATATATGCGGTCAGATCTCCATGGCTCAGCAACATTTTTTTCGAGGGGCAGAACG
ATGAATGCCTCAGACGCTTGGCATGTGCTGACAAATGTGAAACTTCCCTAATCAGCATGGCATGGAAGAACTGACCCAATTCGTGGGCTCGCCAATC
GAATGACGCATTCCTCGACGACTTTTGAACCGGAGAACCTGAGCTGCGTCGCGAAGGGGGTGGAGGGGCAGGCCACACTGGGCATCCAACCAAATGA
CAACGGACAAGCAATTCAATGTCCCAATGCTGGCGTAGCCAAATCCAAGTCCTTATCTAGATGTCCGGCGAACAGTCGCCCAGATCAAGTTGTAAGA
ATGCGAACATGGCAACAAATGTGCTCGACTCAGGTGTTAAAACTTTTGCATTAAAATGGCGCCCAACGCGGAACGGACACAGGCCTCTCGATCCCAA
ACCATGTGGCCCCCACTTCCTTTGGCTGTGTAAAATTAATACTACACTCGGGGAGGTCCAGCCCGATCAAAACTGAACGTAAATCTTAAACACTTTC
GAGTTCTACCCTGCCCCCGTGCGATTCTCTGATTCTCCGATTCACCGACTCCCTGATTCTCCATTGTGCAGCAGGCTTTTGCAGTCGCACGATCAGC
ACGTTCAGTTCCGAGGGGATCTGCTGCTTCAAGGGGGAAACTGGGATGCTGGATGGTGGATGGTGGATGGTCGACGATCGGCAACCGGTCCACGACA
AATGTGCCAGTCTCAGCAACAAGCCAGGCCGCAGAAATATCTGCAAATGCAGCGAATTGTGCGCAGATTTGTTTACAGAAGACTCTCCGAGTGGCAA
ACTGAGGGAAGACGGATTATCGTGGAGGGAGGAGCACCATGATCATCGTAGATATAATTGACGACATGTTGTCTCACGATCGTGCTAAAGCGATTAA
AGCTAATTTAATGCCCGACTCGGAGATTCACTGCACCCAAAATGTATCCACCAAGAAGTGCACTCCCTCACTTTGAGGTCATGCTCGATTTTCTCTG
TGGAAAGCCTTAACAAAATGCCATAATCAAATTTCTAGCTTCACTTTTGTTATTTCTTGTGGCTGAATTTGTTGTGGGATCGAATGGGCTCATTGTC
GGAATTCCATTGCAATTCTATTGCATGTGTGCATGTCGCCTATTTACTTAAATGCACTTGTTTCACTTGCTCACTTGTAATTACATCCAGGCTTTTA
AGTCAGTCTCTGTTGGGCCAAAAATCAAGTGTTGAATCAACATGAATTGTTTAGCACACGATTCAATTGTTTCGTCTCGACGGAGACGTATAAATAA
ATAAATACGAGACGGCCATGAAATATATATTTATTAGAATAAAAAATGTTAACCGCTATCGGTTTATGACAACTGTTTGTTTAATTGTAAAATATAT
ATTCAGGAGAGGTTTAAAAGATATTTTACAAGTTGCCTACCTTAAAGCTTAACTCTTTTACTAGAATTTCATTTGGATGAAGTTTCAACACACTTTA
AAATTTATGTGCTCAGTAATTTGCCAGAGCTGCCCCAATCAACATCAATTGGCTGCCATACTGTCTGAGCATTCTAATTCATTTAATCGAGCTCATT
AGTGGCTCTAAACCATCATGTTTATGCTACCCAATTACCATCGGAAGTGATTCACTTCTGCATGGACGGAGAGATAGCCCTGTGATTTTGATTAGAT
GCCAATTTGTTTATGGCACTCACTAATCCGTCCACAGATCGGATATCCCATATACCATATACCATTTGCCATATTCCATATACCATGTCCCGTATCG
GTTTGATTATGCCCAGCACACTTCGGCTCGTCTTACATGAGCATTTCGATTTTTGGGAGCTCCTTCTCTAATGCGTTACGGATCCATCGAACCCAAT
AAGTTTTAGGCGTTTTAAATTACCCGATATTCGCGTTGCGCGTTTTACGATTGCCATTAAATTTGCTGGCGGTTACCATTGAACAGGCCGAGAAACT
CCAACTGATTAGCTTATTAATTTGTTTTATGTGCTCGAATGGTGGCGGAGTTGTTTCGAATTAATTTATTAATTTATGCGCATAGGAAAACCAACTT
TTCAGTTGGCGTTCGCCCAGCGGCAAAATCTCATTCACAATGGGCATTGTTCGCCCGCATCCGAGAGATACTTACCAAAAAAAAAAACTAACATAAT
ACAGAGAAAGAAACAACAAACTTTGAGGAAAAGTGGTTTTCGACCCACCCCTGTGCGATATTCTTGGCCCTTCGATTTGGGGAATGGGAATGGGCGG
AGTCTAGGCGCATTCTCTGGCCGGCGGAGGGAGCGAGAGAGGCTGCTCCGAGTGCGCACCGCTCACACGAACTCGTTTCGAGTGCCGAGATACATTT
AGCCGGTACGAATACGAATCCAAATAATCCGAGCCAGGGATTTCCACTCAAGCAGCGCCGCTGCCGCTTCGCTGCCGGCGTCGCATTGAGCCACAAA
AGTCGGCTGTTTCGGTGGTTCAGTCGATTCGAGCCACTCAAAGCGAGCGCTACGGGAACGGTCGATCCGCCCGAAGTCGCAGATAAAAAACCTACCA
GATACATTTCGTTCGTTCTGAAACGCTATAACTAAATATATATTCGATTTCAAAACATCGACCATACATTAACTACCTGAAACGGTCGAGTTCACTA
CCCCGCCACGCGTGTGTGTTTTTGTGTGTGTTGCAAGTGAAAGTAATCGCAAGTCCACAGA

+10576 to +11076 (500bp) Enhancer 3 Minimal Fragment

CACCCCTGTGCGATATACTTGGCCCTTCGATTTGGGGAATGGGAATGGGCGGAGTCTAGGCGCATTCTCTGGCCGGCGGAGGGAGCGAGAGAGGCTG
CTCCGAGTGCGCACCGCTCACACGAACTCGTTTCGAGTGCCGAGATACATTTAGCCGGTACGAATACGAATCCAAATAATCCGAGCCAGGGATTTCC
ACTCAAGCAGCGCCGCTGCCGCTTCGCTGCCGGCGTCGCATTGAGCCACAAAAGTCGGCTGTTTCGGTGGTTCAGTCGATTCGAGCTACTCAAAGCG
AGCGCTACGGGAACGGTCGATCCGCCCGAAGTCGCAGATAAAAAACCTACCAGATACATTTCGTTCGTTCTGAAACGCTATAACTAAATATATATTC

GATTTCAAAACATCGACTATACATTAACTACCTGAAACGGTCGAGTTCACTACCCCGCCACGCGTGTGTGTTTTTGTGTGTGTTGCAAGTGAAAGTA
ATCGCAAGTCCACAGG

+11149 to 14024 (2872bp) Intron 1-4

GTAATCACATAGTCGTAGTGCTCTCCTCGCGAAGCTTTAAAAGTGATGTGGTTGAGACGGCTGTGCCGTCGGTTATTACTATTACTAGTATTGCTAG
TGTTATGACTATGATGACGGCGGTAGCTTCCTTGGTGGTTGCGCCTTGTGGGGCTTCACCTAGTCGGGGAGTAGTATCCAAAAAGTGAAACTCCATG
GCGAGATAACGCTTCGACTCTCATTTATCAAGCCTGGATGGAGTCTAATATATGTACGAACAACAGTTTAGGATGCTTTAAGCTGATCTATTGGCCG
CCGTGATATCATAGCACACTTCATATATAAATCTAGTCCAGCTTGACAACTAAGTCGTGTTCAGATGCTATTCGATTTCATAAATCTAAGCGAATAA
ATCGTGCAAATACACTCGAAGAAATACAATTTCATTGGGTTGCTTGAAAATGTATGGAACGTTACTCATTCACAGAGGATTATCAATTTTATAGACC
CATCCTGCGAAGAAAAGCGCTTTAATGACTGCTCATTGTTGGGAAATCGTTAATGGGGATAAAGATTATGGGCACCTGACCAAAATTTTATTACAAC
GCATTAATCGGCTTAACTTTTGGCTGTGGGGTAATGAAGCAAACAAGTTGAGTCCCAAAAGGTCATTAAAAACGCTTAATAAAGTGCCGAAATAGTG
ACAAACGTTTTTCCAATTCGCTGCTGATGCATTTCTCCCATCAAATTACCAAAGCCTTTTCATTCACTGCACGCTTGCGATGCAAAGTCTGGCCGAG
ATTAGCGTAAAGTTCGTTTCCCGACGATTTAATGGAACGGCATTCTCCAGGCTTTTATGGGTCCCTAAACTACGGCTAAGACAAAGTCGGATCGAAG
GAAACGTGACGAACGTGGAGTGGCCGGATGGCCGGATGGTTAAGGCGAAATATTAATAGAGCATAAATTACAGCTCTAGTGGGTCTCTGGGTGCCGG
CTTTATGGGAATTTAAAGAGCCTGGCCCACAAAAGCCAGAGCTGGGCTACGGCATTCGTCCAGCGGCATTAATCACATTTTAATTAAGTTTAAGCCG
TAATCGTAAAAATTAACACGCCATAATTCGACTGCGACAATACGCGCTGCATGTAATTTATGACAAAGAGAATTCACATCGGTGTGCGTGTGTGCGA
GTGTGTGTGGGGGGGGGGGGGGCGGTGGAGGAGTCGAAATATTGATTATGGCCACTGCGATTGACACTTGGCGATTGTTGATTATACTACCACGATC
GTGGCCCAAAACGTAATTAACGCGCCAAAGCGTTAAGGTGCATGGGATAGGTCCCATGCCATAGCAGCCCCTTCCTTCGATTCCACTTCGTCCACCA
GAAGATACAAATTTTCCTCTTGTTTATTTTGATTTTTATCGCGGGGACTCGAGGGGGACTCAAGGGGTTTGTAGGGGTCTTCGGGGTCTTAGGGCCG
GGTTAATAAAAATTTGTCGCCGTCTTCTTGTCTTGTCTTTTGTTTGCCTGCCTTTTTGTGACCGAGTGTGTGTTTTAATCTTCCTCTAAAGCAGC
AGAAGAGACAAAGAGATTACGATCACAGGAATTTCGTTAAAGATGCCCACAAACAGGTCTTTATACCACATATCTCCCACTCTTTTCCGCAGCTGGA
ACCAACCAAGCCGGCCCAACCAAAACCCCCCCAGATACTGATTCGAGTGTTGTCTGTGTTAATGTTTACGTTGTCAGCTTGTGCCATAAATTAGTTT
AGTAAAAGGTTGCATTTGACTCTTCCCTTTCCCCCCCCCCCCCTTTTTTTTGTTGGCCCCTCACCAGCTCACTTTTGCATACAACTTCGGACTCGAA
TTCGGTTGCTCGTGCAGCACGCAATCCTGCAGAATTCGCGACCCGAGATCGCAACTCCAATGCGCAGCTCATCGAAACGCTACCGTTCGGCAATCTG
TCCGCTTGTCCGCCGCTGCGCATGCGCGTGTTCCCTTGGTCCGTCGACAAATCTGAGCAAACTGCGTCCTGCTGCCCCCCACCAGATCACCGGATGA
TGGACAGTGCGTGTGTGTGGTCATCTCGCCGGACGGCAGAAGCTGTCAACCGAAGCCGCTCAGCTTTCGCTCCCTTCCCGCCCTTCTTTTTTTGTTT
TTTTTTTTGTTTTGAGGGACTTCTTTAGGGGCGGAGAGGCGCACAAATTCCAGCACCTGGGCTTGCCGCGCCCCTTAGTCCGCCTTCGATTTATCT
GGCTTCCGTTCGATTTGCATACATGTCTTCTTAAGGAGCGTTTTTTTTTTGACCATTTGTCAAAATCATTCTGGCAAAAGCTGAATTGTTAAAGCTT
TATTTTTATAAAACCTAGTAAGTGGATGTAAAGGACGTTCTATTTTATGCCATATCTAGAGACACAATCTTTCCTCGAATGTCTGTATACTTAAATG
TCATCTTTGTTCCATCTAGCCATTTTGCATCCTTATCGAAATCCGCTGCCACCTGCTGCTTTTCCGGGCACTACCACCTCCCCCCCCCCTTTCCGAC
TTCCCCTCCAAATGGCGCCGCACATCCGAGTAACAGTTGAGTTAAACTTTTTCCCACGCACAAGCTCGGGCAGCGAAAATCGCTTGGCGCAGCAGCA
AATGGCGATTGCGAATTATGTAAAATTTGCTGTTTTCTTTCGCCACTCGCACTGGATAACCCAAATAGAGTTTCAGGCGGTGGAAGTGCCGAGCTCA
GCAGGGCGATTCCACGCCAGACGCTGAGGTGTGAGTGCGTCCGCCTTGTTTATAAACAAATTCTTTCCAGGGCCGGCGAAAATCCAAAAAAAATCAC
AAAAATTAACATTCAGTATAAGTATATATTTTAATGTAATTTTCTTCGCTTTTTTTCAG

+14072 to +16647 (2576bp) Intron 2

GTAGGTTCAAATAAAATAAAATATATATAAATATACTTATTCATAAACATGTAATTTAGGTACTTTTATGAAATAGATTTCTTAAAAGTGTAATATG
TTCTAACTAAAACACATATAGGGGAAATAATAGTTTGCATATATTTATAGGTTGAAACCTAAATTATGAGTCTTTTACCAACTTGCTTCCCAGGATC
CTGAAGAAAAAGGTTTCCCTCTCTGTAAGCGTAGACAATTTGTAGCAGAACGGCGAGAACATCCTAACACTTGACAAGAGGCTCACCATTTTCAATT
GGTTTCGATTGAAAAGTGGCCATGGTCGGATCGTCGTAAGGGAAGGGAAGTGCACATTTTGCATGTGGTCCACACAACCTGCCACATGCCCCGGCAG
AAATTCAAGGAATTCGGTGCACGCTTCCGCTGCGACACTGAAGCGAACCCAAGACCGAAATCCAAAATCCAAAAACCGAAATCCGAAAAACAAAAAG
AACCGAAAAGTGTCAGGGCACTTAACACTTGCCAAGGGGCATGGTGGACATCGTAGGGACACGAGGCGGTGCAGGGCCAACTACTTAAAAGAGGCTT
AAAGGCGGCAACAGTTGCGGCTTAGTGCTAAAGACCTCTCAACCTCCCTCTTCGATAATTTCTATTATAATATTCGTAAATCTCCCATTGGTCAGCC
CATATTGTGAGGAGAGCAGATCTCAAAGCCAAAGTTTGGGTTGGGTTTCCTCCCTCCATTTGGCGCACGCGTCGTTCTGCGCTGGGAAAATGATTTT
CCCCCTTTCACCAGCTGCTCCCCTTTTACCATTTTCCCTCTTGTTGTGGCTGCCAGCAAGATAAATGTGGCCCCTTTCCAGCCGAGCGAAAGAATCT
CAAGGTGTCAGATTCCTTTGGAAATTGGGCACTTAATTTACCTTCCTATTAAAATTATGAAAAATTGTTAAATATTTTCCAAGCCTTATGGGGGGAT
GGGGGGAAATCGTAGGCGGAAAAAGTGGAAATATGGTATACGGTATAGTCGAAGGAAGAAAGTGAGGCAGATAAATCATTTGAGTAGAGAGTAATTT
AAAATAATTATCCTCCATAGGGAAATAACGCGGTGTTTAAATGATTTTATCTTGCTACTTTAAGATAGAAAATATGGGATTTAATTTGCCAGCTGAT
TGTAAAAAACTCATCTTAATTGCATCGAAAAGGATTGAATTTCTCCCCCAATTTGTCTCCATTTTTCCCCCAAAATATCGAAAAGCCTTTTCTTTGT
TTTCATTTTCCCGTAGCTCTGATTTATTTGACTTTCGACTGCTGCTCAGTTTTATTTGATTTTTAGTGAGCCCTCGTAGATTTTCCAATTTGTCCAC
TTTAATAATGTCCTACTCGAAAAGCAATAACATCAGAGTAACAGAACAGAAAAAAAAACATCAAAACACAAATCGTTAAATATATGTATATAAAAGA
AATATTTGTCGCTCAACATTTGCTGCACACATGGCCATGGCAAGGGAATGGGGGGGGGGATGGGTCAGGACTTGTCCGGGACACTCCGCACATGCCA
CCAAAAGGCGGACCCAGCGATCCGCTCAAGTGCCCCGCACCGATTCCAAGCGATTCCTCTTCGAGATCCCAGTAAACAACCCGAACAAATCCAGCAA
CAGGAAGAGGGAAAGAGAACGGCCAGATCGTAGAAAAATATTTATAACACTTGACAAGATTTGGAAGACCTCTTCGCTCGGGTCTTCGACGGGGAAG
CACTTGACTTGGTCCAAGTGGCCCGAAGGGGATCGGGGAATGGGCAACCGAGAGCAGAACGACTACGTGCCGTTAATTTAATGGTTGTTTAAAGATT
ATTGGAAACTATTTTATGTGTTTCCTTAACGAGCAAAAGGTTCTGTGTTTCGGTTCTCCTCCACACAAAGAAAAAATCCTCATGTGTGTTTTGTGTA
CTATTTTATACTCAATCCTCAGTCGGCCTATTAATAATTACAAATCGTCTTGAAGTCGCTTGAAATTCATCAGTTTCCAATATTGAAGATATAATTA
CATATTTCTAGCTTTATTTTAGAGTATTAAAAGGGAATCATAATTTAATAATTTGTAATTTAATAACTAGTTCGCTTCGGGCTTTAGCTATTTATAA
GCACAATTAAGCTGTAAGTACACGTTTTATTAAACAAATGAGCCTAAAATAAATACTTTGATTTAGCCGCCACCTTTTTGATGGCATATATAAATTA
AATTAACCGGTTTTAATATAAATACCTCGATTGATATAATGCAGTCCCAGTGACTCGGTTATTACATTAGTCATGTTCGCCGCCTAAGGATATATTT
CATTTGCTAAGAACTCGTTTTTAAATATTCATAAGCATAAATTGTAGAAATTATATAGTCAAGTTCGATTTAAATATCAAATGTGACATTACAATTT
AAGTATTTCAGCTTTTGTTATTTGTGAATGAATTGTTTACATTTAAAACGGCTTAAAGGTCTGTGTTTCATTGTATATTCCCACACTTGACACCACC
ACCCCATTAATTGGCTCACCCACTTATGACGCCTCTCATCTTATCTTCTTGCAG

+16648 to +18402 (1749bp) Exon 3

CAATCTGTCACAGCAGCAGCAGCAACAGCAACCCCAGCAGCAACAGACGCATCAGCAGCAACAACAGCAGCAGCAGCAATCCCATCAGCAATCCCAT
TCCAGCACCGTGTTGGCCAGCAATGGACCCAGTAGCGCCGGTGCCGGCATGGGTGTCGGTGTGGGCGGAGGCGGTGGCAGTGGAGGAGGAGTAGGAG
GCGGAGTTGGCCAGTGCAGTCCGCTGGGACTGCCGCCGCAGAGCCAGCCGCTCCAGCCGACAATAGGATCGCTGGCCTCGCTGAGCGGTCACTACTC
GAACGGTAATGCCAATCCGAATGTGAACTCGAGCAGCTGCAGTCTGGCCACAGCATCCAGTTTTGCGCAGTCCGCCGGCAGCAGTTTCTCCACATAT

CAACAGGCTGGTGGCACCAGCGGTGGAGTTTCTGGCGAGGATGGCGTGGTGGGCGGAGCAACTGTGATGTCGCACTGGACGCACGATGGCACTGGCT
CGAGTGCAGCGGTCAAGTCGGAGTCCCGCAGCCCGGGCCAAGTGCACGCATCGCTGGACAACGGCTCGGTGGCCGGATCCAATTTGTACGGCTGCAG
CTCGGCCAGCAATCCGCTGGACGGAGGAGCAGTGGCGGTCAACTCTTCGGCAGTGGCAGCGGCAGCAGCAGCGGTCTACGACGGCAAACATGACTAC
TACTACTACAACAGCATGCAGCAGTACACGCCGCCGCCCTTCTACTCCGGATACGGAACTCCTTATGCGGCGGCAACGGCGGCACGGCAGGCCAAGA
TGGAACCCGGAGCGGCAGCTGCGGCGGCTGCCTACTTGACGCCCAGCTATGCCGCCAGCGGCAACAACAACTCGCAGCTGTACAGCAGTCCGTACGC
CGGCTACAACAACTTCGGGCAGCAGGACTACGGCGGCTACTACAACGAGCAGTACGGCAACTATTACAGTCCGGCCAACTACTCACCGTATGCGGTC
AGCTCGCCCAGCTCGAGTGCGAGTCATGGACATGGCTTCCATGTGGCGGCCTCCTCGAATCTCTCCGAGAGTCCCACGGACACCCACTCGACGACGC
CGGTGCACCAGACCACCCACTCGCCGCACTCCCCGCTCCCGATCTCGCCGAGCACTGGCTCCGGCATTGGCCCGCTGGGCAATGTGTCCGCGGCAGC
TGCGGCCGCTGCTCTCAACTCGAGCGGAGGCAGCAGTGTGGGTACCGCCGGCTCTGGGGGCGTGGCAACGAGCAAGACCACGCCCACGGGTAAGACG
GGTCGGGCGCGTGGTAGACGCCATCAGCAGCCCAGCCCCACCAGAAGCACTGCCTCGGACACCGGGAACAGTGAGGCGGTGAAGCCACCGGAGCGGG
TGTTCGTCTGGGATCTGGACGAGACGCTCATCATCTTCCACACGCTGCTGTCGGGCAGCTATGCCAACCGATACACCAAAGACCACAGCTCCCTGAT
GACCATCGCCTTCCGCATGGAGGAGATGGTCTTCAACATGGCCGACACGCATTTCTTCTTCAACGAGATCGAGGAGTGCGACCAGGTGCACATCGAC
GATGTCAGCTCGGACGACAATGGCCAGGACCTGAGCGCCTACAACTTCGCCACGGATGGCTTCCACACGAACACTCCACCAGGCGCCCCGCCCAATC
TCTGCCTGCCCACCGGTGTGAGGGGCGGCGTCGATTGGATGCGCAAGCTGGCCTTCCGCTACCGCAAGATCAAGGACATCTACAATAGCTATCGTGG
AAA

+18403 to +18785 (383bp) Intron 3 + Intron 4 + Intron 4

CTGCGGGAAATGGAAGGGAACAAAACAAAAACTGGCTATATCTCGGATCCATCCACCATCGCCATCCTCAACTCACCGATTTTGTGCGCACTGTAAA
TGTTCTCGATGTTGAAGATGCCGCCCAATCCGAACAGCAGGACCTTGGCCAGCGCCGGGGCCAGTTGCGTGGAGGTTACCAGCACGTTGACGCAGTT
CTCCCGCTGGGAGATCATGCTCAGGCACTTGAGCGCCAGCGTGGCCCAGTTGTCGGTCGCCACCTCGATTTCCGAGCGTATCTGCAGCCAGGCCTCG
CGTTTTCCGGGTCCCAGAAGGGTGCCAACACTGGAAGAACATTCGATCAGTTAGTAACCTATGAATCCGAAAGCGCATCCCCCAATACTCAC

+18933 to +19869 (937bp) Enhancer 4

CCCTCTACACTGCCCTTGACATGGGCTTCTTATGAAAGGCCAAACTGTAAGGGATTCGAAGCGGTTTTGAGTACAAACAGCAAAATGTTTAATTAAT
TTATTAAAATATGTATGTGTGTGTGTGCGTGTGAGACAAGCAACAAATGAAAACTGTAAACCAGCGCAAAATAATTTAATTATTTTGTTTAAACATT
TATCATTTAACGCCAAGACTTTTTGTATTATATAGTTTTTAAACACCTAATCAACGATCGTAACAATTCTCGCACGAAGTTGTTCAAGTGTATAATT
AACAAGTAAATAAATTAACGATATACATACATACGTACGTATTTAGCACCCTAGAGTAGCAAATAATAACAGACCGATACGCATCCTGGCTGGAGAA
GCGGAGCAAACACAACAAAAATTAGTTTAAAGTTCTTAGTTTAAAAGCCGAAGCATAATTATAATGAGTATAAATAATTCGACAAAGCCGTAGTATT
CAAATTTTAAATAACTATTATATAGCTGCATATATTAAACTATATTTAAAATATAAAACCAAGTAATAAAAGAGCAAATCCAACAGCAACGCACTCT
ATTAAAGCATAAGCCTGAGCATTTTTTATTGGGAAGGACTATGAGTAATATGGTCTAAATATGGTGATTTGTTCTTTAATCTTTCTTTGATAACTAT
GTTTTTGCACTAAACGTTTCTTACGTAATGTGTCACATGTTATATAAGAATAAAAAGGAATGGACAATGGAATTAATCCAATTTTGAGTTAAGATAT
TAATATATTCGGATTTAATGATGTGTAATTTTGTAAACTTACAATGTAAAAACCATTCTGTAGAATACGCATCAATGTATAAGTTTATGACATGAAC
TCCAGATGGCGCCCTTGCTGTTTTTACGCAGGCAGATTTAACCATTACTTACATGTACACTACA

319bp Spacer

GAATTCTGAAAGATCTCAATTAGCTAACCGAATATCTGTGGAAGTTTTAGTATGTTGGGTTTTGAATGGATGTATATCTCATGTATTTACGGCAGCT
ACAAATTCCTGGACCACACGCATATTGCATAACTCGCACAAAGTATATTTCACCTCAAATTAAAACCCGAAGAAAGAAGCAAAATCCTAGTCAATTC
CTAGAGCTATTCAAACCTGACTCCTGGTGCTCTCAATCATATTTTCCACATCAAGTGCGCATAATTGCTATCCTTTAATGCGTTCCTCTAGCTCCGA
AATGGCCAAAATGGTAGCAGTTGTCTAGA

S2 Table. A list of primer sequences that were used to clone genomic fragments into vectors containing either a lacZ transcriptional reporter and/or the *eya* RB cDNA isoform. Sequences that are listed in red were unable to drive expression of the lacZ reporter in the retina. Sequences listed in green define *eya* retinal enhancers.

Location: -8714 to -6333, Size: 2379bp, Cloning Type: RED StuI-XbaI, Vector: placZ.attB
5' primer: 5'ATA ATA AGG CCT TGT AAA CAT GTT GGC GAC TCG AAT TC-3'
3' primer: 5'ATA ATA TCT AGA GAT GGCCAT ATA GAC ATT GAC ATT GGG-3'

Location: -6332 to -3831, Size: 2501bp, Cloning Type: RED NotI-KpnI, Vector: placZ.attB
5' primer: 5'-ATA ATA GCG GCC GCA TCG GAA TAG AAA GCG TGT CTT TTA TG-3'
3' primer: 5'-ATA ATA GGT ACC CTT GGC CTG GCT GAT TCC CGA G-3'

Location: -3830 to -897, Size: 2934bp Enhancer 1 Large Fragment, Cloning Type: RED HindIII-KpnI Vector: placZ.attB
5' primer: 5'-ATA ATA AAG CTT ACT ACA CCT CGT ACC AAA TTC TCG G-3'
3' primer: 5'-ATA ATA GGT ACC GGC CAG TTT CGT CTC CTC TTT TGC-3'

Location: -1171 to -897, Size: 275bp, Enhancer 1 Minimal Fragment, Cloning Type: Gateway, Vectors: pglacZ.attB and pg-eyaRB cDNA.attB
5' primer: 5'-AAA TAT TTG GAT ATG TGG GGG AAA GGG-3'
3' primer: 5'-CAG TTT CGT CTC CTC TTT TGC-3'

Location: -896 to -577, Size: 319bp, Enhancer E, Cloning Type RED HindIII-KpnI, Vectors: placZ.attB and p-eyaRB cDNA.attB
5' primer: 5'-ATA ATA AAG CTT CCG TAT GTC TCC TAG TCT GCC CTG TG-3'
3' primer: 5'-ATA ATA GGT ACC TTA ACT GAC CTG CTC AAC TCA AAT CCG-3'

Location: -576 to +10, Size: 586bp, Enhancer 2 Large Fragment, Cloning Type RED HindIII-KpnI, Vector: placZ.attB
5' primer: 5'-ATA ATA AAG CTT ATT TGA GTT GAG CAG GTC AGT TAA TAT TAC-3'
3' primer: 5'-ATA ATA GGT ACC TCA ACT GAT TCG ACT TGG TCG-3'

Location: -576 to +50, Size: 626 Enhancer 2 in Promoterless Vector, Cloning Type: RED HindIII-KpnI and Gateway, Vectors: pglacZ.attB w/o hsp70 promoter
5' primer: 5'-ATA ATA AAG CTT ATT TGA GTT GAG CAG GTC AGT TAA TAT TAC- 3'
5' primer: 5'-ATT TGA GTT GAG CAG GTC AGT TAA TAT-3'
3' primer: 5'-ATA ATA GGT ACC GTG GTC CGC TTT CGC CAC GAA TGT CAC ATA AAG CTG CGT GTC AAC TGA TTC GAC TTG GTC G-3'
3' primer: 5'-GTG GTC CGC TTT CGC CAC GAA TG-3'

Location: -1171 to +10, Size: 1181bp, Composite Enhancer, Cloning Type: Gateway, Vector: pglacZ.attB and pg-eyaRB cDNA.attB
5' primer: 5'-AAA TAT TTG GAT ATG TGG GGG AAA GGG-3'
3' primer: 5'-TCA ACT GAT TCG ACT TGG TCG AAA AGC-3'

Location: -1171 to +50, Size: 1221bp, Composite Enhancer in Promoterless Vector, Cloning Type: RED HindIII-KpnI and Gateway, Vector: pglacZ.attB w/o hsp70 promoter
5' primer: 5'-ATA ATA AAG CTT AAA TAT TTG GAT ATG TGG GGG AAA GGG-3'
5' primer: 5'-AAA TAT TTG GAT ATG TGG GGG AAA GGG-3'

3’ primer: 5’-ATA ATA GGT ACC GTG GTC CGC TTT CGC CAC GAA TGT CAC ATA AAG CTG CGT GTC AAC TGA TTC GAC TTG GTC G-3’
3’ primer: 5’-GTG GTC CGC TTT CGC CAC GAA TG-3’

Location: +529 to +4272, Size: 3744bp, Intron 1-1, Cloning Type: RED StuI-XbaI, Vector: placZ.attB
5’ primer: 5’-ATA ATA AGG CCT GTA AGT TGA AAG ATC TCA ATT AGC TAA CCG-3’
3’ primer: 5’-ATA ATA TCT AGA TCT AAG AAA AAC TGT CAC GAC TGC TAA CG-3’

Location: +3957 to +7672, Size: 3698bp, Intron 1-2, Cloning Type: RED EcoRI-XbaI, Vector: placZ.attB
5’ primer: 5’-ATA ATA GAA TTC GTG AAA ACA AAA CTT GCG CCT CAT TTC C-3’
3’ primer: 5’-ATA ATA TCT AGA GGG CGT TTG GCT GGG TCT TGA TAC AC-3’

Location: +7330 to +11076, Size: 3747bp, Enhancer 3 Large Fragment, Cloning Type: RED NotI-KpnI, Vector: placZ.attB
5’ primer: 5’-ATA ATA GCG GCC GCT TTG CTT CGC CTC GGT CAC TAT GGC-3’
3’ primer: 5’-ATA ATA GGT ACC TGT GGA CTT GCG ATT ACT TTC ACT TGC-3’

Location: +10576 to +11076, Size: 500bp, Enhancer 3 Minimal Fragment, Cloning Type: Gateway, Vectors: pglacZ.attB and pg-eyaRB cDNA.attB
5’ primer: 5’-CAC CCC TGT GCG ATA TAC TTG GC-3’
3’ primer: 5’-CCT GTG GAC TTG CGA TTA CTT TCA C-3’

Location: +11149 to +14024, size: 2872bp, Intron 1-4, Cloning Type: RED StuI, Vector: placZ.attB
5’ primer: 5’-ATA ATA AGG CCT GTA ATC ACA TAG TCG TAG TGC TCT CC-3’
3’ primer: 5’-ATA ATA AGG CCT CGT GTG GTC TGT CTT GGG ACG TTT AAC-3’

Location: +14072 to +16647, Size: 2576bp, Intron 2, Cloning Type: RED HindIII-XbaI, Vector: placZ.attB
5’ primer: 5’-ATA ATA AAG CTT CCA CAC GGA TAC ACA TGA ACG CAA CC-3’
3’ primer: 5’-ATA ATA TCT AGA CTG CAA GAA GAT AAG ATG AGA GGC GTC-3’

Location: +16648 to +18402, Size: 1749bp, Exon 3, Cloning Type: Gateway, Vector: pglacZ.attB
5’ primer: 5’-CAA TCT GTC ACA GCA GCA GCA GC-3’
3’ primer: 5’-TTT CCA CGA TAG CTA TTG TAG ATG TCC-3’

Location: +18403 to +18785, Size: 383bp, Intron 3 + Exon 4 + Intron 4, Cloning Type: RED HindIII-XbaI, Vector: placZ.attB
5’ primer: 5’-ATA ATA AAG CTT GTG AGT ATT GGG GGA TGC GCT TTC G-3’
3’ primer: 5’-ATA ATA TCT AGA GAT CCG CTC ATA GCA GGT TTC ATG GC-3’

Location: +18933 to +19869, Size: 937bp, Enhancer 4, Cloning Type: Gateway, Vectors: pglacZ.attB and pg-eyaRB cDNA.attB
5’ primer: 5’-CCC TCT ACA CTG CCC TTG ACA TGG-3’
3’ primer: 5’-TGT AGT GTA CAT GTA AGT AAT GGT TAA-3’

Location: +535 to +840, Spacer, Size: 319bp, Cloning Type: Gateway, Vectors: pglacZ.attB and pg-eyaRB cDNA.attB
5’ primer: 5’-GAA TTC TGA AAG ATC TCA ATT AGC TAA-3’
3’ primer: 5’-TCT AGA CAA CTG CTA CCA TTT TGG CC-3’

eya RB+3’UTR cDNA, Cloning Type: RED EcoRI-NdeI
5’ primer: 5’-ATA ATA GAA TTC ATG TTG TAT AAT GTG CCG TGC TAT C-3’
3’ primer: 5’-ATA ATA CAT ATG AGG CTT ATG CTT TAA TAG AGT GCG TTG C-3’

Gateway Cassette and hsp70 promoter from pg-RFP.attB, Cloning Type: RED EcoRI
5’ primer: 5’-ATA ATA GAA TTC CGT ATG GCA ATG AAA GAC GGT G-3’
3’ primer: 5’-ATA ATA GAA TTC GGG TGT GAG TTC TTC TTC TTT CTC GGG-3’

S3 Table. A list of sequencing primers that were used to determine the breakpoints of the *eya*^{1} deletion.

Genomic location	Primer sequence
-2627 to -2610	5’-TTATCCGAAAGGAGGACC-3’
-2208 to -2187	5’-ATGAGCAAAGTCACTCCCCTCC-3’
-1730 to -1711	5’-TGGAGTAGTTGGGCAGGTTG-3’
-1270 to -1253	5’-CATTGAGTGCTTTTCCGC-3’
-734 to -711	5’-AAAGAGGAGACCGAGACCCAGAAC-3’
-193 to -176	5’-AAAAGCGAGTCCTGATGC-3’
385 to 406	5’-CCATTTGACATTTCCACTGTGC-3’
891 to 909	5’-TGCTACTACGCATTTGCCC-3’
-2536 to -2518	5’-AATCACTTGGCATCCGAGC-3’
-1950 to -1932	5’-GCTGGAAGTTGACCGATTC-3’
728 to 748	5’-CAGGAGTCAGGTTTGAATAGC-3’
1083 to 1102	5’-CCATTGAGTTACAGCCCTTG-3’

S4 Table. A list of primer sequences that were used to detect *so*, *eya* RB and *eya* RA transcripts using qRT-PCR.

Name	Sequence	Reference
so F	5’-GCCTGTGTTTGCGAGGTTCT-3’	Fly PrimerBank*
so R	5’-TGCAGCTTATCACATTGTGGC-3’	
eyaI F	5’-AATGCCATACAACTACGCTGC -3’	ApE
eyaI R	5’-GTATCCGTGTGGTCTGTCTTG-3’	
eyaII F	5’-GGAGCAGCCACAACACTTG-3’	ApE
eyaII R	5’-CGTGTGGTCTGTCTTGGGA-3’	
eyaI F endo	5’-CGCAAGTCCACAGAATGGTCAC-3’	ApE

* G3 (Bethesda). 2013 Sep 4;3(9):1607-16. doi: 10.1534/g3.113.007021.

S5 Table. A feature list of the *eya* locus. Included in this list are the positions of So binding sites, So ChIP peaks, position of retinal enhancers, as well as the position of introns and exons.

Eya locus -8714 to 19869: Osm-6 to Insulator
So Chip-seq peaks in purple

Coordinates	Position on Schematic	Additional Notes
-8714 to -6333	Most upstream fragment (no expression)	
-8714 to -7088	**So Chip-seq Peak #1**	**Contained within and beyond most upstream fragment also covers PSE enhancer**
-8089 to -8080	**So binding site (Yan B)**	**Contained within most upstream fragment**
-8088 to -8082	**So binding site (Berger B)**	**Contained within most upstream fragment**
-7884 to -7150	**PSE Enhancer**	**Contained within most upstream fragment**
-7565 to -7560	**So binding site (Hazbun B)**	**Contained within PSE Enhancer**
-6332 to -3831	2nd upstream fragment (no expression)	
-5765 to -5759	**So binding site (Berger A)**	**Contained within 2nd upstream fragment**
-5764 to -5759	**So binding site (Noyes, Hazbun A)**	**Contained within 2nd upstream fragment**
-5565 to -5560	**So binding site (Noyes, Hazbun A)**	**Contained within 2nd upstream fragment**
-4460 to -4455	**So binding site (Noyes, Hazbun A)**	**Contained within 2nd upstream fragment**
-3830 to -897	**Enhancer #1 large fragment**	
-1470 to -1465	**So binding site (Hazbun B)**	**Located outside of minimal enhancer #1 fragment**
-1171 to -897	**Enhancer #1 minimal fragment**	
-896 to -577	**Extant Enhancer**	
-614 to -609	**So binding site (Hazbun B)**	**Contained within Extant Enhancer**
-576 to 10	**Enhancer #2 large fragment**	
-448 to 396	**So Chip-seq Peak #2**	**Contained within enhancer #2 and 5' UTR of RB**
-282 to 10	**Enhancer #2 minimal fragment**	
1 to 474	5' UTR eya RB	NOT A CONSTRUCT
475 to 528	Exon 1	53 bp in size NOT A CONSTRUCT
529 to 14024	Intron 1	Divided into 4 pieces due to size
529 to 4272	Intron 1-1 fragment (no expression)	
3548 to 5986	**So Chip-seq Peak #3**	**Spans Intron 1-1 and 1-2 fragments and So site in 1-2**
3957 to 7672	Intron 1-2 fragment (no expression)	Overlaps slightly with Intron 1-1 fragment
4979 to 4984	**So binding site (Noyes, Hazbun A)**	**Contained within Intron 1-2 fragment**
6857 to 6862	**So binding site (Hazbun B)**	**Contained within Intron 1-2 fragment**
7330 to 11076	**Enhancer #3 large fragment**	Overlaps slightly with Intron 1-2 fragment
7430 to 7435	**So binding site (Noyes, Hazbun A)**	**Outside of minimal Enhancer #3 fragment**
7649 to 7654	**So binding site (Noyes, Hazbun A)**	**Outside of minimal Enhancer #3 fragment**
9875 to 11376	**So Chip-seq Peak #4**	**Outside and within minimal Enhancer #3 fragment**
10137 to 10142	**So binding site (Hazbun B)**	**Outside of miminal Enhancer #3 fragment but within Chip-seq peak #3**
10576 to 11076	**Enhancer #3 minimal fragment**	
11077 to 11148	Exon 1A	71 bp in size NOT A CONSTRUCT
11149 to 14024	Intron 1-4 fragment (no expression)	
11444 to 11450	**So binding site (Berger B)**	**Contained within Intron 1-4 fragment**
14025 to 14071	Exon 2	46 bp NOT A CONSTRUCT

14072 to 16647	Intron 2 (no expression)	
16648 to 18402	Exon 3 (no expression)	1754 bp in size THIS IS A CONSTRUCT
18080 to 18085	**So binding site (Hazbun B)**	**Contained within Exon 3 fragment**
18403 to 18464	Intron 3 (no expression)	Combined with Exon 4 and Intron 4 due to small size
18465 to 18709	Exon 4 (no expression)	244 bp in size part of a construct
18710 to 18785	Intron 4 (no expression)	Combined with Intron 3 and Exon 4 due to small size
18786 to 18967	Exon 5	181 bp in size NOT A CONSTRUCT
18933 to 19869	**Enhancer #4**	**Overlaps part of Exon 5**
18968 to 19530	3’ UTR	Contained within Enhancer #4
19298 to 19303	**So binding site (Hazbun B)**	**Contained within Enhancer #4 in 3’ UTR**
19531 to 19869	End of 3’UTR to genomic insulator	Contained within Enhancer #4

REFERENCES

1. Davidson EH (2010) Emerging properties of animal gene regulatory networks. Nature 468: 911±920. doi: 10.1038/nature09645 PMID: 21164479

2. Davidson EH, Levine MS (2008) Properties of developmental gene regulatory networks. Proc Natl Acad Sci U S A 105: 20063±20066. doi: 10.1073/pnas.0806007105 PMID: 19104053

3. Levine M, Davidson EH (2005) Gene regulatory networks for development. Proc Natl Acad Sci U S A 102: 4936±4942. doi: 10.1073/pnas.0408031102 PMID: 15788537

4. Peter IS, Davidson EH (2015) Genomic Control Processes: Academic Press. 448 p.

5. Kumar JP (2010) Retinal determination the beginning of eye development. Curr Top Dev Biol 93: 1±28. doi: 10.1016/B978-0-12-385044-7.00001-1 PMID: 20959161

6. Quiring R, Walldorf U, Kloter U, Gehring WJ (1994) Homology of the eyeless gene of Drosophila to the Small eye gene in mice and Aniridia in humans [see comments]. Science 265: 785±789. PMID: 7914031

7. Serikaku MA, O'Tousa JE (1994) sine oculis is a homeobox gene required for Drosophila visual system development. Genetics 138: 1137±1150. PMID: 7896096

8. Mardon G, Solomon NM, Rubin GM (1994) dachshund encodes a nuclear protein required for normal eye and leg development in Drosophila. Development 120: 3473±3486. PMID: 7821215

9. Czerny T, Halder G, Kloter U, Souabni A, Gehring WJ, et al. (1999) twin of eyeless, a second Pax-6 gene of Drosophila, acts upstream of eyeless in the control of eye development. Mol Cell 3: 297±307. PMID: 10198632

10. Cheyette BN, Green PJ, Martin K, Garren H, Hartenstein V, et al. (1994) The Drosophila sine oculis locus encodes a homeodomain-containing protein required for the development of the entire visual system. Neuron 12: 977±996. PMID: 7910468

11. Bonini NM, Leiserson WM, Benzer S (1993) The eyes absent gene: genetic control of cell survival and differentiation in the developing Drosophila eye. Cell 72: 379±395. PMID: 8431945

12. Jemc J, Rebay I (2007) The eyes absent family of phosphotyrosine phosphatases: properties and roles in developmental regulation of transcription. Annu Rev Biochem 76: 513±538. doi: 10.1146/annurev. biochem.76.052705.164916 PMID: 17341163

13. Tadjuidje E, Hegde RS (2013) The Eyes Absent proteins in development and disease. Cell Mol Life Sci 70: 1897±1913. doi: 10.1007/s00018-012-1144-9 PMID: 22971774

14. Xu PX (2012) The EYA-SO/SIX complex in development and disease. Pediatr Nephrol.

15. Ostrin EJ, Li Y, Hoffman K, Liu J, Wang K, et al. (2006) Genome-wide identification of direct targets of the Drosophila retinal determination protein Eyeless. Genome Res 16: 466±476. doi: 10.1101/gr. 4673006 PMID: 16533912

16. Pappu K, Mardon G (2002) Retinal specification and determination in Drosophila. Results Probl Cell Differ 37: 5±20. PMID: 25707066

17. Braid LR, Verheyen EM (2008) Drosophila nemo promotes eye specification directed by the retinal determination gene network. Genetics 180: 283±299. doi: 10.1534/genetics.108.092155 PMID: 18757943

18. Bessa J, Gebelein B, Pichaud F, Casares F, Mann RS (2002) Combinatorial control of Drosophila eye development by eyeless, homothorax, and teashirt. Genes Dev 16: 2415±2427. doi: 10.1101/gad. 1009002 PMID: 12231630

19. Wang CW, Sun YH (2012) Segregation of eye and antenna fates maintained by mutual antagonism in Drosophila. Development 139: 3413±3421. doi: 10.1242/dev.078857 PMID: 22912416

20. Atkins M, Jiang Y, Sansores-Garcia L, Jusiak B, Halder G, et al. (2013) Dynamic rewiring of the Drosophila retinal determination network switches its function from selector to differentiation. PLoS Genet 9: e1003731. doi: 10.1371/journal.pgen.1003731 PMID: 24009524

21. Rebay I (2015) Multiple Functions of the Eya Phosphotyrosine Phosphatase. Mol Cell Biol 36: 668±677. doi: 10.1128/MCB.00976-15 PMID: 26667035

22. Pignoni F, Hu B, Zavitz KH, Xiao J, Garrity PA, et al. (1997) The eye-specification proteins So and Eya form a complex and regulate multiple steps in Drosophila eye development. Cell 91: 881±891. PMID: 9428512

23. Silver SJ, Davies EL, Doyon L, Rebay I (2003) Functional dissection of eyes absent reveals new modes of regulation within the retinal determination gene network. Mol Cell Biol 23: 5989±5999. doi: 10.1128/MCB.23.17.5989-5999.2003 PMID: 12917324

24. Tootle TL, Silver SJ, Davies EL, Newman V, Latek RR, et al. (2003) The transcription factor Eyes absent is a protein tyrosine phosphatase. Nature 426: 299±302. doi: 10.1038/nature02097 PMID:14628053

25. Jin M, Jusiak B, Bai Z, Mardon G (2013) Eyes absent tyrosine phosphatase activity is not required for Drosophila development or survival. PLoS One 8: e58818. doi: 10.1371/journal.pone.0058818 PMID:23554934

26. Ohto H, Kamada S, Tago K, Tominaga SI, Ozaki H, et al. (1999) Cooperation of six and eya in activation of their target genes through nuclear translocation of Eya. Mol Cell Biol 19: 6815±6824. PMID:10490620

27. Anderson AM, Weasner BM, Weasner BP, Kumar JP (2012) Dual transcriptional activities of SIX proteins define their roles in normal and ectopic eye development. Development 139: 991±1000. doi: 10.1242/dev.077255 PMID: 22318629

28. Weasner BM, Kumar JP (2013) Competition among gene regulatory networks imposes order within the eye-antennal disc of Drosophila. Development 140: 205±215. doi: 10.1242/dev.085423 PMID:23222441

29. Halder G, Callaerts P, Flister S, Walldorf U, Kloter U, et al. (1998) Eyeless initiates the expression of both sine oculis and eyes absent during drosophila compound eye development. Development 125:2181±2191. PMID: 9584118

30. Bui QT, Zimmerman JE, Liu H, Gray-Board GL, Bonini NM (2000) Functional analysis of an eye enhancer of the Drosophila eyes absent gene: differential regulation by eye specification genes. Dev Biol 221: 355±364. doi: 10.1006/dbio.2000.9688 PMID:10790331

31. Zimmerman JE, Bui QT, Liu H, Bonini NM (2000) Molecular genetic analysis of Drosophila eyes absent mutants reveals an eye enhancer element. Genetics 154:237±246. PMID: 10628984

32. Hazbun TR, Stahura FL, Mossing MC (1997) Site-specific recognition by an isolated DNA-binding domain of the sine oculis protein. Biochemistry 36: 3680±3686. doi: 10.1021/bi9625206 PMID:9132021

33. Jusiak B, Karandikar UC, Kwak SJ, Wang F, Wang H, et al. (2014) Regulation of Drosophila eye development by the transcription factor Sine oculis. PLoS One 9: e89695. doi: 10.1371/journal.pone.0089695 PMID: 24586968

34. Jusiak B, Wang F, Karandikar UC, Kwak SJ, Wang H, et al. (2014) Genome-wide DNA binding pattern of the homeodomain transcription factor Sine oculis (So) in the developing eye of. Genom Data 2: 153±155. doi: 10.1016/j.gdata.2014.06.016 PMID:25126519

35. Karandikar U, Jin M, Jusiak B, Kwak S, Chen R, et al. (2014) Drosophila eyes absent is required for normal cone and pigment cell development. PLoS One 9: e102143. doi: 10.1371/journal.pone.0102143 PMID: 25057928

36. Ready DF, Hanson TE, Benzer S (1976) Development of the Drosophila retina, a neurocrystalline lattice. Dev Biol 53: 217±240. PMID: 825400

37. Milani R (1941) Two new eye-shape mutant alleles in Drosophila melanogaster. D I S 14: 52.

38. Salzer CL, Kumar JP (2009) Position dependent responses to discontinuities in the retinal determination network. Dev Biol 326: 121±130. doi: 10.1016/j.ydbio.2008.10.048 PMID: 19061881

39. Kumar JP (2011) My what big eyes you have: how the Drosophila retina grows. Dev Neurobiol 71:1133±1152. doi: 10.1002/dneu.20921 PMID: 21604387

40. Baker NE, Firth LC (2011) Retinal determination genes function along with cell-cell signals to regulate Drosophila eye development: examples of multi-layered regulation by master regulators. Bioessays 33:538±546. doi: 10.1002/bies.201000131 PMID: 21607995

41. Pankratz MJ, Busch M, Hoch M, Seifert E, Jackle H (1992) Spatial control of the gap gene knirps in the Drosophila embryo by posterior morphogen system. Science 255: 986±989. PMID: 1546296

42. Driever W, Thoma G, Nusslein-Volhard C (1989) Determination of spatial domains of zygotic gene expression in the Drosophila embryo by the affinity of binding sites for the bicoid morphogen. Nature 340: 363±367. doi: 10.1038/340363a0 PMID: 2502714

43. Perry MW, Boettiger AN, Levine M (2011) Multiple enhancers ensure precision of gap gene-expression patterns in the Drosophila embryo. Proc Natl Acad Sci U S A 108: 13570±13575. doi: 10.1073/pnas. 1109873108 PMID: 21825127

44. Schroeder MD, Pearce M, Fak J, Fan H, Unnerstall U, et al. (2004) Transcriptional control in the segmentation gene network of Drosophila. PLoS Biol 2: E271. doi: 10.1371/journal.pbio.0020271 PMID:15340490

45. Bothma JP, Garcia HG, Ng S, Perry MW, Gregor T, et al. (2015) Enhancer additivity and non-additivity are determined by enhancer strength in the Drosophila embryo. Elife 4.

46. Small S, Arnosti DN, Levine M (1993) Spacing ensures autonomous expression of different stripe enhancers in the even-skipped promoter. Development 119: 762±772. PMID: 8187640

47. Spratford CM, Kumar JP (2015) Extramacrochaetae functions in dorsal-ventral patterning of Drosophila imaginal discs. Development 142: 1006±1015. doi: 10.1242/dev.120618 PMID: 25715400

48. Kawakami K, Ohto H, Takizawa T, Saito T (1996) Identification and expression of six family genes in mouse retina. FEBS Lett 393: 259±263. PMID: 8814301

49. Ihry RJ, Sapiro AL, Bashirullah A (2012) Translational control by the DEAD Box RNA helicase belle regulates ecdysone-triggered transcriptional cascades. PLoS Genet 8: e1003085. doi: 10.1371/journal.pgen.1003085 PMID: 23209440

50. Pfaffl MW, Horgan GW, Dempfle L (2002) Relative expression software tool (REST) for group-wise comparison and statistical analysis of relative expression results in real-time PCR. Nucleic Acids Res 30: e36. PMID: 11972351

51. Hu Y, Sopko R, Foos M, Kelley C, Flockhart I, et al. (2013) FlyPrimerBank: an online database for Drosophila melanogaster gene expression analysis and knockdown evaluation of RNAi reagents. G3 (Bethesda) 3: 1607±1616.

52. Pauli T, Seimiya M, Blanco J, Gehring WJ (2005) Identification of functional sine oculis motifs in the autoregulatory element of its own gene, in the eyeless enhancer and in the signalling gene hedgehog. Development 132: 2771±2782. doi: 10.1242/dev.01841 PMID: 15901665

53. Berger MF, Badis G, Gehrke AR, Talukder S, Philippakis AA, et al. (2008) Variation in homeodomain DNA binding revealed by high-resolution analysis of sequence preferences. Cell 133: 1266±1276. doi: 10.1016/j.cell.2008.05.024 PMID: 18585359

54. Noyes MB, Christensen RG, Wakabayashi A, Stormo GD, Brodsky MH, et al. (2008) Analysis of homeodomain specificities allows the family-wide prediction of preferred recognition sites. Cell 133: 1277±1289. doi: 10.1016/j.cell.2008.05.023 PMID: 18585360

55. Yan H, Canon J, Banerjee U (2003) A transcriptional chain linking eye specification to terminal determination of cone cells in the Drosophila eye. Dev Biol 263: 323±329. PMID: 14597205

APPENDIX 2

Teashirt and Tiptop control growth and developmental plasticity within the *Drosophila* eye-antennal disc

This chapter is under revision for publication in *PLoS Genetics*

Pallilyil S, Zhu J, Baker LR, Neuman SD, Bashirullah A, Kumar JP. (2017) Teashirt and Tiptop control growth and developmental plasticity within the *Drosophila* eye-antennal disc. *PLoS Genet*. Under revision.

ABSTRACT

The earliest steps in the specification of the developing *Drosophila* compound eye involve the action of fourteen transcription factors whose activities are interwoven into a complex gene regulatory circuit called the retinal determination (RD) network. Loss-of-function mutants are characterized by a failure in eye development and the homeotic conversion of retinal progenitors into adjacent non-ocular structures such as antennae, maxillary palps, and head epidermis. Remarkably, forced expression of these same network genes in non-retinal tissues is sufficient to drive ectopic eye formation, a phenotype that is consistent with a model in which these factors sit atop the entire eye/lens gene regulatory network. Several RD genes such as *teashirt* (*tsh*) and the Pax6 ortholog *twin of eyeless* (*toy*) are first expressed throughout the entire nascent eye-antennal disc only to have their expression restricted to the eye field later in development. While its role in eye development has been heavily scrutinized, very little is known about the function of the RD network in non-retinal tissues that are also derived from the eye-antennal disc. Here we show that Tsh cooperates with Toy to promote survival of the entire nascent disc by suppressing apoptosis. The need to block cell death within the antenna and head epidermis appears dispensable later in development as the expression of *tsh* and its paralog *tiptop (tio)* are restricted to just the undifferentiated cells of the eye field. If these genes continue to be expressed within the antennal field, then the head epidermis and aristal segments are transformed into eyes. The path to eye formation can be diverted towards a leg fate if Pax6 expression is inhibited. Our findings shed new light on how growth and plasticity of the entire eye-antennal disc is controlled, and indicate that the RD network plays a larger role than has been previously appreciated.

INTRODUCTION

It is well established that the wide and diverse set of cell types that make up a metazoan are generated, in part, by the use of a rather limited set of site-specific DNA binding proteins. Many mechanisms are put in place to maximize the potential that these transcription factors possess. For example, transcription factors are known to be able to activate a target gene in one cell type while repressing the same target gene in a different cell type. Transcription factors can also bind to and activate (or repress) a set of target genes in one cell type while controlling the expression of a separate set of genes in another cell type. These shifting activities are often associated with alterations in the epigenetic landscape, changes in the availability of co-factors, and in the modifications (i.e. phosphorylation) that are placed upon the transcription factor. An interesting aspect of transcription factors is the patterns in which they are expressed: some transcription factors are expressed in very broad patterns early in development only to be found in much more restricted patterns later. These changes in expression patterns often reflect shifts in the roles that these DNA binding proteins play in development. The eye antennal disc of the fruit fly is an ideal model system for understanding the correlation between the expression patterns of transcription factors and their shifting roles in development.

During *Drosophila* embryogenesis, several different populations of cells coalesce to form the eye-antennal disc [1]. This monolayer epithelium eventually gives rise to a number of head structures, including the visual system (compound eyes and ocelli), the olfactory system (antennae and maxillary palps), and the surrounding head epidermis. Mosaic clone analysis and transplantation experiments using disc fragments have identified the physical locations of each tissue within the late third larval instar disc [2-6].

At this late stage of development, physical landmarks distinguish the major regions of the eye-antennal disc from one another, while gene expression and protein distribution patterns can identify much more discrete domains. In contrast, between mid-embryogenesis and the beginning of the second larval instar, the eye-antennal disc does not have any obvious physical markings that would distinguish one region from another, nor are there many genes expressed in discrete patterns. In fact, many genes that occupy very restricted patterns later in development often were first ubiquitously expressed earlier in development. While the signals that trigger tissue fate specification and gene expression restriction are yet to be well defined, it is clear that the changes in temporal/spatial expression patterns can be important because the roles of many proteins shift during development.

One poignant example is the case of the two *Drosophila* Pax6 genes, *eyeless* (*ey*) and *twin of eyeless* (*toy*). Starting at stage 12 of embryogenesis and continuing through the first larval instar, both *ey* and *toy* are expressed throughout the entire eye-antennal disc, only to be restricted later to a stripe of undifferentiated cells ahead of the advancing morphogenetic furrow in the eye field [7-9]. The simultaneous removal of these proteins early in development, when they are universally expressed in the eye-antennal disc, leads to the elimination of the entire disc and all associated head structures that are derived from the disc [10,11]. Ey/Toy appears to promote proliferation of the disc through the activity of the Pax6(5a) homolog Eyegone (Eyg), the zinc finger transcription factor Teashirt (Tsh), and the Notch (N) signaling pathway during early stages of development [10]. If Ey/Toy are necessary for tissue proliferation early in development, then why is expression of both these genes lost from the antennal and head epidermal portions of the

disc even as both domains continue to proliferate and grow? The answer lies in experiments involving targeted expression of *ey/toy* in the antennal field; in these situations, ectopic eyes are induced [8,12]. By the early second larval instar *ey/toy* are not expressed in the antennal and head epidermal regions, as they are mainly required at this time for specification and continued growth of the eye field. It thus appears that Pax6 plays two roles in development: cell proliferation and tissue specification. The changing temporal expression pattern of Pax6 genes over time is critical for separating the two functions of Pax6 in both time and space. This ensures that development of the eye-antennal disc and formation of the entire fly head occur correctly.

To better understand the mechanisms of how these developmental genes alter their roles as their expression patterns change, we analyzed other genes that might play similar roles to that of Ey/Toy in eye-antennal disc development. We focused on *tsh* and its paralog *tiptop* (*tio*), as both genes promote proliferation of the eye field, and because Tsh mediates the effect that Ey/Toy have on the development of the entire eye-antennal disc [10,13-15]. While both genes are known to participate in the specification of the eye, their exact roles in eye development and the positions that they occupy within the RD network hierarchy are not well understood. *tsh*, like *toy*, is first expressed throughout the entire eye-antennal disc early in development before it is then later restricted to the same set of *toy* expressing undifferentiated cells in the eye field. Here we show that the simultaneous removal of Toy and Tsh proteins results in the complete loss of both eye-antennal discs and in headless animals that die as pharate adults. This interaction is very specific to this pair of proteins, as the concurrent removal of Ey and Tsh proteins does not affect growth of the disc, nor does the concomitant loss of Tio with either Pax6

member. We demonstrate that Toy and Tsh act to suppress apoptosis in the disc and propose that the headless phenotype in *toy/tsh* double mutants results from massive increases in cell death levels within the eye-antennal disc. The role for Tsh in early disc growth has remained hidden up to this point, and is only revealed when Toy protein levels are simultaneously reduced.

Despite its ability to promote tissue growth, the restriction of Tsh to the eye field later in development is necessary, since prolonged expression within the antennal field, like Toy, also induces ectopic eye formation [16]. We demonstrate here that during the induction of ectopic eyes within the ventral head epidermis and arista, Tsh not only initiates expression of retinal selector genes such as *ey*, *sine oculis* (*so*), and *eyes absent* (*eya*), but it also independently represses the expression of antennal/head epidermal selector genes such as *cut (ct), Lim1, aristaless (al),* and *spineless (ss)*. If *ey* is removed, then the arista is converted into a tarsal leg segment instead. But if lower level network members such as *so* and *eya* are removed (while maintaining *ey*), then the arista develops into a mass of epidermal tissue. Forced expression of Tio within the antennal disc leads to similar changes in selector gene expression and tissue fate specification. However, unlike *tsh*, *tio* is never expressed within the antennal field but is always restricted to the undifferentiated cells of the developing eye. This is consistent with our findings that only Tsh cooperates with Toy to promote the early growth of the entire eye-antennal disc. Our data indicates that while Tsh/Tio proteins are functionally redundant in the eye [13,17], changes in promoter/enhancer elements are likely to have played a key role in how these proteins differentially affect early eye-antennal disc development.

Our findings shed new light on the role that the RD gene network plays in the growth and specification of the entire eye-antennal field. In addition to demonstrating that the network plays a much larger role than previously appreciated, our study furthers our understanding of the shifting roles that many transcription factors play during development and the mechanisms by which tissues take advantage of such distinct activities. This report also describes a hitherto unknown functional difference between Tsh and Tio proteins.

MATERIALS AND METHODS

Fly stocks

The following fly stocks were used in this study: (1) *DE-GAL4* (Georg Halder), (2) *ey-GAL4* (BDSC), (3) *tio-GAL4* (Kwang Choi), (4) *eya-GAL4*, (5) *dpp-GAL4* (Graeme Mardon), (6) *hsFLP*^{22} (BDSC), (7) *Actin5C>y*$^{+}$*>GAL4, UAS-GFP S65T* (BDSC), (8) *Actin5C>y*$^{+}$*>GAL4, UAS-lacZ* (BDSC), (9) *UAS-tsh* RNAi (BDSC), (10) *UAS-tio* RNAi (BDSC), (11) *UAS-ey* RNAi (BDSC), (12) *UAS-toy* RNAi (BDSC), (13) *tub-GAL80*^{ts} (BDSC), (14) UAS-RedStinger, UAS-FLP, Ubi-p63E(FRT.STOP)Stinger (BDSC), (15) *UAS-GFP* (BDSC), (16) *UAS-ey*, (17) *UAS-eya,* (18) *UAS-so,* (19) *UAS-tsh*, (20) *UAS-tio*, (21) *UAS-tsh ΔZnF1*, (22) *UAS-tsh ΔZnF2*, (23) *UAS-tsh ΔZnF3*, (24) *UAS-tio ΔZnF1*, (25) *UAS-tio ΔZnF2*, (26) *UAS-tio ΔZnF3*, (27) *UAS-tio ΔZnF4*, (28) *UAS-Tc tsh/tio*, (29) *UAS-tsh* (Amit Singh), (30) *UAS-eyg* (BDSC), (31) *UAS-p35* (BDSC), (32) UAS-*DIAP1* (BDSC), (33) *eyg-GFP* (BDSC), (34) *eya*^{2} (Nancy Bonini), (35) *so*^{1} (Larry Zipursky), (36) *ey*^{LB}, (37) *ss* 522$^{(1-5)}$*-lacZ* (Ian Duncan). BDSC = Bloomington Drosophila Stock Center. Stocks without a donor were generated in our lab. All crosses (except for GAL80 temperature shift experiments) were conducted at 25°C.

Antibodies and Microscopy

The following primary antibodies and stains were used: chicken anti-β-gal (1:800, Abcam), guinea pig anti-Toy (1:500, Henry Sun), guinea pig anti-Ss (1:100), mouse anti-Ey (1:100, DSHB), mouse anti-Cut (1:100, DSHB), mouse anti-Eya (1:4, DSHB), mouse anti-Dac (1:100, DSHB), mouse anti-Antp (1:100), mouse anti-Dll (1:500, Dianne Duncan), rabbit anti-GFP (1:1000, Invitrogen), rabbit anti-cleaved Dcp-1 (1:100, Cell

Signaling Technologies), rabbit anti-Tsh (1:3000, Stephen Cohen), rabbit anti-Hth (1:1000, Richard Mann), rabbit anti-PH3 (1:20,000, Abcam), rabbit anti-Lim1 (1:1000, Juan Botas), rat anti-ELAV (1:100, DSHB), rat anti-Al (1:1000, Gerard Campbell), Hoechst 33342 (1:2000, Invitrogen). DSHB = Developmental Studies Hybridoma Bank. Secondary fluorophore-conjugated antibodies and phalloidin-fluorophore conjugates (for detection of F-actin) are from Molecular Probes. Imaginal discs were prepared as described previously in [71]. TUNEL Assay (Sigma-Aldrich) was performed as per manufacturer's instructions. For adult antennae, adult fly heads were removed using a surgical blade and were placed in a concave depression glass slide containing isopropanol. Using forceps the antennae were then dissected away from 544 the adult heads while the tissue incubated in isopropanol. The dissected antennae were then allowed to air dry and then mounted on a glass slide using Permount (Fisher Scientific). Adult eyes, heads, and antennae were imaged with a Zeiss Discovery Light Microscope or a Leica M205FA Stereo Microscope.

GAL80 inducible expression system

tub-Gal80^{ts}; DE-GAL4, toy RNAi, tsh RNAi embryos were first collected for an hour at either 18°C or 30°C as per the experiment and then further incubated at the egg laying temperature for defined periods of time before being transferred to the opposite temperature. Eye-antennal imaginal discs were dissected at specific time points after the temperature shift or from third instar larvae.

Clonal induction and data analysis

The heat shock flp-out over-expression system was used to induce clones overexpressing *tsh* RNAi and/or *toy* RNAi. Embryos of the appropriate genotype were collected after an egg laying period of 1hr at 25°C. Clones were induced at 24hrs after egg lay (AEL) by a single heat shock pulse of 15min in a 37°C water bath. Larvae were returned to 25°C and eye antennal discs were dissected at specific time points. For each genotype clones in three different regions were measured: eye region, antennal region and eye progenitor region (see Figure 5A,B). Adobe Photoshop CS 5.1 was used to outline and measure the area of the clones induced in the eye antennal disc (in pixels). Statistical significance was calculated using one-way ANOVA with GraphPad Prism.

EdU incorporation and PH3 assay

Click-iT EdU Alexa Fluor 555 imaging Kit (Invitrogen) was used to detect the cells in S phase. The protocol provided by the manufacturer was adapted and standardized for the eye-antennal imaginal discs. First, the eye-antennal discs were dissected in PBS and incubated in 50 μM EdU containing PBS for 15mins. This was followed by fixation in Paraformaldehyde-Lysine-Periodate (PLP) fixative as described in [71]. The fixed discs were then sequentially washed in 0.1% TritonX PBS and 3% BSA containing PBS. Next, eye-antennal discs were incubated with Click-iT reaction cocktail as per the manufacturer's instructions followed by washing in 3% BSA containing PBS and 0.1% TritonX PBS. This was followed by standard immunostaining with pH3 antibody to detect the cells in M phase. Finally, for nuclear staining the eye-antennal imaginal discs were stained with Hoechst 33342. Eye-antennal discs were imaged using Leica SP5 confocal. Total cell numbers as well as EdU and PH3 positive cell density were measured using

Imaris Image Analysis Software. Statistical significance was calculated using a paired t-test.

RT-qPCR

RNA from wild type (control), *DE>toy* RNAi*, DE>ey* RNAi*, DE>tsh* RNAi, and *DE>tio* RNAi eye-antennal imaginal discs was isolated as described by [25] and subjected to RT-qPCR analysis as described in [72]. For each genotype, RNA isolation, cDNA synthesis and qPCR was performed on three separate biological replicates with each sample consisting of approximately 50 third larval instar eye-antennal imaginal discs.

The following primers were used to detect *toy, ey, tsh, tio* and *so* transcripts using RT-qPCR: *toy* F: 5'-CCA GAG GCA CGT ATT CAG GTT TGG-3'; *toy* R: 5'-TTA TTT GCC GTG CTG GTT CGA C-3' (QuantPrime) [73]; *ey* F: 5'-TGG TAG GTC AAT CAC CCA ACC-3'; *ey R: 5'*-GCT GCT GTA GTG CCT GAT GG-3'; *tsh* F: 5'-TCG CAC CAA TCT TTA TGG AAG G; *tsh* R: GTA CCT ACA GAG AGA TCG AGT GG-3'; *tio* F: 5'-GAG GCC GTC ATG CTG GAA AT-3'; *tio* R: 5'-ATG CGA CTC ATT CGA TGG ACA-3`; *so* F: 5'-GCC TGT GTT TGC GAG GTT CT-3-; *so* R: 5'-TGC AGC TTA TCA CAT TGT GGC-3' (FlyPrimerBank) [74].

RESULTS

Tsh, but not Tio, alongside Toy is essential for eye-antennal disc development

Within the *Drosophila* eye, the Pax6 transcription factors, Ey and Toy, sit atop a gene regulatory network that controls both tissue fate specification and cell proliferation (Fig 1A,B). A recent report from our group demonstrated that the combined loss of both Pax6 members leads to the complete elimination of the eye-antennal discs and this in turn results in headless animals that die as pharate adults [10]. In the course of searching for downstream targets of Ey/Toy, we determined that their influence on disc growth is exerted through the activities of Tsh, Eyg, and Notch signaling. We began this study by asking what happens if either Ey or Toy protein levels are simultaneously reduced along with Tsh. We included Tio, since both proteins are thought to function redundantly in the eye [13,15]. To answer this question we used a Dorsal Eye (DE) – GAL4 line to drive expression of combinations of RNAi lines. The DE-GAL4 line is an insertion within the *mirror* (*mirr*) locus [18]. Early in development, it drives expression in all cells of the eye-antennal disc, but later in development its expression is restricted to the dorsal half of the eye and a subset of peripodial cells (S1A-B Fig) [10]. Driving RNAi lines that individually target *toy*, *ey*, *tsh*, and *tio* with DE-GAL4 has no effect on compound eye development (S1C,E,G,I Fig) despite the complete elimination of all four proteins from the dorsal half of the eye (S1D,F,H,J Fig). We also looked at transcript levels in whole late third larval instar expecting to see a reduction in expression levels of approximately 50%, since the DE-GAL4 line is driving expression of the RNAi lines in about half of cells within the eye disc at this time. For *toy*, *tsh* and *tio* we do indeed see such a reduction (S1K Fig). However, the transcript levels of *ey* appear to be unaffected (S1K Fig). Since Ey protein

levels are completely lost in the dorsal half of the eye disc (S1F Fig), we assume that there must be compensation of gene expression within the ventral half of the eye disc through a mechanism that we do not yet understand. To ensure that the knockdown of gene expression that we observe is specific, we looked at the expression of several other RD genes including *so*. As predicted, we do not see a reduction in *so* expression when we are targeting the *ey/toy* and *tsh/tio* gene pairs (S1K Fig). We then expressed different combinations of RNAi lines with DE-GAL4. The concurrent reduction of Toy and Tsh eliminates the eye-antennal discs and results in pharate lethal headless adults (Fig 1C-H). The headless phenotype is identical to the combined loss of Ey and Toy [10], and confirms that Tsh lies genetically downstream of Pax6. Interestingly, the loss of eye-antennal discs is specific to the Toy/Tsh genetic combination, as neither the concurrent loss of Ey and Tsh nor the concomitant removal of Tio with either Pax6 protein has any effect on disc development (Fig 1I-K). Our results also suggest that, in this context, Tio cannot compensate for the loss of its paralog, Tsh. We also confirmed that the *tsh* RNAi line is capable of inducing a phenotype on its own: the wings display an outstretched posture that is similar to the *aeroplane-like* allele of *tsh* (S4A Fig) [19,20].

Toy/Tsh control eye-antennal disc development during embryogenesis and the first larval instar

The above result is the first demonstration that Tsh plays a role in the development of the entire eye antennal disc. It is also consistent with a previous study showing that Tsh physically interacts with Pax6 to control growth in the eye field [21]. In that report, it was proposed that Tsh functions within a tertiary biochemical complex that includes Ey

and Homothorax (Hth) to control cell proliferation. To determine the developmental stages at which Toy and Tsh are functioning together, we introduced a temperature sensitive GAL80 construct [22] to temporally modulate the activity of GAL4 and in turn regulate the timing of *toy*/*tsh* RNAi expression. At 18°C (the permissive temperature) GAL80 inhibits the activity of GAL4, thereby silencing the RNAi lines and allowing for normal expression of *toy* and *tsh*. Animals kept at this temperature throughout development emerge as adults that are indistinguishable from wild type. In contrast, GAL80 is non-functional at 30°C (the restrictive temperature), which allows for the expression of the RNAi lines and for the suppression of both genes. At this temperature, larvae lack eye-antennal discs and the pharate adults are completely headless. By toggling between the permissive and restrictive temperatures, we can temporally control *toy* and *tsh* expression and determine when both genes are required for disc development. When going back and forth between different temperatures, we had to take into account the dynamics of endogenous protein loss and recovery. We have determined that once animals have been shifted to 30°C and RNAi expression is initiated, it takes roughly 8hrs for Toy [10] and 12hrs for Tsh proteins to 234 be erased from the disc (S2A-D Fig). Once flies are returned to 18°C and the expression of RNAi lines has ceased, it takes approximately 40hrs for Toy [10] and 38hrs for Tsh (S3A-F Fig) to return to wild type levels. We first kept animals at the permissive temperature (18°C) for varying amounts of time before shifting to the restrictive temperature (30°C). Depending on when Toy/Tsh are removed, we see a range of phenotypes with headless flies on one extreme and wild type looking flies on the other (Fig 2A-L). Animals with more severe defects are the ones in which the removal of Toy/Tsh began earlier in development (Fig 2M). We also conducted the opposite

experiment, in which animals were kept at the restrictive temperature (30°C) for varying lengths of time before returning them to the permissive temperature (18°C). Again, depending upon the time at which Toy/Tsh proteins are restored, we see a range of mild to severe phenotypes (Fig 3A-L). Severe defects such as the complete loss of the eye antennal discs are most often associated with the knockdown of *toy/tsh* levels for longer periods of time (Fig 3M). After taking into consideration the effect that different temperatures have on developmental rates, as well as the time that it takes for Toy/Tsh proteins to either be depleted or recovered, we propose that the critical window for Toy/Tsh control of eye-antennal disc development is between stage 16 of embryogenesis and the end of the first larval instar (Fig 2M, 3M).

In order to confirm this timeline, we simultaneously knocked down *toy/tsh* using several different GAL4 drivers that initiate their expression at different times in development. Expression of the *toy/tsh* RNAi lines with *ey*-GAL4, which is activated during embryogenesis, also results in larvae lacking eye antennal discs and pharate lethal headless adults (Fig 4A-C,G,J). This effect is synergistic, as expression of the individual RNAi lines with *ey*-GAL4 has much milder effects on the eye and head (S4B-E Fig). In contrast, removing Toy/Tsh simultaneously or individually with a *tio*-GAL4 driver, whose expression begins during the mid-second larval instar has no effect on the eye-antennal disc or the adult head (Fig. 4D-F,H,J, S4H-K Fig). The GAL4 line does drive expression of transcriptional reporters in the eye ahead of the morphogenetic furrow (Fig 4H), and we are confident that it is driving expression of the RNAi lines at sufficiently highly levels, since we observe defects in leg development (S4L-P Fig). *tio*-GAL4 drives expression in regions within the leg disc that will give rise to the adult pleura and coxa (S4L Fig). If Tsh

is removed from these regions, then the leg discs are duplicated (S4M Fig). The resulting adult legs are considerably smaller than their wild type counterparts and are often internalized within the adult fly (S4N-P Fig). This phenotype is consistent with the known role of Tsh in *Drosophila* leg development [23,24]. Based on the leg phenotypes associated with the *tio-GAL4, UAS-tsh* RNAi strain, we are confident that the lack of observable phenotypes in the eye-antennal disc are due to the late onset of the *tio* enhancer and not because of a technical issue with the driver. We also tried to remove Toy/Tsh with an *eya*-GAL4 driver, which begins its expression at the start of the second larval instar (Fig 4I) [25]. Individual knockdown of *toy* does not have an effect on the disc with this driver (S4F,G Fig) but animals in which expression of *tsh* is reduced die during embryogenesis (Fig 4J), so we were unable to use this driver. The results from the other three drivers (*DE-GAL4*, *ey*-GAL4, *tio*-GAL4) are consistent with the GAL80 time course experiments and indicate that Toy/Tsh function together during late embryogenesis and through the first larval instar to promote growth of the eye antennal disc. This timeline for Toy/Tsh is consistent with the critical period for Ey/Toy function and is consistent with data that places *tsh* genetically downstream of both Pax6 genes [10]. It is also consistent with a role for Tsh in promoting growth as proposed by [21], with the important difference that these two studies are addressing how Tsh interacts with distinct Pax6 proteins.

Increased cell death is the principal cause of the headless phenotype in *toy/tsh* mutants

We then used the flp-out over-expression system to generate mosaic clones in which the *toy* and *tsh* RNAi lines were simultaneously expressed in smaller cell

populations. This allows us to measure the effect that the loss of both genes has on tissue growth. The size of the *toy*/*tsh* double knockdown clones and clones in which each gene had been knocked down individually were compared to GFP control clones. The growth of each type of clone was examined within the entire eye field (Fig 5A, dark blue), the antennal field (Fig 5A, purple), and just the retinal progenitor domain (Fig 5B, light blue). Within the antennal field, control, individual RNAi, and double RNAi-expressing clones are recovered with equal frequency and are of nearly identical sizes (Fig 5C-G). This is most likely due to the fact that expression of both *toy* and *tsh* become segregated to the eye field during the second larval instar, thus rendering the expression of the RNAi lines largely ineffective. In contrast, within the eye field and retinal progenitor region, clones in which both *toy* and *tsh* were simultaneously knocked down are rare and significantly smaller than either control or individual RNAi-expressing clones (Fig 5C-G). These findings are consistent with the above experiments using DE-GAL4, where we see that the loss of individual factors has no effect on growth but the concurrent loss of both Toy/Tsh appears to either block cell proliferation, induce apoptosis, or both. Since several RD genes are known to participate in promoting growth and blocking cell death [10,14,21,25-31], we asked if the loss of Toy/Tsh proteins affect the expression of any of these other network members. We analyzed the expression of *ey*, *eya*, *eyg*, *dachshund* (*dac*), and *hth* in clones lacking both Toy and Tsh, and in all cases, the expression patterns and levels of these genes were unaffected (S5A-F Fig), suggesting that the regulation of growth by Toy/Tsh is likely independent of the known RD gene network.

We then attempted to determine if the headless phenotype is caused by an increase in apoptosis, a lack of cell proliferation, or both. Using TUNEL staining and

antibodies against the cell death marker Dcp-1 [32], we observed dying cells in the dorsal half of the eye when Toy/Tsh levels are reduced (Fig 6A-D, yellow arrows). In this experiment, the RNAi lines were expressed only later in development to ensure that there is an actual disc to examine. By the time we start inducing RNAi expression, expression of the DE-GAL4 driver has been already segregated to the dorsal half of the eye, so that is why cell death is only observed in the dorsal compartment. The suppression of cell death that we observe is consistent with the ability of mammalian Tsh proteins to suppress the expression of the caspase gene, CASP4 [33]. We then asked whether we could restore eye and head development to the *toy/tsh* double knockdown animals by blocking cell death via expression of two apoptosis inhibitors, DIAP1 and P35 [34,35]. In both cases, substantial levels of the eye and head were restored (Fig 6F,G,I,J,L,M,N). This is in contrast to the higher percentage of animals lacking any rescue that is seen when a control UAS-GFP transgene is expressed in the double knockdown background (Fig 6E,H,K,N).

We also examined the cell cycle profile of Toy/Tsh deficient cells. Since DE-GAL4 drives expression only in the dorsal compartment later in development, we were able to use EdU staining and PH3 to look at potential differences in S phase and M phase populations within the dorsal (mutant) and ventral (wild type) compartments. Despite detecting significantly fewer total cells in the dorsal mutant tissue (Hoechst positive), we do not observe any significant difference in the densities of S and M phase cells between wild type tissue and those that lack both proteins (S6A-H Fig), and as such did not pursue any rescue experiments with cell proliferation promoting genes. In total, this set of results suggests that Toy/Tsh are suppressing apoptosis during the early stages of eye-antennal

disc development and that the reduced size of double mutant clones and headless phenotypes are mainly the result of the inappropriate induction of cell death.

Tsh/Tio in the antenna down-regulates non-ocular antennal and head epidermal genes

From the results we have shown above, we know that Tsh and Toy are required to promote growth of the eye-antennal disc. Then why are these proteins segregated to the eye field and removed from the antennal and head epidermis fields? The answer appears to lie in the shifting roles that these proteins play in development. During the second larval instar, both Toy and Tsh proteins are restricted to the retinal progenitor zone ahead of the advancing morphogenetic furrow (Fig 7A-C) [8,21,36]. If either protein is allowed to remain in the antennal field, then ectopic eyes are induced [8,16]. We sought to further our understanding of how Tsh and Tio alter the fate of the antennal and head epidermal fields. To do this we used a *dpp*-GAL4 driver (Fig 7D) and the flp-out system to mis-express each gene within the antennal field and assay changes in gene expression and adult phenotypes. Expression of either *tsh* or *tio* in the antennal field inhibits the expression of *cut* (*ct*), a gene necessary for sensory organ formation (Fig 7C,E-H, yellow arrows) [37-39]. This finding is consistent with a recent study showing that Tsh/Tio negatively regulates *ct* expression during renal tubule development [40], suggesting that the observed cross-regulatory relationship is not tissue-specific. Moreover, the ability to repress *ct* is at least 250 million years old, as the *tsh*/*tio* homolog in the red flour beetle, *Tribolium castaneum*, can also inhibit *ct* expression when it is forcibly expressed within the *Drosophila* antennal disc (Fig 7I,J, yellow arrows). Tsh and Tio are zinc (Zn) finger

transcription factors [41,42], and in a prior study, we deleted each Zn finger individually and showed differential use of these DNA/protein binding domains in the context of inducing ectopic eyes and promoting cell proliferation [15]. Here we expressed those deletion constructs within the antenna in an attempt to determine which Zn finger might be necessary for inhibiting *ct* expression. None of the individual deletion proteins were compromised in their ability to repress *ct* expression (S7A-G Fig, orange arrows), which suggests that the Zn finger domains may function redundantly in this context and the loss of any one domain may be compensated for by the other Zn fingers.

Tsh/Tio repression of *cut* expression is independent of the Ey/So/Eya module

Tsh induces ectopic eye formation in part by activating the expression of several RD genes, including *ey*, *eya*, *so*, and *dac* [16,17]. An example is presented in S8A,B Fig, in which the forced expression of *tsh* induces both *eya* expression and ectopic eye formation. Many of these genes are also thought to inhibit the expression of antennal/head epidermis genes such as *ct* [11,43-45]. We set out to determine if the repression of *ct* is due to Tsh/Tio or if it is the indirect consequence of activating one or more of these other retinal network genes instead. To do this, we forcibly expressed *tsh* within the antenna in ey^{LB}, eya^{2}, and so^{1} loss-of-function mutant backgrounds. Each mutant is characterized by the absence or severe disruption of the eye that is caused by deletions of eye-specific enhancers [27,46] (Baker and Kumar, unpublished). The loss of these enhancers completely eliminates expression of each gene within the developing eye. It also prevents ectopic eye formation from being induced by the expression of *tsh/tio* [16]. *ct* is expressed normally within the antenna of all three mutants (Fig 8A,D,G), but is

still repressed when either *tsh* or *tio* is forcibly expressed (Fig 8B,C,E,F,H,I), suggesting that the repression of *ct* is mediated by Tsh/Tio independent of the *ey/so/eya* module. Further evidence to support this conclusion comes from the observation that Ey is able to repress *ct* only when an ectopic eye is induced (S8C,D Fig) and from the fact that the forced expression of either *eya* or *so* is insufficient to inhibit *ct* expression (S8E,F Fig).

Expression of *tsh/tio* transforms the arista into eyes, tarsal legs, and head epidermis

Surprisingly, in addition to ectopic eye formation within the head epidermis that is derived from the antennal field [16,17], our own analysis indicates that targeted expression of *tsh/tio* can induce other types of homeotic transformations. Tsh/Tio can also induce a transformation of the arista into ectopic eyes, tarsal leg segments, or a mass of head epidermal tissue [16,17] (Fig 9A-D). The ability to transform a portion of the antenna into the homologous leg segment is consistent with a report showing that Tio functions as a selector gene for promoting leg development in the milkweed bug, *Oncopeltus fasciatus* [47]. Surprisingly, blocking eye formation through mutations in *ey*, *so*, and *eya* does not revert the transformed tissue back to an arista as one might have expected. Instead, the percentages of the other types of homeotic transformations rise compensating for the loss of the arista–eye fate switch. For example, if *ey* is removed (while *tsh/tio* is still expressed), then arista–leg transformations increase to 80% from a starting point of 30% (Fig 9E). Similarly, if *so* or *eya* are removed, while expression of *ey* and *tsh*/*tio* is maintained (S9U-Z Fig), then the number of arista–head epidermis transformations rises, while the arista–leg fate drops back to about 35% (Fig 9E).

Down-regulation of *ss* by Tsh/Tio is the underlying cause of the arista–leg transformation

We were most interested in understanding the mechanisms underlying the arista–leg transformation. Since the antenna can be transformed into a complete leg when the Hox gene *Antennapedia* (*Antp*) is inappropriately expressed in the antenna [48], we began our analysis by looking at whether *Antp* is activated when *tsh/tio* is mis-expressed. In wild type and ey^{LB} mutants the antenna does not express *Antp* [49] (Fig 9F). *Antp* is kept off in wild type discs (in most cases), despite the forced expression of *tsh/tio* (S9A,B Fig). In contrast, *Antp* expression is activated quite frequently within the antennal field when *tsh*/*tio* are expressed in ey^{LB} mutants. This increase in *Antp* expression might indicate a role for Pax6 in repressing *Antp* transcription. This would complement a post-transcriptional activity that Pax6 and Hox proteins are reported to play in inactivating each other [50]. However, *Antp* is activated within the ventral head epidermis (Fig 9G,H, green arrows), which is not the position from which the arista is formed. Thus, in this case, we don't believe that Antp is mediating the arista–leg transformation. Instead, we believe that the arista–leg transformation that we are seeing is actually due to a loss of *spineless* (*ss*) expression. We pursued this model since the Tsh/Tio induced arista–leg transformation that we observe is reminiscent of transformations that characterize the *aristapedia* allele of *ss* (ss^{a}) [51,52].

Ss protein is distributed within the aristal segment in both wild type and ey^{LB} mutant discs (Fig 9I). However, if *tsh*/*tio* are expressed within the *dpp*-GAL4 domain, then *ss* expression is lost in the arista (Fig 9J,K, red arrows). A transcriptional reporter (*ss-lacZ*) that drives expression within the aristal segment [53] is also responsive to Tsh/Tio (Fig

9L-N), suggesting that both genes are acting on the *ss* aristal enhancer. While it is not clear if either Tsh or Tio is directly binding to the enhancer, our model is that the arista–leg transformation is due to an inhibition of *ss* expression by Tsh/Tio. Additionally, we have evidence suggesting that the repression of *ss* is independent of *Distalless (Dll)* and *hth,* two key antennal selector genes that are upstream regulators of *ss* [52,54-56]. The expression of neither gene is affected when *tsh*/*tio* are expressed within the antenna (S9F-K Fig).

We also tested *Lim1* and *aristaless (al),* both of which are expressed in the distal most segments of the antenna and leg [57,58]. Upon induction of Tsh/Tio, *al* and *Lim1* are always lost within the ventral head epidermis in both wild type and ey^{LB} mutant antennal discs (S9L-Q Fig, Fig 10A-C). In about 14% of the wild type discs we see that both genes are maintained in the arista and *ey* expression is not initiated in either the arista or the ventral head epidermis (Fig 10A). We predict that these discs will eventually give rise to animals that do not have ectopic eyes. In contrast, within the majority of discs we observe an induction of *ey* in addition to the loss of *al* and *Lim1* within the ventral head epidermis (Fig 10B, green arrow). These discs will most likely give rise to adult heads that contain ectopic eyes on the ventral head as earlier reported [13,15-17]. Interestingly, we also observe discs in which *al* and *Lim1* are lost, while *ey* is ectopically expressed within the aristal segment. We predict that the adult heads derived from these discs will harbor the arista–eye transformation (Fig 10C, Fig 9B). Our results suggest that the presence of both Al and Lim1 combined with loss of Ss in the aristal ring is critical for the arista–leg transformation, and that loss of Al and Lim1 in the arista is due to *ey* induction. A more complicated situation involves Dac, which is lost within the A3 ring (S9R-T Fig, orange

arrow) but activated in the ventral head epidermis (S9R-T Fig, green arrows). Our results suggest that transformation of ventral head epidermis into eyes and the arista into eyes, legs, and head epidermis is the result of two distinct but equally important events: (1) activation of the RD network and (2) inhibition of an endogenous non retinal gene regulatory network.

DISCUSSION

The RD gene network is thought to control many aspects of early eye development, including the promotion of cell proliferation, the suppression of apoptosis, the selection of tissue fate, and the initiation/progression of the morphogenetic furrow. Several reports over the last decade and a half [11,59-61] have hinted that it is also responsible for the development of the rest of the eye-antennal disc, which, in addition to the eye, gives rise to the antenna, ocelli, head epidermis, and maxillary palps. We have recently shown that Ey and Toy, which sit at the top of the entire eye/lens gene regulatory network, control growth of the entire eye-antennal disc [10]. Without Ey/Toy, the entire eye-antennal disc fails to grow and the adults are headless. This loss is caused by an increase in apoptosis and a dramatic decrease in cell proliferation. In that report and in the results described here, we suggest that the control of tissue growth downstream of Ey/Toy is bifurcated into two branches (Fig 11). One branch involves the promotion of cell proliferation by Eyg and the Notch signaling pathway [10]. In this report, we describe that Ey/Toy also suppresses apoptosis and that this occurs through Tsh, another member of the RD network (Fig 11). The ability of Tsh to suppress cell death appears to be conserved from flies to mammals [33]. Both of these activities appear to be taking place during embryogenesis and the first larval instar.

By the second larval instar, the expression patterns of *tsh*, *eyg*, *ey*, and *toy*, which started off quite broad and throughout the entire eye-antennal disc, are now restricted to a zone of undifferentiated retinal progenitor cells within the eye (Fig 7A-C) [7-9,28]. All of the available evidence accumulated so far points to a model in which these genes, together with the other RD network members, function within the retinal progenitor cells

to promote the growth and specification of the eye (Fig 11) [62-65]. If the network is disrupted then the eye fails to be specified, the morphogenetic furrow fails to initiate, the eye field experiences a dramatic rise in cell death, and the tissue fails to proliferate. In addition, several selector genes that are expressed in the antenna and head epidermis are now de-repressed within the retinal progenitor zone [11,43,45,66]. This suggests that an additional role of the RD network is to prevent non-ocular selector genes from being expressed in the eye and promoting inappropriate fates from being selected (Fig 11).

If Ey, Toy, Eyg, and Tsh play such vital roles in promoting tissue growth then why are they segregated away from the antenna and head epidermis when it continues to proliferate and grow? It is because their continued expression in the antennal disc induces ectopic eye formation within the adult antenna and ventral head epidermis [8,12,16,28]. This shifting role requires that the expression of these genes be segregated away from the antennal disc. We focused on the ectopic expression of *tsh* and *tio* because these genes lead not only to the formation of ectopic eyes within the arista and head epidermis, but both genes also transform the arista into tarsal legs and head epidermal tissue (Fig 12, left panel). The ability to induce so many different fate transformations is a unique trait amongst all members of the RD network. All other network members, when expressed in the antenna, just induce ectopic eye formation [64]. Another unique feature of Tsh/Tio is that the arista–eye transformation can be redirected towards the arista–leg and arista–head epidermis fate switch if another RD gene is simultaneously reduced while *tsh*/*tio* are being expressed (Fig 12, left panel). In all other cases, if you induce ectopic eyes with one gene and simultaneously remove another gene, the ectopic eye simply reverts to endogenous tissue fate [67-70].

During our investigation of these different types of transformations, we observed several interesting trends in gene expression alterations. For example, in order for Tsh/Tio to transform the arista into an eye, the *Lim1*, *al*, and *ss* selector genes must all be turned off while the *ey*/*eya*/*so* retinal genes are all activated. In contrast, the arista–leg transformation occurs when *Lim1* and *al* remain activated while *ss* is turned off. Interestingly, it is not just the state of the antennal selector genes that is important. Instead, the state of the RD genes is just as critical (Fig 12, right panel). When the arista transforms into a leg, *ey*/*eya*/*so* are all off, while in the arista–head epidermis transformation *ey* expression is activated (Fig 12, right panel). These findings suggest that the induction of ectopic eyes involves two distinct but equally essential processes: (1) the activation of the RD network and (2) the repression of endogenous non-ocular gene regulatory networks. While that former activity is not surprising and has been shown in multiple publications, the latter role in repressing endogenous gene regulatory networks has been underappreciated. In fact, current thinking has been that the induction of ectopic eyes is the simple result of expressing an eye specification gene (and the entire network as well) at levels that are significantly higher than the endogenous network (due to the use of mis-expression systems such as UAS/GAL4). We propose that the induction of ectopic eyes is a more complicated developmental event with the deliberate promotion of the retinal pathway occurring simultaneously with the purposeful suppression of non-ocular endogenous networks. One could also extend this concept to any cell or tissue fate change, particularly homeotic-class transformations of entire imaginal discs and/or body segments.

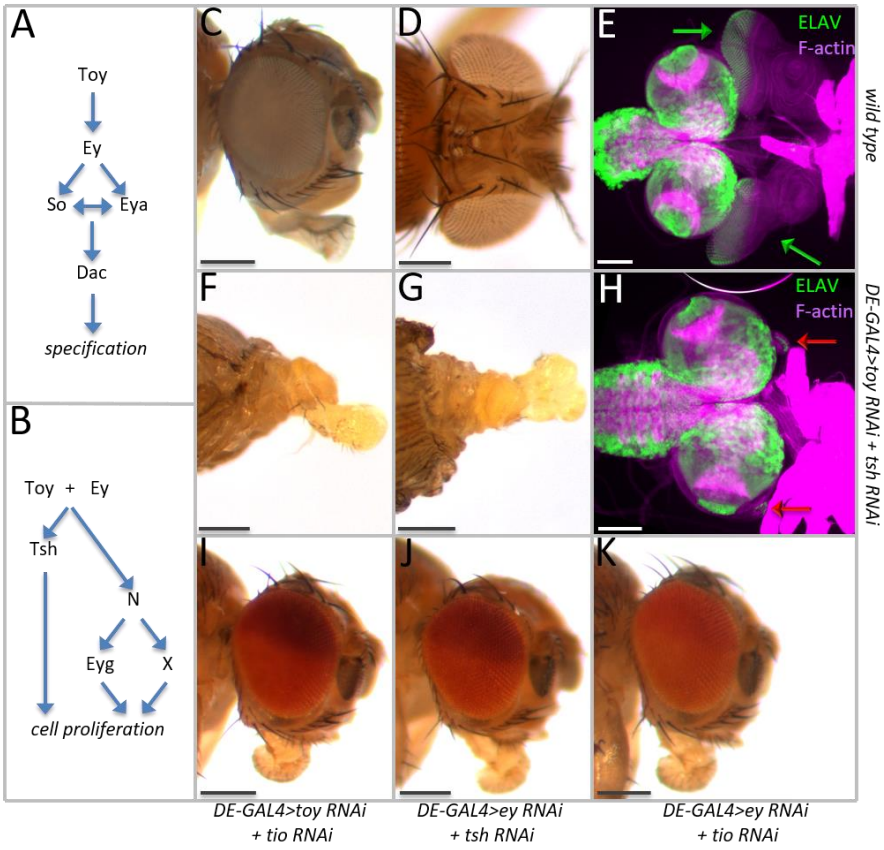

Figure 1. Simultaneous removal of Toy/Tsh eliminates the eye-antennal disc. (A) Schematic diagram of how the RD network regulates eye specification. **(B)** Schematic of how the RD network might control cell proliferation as described by Zhu et al., 2017. **(C)** Side view of a wild type head. **(D)** Dorsal view of a wild type head. **(E)** Light microscope image of a pair of eye-antennal discs (green arrows) from a wild type third instar larva. **(F)** Side view of a *DE>toy RNAi + tsh RNAi* pharate lethal headless adult. **(G)** Dorsal view of a *DE>toy RNAi + tsh RNAi* pharate lethal headless adult. **(H)** Light microscope image of the brain complex from a *DE>toy RNAi + tsh RNAi* third instar larva. The eye-antennal discs (red arrows) are rudimentary in size. **(I)** Side view of a *DE>toy RNAi + tio RNAi* adult head. **(J)** Side view of a *DE>ey RNAi + tsh RNAi* adult head. **(K)** Side view of a *DE>ey RNAi + tio RNAi* adult head. (Scale bars, 100 µm).

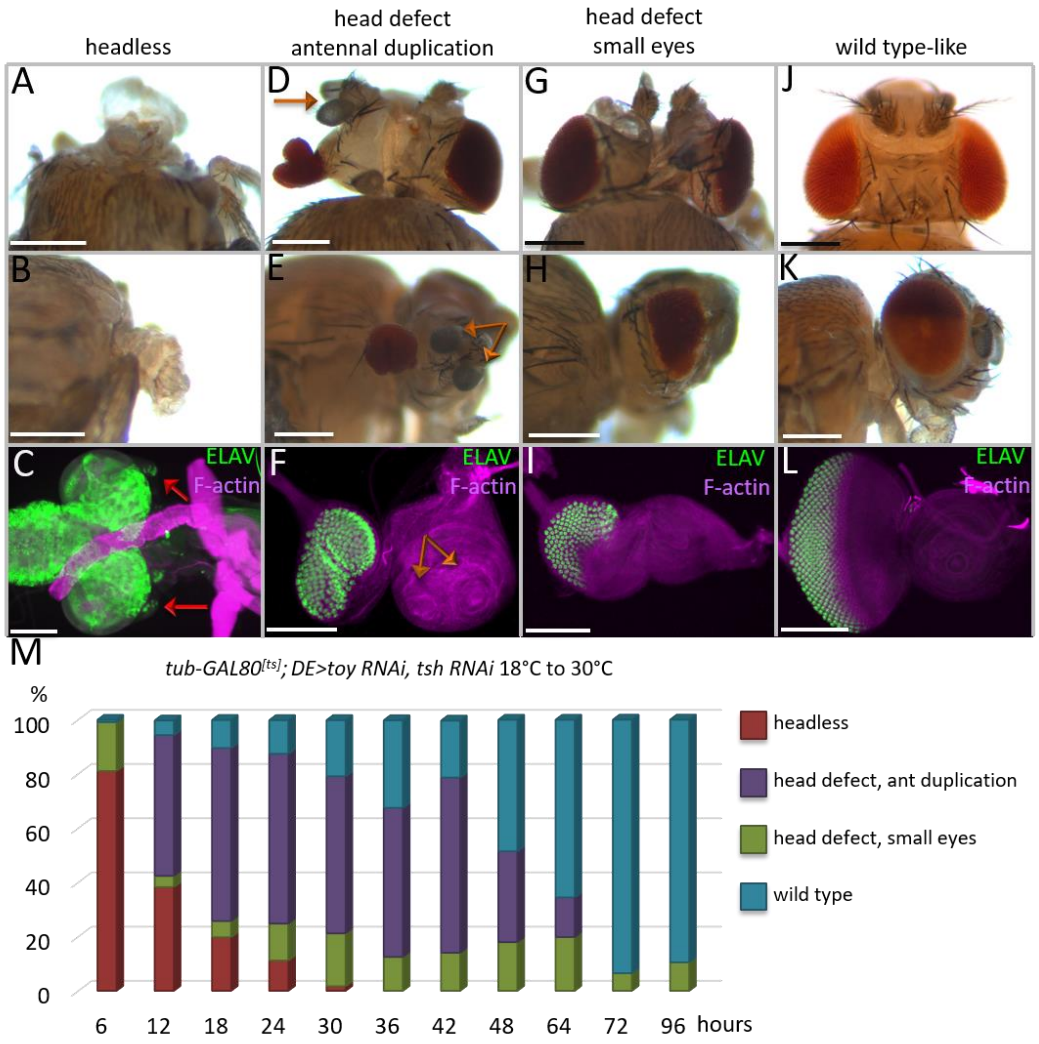

Figure 2. Toy/Tsh are required during successive temporal waves for eye-antennal disc development. (A-M) *tub-GAL80^{ts}; DE>toy RNAi + tsh RNAi*. **(A,D,G,J)** Dorsal view of adult heads. **(B,E,H,K)** Side view of adult heads. **(C,F,I,L)** Light microscope images of eye-antennal discs from third instar larvae. Anterior is to the right. Eye-antennal discs were stained with an antibody that recognizes the pan neuronal marker ELAV. Removal of Toy and Tsh at different times in development results in four major categories of phenotypes: **(A-C)** Headless, the red arrows mark the greatly reduced eye-antennal discs. **(D-F)** Head defects with antennal duplications, the orange arrows mark the duplicated antennal segments. **(G-I)** Head defects with small eyes. **(J-L)** Wild type-looking

heads and eye-antennal discs. **(M)** Time-course of Toy/Tsh removal during development. Embryos/larvae were first kept at the permissive temperature of GAL80 (18°C) for the times listed on the X-axis before being shifted to the non-permissive temperature (30°C). Animals were either dissected as late third instar larvae or allowed to reach the pharate adult stage. The graph shows the percentage of animals that have each of the four phenotypes (Y-axis) during each experiment. (N ≥ 100 in each experiment) (Scale bars, 100 μm).

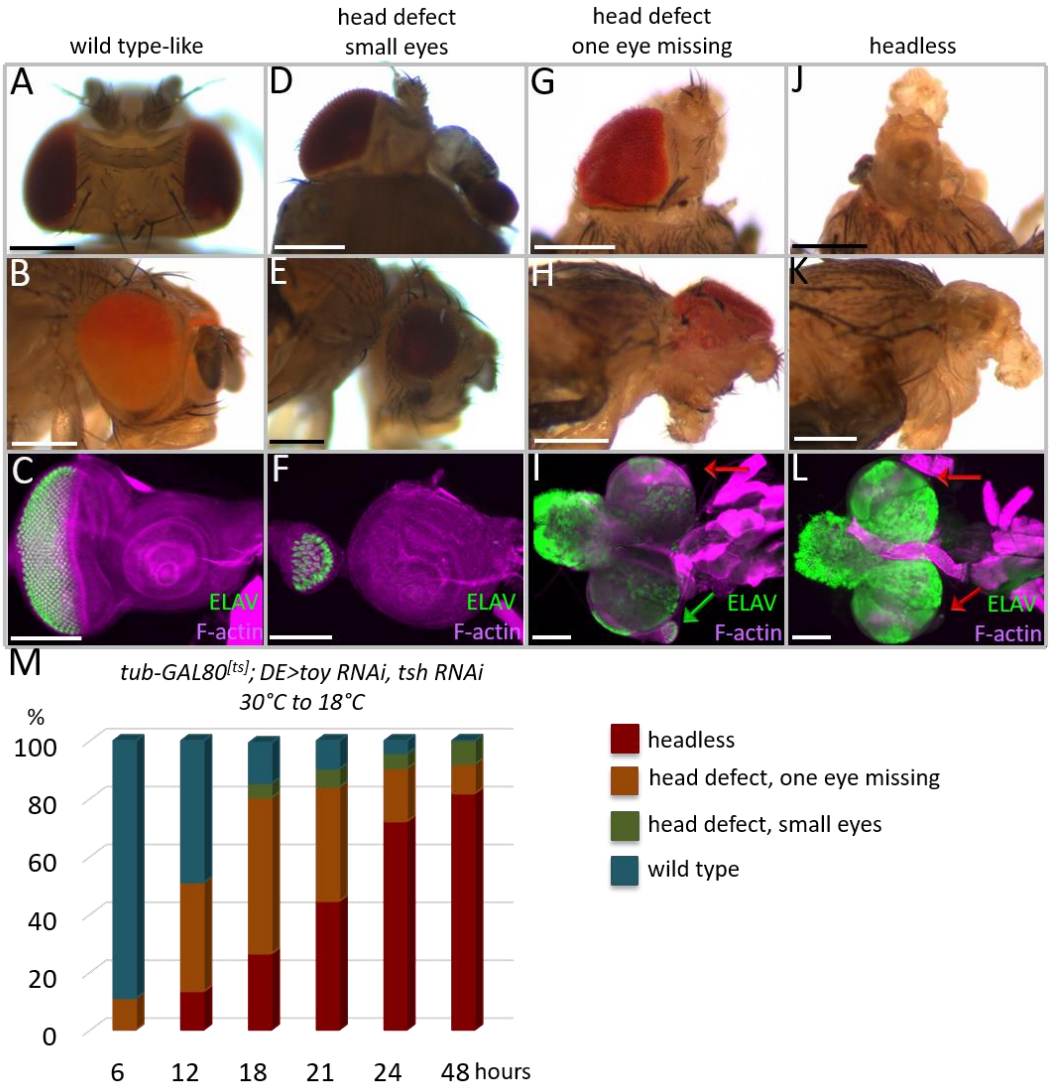

Figure 3. Toy/Tsh are required for growth of the entire eye-antennal eye disc during early larval instars. (A-M) *tub-GAL80^{ts}; DE>toy RNAi + tsh RNAi*. **(A,D,G,J)** Dorsal view of adult heads. **(B,E,H,K)** Side view of adult heads. **(C,F,I,L)** Light microscope images of eye-antennal discs from third instar larvae. Anterior is to the right. Eye-antennal discs were stained with an antibody that recognizes the pan neuronal marker ELAV. **(M)** Time-course for the restoration of Toy/Tsh to the eye-antennal disc. Embryos/larvae were first kept at the non-permissive temperature of GAL80 (30°C) for the times listed on the X-axis before being shifted to the permissive temperature (18°C). Animals were either dissected

as late third instar larvae or allowed to reach the pharate adult stage. The graph shows the percentage of animals that were scored (Y-axis) during each experiment. Depending upon the temporal window at which Toy/Tsh are restored to the eye antennal discs, it is possible to either fully **(A-C,M)** or partially **(D-I)** rescue defects to the eye, antenna, and head epidermis. However, it becomes exceedingly difficult to restore the eye-antennal disc after the first larval instar. (N ≥ 100 in each experiment) (Scale bars, 100 μm).

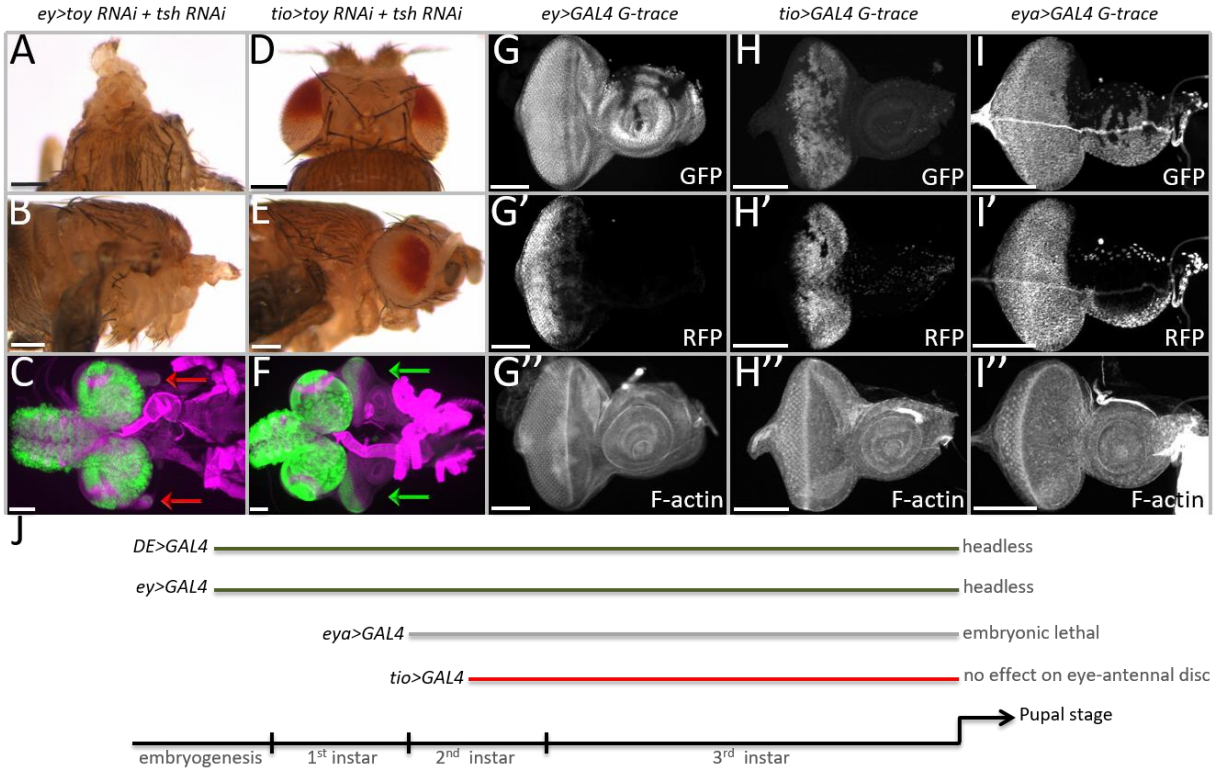

Figure 4. Toy/Tsh are required for growth of the eye-antennal disc prior to the segregation of the eye and antennal fields. (A-C) *ey-GAL4, UAS-toy RNAi + UAS-tsh RNAi.* Removal of Toy/Tsh using the *ey-GAL4* driver results in the loss of the eye-antennal imaginal discs and in headless pharate lethal flies. **(D-F)** *tio-GAL4, UAS-toy RNAi + UAS-tsh RNAi*. Loss of Toy/Tsh using the *tio-GAL4* driver has no effect on the development of the eye-antennal disc. **(G-I)** Light microscope images of third larval instar eye-antennal discs showing historical (GFP) and real-time (RFP) expression patterns of *ey-GAL4* **(G),** *tio-GAL4* **(H)** and *eya-GAL4* **(I)**. Anterior is to the right in all images of eye-antennal discs. **(J)** Schematic depicting the onset of expression of individual GAL4 lines used in this study. Removal of Toy/Tsh using early drivers (*DE-GAL4* and *ey-GAL4*) leads to the loss of the eye-antennal discs and in headless pharate lethal adults. However, removal of Toy/Tsh with the late acting driver (*tio-GAL4*) has no effect on eye-antennal

disc development. This suggests that the critical window for Toy/Tsh in promoting growth of the eye-antennal discs lies between stage 12 of embryogenesis and the middle of the second larval instar. These results are consistent with the time-course experiments described in Figures 2 and 3. (Scale bars, 100 μm).

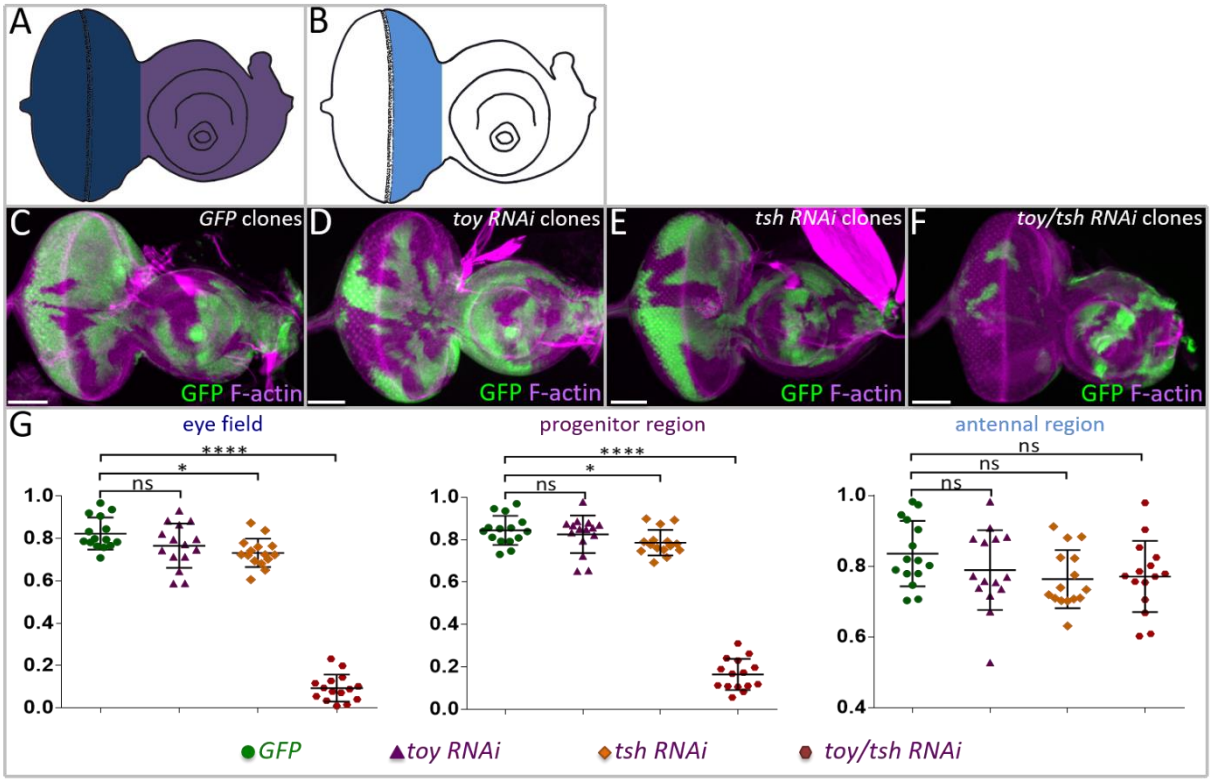

Figure 5. Loss of Toy/Tsh in clones leads to a loss of tissue growth. (A,B) Drawings of third larval instar eye-antennal discs in which the entire eye field (dark blue), retinal progenitor domain (light blue) and antennal region (purple) are demarcated. **(C-F)** Light microscope images of eye-antennal discs containing *wild type* **(C)**, *toy RNAi* **(D)**, *tsh RNAi*, and *toy/tsh RNAi* clones – all clones are marked by GFP. Anterior is to the right. **(G)** Comparison of clone size in the eye field, retinal progenitor domain, and antennal field. The individual loss of Toy or Tsh has no effect on the size/growth of the clone. However, the combined loss of Toy/Tsh inhibits clone growth within the progenitor region and eye field. As the expression of both genes is withdrawn from the antennal disc by the end of the first larval instar, there is no noticeable effect on clone size within the antenna. N=15 per genotype, *P ≤ 0.1, **P ≤ 0.01, ***P ≤ 0.001, ****P ≤ 0.0001 (Scale bars, 50 µm).

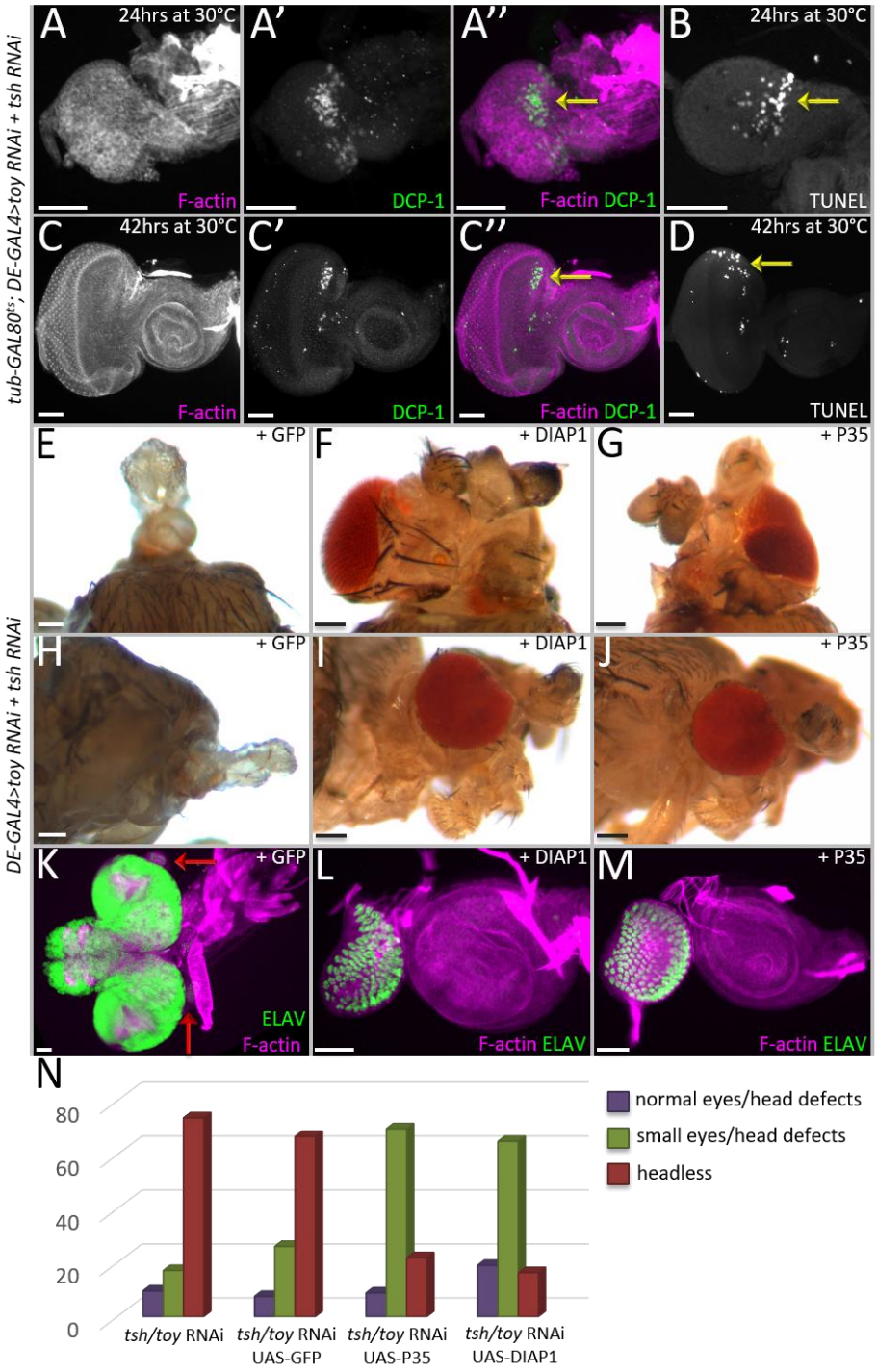

Figure 6. Cell death is a leading cause of the headless phenotype in *tsh/toy* mutant animals. (A-D) Light microscope images of eye-antennal discs showing apoptotic cells in the dorsal compartment (yellow arrows) where Toy and Tsh are removed. **(A-D)** *tub-*

GAL80^{ts}; DE>toy RNAi + tsh RNAi **(A,B)** 24hrs at 30°C **(C,D)** 42hrs at 30°C. **(E-J)** Dorsal and side views of adult heads in which expression of P35 and DIAP1 has partially restored eye and head development. **(K-M)** Light microscope images of eye-antennal discs showing partial restoration of the eye-antennal disc. **(E,H,K)** *DE-GAL4, UAS-toy RNAi, UAS-tsh RNAi, UAS-GFP*. **(F,I,L)** *DE-GAL4, UAS-toy RNAi, UAS-tsh RNAi, UAS-DIAP1*. **(G,J,M)** *DE-GAL4, UAS-toy RNAi, UAS-tsh RNAi, UAS-P35*. **(N)** Graph quantifying the degree of rescue when cell death is blocked. (N ≥ 25 in each experiment) (Scale bars, 50 µm).

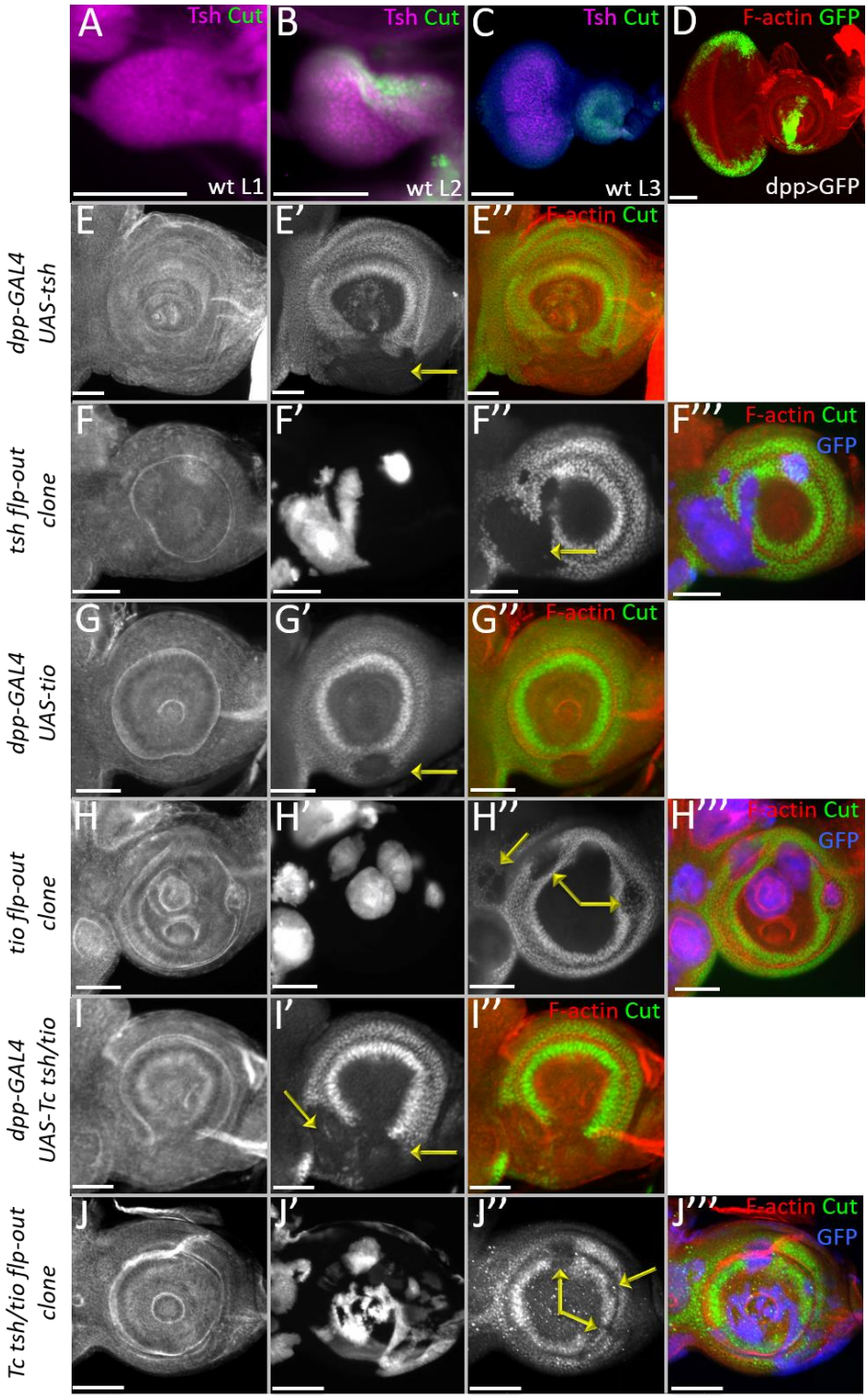

Figure 7. Continued presence of Tsh/Tio in the antennal disc inhibits *cut* expression. (A-I) Light microscope images of antennal discs. **(A)** Wild type first instar

eye-antennal disc. Tsh protein is expressed throughout the entire disc. Cut protein is not yet detected. **(B)** Wild type second instar eye antennal disc. Tsh protein continues to be found throughout the disc while Cut protein is found within the antennal portion. **(C)** Wild type third instar eye-antennal disc. Tsh protein is found just within the undifferentiated cells of the eye field while Cut protein is exclusively seen in the antennal field. **(D)** *dpp-GAL4, UAS-GFP*. The *dpp-GAL4* construct drives expression along the posterior-lateral margins of the eye field and within a ventral sector of the antennal disc. **(E,G,I)** Expression of Drosophila Tsh, Tio, or Tribolium Tsh/Tio using *dpp-GAL4*. In all cases *cut* expression is inhibited within the *dpp-GAL4* domain. **(F,H,J)** Expression of Drosophila *tsh, tio,* or *Tribolium tsh/tio* using flp-out over-expression clones. Yellow arrows in each panel demarcate areas where *cut* expression is repressed. Posterior is to the right. (Scale bars, 50 µm).

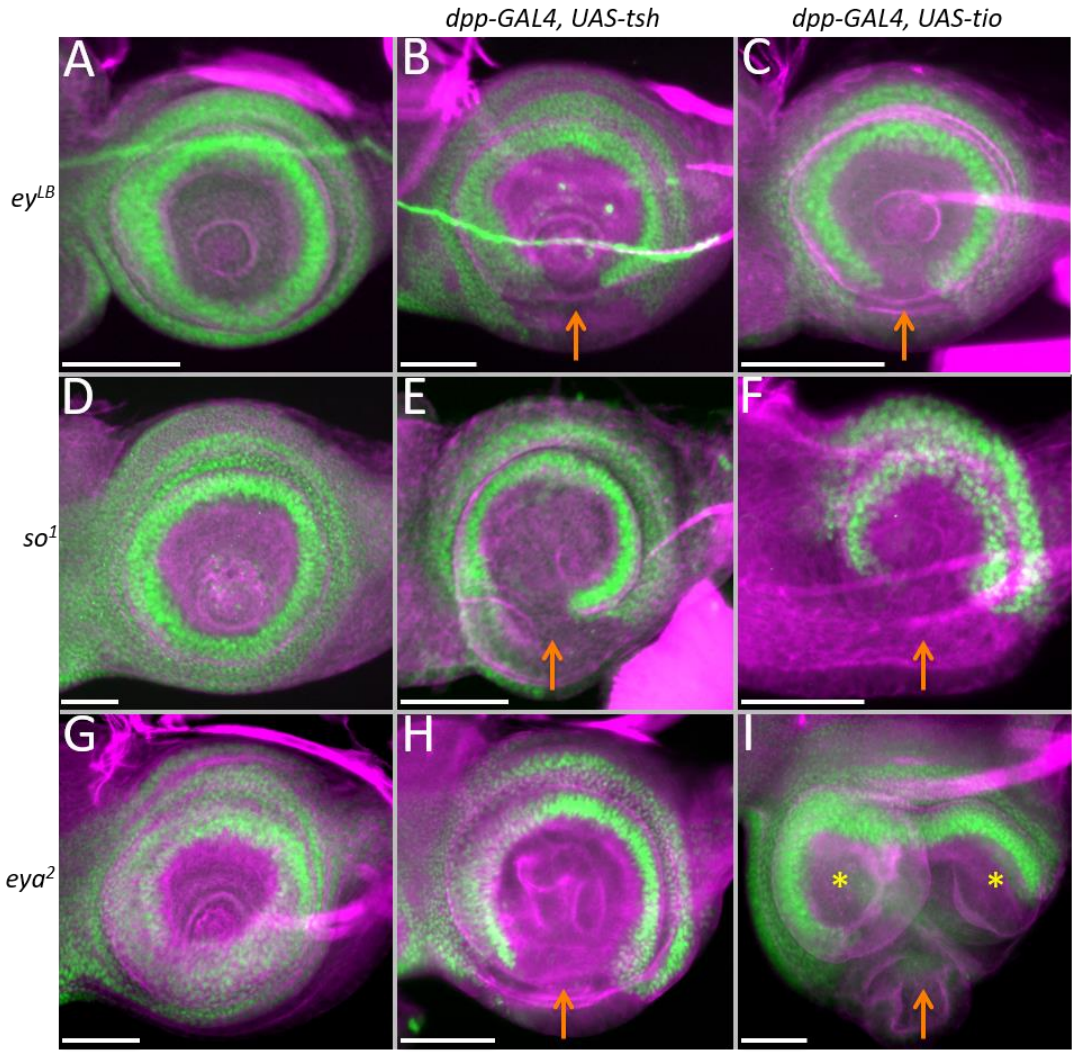

Figure 8. Repression of *cut* by Tsh/Tio is independent of the retinal determination network. (A,D,G) *cut* expression in the antennal disc of ey^{LB}, so^{1}, and eya^{2} mutant antennal discs. Note that in these mutants *cut* expression is identical to wild type. **(B,C,E,F,H,I)** Loss of *cut* expression when *tsh* **(B,E,H)** or *tio* **(C,F,I)** continues to be expressed in the antenna with *dpp-GAL4*. Orange arrows demarcate zones where *cut* expression is down regulated. Yellow asterisks mark the duplicated antennal segments. Posterior is to the right. (Scale bars, 50 µm).

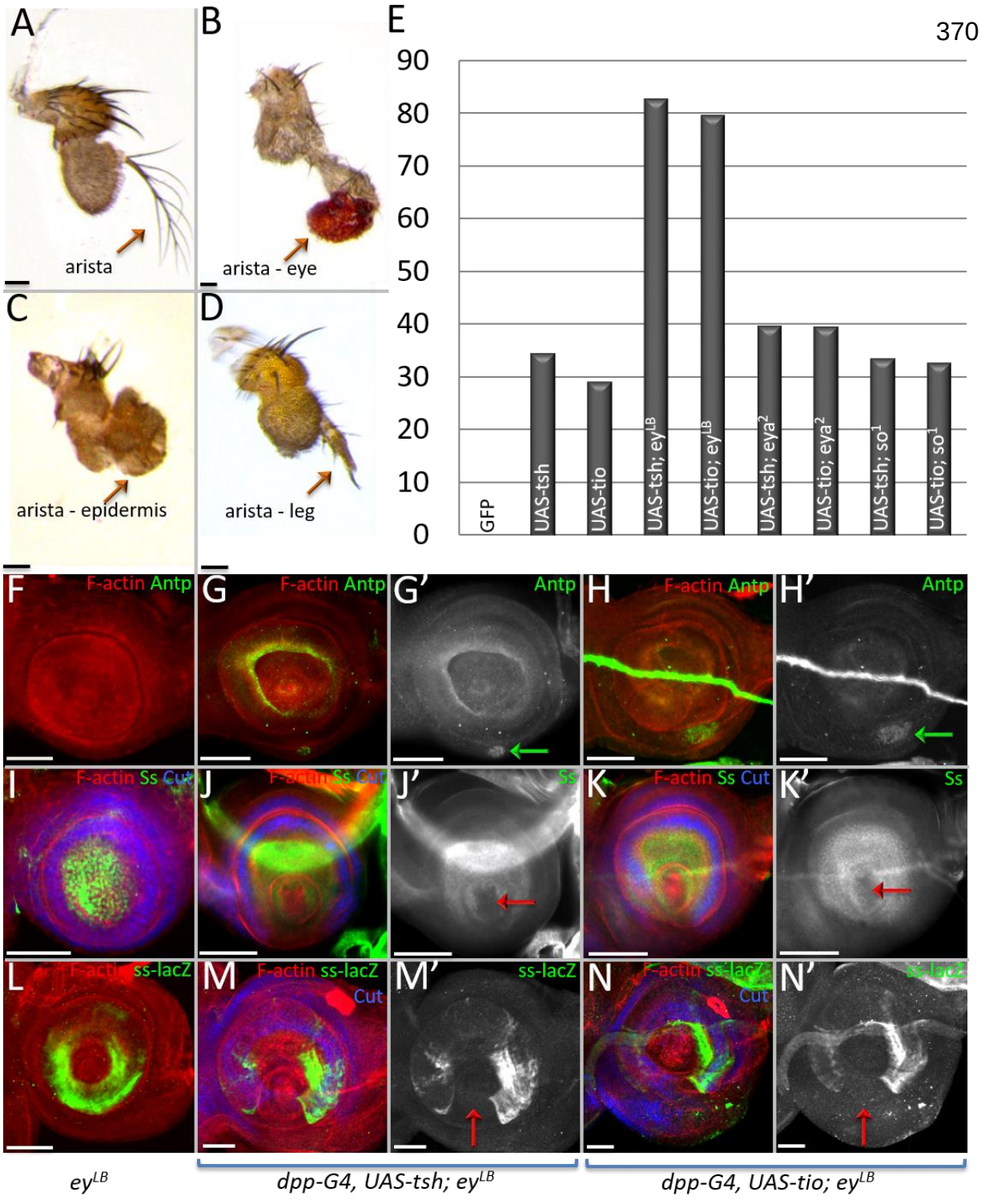

Figure 9. Continued expression of *tsh/tio* in the antennal disc alters its fate. (A-D) Light microscope images of adult antennal segments. **(A)** Wild type antenna with arista. **(B)** *dpp-GAL4, UAS-tsh*; the arista has been converted into an ectopic eye. **(C)** *eya*^{2}, *dpp-*

GAL4, UAS-tsh; the arista is transformed into head epidermal mass. **(D)** *dpp-GAL4, UAS-tsh*, ey^{LB}; the arista has been transformed into the leg tarsal segment. **(E)** Chart documenting the percentage of arista to leg transformations when *tsh/tio* are expressed in wild type and RD gene mutants (N ≥ 35). **(F-N)** Light microscope images of third larval instar antennal segments. Posterior is to the right in all antennal disc images. **(F,I,L)** ey^{LB} **(G,J,M)** *dpp-GAL4, UAS-tsh;* ey^{LB} **(H,K,N)** *dpp-GAL4, UAS-tio;* ey^{LB} **(F)** *Antp* is not expressed normally in the antennal field. **(G,H)** Tsh/Tio are capable of activating *Antp* expression (green arrows). **(I)** Ss protein is present throughout the entire aristal segment. **(J,K)** Tsh/Tio repress *ss* expression within a portion of the aristal segment (red arrows). **(L)** A *ss-lacZ* construct is expressed within a subdomain of the aristal segment. **(M,N)** Tsh/Tio are capable of repressing the activity of the *ss* antennal enhancer (red arrows). (Scale bars, 50 μm).

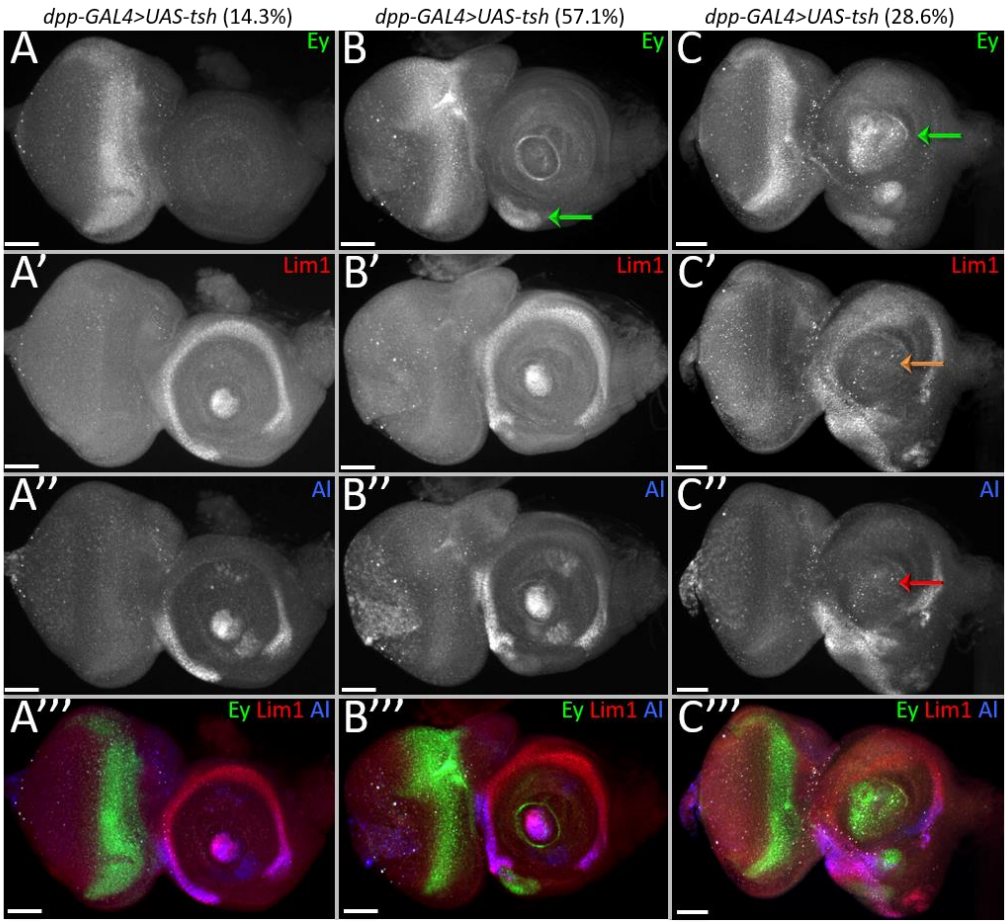

Figure 10. Homeotic transformations mediated by ectopic expression of Tsh. (A-C) Light microscope images of *dpp-GAL4, UAS-tsh* third larval instar eye-antennal discs. **(A)** In this example, the targeted expression of *tsh* does not induce *ey* expression (14.3%). The adult tissues are slightly disrupted without any homeotic transformations. **(B)** In some discs (57.1%), the expression of *tsh* induces *ey* expression within the head epidermis (green arrow) which results in the transformation of head epidermis into eye tissue. **(C)** In some others (28.6%), the expression of *tsh* can activate *ey* (green arrow) and repress both *Lim1* (orange arrow) and *al* (red arrow) expression within the aristal segment. This transforms the arista into a compound eye. Anterior is to the right. N = 21 (Scale bars, 50 µm).

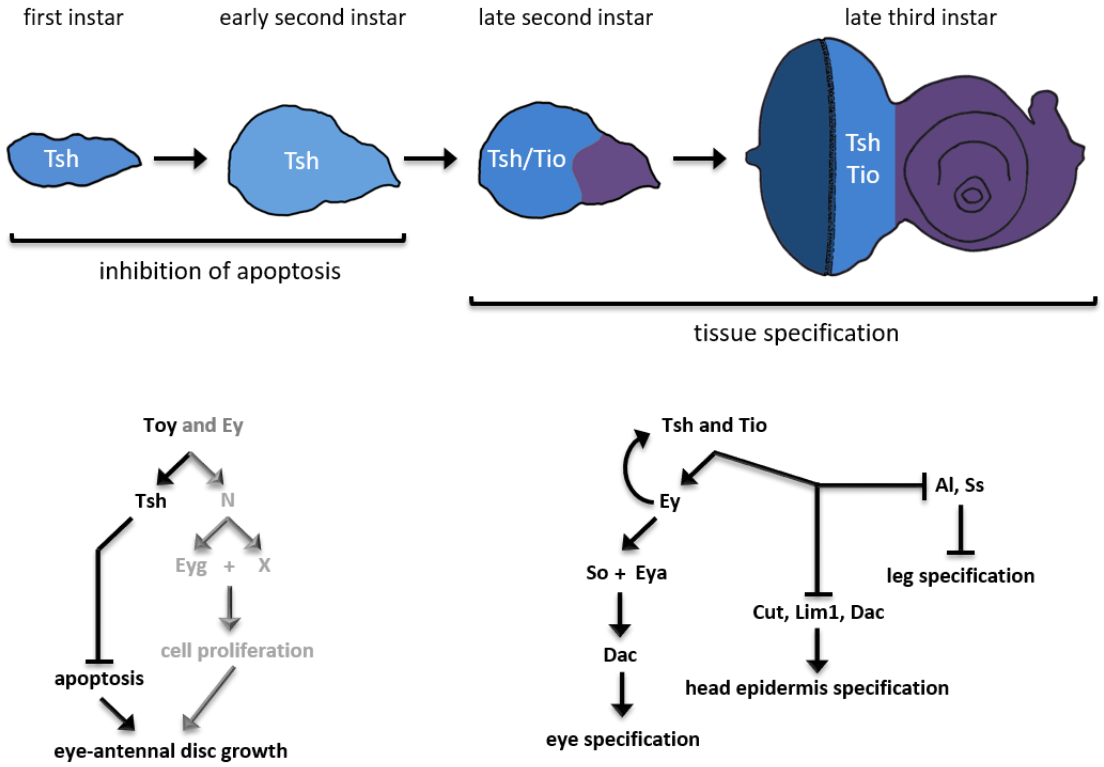

Figure 11. Summary of the role that Tsh/Tio play in the eye-antennal disc. Within the first and early second larval instars, *tsh* is expressed throughout the entire eye-antennal disc. During these developmental stages, Tsh cooperates with Toy to suppress apoptosis. In their combined absence, the entire eye-antennal disc is lost. Prior findings from our group have indicated that N/Eyg function in parallel to Tsh to promote cell proliferation throughout the entire disc (grey lettering, Zhu et al., 2017). The Pax6 proteins Toy and Ey function upstream of all three Tsh, N, and Eyg (Zhu et al., 2017; this report). During the late larval second instar, *tsh* expression is restricted to the eye disc and *tio* expression is initiated (also within the eye disc). By the third larval instar both proteins are restricted to the undifferentiated cells ahead of the advancing morphogenetic furrow. If Tsh/Tio remains in the antennal field during these later developmental stages they induce ectopic eyes, suppress head epidermis development, and relieve the default repression on leg development.

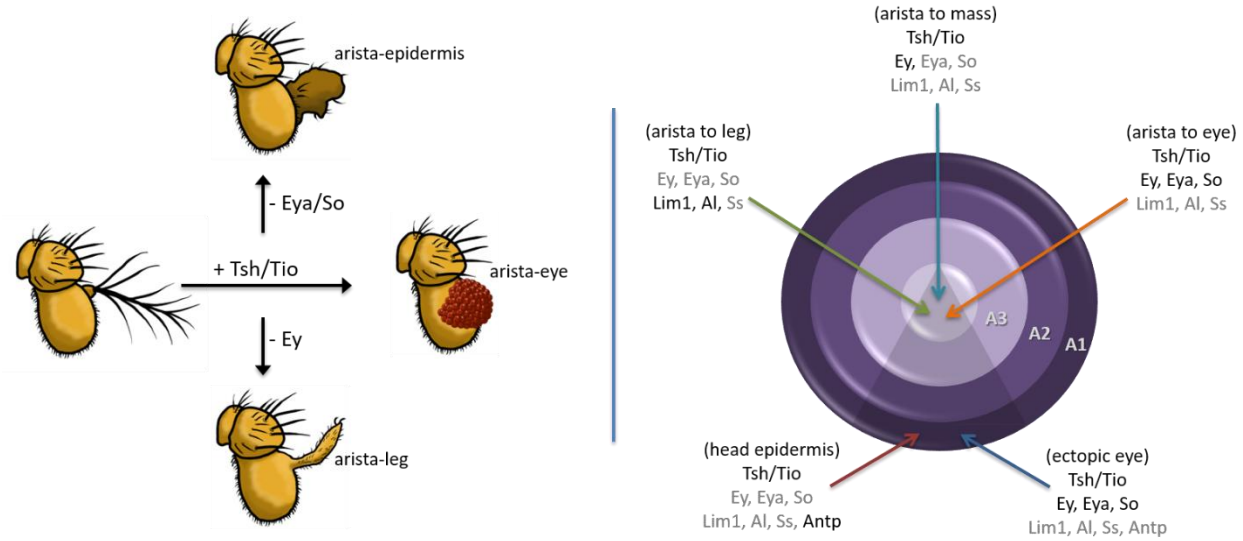

Figure 12. Summary of Tsh/Tio dependent antennal transformations. (Left panel) If Tsh/Tio remain in the antennal disc, then the arista can be transformed into an ectopic eye. Similar transformations of the ventral head epidermis are also observed (not depicted). If *ey* expression is eliminated, then Tsh/Tio transform the arista into the tarsal portion of the leg. Interestingly, if *ey* expression is maintained but transcription of downstream members such as *eya* and *so* are lowered, then the arista does not take on a particular alternate fate but instead grows as head epidermal mass. **(Right panel)** The positions of the various transformations that are caused by the presence of Tsh/Tio in the antennal discs are depicted. Included are the on/off states of a number of eye, antennal, and head epidermal genes. Genes coded in black are in the “on” state while genes listed in grey are in the “off” state. Our results indicate that the arista–leg transformation appears to be due to the loss of *ss* rather than an up-regulation of *Antp*. The repression of antennal and head epidermal genes by Tsh/Tio appears to occur independently of the Ey/Eya/So module of the RD network.

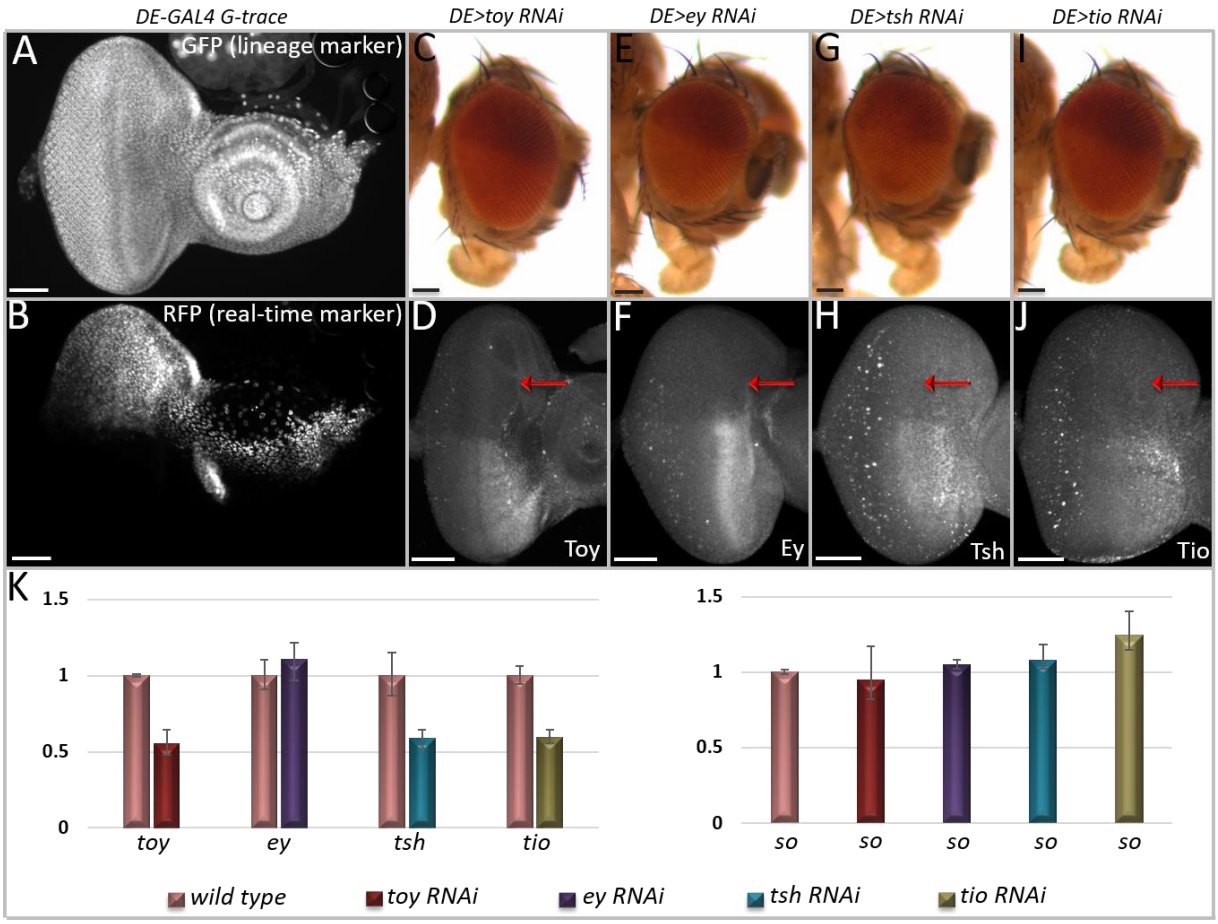

Supplemental Figure 1. The RNAi lines used in this study are efficacious in reducing target gene transcripts and protein levels. (A,B) Light microscope images showing the lineage tracing **(A)** and real time **(B)** expression of the *DE-GAL4* driver. Since GFP (lineage marker) is present in all cells of the imaginal disc **(A)**, the driver should be expressed throughout the entire disc at some point in development. In a previous study (Zhu et al., 2017) we confirmed that *DE-GAL4* driver is expressed throughout the disc during embryogenesis and the first larval instar. **(C,E,G,I)** Light microscope images of adult heads. **(D,F,H,J)** Light microscope images of third instar eye discs. **(C,D)** *DE>toy RNAi* **(E,F)** *DE>ey RNAi* **(G,H)** *DE>tsh RNAi* **(I,J)** *DE>tio RNAi*: expression of each RNAi individually has no effect on the overall structure of the adult head **(C,E,G,I)** even though

each RNAi line reduces levels of the target below detection levels (**D,F,H,J,** red arrows). **(K)** Quantitative RT-PCR showing target transcript levels from entire wild type and mutant eye-antennal discs. The remaining transcripts in each mutant sample are from the ventral half of the disc. Note that the expression of *toy*, *tsh*, and *tio* is reduced by approximately 50%, which is expected based on the *DE-GAL4* pattern. *ey* transcripts appear unaffected although we observe a complete elimination of Ey protein in the dorsal half of the eye **(F)**. One possible explanation is that there is compensatory expression of the *ey* gene within the ventral half of the retina. Note that *so* expression is not affected in any of the mutants, which is expected since the eyes are structurally normal. All qPCR samples were run in biological triplicate and normalized to the reference gene *rp49*. (Scale bars, 50 μm).

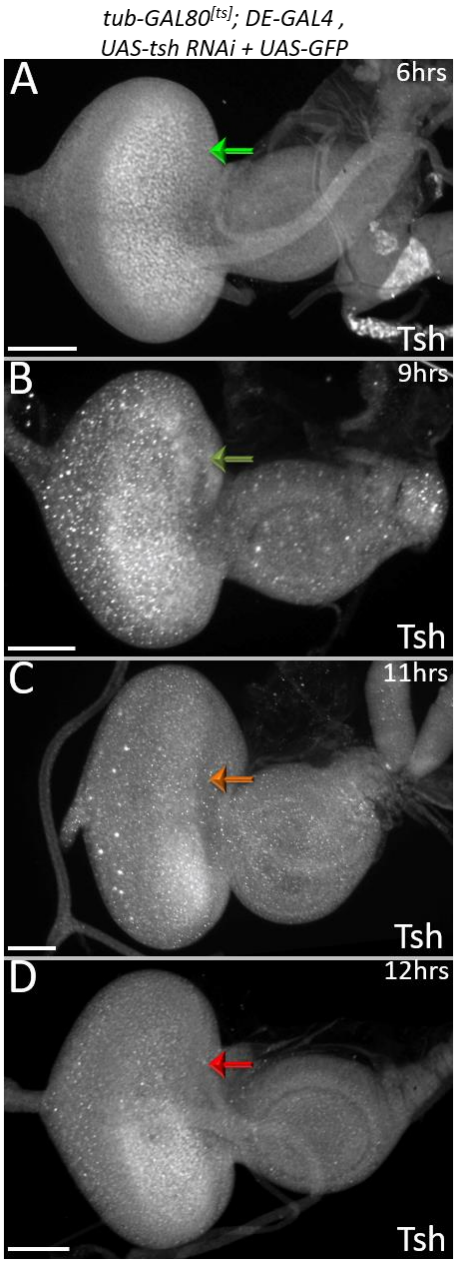

Supplemental Figure 2. Tsh protein is completely removed after 12hrs of RNAi treatment. (A-D) *tub-GAL80^{ts}; DE> UAS-tsh RNAi + UAS-GFP.* Light microscope images of third larval instar eye-antennal discs. Embryos and larvae were raised at 18°C (permissive temp for GAL80) until the third larval instar and then shifted to the non-permissive temperature (30°C). Larvae were dissected and Tsh protein level was monitored in the dorsal compartment at 6hrs (**A**, bright green arrow), 9hrs (**B**, dark green arrow), 11hrs (**C**, orange arrow), and 12hrs (**D**, red arrow) after RNAi induction. Tsh protein is completely eliminated from the dorsal half of the retina by 12hrs. In Zhu et al., 2017 we showed that Toy protein is eliminated after 10hrs of RNAi treatment. These temporal windows are incorporated into our calculations for determining the critical windows for Toy/Tsh activity. (Scale bars, 50 µm).

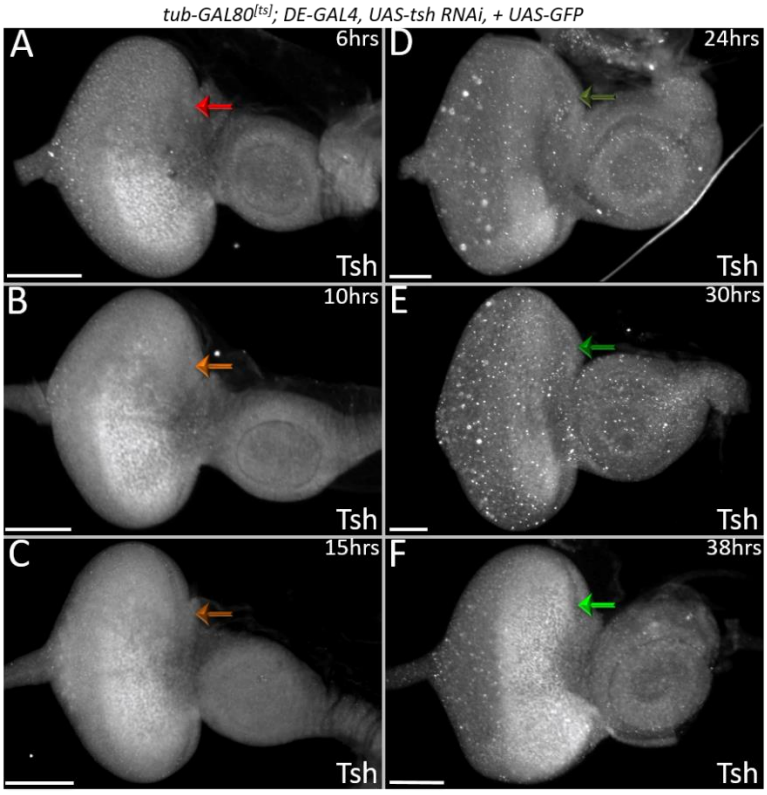

Supplemental Figure 3. Restoration of Tsh protein takes 38hrs after RNAi induction ceases. (A-F) *tub-GAL80^{ts}; DE> UAS-tsh RNAi + UAS-GFP*. Light microscope images of third larval instar eye-antennal discs. Embryos and larvae were raised at 30°C (non-permissive temp for GAL80) until the third larval instar and then shifted to the permissive temperature (18°C). Larvae were dissected and Tsh protein level was monitored in the dorsal compartment at 6hrs (**A**, red arrow), 10hrs (**B**, bright orange arrow), 15hrs (**C**, dark orange arrow), 24hrs (**D**, hunter green arrow), 30hrs (**E**, evergreen green arrow), and 38hrs (**F**, bright green arrow) after RNAi induction ceased. Tsh protein has recovered to wild type levels by 38hrs. In Zhu et al., 2017 we demonstrated that Toy protein levels recover 44hrs after RNAi induction has ended. These temporal windows are incorporated into our calculations for determining the critical windows for Toy/Tsh activity. (Scale bars, 50 µm).

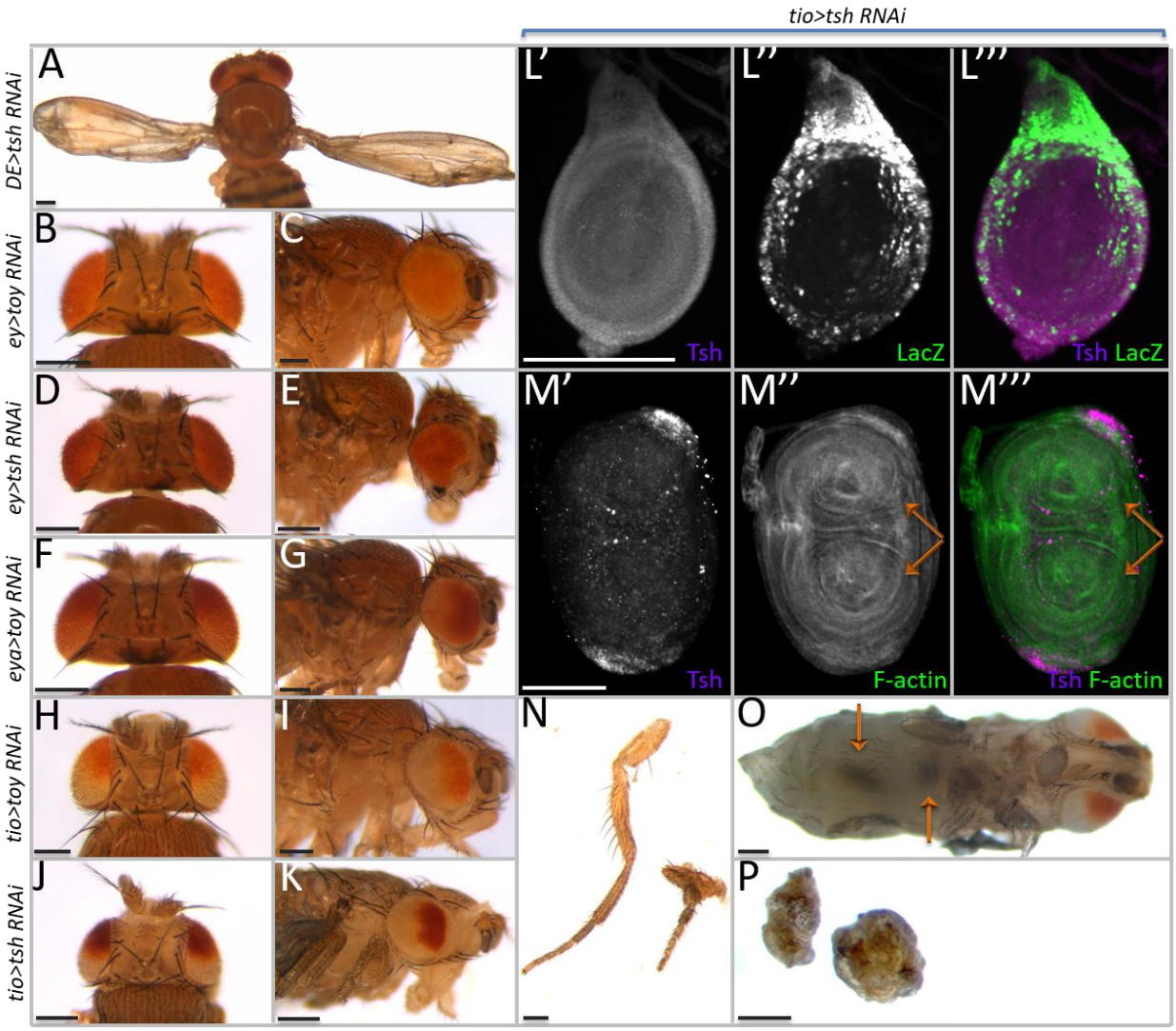

Supplemental Figure 4. Effect of losing either Toy or Tsh individually using *DE-GAL4*, *ey-GAL4*, *eya-GAL4* and *tio-GAL4*. (A) *DE-GAL4, UAS-tsh RNAi*, abnormal wing posture that is similar to the *aeroplane-like* (*ae-l*) allele of *tsh*. **(B,C)** *ey-GAL4, UAS-toy RNA*i, normal head structure**. (D,E)** *ey-GAL4, UAS-tsh RNAi;* ventral eye development is inhibited. **(F,G)** *eya-GAL4, UAS-toy RNAi*; normal head structure. **(H,I)** *tio-GAL4, UAS-toy RNAi*; normal head structure. **(J,K)** *tio-GAL4, UAS-tsh RNAi*; normal head development. **(L)** *tio-GAL4, UAS-lacZ* leg disc showing *tio* expression pattern. **(M-P)** *tio-GAL4, UAS-tsh RNAi*. **(M)** The loss of Tsh leads to the duplication of the leg disc (orange

arrows). This is similar to the antennal duplication that results from the loss of Tsh. **(N)** The resulting adult legs (right) are considerably smaller than their wild type counterparts (left). **(O)** Some adult legs fail to extend and are often buried within the abdomen, orange arrows. **(P)** The internalized adult legs after dissection. (Scale bars, 100 μm).

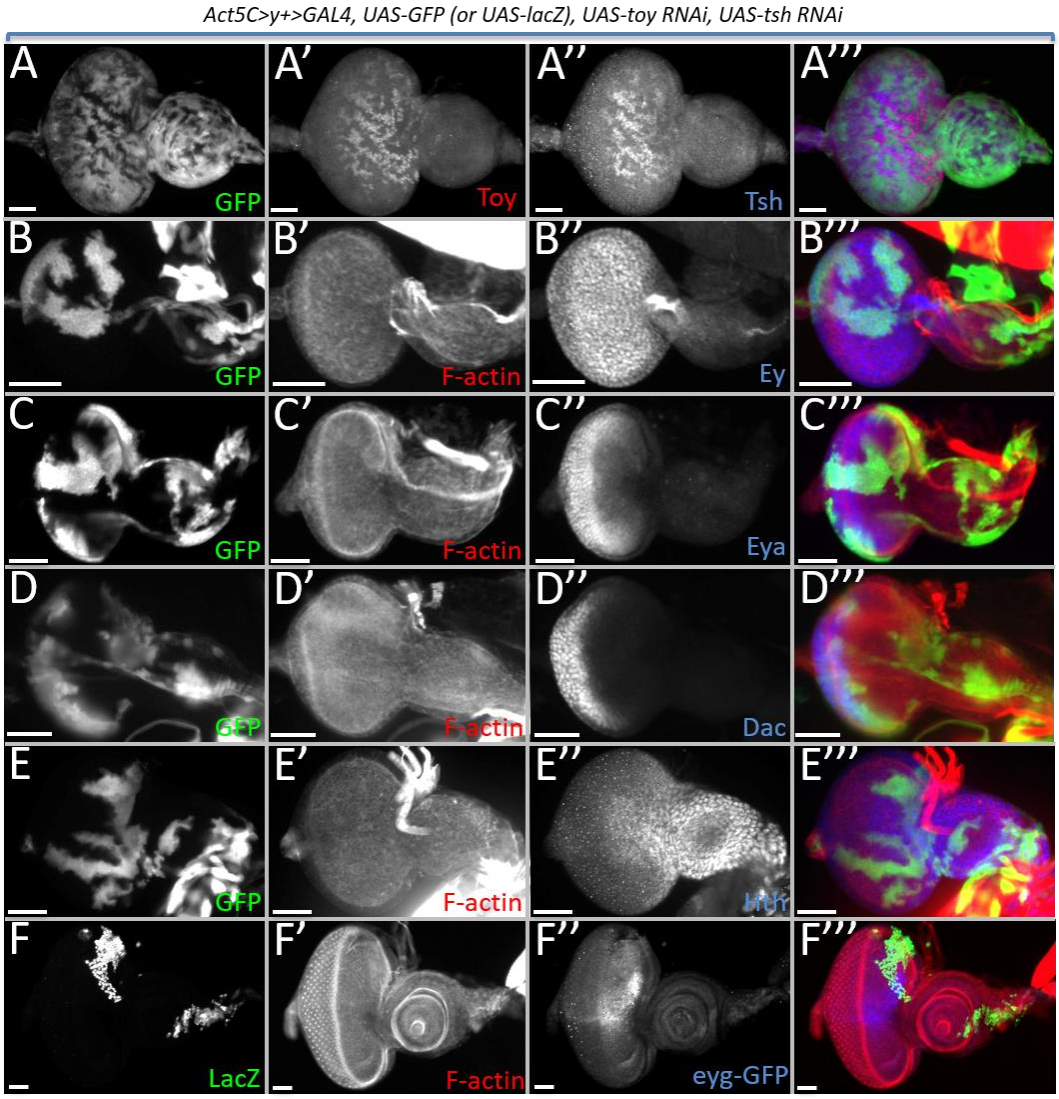

Supplemental Figure 5. Control of early eye-antennal disc development by Toy/Tsh is independent of the RD network. (A-F) Light microscope images of eye-antennal discs from either *Act5C>y+>GAL4, UAS-GFP, UAS-toy RNAi, UAS-tsh RNAi* **(A-E)** or *Act5C>y+>GAL4, UAS-LacZ, UAS-toy RNAi, UAS-tsh RNAi* **(F)** containing clones simultaneously expressing *toy* RNAi and *tsh* RNAi constructs (marked with GFP or LacZ). **(A)** In clones, the RNAi constructs efficiently knockdown expression of both *toy* and *tsh*. **(B-F)** The expression of *ey* **(B)**, *eya* **(C)**, *dac* **(D)**, *hth* **(E)**, and *eyg-GFP* **(F)** are not affected by the combined loss of Toy/Tsh. Anterior is to the right. (Scale bars, 25 µm).

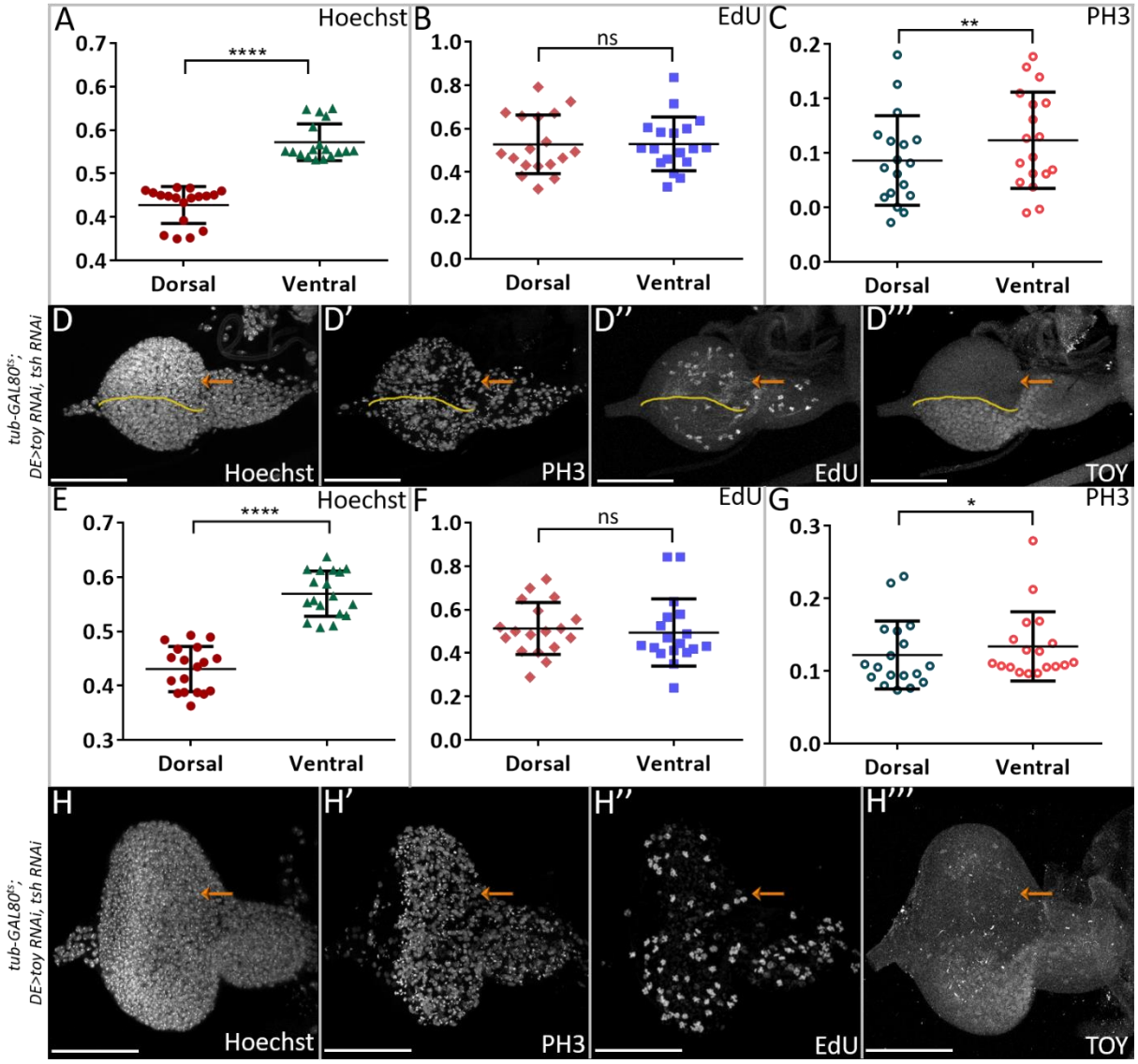

Supplemental Figure 6. Defects in cell proliferation are not a significant contributor to the headless phenotype of removing Tsh/Toy. (A-C, E-G) In these graphs the density of Hoechst, EdU, and PH3 positive cells in the dorsal and ventral compartments after *toy/tsh* have been knocked-down for 24hrs **(A-C)** and for 36hrs **(E-G)** is presented. **(A and E)** To account for the difference in cell number between dorsal and ventral compartments, a ratio of Hoechst positive cells in dorsal (or ventral) to the total number of cells in the entire disc (D+V) was determined. **(B,C,F,G)** To accurately determine the percentage of cells in each compartment that express either EdU or PH3, we divided the

number of cells expressing these markers within a single compartment by the total number of Hoechst positive cells in the same compartment. Each graph is therefore comparing ratios of EdU and PH3 positive cells within the dorsal and ventral domains of the eye disc. All eye discs were of the following genotype: *tub-GAL80^{ts}; DE-GAL4, UAS-toy RNAi, UAS-tsh RNAi*. **(A,E)** The loss of Toy/Tsh results in a dorsal compartment that contains significantly fewer cells than the ventral compartment. **(B,C,F,G)** However, there are only slight differences in the percentage of cells that are in either S or M phases of the cell cycle. **(D-D’’’)** Light microscope images of discs that were analyzed for panels A-C. The yellow line demarcates the midline. The orange arrows mark the dorsal compartment where both *toy* and *tsh* expression is knocked-down. **(H-H’’’)** Light microscope images of discs that were analyzed for panels E-G. The orange arrows mark the dorsal compartment where both *toy* and *tsh* expression is knocked down. Anterior is to the right. N = 18 in each experiment, *$P \leq 0.1$, **$P \leq 0.01$, ***$P \leq 0.001$, ****$P \leq 0.0001$ (Scale bars, 50 µm).

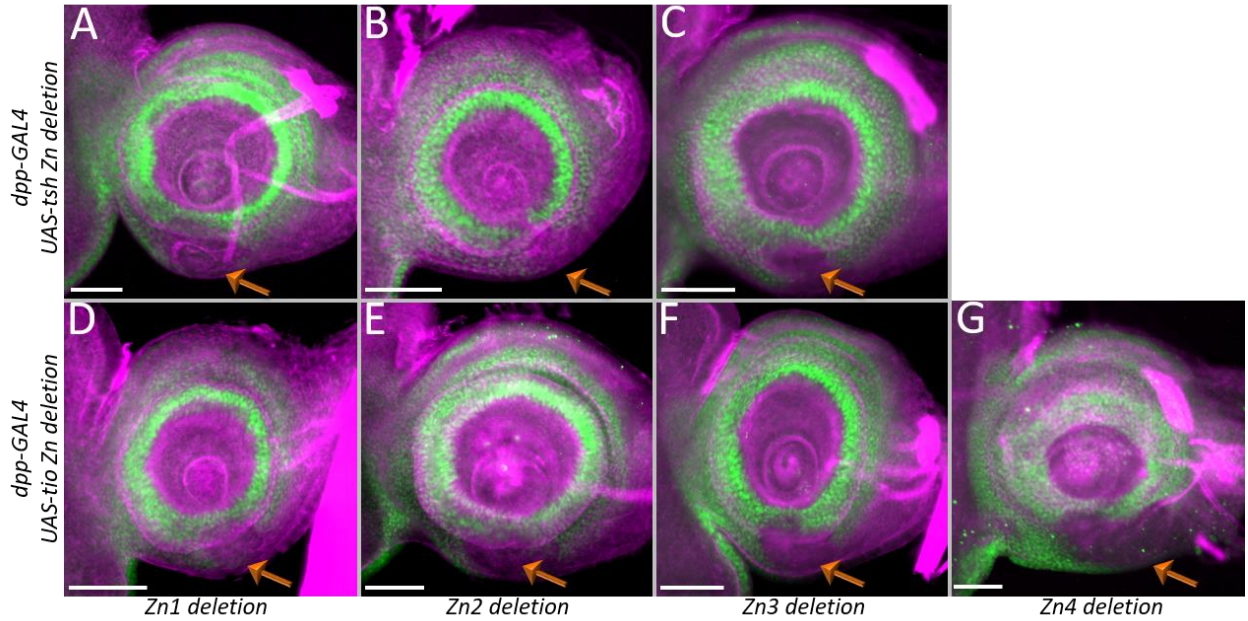

Supplemental Figure 7. The Zn finger domains of Tsh/Tio function redundantly. (A-G) Light microscope images of third instar antennal discs in which Tsh/Tio protein variants are expressed via *dpp*-GAL4. Each panel depicts the effect that removal of an individual zinc finger domain has on the ability of either Tsh or Tio to repress *cut* expression. In all cases, the deletion of an individual zinc finger domain does not impair the ability to repress *cut* within the antenna. This suggests that the zinc fingers either work redundantly or cooperatively to enable Tsh and Tio to bind to their DNA targets. Posterior is to the right. (Scale bars, 50 µm).

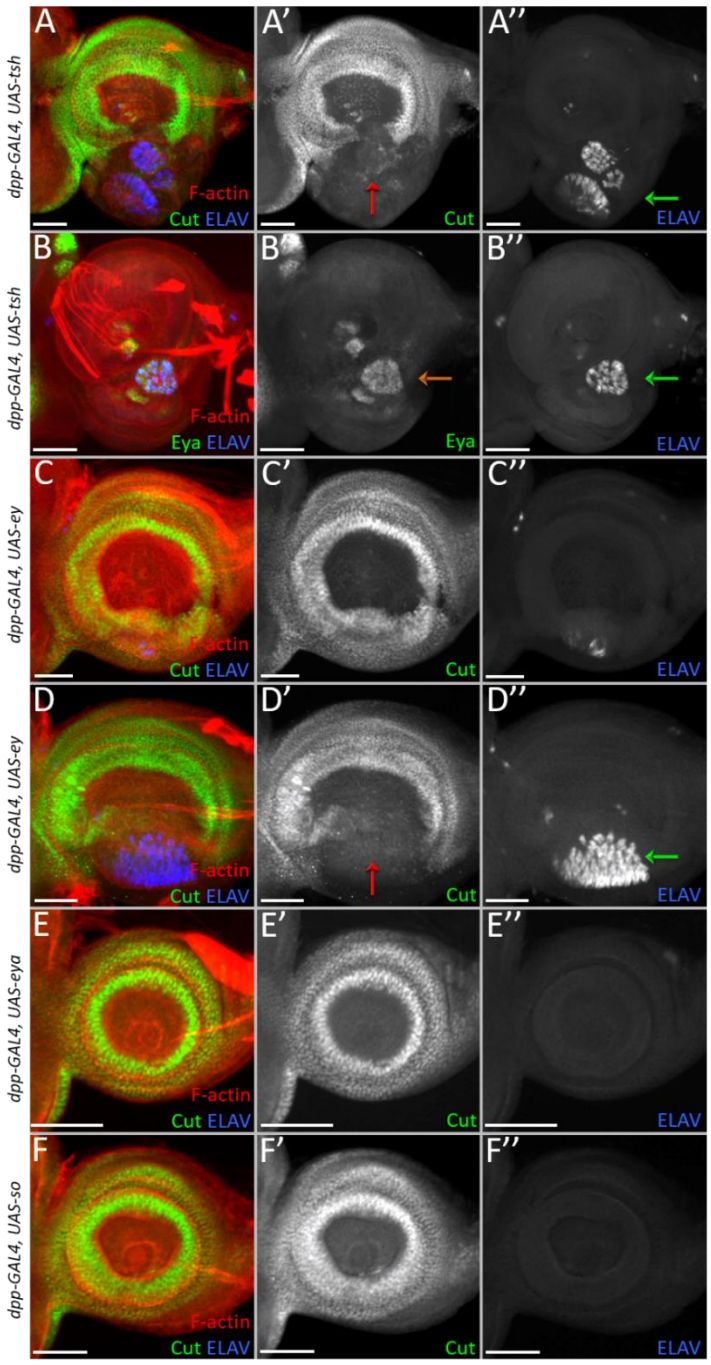

Supplemental Figure 8. Repression of *cut* does not function through the core RD network. (A-F) Light microscope images of third instar antennal discs. **(A,B)** Forced expression of *tsh* induces *eya* expression (orange arrow), induces the formation of an ectopic eye (green arrows) and represses *cut* expression (red arrow). **(C,D)** The repression of *cut* (red arrow) by *ey* occurs only when an ectopic eye is induced (green arrow). This is different than *tsh*, which can repress *cut* in the absence of ectopic eye formation. **(E,F)** Neither *so* nor *eya* appear capable of repressing *cut* within the *dpp-GAL4* ventral expression domain. Posterior is to the right. (Scale bars, 50 µm).

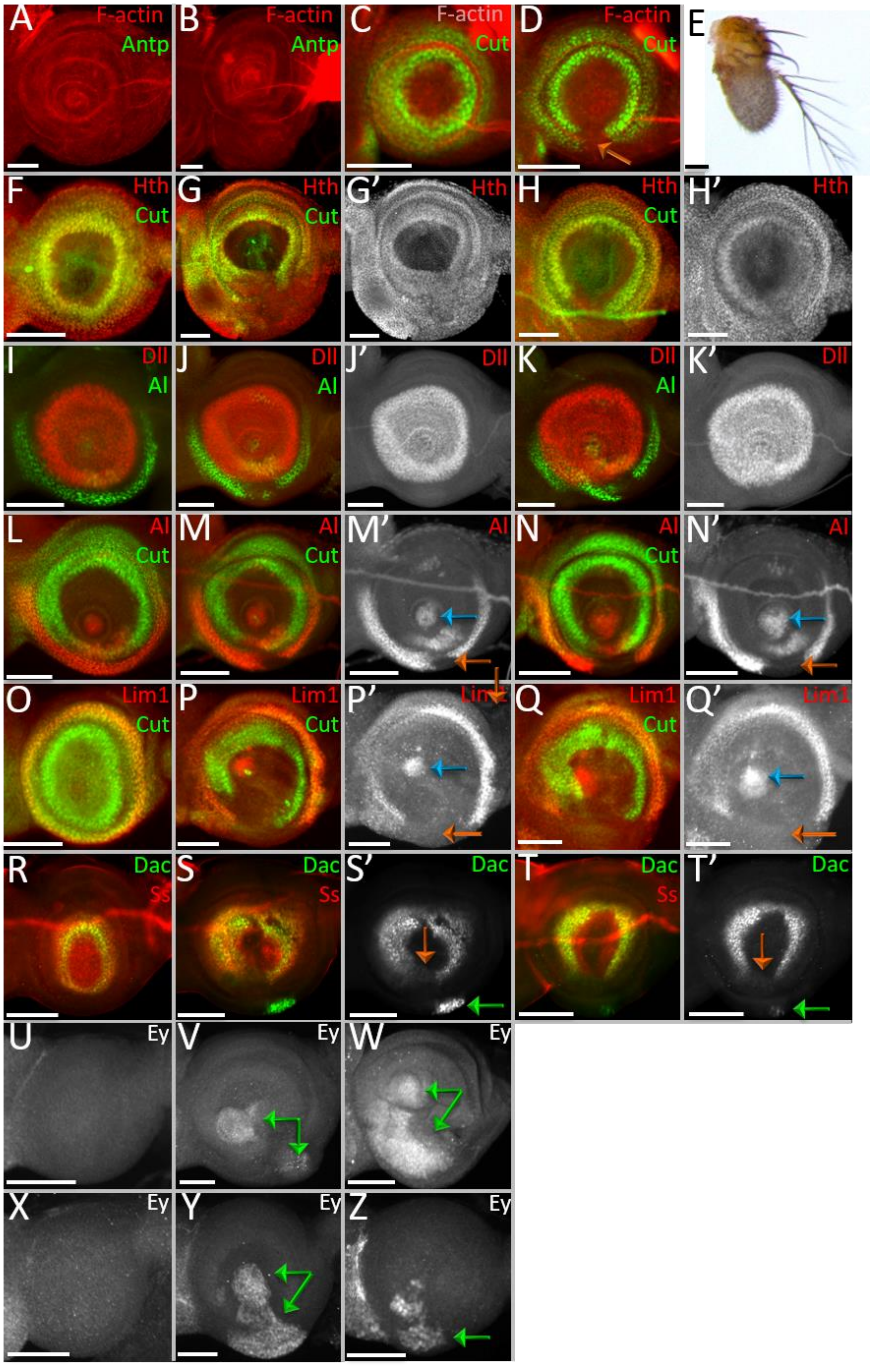

Supplemental Figure 9. RD gene expression patterns. (A-D, F-Y) Light microscope images of third instar antennal discs. **(E)** Light microscope image of an adult antenna and arista. **(A)** wild type – *tsh* expression does not induce *Antp* transcription. **(B)** wild type – *tio* expression does not induce *Antp* transcription. **(C)** wild type – *cut* expression pattern. **(D)** *dpp-GAL4, UAS-cut RNAi* – *cut* expression is lost in the *dpp* expression domain. **(E)**

dpp-GAL4, UAS-cut RNAi – the arista is unaffected by the loss of *cut*. **(F)** *ey^{LB} – hth* expression pattern. **(G,G')** *dpp-GAL4 UAS-tsh; ey^{LB} – hth* expression is unaffected within the *dpp* expression domain. **(H,H')** *dpp-GAL4 UAS-tio; ey^{LB} – hth* expression is unaffected within the *dpp* expression domain. **(I)** *ey^{LB}– Dll* expression pattern. **(J,J')** *dpp-GAL4 UAS-tsh; ey^{LB} – Dll* expression is unaffected within the *dpp* expression domain. **(K,K')** *dpp-GAL4 UAS-tio; ey^{LB} – Dll* expression is unaffected within the *dpp* expression domain. (L) *ey^{LB}– al* expression pattern. *dpp-GAL4 UAS-tsh; ey^{LB} – al* expression is lost within the head epidermis (orange arrow) but is unaffected within the aristal segment. **(N,N')** *dpp-GAL4 UAS-tio; ey^{LB} – al* expression is lost within the head epidermis (orange arrow) but is unaffected within the aristal segment. **(O)** wild type – *Lim1* expression pattern. **(P,P')** *dpp-GAL4 UAS-tsh; ey^{LB}*– Like *al*, *Lim1* expression is inhibited by the expression of *tsh*. **(Q,Q')** *dpp-GAL4 UAS-tio; ey^{LB}* – Like *al, Lim1* expression is inhibited by the expression of *tio*. (R) *ey^{LB} – dac* and *ss* expression pattern. **(S,S')** *dpp-GAL4 UAS-tsh; ey^{LB} – dac* expression is induced within the head epidermis by Tsh (green arrow) independent of Ey. A portion of its normal pattern (orange arrow) is lost simultaneously. **(T,T')** *dpp-GAL4 UAS-tio; ey^{LB} – dac* expression is induced within the head epidermis by Tio (green arrow) independent of Ey. A portion of its normal pattern (orange arrow) is lost simultaneously. **(U)** *so^{1}* – Ey protein is not found within the antennal disc of *so^{1}* mutants. **(V,W)** Both Tsh **(V)** and Tio **(W)** are capable of activating *ey* (green arrows) expression within the ventral antenna. **(X)** *eya^{2}* - Ey protein is not found within the antennal disc of *eya^{2}* mutants. **(Y,Z)** Both Tsh **(Y)** and Tio **(Z)** are capable of activating *ey* (green arrows) expression within the ventral antenna). Posterior is to the right. (Scale bars, 50 µm).

REFERENCES

1. Jurgens J, Hartenstein V (1993) The terminal regions of the body pattern. In Bate, M and Martinez Arias, A (eds), Cold Spring Harbor Laboratory Press, Cold Spring Harbor, NY pp 687-746.

2. Vogt M (1946) Zur labilen Determination der Imagin-alscheiben von Drosophila. I. Verhalten verschieden-altriger Imaginalanlagen bei operative Defektsetzung. Biol Zbl 65: 223-238.

3. Gehring W (1966) [Cell heredity and changes of determination in cultures of imaginal discs in Drosophila melanogaster]. J Embryol Exp Morphol 15: 77-111.

4. Ouweneel WJ (1970) Normal and abnormal determination in the imaginal discs of Drosophila, with special reference to the eye discs. Acta Embryol Exp (Palermo) 1: 95-119.

5. Baker WK (1978) A fine-structure gynandromorph fate map of the Drosophila head. Genetics 88: 743-754.

6. Haynie JL, Bryant PJ (1986) Development of the eye-antenna imaginal disc and morphogenesis of the adult head in Drosophila melanogaster. J Exp Zool 237: 293-308.

7. Quiring R, Walldorf U, Kloter U, Gehring WJ (1994) Homology of the eyeless gene of Drosophila to the Small eye gene in mice and Aniridia in humans [see comments]. Science 265: 785-789.

8. Czerny T, Halder G, Kloter U, Souabni A, Gehring WJ, et al. (1999) twin of eyeless, a second Pax-6 gene of Drosophila, acts upstream of eyeless in the control of eye development. Mol Cell 3: 297-307.

9. Kumar JP, Moses K (2001) EGF receptor and Notch signaling act upstream of Eyeless/Pax6 to control eye specification. Cell 104: 687-697.

10. Zhu J, Palliyil S, Ran C, Kumar JP (2017) Drosophila Pax6 promotes development of the entire eye-antennal disc, thereby ensuring proper adult head formation. Proc Natl Acad Sci U S A 114: 5846-5853.

11. Wang CW, Sun YH (2012) Segregation of eye and antenna fates maintained by mutual antagonism in Drosophila. Development 139: 3413-3421.

12. Halder G, Callaerts P, Gehring WJ (1995) Induction of ectopic eyes by targeted expression of the eyeless gene in Drosophila. Science 267: 1788-1792.

13. Bessa J, Carmona L, Casares F (2009) Zinc-finger paralogues tsh and tio are functionally equivalent during imaginal development in Drosophila and maintain their expression levels through auto- and cross-negative feedback loops. Dev Dyn 238: 19-28.

14. Peng HW, Slattery M, Mann RS (2009) Transcription factor choice in the Hippo signaling pathway: homothorax and yorkie regulation of the microRNA bantam in the progenitor domain of the Drosophila eye imaginal disc. Genes Dev 23: 2307-2319.

15. Datta RR, Weasner BP, Kumar JP (2011) A dissection of the teashirt and tiptop genes reveals a novel mechanism for regulating transcription factor activity. Dev Biol 360: 391-402.

16. Pan D, Rubin GM (1998) 942 Targeted expression of teashirt induces ectopic eyes in Drosophila. Proc Natl Acad Sci U S A 95: 15508-15512.

17. Datta RR, Lurye JM, Kumar JP (2009) Restriction of ectopic eye formation by Drosophila teashirt and tiptop to the developing antenna. Dev Dyn.

18. Morrison CM, Halder G (2010) Characterization of a dorsal-eye Gal4 Line in Drosophila. Genesis 48: 3-7.

19. Soanes KH, Bell JB (2001) The drosophila aeroplane mutant is caused by an I949 element insertion into a tissue-specific teashirt enhancer motif. Genome 44:919-928.

20. Soanes KH, Bell JB (1999) Rediscovery and further characterization of the aeroplane (ae) wing posture mutation in Drosophila melanogaster. Genome 42: 403-411.

21. Bessa J, Gebelein B, Pichaud F, Casares F, Mann RS (2002) Combinatorial control of Drosophila eye development by eyeless, homothorax, and teashirt. Genes Dev 16: 2415-2427.

22. McGuire SE, Le PT, Osborn AJ, Matsumoto K, Davis RL (2003) Spatiotemporal rescue of memory dysfunction in Drosophila. Science 302: 1765-1768.

23. Erkner A, Gallet A, Angelats C, Fasano L, Kerridge S (1999) The role of Teashirt in proximal leg development in Drosophila: ectopic Teashirt expression reveals different cell behaviours in ventral and dorsal domains. Dev Biol 215: 221-232.

24. Wu J, Cohen SM (2000) Proximal distal axis formation in the Drosophila leg: distinct functions of teashirt and homothorax in the proximal leg. Mech Dev 94: 47-56.

25. Weasner BM, Weasner BP, Neuman SD, Bashirullah A, Kumar JP (2016) Retinal Expression of the Drosophila eyes absent Gene Is Controlled by Several Cooperatively Acting Cis-regulatory Elements. PLoS Genet 12: e1006462.

26. Shaham O, Menuchin Y, Farhy C, Ashery-Padan R (2012) Pax6: a multi-level regulator of ocular development. Prog Retin Eye Res 31: 351-376.

27. Bonini NM, Leiserson WM, Benzer S (1993) The eyes absent gene: genetic control of cell survival and differentiation in the developing Drosophila eye. Cell 72: 379-395.

28. Jang CC, Chao JL, Jones N, Yao LC, Bessarab DA, et al. (2003) Two Pax genes, eyegone and eyeless, act cooperatively in promoting Drosophila eye development. Development 130: 2939-2951.

29. Dominguez M, Ferres-Marco D, Gutierrez-Avino FJ, Speicher SA, Beneyto M (2004) Growth and specification of the eye are controlled independently by Eyegone and Eyeless in Drosophila melanogaster. Nat Genet 36: 31-39.

30. Chao JL, Tsai YC, Chiu SJ, Sun YH (2004) Localized Notch signal acts through eyg and upd to promote global growth in Drosophila eye. Development 131: 3839-3847.

31. Jemc J, Rebay I (2007) Identification of transcriptional targets of the dual function transcription factor/phosphatase eyes absent. Dev Biol 310: 416-429.

32. Song Z, McCall K, Steller H (1997) DCP-1, a Drosophila cell death protease essential for development. Science 275: 536-540.

33. Kajiwara Y, Akram A, Katsel P, Haroutunian V, Schmeidler J, et al. (2009) FE65 binds Teashirt, inhibiting expression of the primate-specific caspase-4. PLoS One 4: e5071.

34. Hay BA, Wolff T, Rubin GM (1994) Expression of baculovirus P35 prevents cell death in Drosophila. Development 120: 2121-2129.

35. Hay BA, Wassarman DA, Rubin GM (1995) Drosophila homologs of baculovirus inhibitor of apoptosis proteins function to block cell death. Cell 83: 1253-1262.

36. Bessa J, Casares F (2005) Restricted teashirt expression confers eye-specific responsiveness to Dpp and Wg signals during eye specification in Drosophila. Development 132: 5011-5020.

37. Bodmer R, Barbel S, Sheperd S, Jack JW, Jan LY, et al. (1987) Transformation of sensory organs by mutations of the cut locus of D. melanogaster. Cell 51: 293-307.

38. Todi SV, Sharma Y, Eberl DF (2004) Anatomical and molecular design of the Drosophila antenna as a flagellar auditory organ. Microsc Res Tech 63: 388-399.

39. Ebacher DJ, Todi SV, Eberl DF, Boekhoff-Falk GE (2007) Cut mutant Drosophila auditory organs differentiate abnormally and degenerate. Fly (Austin) 1: 86-94.

40. Denholm B, Hu N, Fauquier T, Caubit X, Fasano L, et al. (2013) The tiptop/teashirt genes regulate cell differentiation and renal physiology in Drosophila. Development 140: 1100-1110.

41. Fasano L, Roder L, Core N, Alexandre E, Vola C, et al. (1991) The gene teashirt is required for the development of Drosophila embryonic trunk segments and encodes a protein with widely spaced zinc finger motifs. Cell 64: 63-79.

42. Laugier E, Yang Z, Fasano L, Kerridge S, Vola C (2005) A critical role of teashirt for patterning the ventral epidermis is masked by ectopic expression of tiptop, a paralog of teashirt in Drosophila. Dev Biol 283: 446-458.

Salzer CL, Kumar JP (2009) Position dependent responses to discontinuities in the retinal determination network. Dev Biol 326: 121-130.

44. Anderson AM, Weasner BM, Weasner BP, Kumar JP (2012) Dual transcriptional activities of SIX proteins define their roles in normal and ectopic eye development. Development 139: 991-1000.

45. Weasner BM, Kumar JP (2013) Competition among gene regulatory networks imposes order within the eye-antennal disc of Drosophila. Development 140:205-215.

46. Cheyette BN, Green PJ, Martin K, Garren H, Hartenstein V, et al. (1994) The Drosophila sine oculis locus encodes a homeodomain-containing protein required for the development of the entire visual system. Neuron 12: 977-996.

47. Herke SW, Serio NV, Rogers BT (2005) Functional analyses of tiptop and antennapedia in the embryonic development of Oncopeltus fasciatus suggests an evolutionary pathway from ground state to insect legs. Development 132: 27-34.

48. Schneuwly S, Kuroiwa A, Gehring WJ (1987) Molecular analysis of the dominant homeotic Antennapedia phenotype. Embo J 6: 201-206.

49. Wirz J, Fessler LI, Gehring WJ (1986) Localization of the Antennapedia protein in Drosophila embryos and imaginal discs. EMBO J 5: 3327-3334.

50. Benassayag C, Plaza S, Callaerts P, Clements J, Romeo Y, et al. (2003) Evidence for a direct functional antagonism of the selector genes proboscipedia and eyeless in Drosophila head development. Development 130: 575-586.

51. Struhl G (1982) Spineless-aristapedia: a homeotic gene that does not control the development of specific compartments in Drosophila. Genetics 102: 737-749.

52. Duncan DM, Burgess EA, Duncan I (1998) Control of distal antennal identity and tarsal development in Drosophila by spineless-aristapedia, a homolog of the mammalian dioxin receptor. Genes Dev 12: 1290-1303.

53. Duncan D, Kiefel P, Duncan I (2010) Control of the spineless antennal enhancer: direct repression of antennal target genes by Antennapedia. Dev Biol 347:82-91.

54. Dong PD, Chu J, Panganiban G (2000) Coexpression of the homeobox genes distal-less and homothorax determines drosophila antennal identity [In Process Citation]. Development 127: 209-216.

55. Dong PD, Dicks JS, Panganiban G (2002) Distal-less and homothorax regulate multiple targets to pattern the Drosophila antenna. Development 129: 1967-1974.

56. Emmons RB, Duncan D, Duncan I (2007) Regulation of the Drosophila distal antennal determinant spineless. Dev Biol 302: 412-426.

57. Campbell G, Tomlinson A (1998) The roles of the homeobox genes aristaless and Distal-less in patterning the legs and wings of Drosophila. Development 125:4483-4493.

58. Tsuji T, Sato A, Hiratani I, Taira M, Saigo K, et al. (2000) Requirements of Lim1, a Drosophila LIM-homeobox gene, for normal leg and antennal development. Development 127: 4315-4323.

59. Jiao R, Daube M, Duan H, Zou Y, Frei E, et al. (2001) Headless flies generated by developmental pathway interference. Development 128: 3307-3319.

60. Kronhamn J, Frei E, Daube M, Jiao R, Shi Y, et al. (2002) Headless flies produced by mutations in the paralogous Pax6 genes eyeless and twin of eyeless. Development 129: 1015-1026.

61. Jacobsson L, Kronhamn J, Rasmuson-Lestander A (2009) The Drosophila Pax6 paralogs have different functions in head development but can partially substitute for each other. Mol Genet Genomics 282: 217-231.

62. Dominguez M, Casares F (2005) Organ specification-growth control connection: new in-sights from the Drosophila eye-antennal disc. Dev Dyn 232: 673-684.

63. Amore G, Casares F (2010) Size matters: the contribution of cell proliferation to the progression of the specification Drosophila eye gene regulatory network. Dev Biol 344: 569-577.

64. Kumar JP (2010) Retinal determination the beginning of eye development. Curr Top Dev Biol 93: 1-28.

65. Kumar JP (2011) My what big eyes you have: how the Drosophila retina grows. Dev Neurobiol 71: 1133-1152.

66. Braid LR, Verheyen EM (2008) Drosophila nemo promotes eye specification directed by the retinal determination gene network. Genetics 180: 283-299.

67. Bonini NM, Bui QT, Gray-Board GL, Warrick JM (1997) The Drosophila eyes absent gene directs ectopic eye formation in a pathway conserved between flies and vertebrates. Development 124: 4819-4826.

68. Pignoni F, Zipursky SL (1997) Induction of Drosophila eye development by Decapentaplegic. Development 124: 271-278.

69. Shen W, Mardon G (1997) Ectopic eye development in Drosophila induced by directed dachshund expression. Development 124: 45-52.

70. Halder G, Callaerts P, Flister S, Walldorf U, Kloter U, et al. (1998) Eyeless initiates the expression of both sine oculis and eyes absent during drosophila compound eye development. Development 125: 2181-2191.

71. Spratford CM, Kumar JP (2014) Dissection and immunostaining of imaginal discs from Drosophila melanogaster. J Vis Exp: 51792.

72. Ihry RJ, Sapiro AL, Bashirullah A (2012) Translational control by the DEAD Box RNA helicase belle regulates ecdysone-triggered transcriptional cascades. PLoS Genet 8: e1003085.

73. Arvidsson S, Kwasniewski M, Riaño-Pachón DM, Mueller-Roeber B (2008) QuantPrime – a flexible tool for reliable high-throughput primer design for quantitative PCR. BMC Bioinformatics 9: 465.

74. Hu Y, Sopko R, Foos M, Kelley C, Flockhart I, et al. (2013) FlyPrimerBank: an online database for Drosophila melanogaster gene expression analysis and knockdown evaluation of RNAi reagents. G3 (Bethesda) 3: 1607-1616.